Universidad Autónoma de Madrid

Departamento de Física de la Materia Condensada
Facultad de Ciencias

Donor and acceptor molecules on metal surfaces: Supramolecular self-assembly, metal-organic coordination networks, and charge-transfer complexes.

Tesis doctoral presentada por

Jonathan Rodríguez Fernández

para optar al Título de Doctor en Ciencias Físicas

Directores de Tesis:

Prof. Rodolfo Miranda Soriano

Dr. José M. Gallego Vázquez

Madrid, Diciembre de 2014

Dedicada a mis seres queridos, en especial a mi tío "Sebi"

Contents

Abstract

This thesis presents a dissertation on supramolecular self-assembly, coordination networks and charge transfer complexes of four molecules: Dicyano-p-quinonediimine (DCNQI), Tetracyanoethylene (TCNE), Tetracyanoquinodimethane (TCNQ) and Tetrathiafulvalene (TTF) at a noble metal surface. Different systems were analyzed by variable temperature scanning tunneling microscopy (STM), X-ray photoelectron spectroscopy (XPS) and the results were compared with theoretical within the density functional theory (DFT).

In the first part of this thesis, the adsorption of the individual molecules (TCNE, TCNQ, and TTF) on a Ag(111) surface was studied.

The growth of TCNE on Ag(111) results in the formation of two different Ag-TCNE coordination networks, depending on the substrate temperature, where the silver adatoms originate from the step etching of the silver substrate. According to DFT calculations and in agreement with XPS measurements, the TCNE molecules are negatively charged ($\sim$ 1 e), taking charge from the substrate and from the silver adatom (the charge on the silver adatoms is 0.45 e).

The adsorption of TCNQ on Ag(111) shows the formation of three different phases, where the molecules are bonded together by hydrogen bonds, but with a strong influence of the interaction of the cyano groups with the silver substrate. Actually, in one of the phases the participation of silver adatoms cannot be completely ruled out. There is also a strong charge transfer from the silver to the TCNQ molecule ($\sim$ 1 e). On the other hand, for a bilayer of TCNQ molecules on Ag(111), the second layer is much more decoupled from the substrate, and the self-assembly is driven exclusively by the formation of hydrogen bonds between the molecules, in a similar behavior to that reported on graphene and Au(111) substrates.

The adsorption of the electron donor TTF on Ag(111) was studied, after room temperature deposition. No isolated or islands could be imaged due to a high molecular diffusivity. Annealing the sample at 350 K results in the formation of well-ordered island where the molecules are slightly tilted with respect to the surface. DFT calculations and XPS measurements show that in this case the charge transfer, although very small ($\sim$ 0.1 e), takes place in the opposite direction, the molecule remaining positively charged.

In the second part of the thesis, mixtures of donor/acceptor molecules (TCNQ-TTF, TCNE-TTF) have been studied on a Ag(111) substrate. The metal surface allows us to expands the variety of such Donor-Acceptor (D-A) networks. We show that these systems exhibit various structural phases, depending on the stoichiometry, each leading to different levels of charge transfer. In particular, both TCNE and TCNQ, both being strong electron acceptors, hold in every case a negative charge close to 1 e. On the contrary, the charge on the TTF molecules, being positive, seems to increase with the TCNQ content. Thus by controlling the stoichiometry ratio in these complexes, we can tune both the structural and the electronic properties (for example, the work-function) of a D-A system.

Finally, in the last part of the thesis on the temperature controlled irreversible transition between the two isomeric forms (trans and cis) of the strong electron acceptor DCNQI, both on Cu(100) and Ag(111) surfaces is reported. The experiments and DFT calculations show that the isomerization barrier is lower than in gas phase or solution due to the fact that charge transfer from the substrate has modified the bond configuration of the molecule. In addition, an Fe-DCNQI coordination network was studied by mixing Fe atoms and DCQNI molecules on Ag(111). After annealing at 380 K, one-dimensional (1-D) network has been observed where one Fe atom is connected to 4 DCNQI, forming chains that assemble together by hydrogen bonds. The electronic structure of this network reveals that the iron atom changes from the metallic state to the oxidized state.

In summary, since charge transfer at the metal organic interface plays an important role in the efficiency of many organic optoelectronic devices, we have studied the effect of charge transfer in model donor, acceptor and donor-acceptor systems on a Ag(111), Cu(100) and Au(111).

Resumen

Esta tesis presenta una disertación sobre autoensamblados supramoleculares, redes de coordinación y complejos de transferencia de carga de cuatro moléculas: Dicyano-p-quinonediimine (DCNQI) , Tetracyanoethylene (TCNE), Tetracyanoquinodimethane (TCNQ) and Tetrathiafulvalene (TTF) en superficies de metales nobles. Diferentes sistemas fueron analizados mediante un microcopio de efecto túnel de temperatura variable (STM), espectroscopía de fotoelectrones emitidos por rayos X (XPS) y los resultados fueron comparados con cálculos teóricos mediante la teoría del funcional de la densidad.

En la primera parte de esta tesis, se ha estudiado la adsorción de moléculas individuales (TCNE, TCNQ y TTF) sobre la superficie de Ag(111).

El crecimiento del TCNE sobre Ag(111) resulta en la formación de dos redes de coordinación diferentes Ag-TCNE, dependiendo de la temperatura del substrato, donde los adátomos se originan desde el escalón atacado del substrato de plata. Según los cálculos de DFT y en acuerdo con las medidas de XPS, las moléculas de TCNE están negativamente cargadas ($\sim$ 1 e), cogiendo carga del substrato y de los adátomos de plata (la carga sobre los adátomos de plata es de 0.45 e).

La adsorción del TCNQ sobre Ag(111) muesta la formación de tres diferentes fases, donde las moléculas están enlazados entre sí mediante enlaces de hidrógeno, pero con una fuerte influencia de la interacción de los grupos cyanos con el substrato de plata. Actualmente, en una de las fases la participación de los adátomos de plata no pueden ser completamente excluidos. También hay una fuerte transferencia de carga del substrato a la molécula TCNQ ($\sim$ 1 e). Por el contrario, para una bicapa de moléculas TCNQ sobre Ag(111), la segunda capa está más desacoplada del substrato, y el autoensamblado está dirigido exclusivamente por la formación de enlances de hidrógeno entre las moléculas, un comportamiento similar ha sido reportado en substratos de grafeno y Au(111).

Después de depositar a temperatura ambiente, se ha estudiado la adsorción del donor de electrones TTF sobre Ag(111). Ni moléculas aisladas o islas pueden ser medidas debido a la alta movilidad molecular. Después de calentar la muestra a 350 K resulta en la formación de islas bien ordenadas

donde las moléculas están ligeramente inclinadas con respecto a la superficie. Los cálculos DFT y las medidas XPS muestran que en el caso de transferencia de carga, aunque muy pequeña ($\sim$ 0.1 e), toma lugar en dirección opuesta, la molécula se matiene positivamente cargada.

En la segunda parte de la tesis, se han estudiado mezclas de moléculas donoras y acceptoras (TCNQ-TTF, TCNE-TTF) sobre el substrato de plata (111). La superficie metálica nos permite ampliar la variedad de tales redes Donor-acceptor (D-A). Nosotros mostramos que estos sistemas exhiben diversas fases estructurales, dependiendo de la estequiometría, cada una de ellas dirigiendo a diferentes niveles de transferencia de carga. En particular, ambos TCNE y TCNQ, ambos siendo fuertes aceptores de electrones, agarrán en cada caso una carga negativa cercana a 1 e. Por el contrario, la carga sobre las moléculas TTF, siendo positivas, parece incrementarse con la aparición de TCNQ. Así controlando la proporción estequiométrica en estos compuestos, nosotros podemos ajustar las propiedades estructurales y electrónicas (por ejemplo, la función de trabajo) del sistema D-A.

Finalmente, en la última parte de la tesis presenta entre dos formas isoméricas (trans y cis) del aceptor de electrones DCNQI, ambos sobre las superficies de Cu(100) y Ag(111). Los experimentos y los cálculos de DFT muestran que la barrera de isomerización es más baja que en fase gas o en solución debido a la transferencia de carga del substrato. Además, se ha estudiado la red de coordinación Fe-DCNQI mezclando átomos de hierro y moléculas DCNQI sobre Ag(111). Después de calentar a 380 K, se han observado redes unidimensionales (1-D) donde un átomo de hierro está conectado a 4 DCNQI, formando cadenas que se autoensamblan por enlaces de hidrógeno. La estructura electrónica de estas redes revela que los átomos de hierro pasan de un comportamiento metálico a un estado oxidado.

En resumen, dado que la transferencia de carga en interfases metal orgánicas juegan un papel importante en la eficiencia de muchos dipositivos optoelectrónicos orgánicos, nosotros hemos estudiado el efecto de transferencia de carga en sistemas modelo de donores, aceptores y donores-aceptores sobre la superficie de Ag(111), Cu(100) y Au(111).

1 Introduction

In the last decades nanotechnology (or nanoscience) has emerged and considered as the next industrial revolution due to the big impact it is having in the scientific and technological advance. This new concept is attributed to physicist Richard Feynmann, who gave a very famous, visionary speech in 1959 during one of his lectures, "There's Plenty of Room at the Bottom", which is essentially based on the ability to manipulate and control individual atoms and molecules. Nanotechnology is a multidisciplinary science that includes a broad area of expertise like physics, chemistry, material science, surface science, organic chemistry, molecular biology, semiconductor physics, etc. Essentially, nanoscience is the study of phenomena and manipulation of materials at the nanometer scale (atomic, molecular and macromolecular, scales) where properties differ significantly from those at a larger scale.

The practical development of nanotechnology is intimately associated with the invention of the Scanning Tunneling Microscope (STM) and the Atomic Force Microscope (AFM) in the early 1980's. Both microscopies are capable at imaging surfaces with atomic resolution, and have revolutionized the imaging and provided a unique capability for the manipulation of atoms and molecules on surfaces at the nanoscale. The STM can be considered as the first step in the realization of Feyman's vision of atom by atom fabrication.

In nanotechnology there are two approaches for fabricating materials or manipulating devices: "top-down", based in the concept of miniaturization, refers to slicing or successive cutting of a bulk material to get nano sized particles; and "bottom-up", that refers to the build up of a material from the

bottom: atom by atom, molecule by molecule to give rise to more complex systems. Both approaches play very important roles in modern industry.

An important discipline inside the 'bottom-up approach" is the supramolecular self-assembly, and in particular, supramolecular assembly on solid surfaces, a complicated process that depends in general on both the molecule-molecule and the molecule-substrate interactions. It is very relevant for a number of applications such as molecular electronics, biosensors, optoelectronic devices.

In this thesis we present several studies of molecular adsorption on metal surfaces. The main topics covered are self-assembly, molecule-substrate interactions, metal-organic coordination networks and charge-transfer complexes investigated with high-resolution STM under ultra-high vacuum (UHV) conditions. The STM results are supported by X-Ray photoelectron spectroscopy (XPS) and density functional theory (DFT) calculations.

Outline of this thesis

This thesis is organized as follows:

Chapter 2 provides the technical background for this work: A brief introduction to scanning tunneling microscopy (STM), x-ray photoelectron spectroscopy (XPS) and the basics of Density Functional Theory (DFT). Also, the experimental set-up and sample preparation will be described in detail.

Chapter 3 describes the adsorption of the individual molecules, two electron acceptor molecules TCNE, TCNQ and one electron donor molecule TTF on Ag(111) surface.

Chapter 4 focuses on the mixture of Donor-Acceptor networks: TCNE-TTF and TCNQ-TTF on Ag(111). We show that these systems have different structural phases, depending on the stoichiometry, each leading to different levels of charge transfer.

Chapter 5 shows the self-assembly of the electron acceptor DCNQI molecules on the metal substrates Cu(100) and Ag(111). Charge transfer is shown to be the responsible for the appearance of two types of islands due to the lowering of the energy barrier for molecular isomerization. The second part of the chapter focuses on the metallorganic chemistry. In particular, it

describes the fabrication and electronic properties of Fe-DCNQI coordination networks.

In **Chapter 6-7** the general conclusions obtained in this thesis are summarized.

Finally, the bibliography and the list of publications are listed.

2

Experimental techniques and theory

This thesis was carried out in the surface science field. In this chapter, we would like to explain the main techniques used during this work: Scanning tunnelling microscopy (STM) and X-Ray photoelectron spectroscopy (XPS); and also, briefly, the basics of the density functional theory (DFT). First of all, we want to introduce why it is important to use ultra high vacuum (UHV) conditions in surface science.

2.1 Ultra high vacuum (UHV)

In surface science experiments ultra-high vacuum is required for two main reasons: i) first, the surface sample must be clean before the experiments, and must continue without unwanted contamination during the experiment; ii) and second, spectroscopic techniques can be used without interference with the residual gas in the chamber.

We can determinate how long the surface can be kept clean with the help of the kinetic theory of the gases. The number F of incident molecules per unit area of surface is given by the Hertz-Knudsen equation [1]:

$$F = \frac{P}{\sqrt{2\pi m K_B T}} \tag{2.1}$$

where P is the pressure, m the molecular mass, k_B the Boltzmann constant and T the temperature. Using this equation we can calculate the time needed

to form a monolayer of absorbed molecules on the surface. In the case of atmospheric pressure this time is close to $10^{-9}s$. However, in UHV conditions (10^{-10} $Torr$) it is close to 10^4 s, which is usually enough time to carry out the experiments.

On the other hand, when using electron spectroscopic techniques, like XPS, electrons must go from the surface to the analyzer; but if the density of molecules in the residual gas in the chamber is high, the electrons can interfere with this residual gas. The average distance that a particle moves in the gas phase between collisions, that is, without interference with the residual gas, is known as the mean free path, and is given by [2, 3]:

$$\lambda = \frac{K_B T}{1.414 P \sigma} \tag{2.2}$$

where σ is the collision cross section. In the case of atmospheric pressure, λ is close to 7×10^{-8} m, but in UHV conditions (10^{-10} $Torr$) it is around 5×10^5 m, longer than the dimensions of the systems.

2.2 Scanning tunneling microscopy (STM)

2.2.1 The basic principles

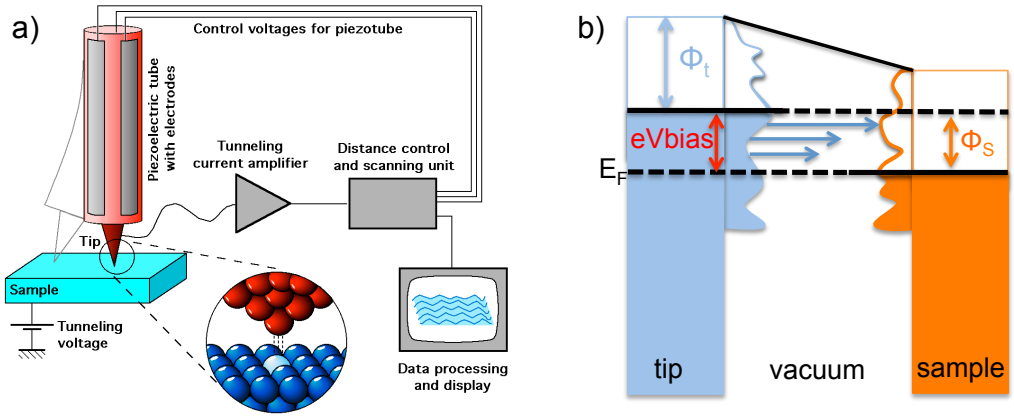

Figure 2.1: *a) Schematic representation of the working principle of an STM (image taken from* `http://en.wikipedia.org/wiki/Scanning_tunneling_microscope`*. b) Energy diagram of the tunneling process for a positive sample bias; ϕ_t and ϕ_s are the workfunctions of the tip and sample, respectively, and E_F is the Fermi level.*

The Scanning tunneling microscope (STM) was invented in 1981 by Gerd Binning and Heinrich Rohrer, who won the nobel Prize in physics in 1986 [4–6]. Actually, this technique is a very powerful tool in surface science. The basic principle of the Scanning tunneling microscopy (STM) is the tunneling effect. This is a pure quantum effect that takes place when two electrodes (with different voltages) are separated by a short distance. In classical mechanics, as shown in figure 2.2, if a particle is confined by a potential barrier and the barrier height is larger than the energy of the particle, the probability of the particle to go through the barrier is zero. In quantum mechanics, however the Schrödinger's equation has solution inside the barrier, and the amplitude of the wavefunction that describes the particle is not zero in this region. So if the barrier is narrow (a few angstroms) and it is not high (a few eV) the probability of the particle to go through the barrier is non-zero.

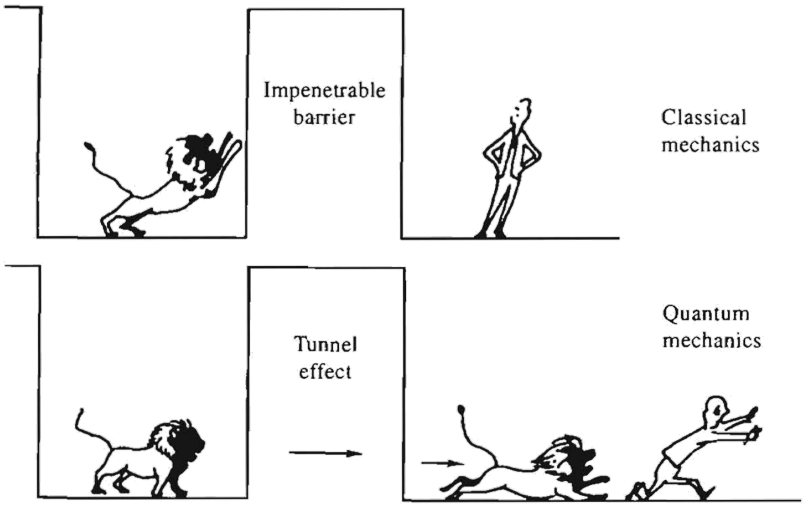

Figure 2.2: *Explanation of the tunneling effect. The illustration shows the difference between classical and quantum theory. Figure taken from [7].*

In an STM, as figure 2.1a shows, one of the electrodes is the tip and the other is the sample, which are separated a few angstroms by the vacuum gap. To control the direction of the tunneling current you need to apply a bias voltage between tip and sample. This bias voltage can be positive or negative. In the first case, if you apply a positive bias voltage to the sample, the electrons go from the occupied states of the tip to the unoccupied states of the sample through the vacuum gap, as shown in figure 2.1b. If the sign of the bias is reversed, that means sample at negative voltage, the electrons go from the occupied states of the sample to the unoccupied states of the tip.

For STM measurement the tip is scanned across the sample, X-Y directions, which can be done in two different ways. The first way is called **constant height mode**: in this case the bias voltage and the distance between the tip and the sample is kept constant during the measurement. The big problem with this mode is that the surface necessarily has to be rather flat, because otherwise the tip can crash with the surface. The second way is the **constant current mode**, which is the most commonly used; in this mode a feedback mechanism adjusts the distance between the tip and the sample to keep the tunneling current constant. In this case the surface does not need to be planar, which allows the measurement of larger areas.

2.2.2 Tunnel effect: the theory

In the decade of the 60s, J. Bardeen developed the formalism to study the tunneling current through a metal-insulator-metal junction [8]. The Schrödinger equation was solved for each electrode separately and the wave function of each electrode was obtained. In this way the tunneling matrix elements $M_{\mu\nu}$ due to the overlap of the states ψ_μ of the tip with the states ψ_ν of the sample can be estimated. In the first-order of perturbation theory, the tunneling current through the two electrodes is given by:

$$I = \frac{2\pi e}{\hbar} \sum_{\mu\nu} f(E_\mu)[1 - f(E_\nu + eV)]|M_{\mu\nu}|^2 \delta(E_\mu - E_\nu) \tag{2.3}$$

where f(E) is the Fermi function; V the bias voltage; and E_μ, E_ν are the energies of the states ψ_μ, ψ_ν (in the absence of tunneling). In the Bardeen formalism the tunneling matrix element is given by:

$$M_{\mu\nu} = \frac{\hbar^2}{2m} \int \overrightarrow{dS}(\psi_\mu^* \overrightarrow{\nabla} \psi_\nu - \psi_\nu \overrightarrow{\nabla} \psi_\mu^*) \tag{2.4}$$

where the integral is over any surface lying entirely within the vacuum region separating surface and the tip. In the limit of zero bias voltage ($E_\nu \approx E_F$), and low temperatures:

$$I = \frac{2\pi e^2 V}{\hbar} \sum_{\mu\nu} |M_{\mu\nu}|^2 \delta(E_\nu - E_F)\delta(E_\mu - E_F) \tag{2.5}$$

The wave function of the tip is not known; however if you suppose that the part of the tip that is close to the surface has a locally spherical shape, you can estimate its wave functions. This is the Tersoff-Hamman model [9, 10]; it is based on the formalism of J. Bardeen, but in here one electrode is a

spherical tip and the other is the sample. In this approximation, assuming that the local density of states of the tip is constant, $M_{\mu\nu}$ is given by:

$$M_{\mu\nu} \approx Re^{KR}\psi_\nu(\overrightarrow{r_0}) \tag{2.6}$$

where R is the radius of curvature of the tip (centered in r_0). With the equation 2.6 and the spherical wavefunctions of the tip, we can then rewrite the equation 2.5 as:

$$I \approx V\rho_t(E_F)e^{2KR}\sum_\nu |\Psi_\nu(r_0)|^2\delta(E_\nu - E_F) \tag{2.7}$$

where $\rho_t(E_F)$ is the density of states of the tip, $K = \sqrt{\frac{2m\Phi}{\hbar}}$ is the inverse decay length for the wave functions in vacuum, and Φ is the work function. Since $\rho(\overrightarrow{r_0}, E) = \sum_\nu |\Psi_\nu(r_0)|^2\delta(E_\nu - E_F)$ is the Local Density of States (LDOS) of the sample, we can see that in this case the tunneling current is proportional to the LDOS of the sample in the tip position.

However, the Tersoff-Hamman formalism is only valid for small bias voltages and tips with spherical form. In the general case, the STM images will depend on the density of states of the sample and of the tip. So, when analyzing the data, we need to take into account also the electronic states of the tip and its geometry.

2.3 X-Ray photoelectron Spectroscopy (XPS)

X-Ray photoelectron Spectroscopy (XPS) is another powerful tool in surface science [11]. This technique is used to study the elemental composition of the surface, but also the chemical and electronic states of the elements within a material, to detect unwanted materials like impurities or contamination and chemical shift in the elements due to charge transfer, covalent bonds, etc. XPS is based on the photoelectric effect. As shown in figure 2.3, when photons with a certain energy (in the X-ray range) irradiate the sample, they may excite electrons inside the sample. If the energy of the photon is larger than the binding energy of the electron core level, this electron can be ejected from the sample with a kinetic energy given by,

$$E_{Kinetic,sample} = h\nu - E_{Binding} - \Phi_{sample} \tag{2.8}$$

that depends on the initial binding energy of the core level, and therefore carries chemical information about the nature of the element (figure 2.4b).

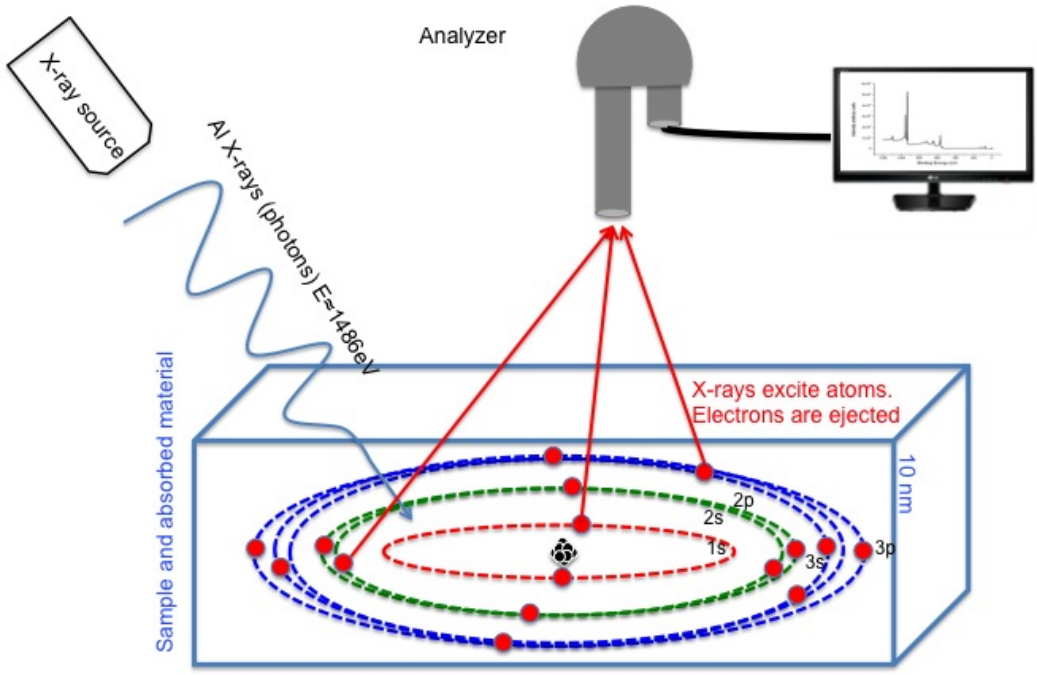

Figure 2.3: *XPS mechanism: the X-rays source emits photons with a fixed energy, $h\nu$. These photons irradiate the sample and excite some core electrons that are ejected out of the sample. An hemispherical electron energy analyzer acquires and measures the kinetic energy of these electrons.*

On the other hand, the hole created when the electron is ejected can be filled after a very short time by different relaxation processes. One of these mechanism is the Auger process: the inner hole is filled by an external electron of the atom, resulting in a release of energy, as shown in figure 2.4a. This energy can be released in the form of an emitted photon, but also by another electron ejected outside the sample. This new electron is called the Auger electron, and its energy, given by

$$E_{Kin}(KL_1L_{23}) = E_K - E_{L1} + E_{L23} \tag{2.9}$$

depends on the atom type (also on the chemical environment). As we can see, photoemission and Auger electron spectroscopy are based on different processes, but in both cases the kinetic energy of the electrons carry information about the chemical composition of the element. An important difference is that the kinetic energy of the Auger electron does not depend on the energy of the photon.

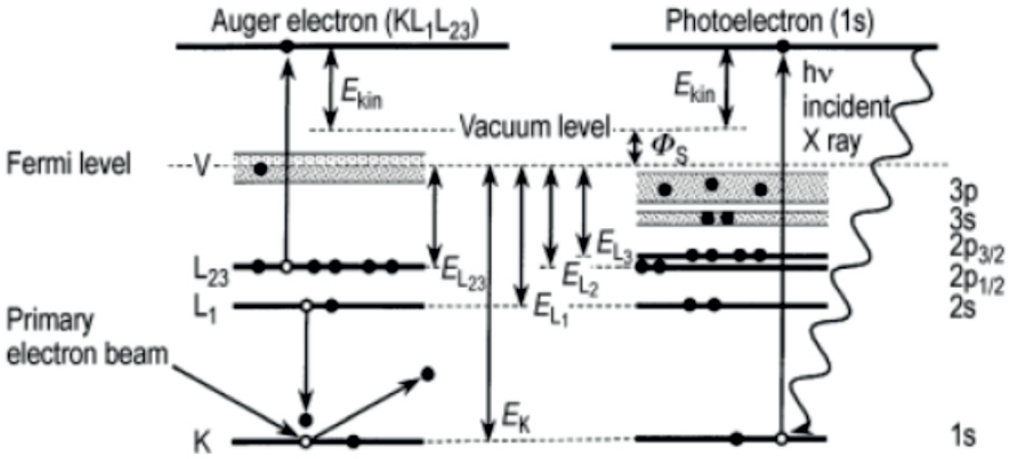

Figure 2.4: *Schematic diagram of the electron emission Auger process (left side) and photoelectron process (right side) in a solid. Electrons involved in the emission process are indicated by open circles (Figure taken from [12]).*

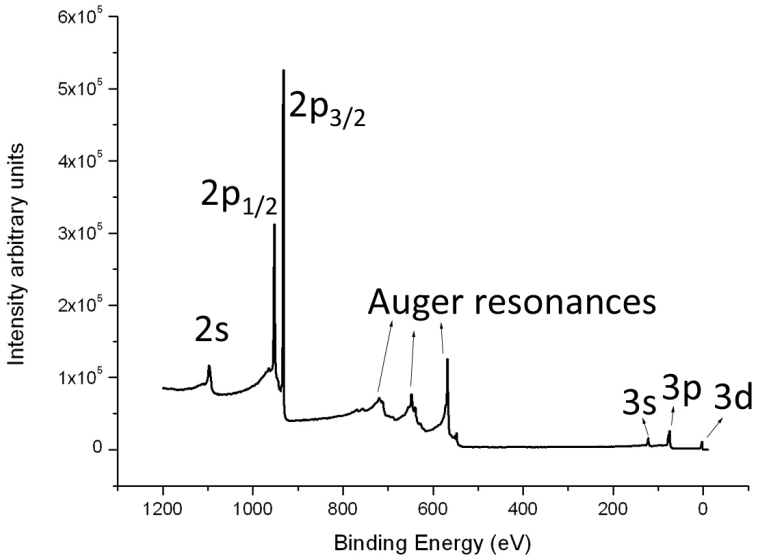

Figure 2.5: *Typical XPS spectra of clean copper(100), where the intensity of the photoelectrons is measured as a function of their binding energy, providing information about their origin and chemical state.*

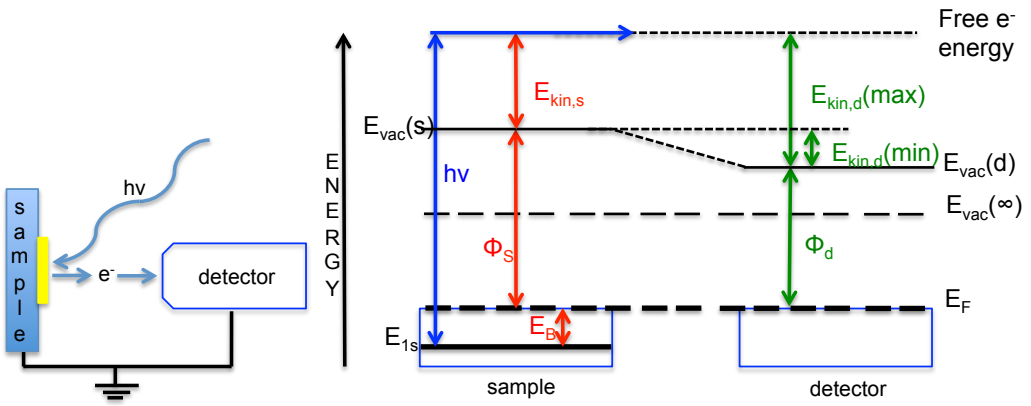

Figure 2.6: *a) Schematic drawing of the XPS technique in which the sample in electrical equilibrium with a detector. b) Schematic energy level for the XPS process.*

In an XPS experiment, the kinetic energy of the emited electrons is measured by an electron energy analyzer. Figure 2.5 shows a typical XPS spectra of clean Copper(100). This type of graphs represent the number of electrons detected by the analyzer versus their kinetic energy (or binding energy, see below). Two types of peaks can be seen in the spectra: the photoemission peaks, related to the photoionization of the different core levels, and the Auger peaks. In the following, we will consider only the photoemission peaks.

According to the photoelectric effect (equation 2.8 and figure 2.6), the kinetic energy of the emitted electron when leaving the sample is given by:

$$E_{Kinetic,sample} = h\nu - E_{Binding} - \Phi_{sample} \tag{2.10}$$

Usually, the work-function of the sample and the analyzer are different, and this causes that the kinetic energy of the sample measured by the analyzer is not equal to the kinetic energy of the electron when leaving the sample. However, due to the energy conservation (figure 2.6)

$$E_{Kinetic,sample} + \Phi_{sample} = E_{Kinetic,detector} + \Phi_{detector} \tag{2.11}$$

Then, when the electron reaches the detector:

$$E_{Kinetic,detector} + \Phi_{detector} = h\nu - E_{Binding} \tag{2.12}$$

and

$$E_{Binding} = h\nu - E_{Kinetic,detector} - \Phi_{detector} \tag{2.13}$$

where $h\nu$ is the energy of photon, $E_{Kinetic}$ is the kinetic energy measured by the analyzer and Φ is the work-function of the detector. Thus, the measurement of the kinetic energy of the photoelectron allows to estimate the binding energy, which is characteristic of each element.

XPS can provide also information about the work-function of the sample. The work-function is the minimun energy needed to remove an electron from a solid to a point immediately outside the solid surface (or the energy needed to move an electron from the Fermi level into the vacuum). According to the energy diagram in figure 2.6b, the minimum kinetic energy of the electrons that reach the detector (that is, those electrons that leave the sample with zero kinetic energy) is given by:

$$E_{SECO} = E_{Kinetic,detector(min)} = \phi_{sample} - \phi_{detector} \tag{2.14}$$

where (SECO) refers to the "secondary electron cut-off". On the other hand, according to equation 2.12, the maximum kinetic energy of the electrons that reach the detector is the energy of those electrons leaving the sample with $E_{binding} = 0$, that is, the electron at the Fermi level of the sample. In this case,

$$E_F = E_{Kinetic,detector(max)} = h\nu - \phi_{detector} \tag{2.15}$$

combining equations 2.14 and 2.15, the work-function of the sample can be written as:

$$\phi_{sample} = h\nu - (E_{SECO} - E_F) \tag{2.16}$$

where it can be observed that the sample work-function is independent of the detector and can be obtained by subtracting form the photon energy the difference in energy between the minimun and maximum kinetic energy measured by the analyzer. In order to measure the SECO of the sample, a negative bias voltage (typically -10 V) is applied to the sample to displace the spectrum and identify doubtlessly the electron cut-off related to sample electrons from those coming from the analyzer.

The chemical shift

XPS measurements can provide information not only about the elements present in the sample, but also about their electronic structure or chemical state. When an atom enters into a combination with another atom or groups

of atoms, an alteration happens in the valence electron density; this might be positive or negative according to whether charge is accepted or donated, causing a consequent alteration in the electrostatic potential affecting the core electrons. These changes in the binding energy are known as chemical shifts, and are typically on the order of electron volts. In an oversimplified picture, we can view the atom as a sphere of radius r with a valence charge q on its surface. The electrons within the sphere feel a potential q/r. If q increases, the potential increases, and hence the binding energy of those electrons inside the sphere also increases. These shifts can be compared with pure compounds of that element, thus enabling the identification of the different chemical state.

This simple analysis of the chemical shift is complicated by other effects (the so-called final state effects) related to how the other electrons respond to the hole being created in the photoemision process.

One effect that always occurs is the decrease of the total energy of the ion due to the relaxation of the remaining electrons towards the hole (the screening of the hole), which allows the photoelectron to go away with greater kinetic energy (i.e., a lower apparent binding energy). Contributions to the relaxation energy arise from both the atom containing the core hole and from its surrounding atoms. Thus, for example, for atoms in a molecule close to a metal surface, the screening is higher, and the measured binding energy lower, than for the same atoms in the same molecule far away from the surface.

A different effect, called spin-orbit splitting, is due to the coupling of the spin of the unpaired electron left behind in the orbital from where the photoelectron has been ejected, with the angular momentum of that orbital, giving two possible different energy final states (spin up or down). This happens for all levels except the s levels, which have no orbital angular momentum, and gives raise to double peaks instead of single peaks.

While a core-electron is being ejected, it can lose part of its kinetic energy to excite a valence electron into an empty orbital. This will shift the XPS peaks to apparently higher binding energy. Shake-up structure can provide chemical information because the valence levels are involved. However, these "shake-up satellites" are usually weak because the probability of their occurrence is rather low.

In this thesis will study the interaction between different molecules and a metal surface. The chemical shifts will help us to find out the chemical environment of the atoms involved, which will provide information about the interaction or bonding with the metal surface or with other molecules. In conclusion, XPS measurements will give us information about what happens on the surface.

2.4 Density Functional theory (DFT)

Although this thesis is mainly based on experimental work, we have heavily relied on theoretical calculations to understand and complement the results. The calculations have been made using the Density Functional Theory (DFT). DFT calculations provide good estimations for several physical properties of a metal-organic interface, like atomic structure, work-function, vibrational modes, chemisorption energies, and charge-transfer between molecule and surface. This section is devoted to briefly introduce the basics concepts of DFT.

Density Functional Theory starts from a theorem due to Hohenberg and Kohn [13], later generalized by Levy [14], stating that all ground state properties are functionals of the density. In particular, the ground state energy of an electron system in an external potential, i.e., the potential due to a set of nuclei in a given arrangement, can be found by minimizing the functional with respect to variations in the density. This leads to a set of equations, to be solved self-consistently, involving a local potential $\mu_{XC}(r)$ which describes exchange and correlation effects [15].

$$\{\frac{-\hbar^2}{2m}\Delta + V_S(r) + \mu_{xc,\sigma}(r)\}\Phi_{k,\sigma}(r) = \epsilon_i \Phi_{k,\sigma}(r), \tag{2.17}$$

$$\rho_\sigma(r) = \sum_k^{occ} |\Phi_{k,\sigma}(r)|^2, \rho = \rho_\sigma + \rho_{-\sigma'} \tag{2.18}$$

where V_S is the electrostatic potential due to the nuclei and the electron charge distribution, and σ is a spin label. Since no exact functionals for exchange and correlation are known (except for the free electron gas) some approximations have to be included in order to calculate physical quantities. Basically, two approximations are used in DFT: **(i)** Local-density approximation (LDA), that assumes that exchange-correlation depends on the electron density locally, and **(ii)** Generalized gradient approximation (GGA), that takes density variations into account. The total energy can be written as:

$$E_t = \sum_k^{occ} \epsilon_k + \sum_\sigma \int \rho_\sigma(\epsilon_{xc} - \mu_{xc,\sigma} - \frac{V_e}{2}) d^3r + \sum_{\alpha,\beta} \frac{z_\alpha z_\beta}{|R_\alpha - R_\beta|} \tag{2.19}$$

where V_e is the electrostatic potential due to the electron charge distribution and ϵ_{xc} is a universal potential fundamentally related to μ_{xc} by $\frac{d(\rho\epsilon_{xc})}{d\rho} = \mu_{xc}$.

Most quantum chemical methods use a linear variational expansion for the single particle orbitals

$$\Phi_{k,\sigma}(r) \approx \sum c_{j,k,\sigma}\phi_j(r) \tag{2.20}$$

This converts the differential eigenvalue problem (2.17) into a generalized matrix eigenvalue equation

$$\sum_j h_{i,j,\sigma}c_{j,k,\sigma} = \epsilon_k \sum_j s_{i,j}c_{j,k,\sigma} \tag{2.21}$$

where

$$h_{i,j,\sigma} = \int \phi_i(r)\{\frac{-\hbar^2}{2m}\Delta + V_s(r) + \mu_{xc,\sigma}[\rho_\sigma(r), \rho_{-\sigma}(r)]\}\phi_j(r)d^3r \tag{2.22}$$

and

$$S_{i,j} = \int \phi_i(r)\phi_j(r)d^3r \tag{2.23}$$

DFT methods are typically characterized by the type of orbital expansion functions ϕ_i used, e.g., Gaussian linear combination of atomic orbitals (LCAO), slater type orbital LCAO, numerical LCAO, multiple scaterring, linearized augmented plane waves, etc.

In this thesis, two different methods have been used.

The results presented in chapter 5 for the DCNQI/Cu(100) and in chapter 4 for the mixed TCNQ-TTF/Ag(111) layers were obtained by the group of Fernando Marín in the Universidad Autónoma de Madrid using the VASP package [16]. In VASP, central quantities, like the one-electron orbitals, the electronic charge density, and the local potential are expressed in plane wave basis sets. DFT calculations using the Perder-Burke-Enzerhof (PBE) exchange-correlation functional [17] were performed with the projector augmented wave (PAW) method [18]. The dipole correction and the Grimme's van der Waals correction [19] were included in the DFT total energies. In all cases, the substrate was modeled by placing a four-layer slab of atoms with the unit cell determined by experiments, separated by $\sim$ 25 Å of vacuum in the surface normal direction. A cutoff energy up to 600 eV was chosen for the plane wave expansion. The geometries were optimized using a conjugated-gradient algorithm until the forces on each ion are smaller than 0.02 eV Å^{-1}. A 3×3×1 Monkhorst-Pack grid for k-point smapling was taken for the geometry optimizations [20]. The total energies for the optimized structures were further refined by performing single-point calculations using

finer k-point grids, 4×4×2 and 5×5×2 k-points for the trans- and the cis-self-assembled networks on Cu(100), respectively.

For the rest of the systems in this thesis, DFT calculations were carried out by using the Dmol3 package integrated in the Material Studio program of Accelrys Inc. [21, 22]. This package employs density functional Hamiltonian for molecules and three-dimensional periodic solid and approximates true wavefunctions through an expansion of crystalline orbitals as a linear combination of atomic orbitals. Generalized gradient approximation [19] and PBE, exchange correlation functional, [17] were used throughout. All electrons are included in the calculations. In this case the TS scheme [23] for van der Waals correction was used. The sampling k-point set was generated automatically, depending on the unit cell size, in the approach of Monkhorst-Pack scheme [20]. Concerning the accuracy and computational cost, we employ the DNP basis set (double numerical valence functions plus a polarization p-function on all hydrogen atoms). The local basis cut-off radius was set to $R_c = 0,44nm$.

Population Analysis.

Since we are dealing with donor and acceptor systems and charge transfer complexes, one of the results we are more interested in is charge transfer between molecules, and between molecules and the metal substrate. To get an idea of how the charge is distributed in a system, a population analysis must be carried out. However, once the structure has been optimized and the electronic density calculated, there are different methods to partition the charge. Some of them are based on electronic orbitals (Mulliken, Coulson, ...) and others are based only on the charge density (Bader, Hirshfeld, ...). In this thesis, we have used the Mulliken population analysis. In this method, half of the overlap population between orbitals is assigned to each contributing orbital, giving the total population of each atomic orbital. Summing over all the atomic orbitals on a specific atoms gives us the gross atomic population. The main problem with the Mulliken analysis is that it is highly basis set dependent. However, we have compared the results obtained from Mulliken analysis and from a Hirshfeld analysis, and although the magnitude of the Hirshfeld charges is in general smaller than for Mulliken, the total charge on the molecule is approximately the same in both case (Table 2.1).

In any case, however, it is important to have in mind that the results given in this thesis are just approximate, and probably make more sense when compared with another (in all cases, the same basis set was used).

Table 2.1: *Mulliken and Hirshfeld values for TCNE and TCNQ molecules when adsorbed on Ag(111).*

	TCNE			TCNQ		
	Dmol3			Dmol3		
	Mulliken	Hirsfeld		Mulliken	Hirsfeld	
N	-0.30	-0.23	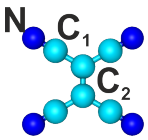	-0.31	-0.24	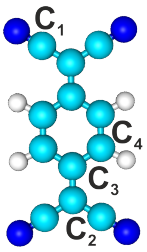
C1	+0.16	+0.04		+0.16	+0.05	
C2	-0.16	-0.05		-0.23	-0.06	
C3				+0.05	-0.02	
C4				-0.12	-0.06	
H				+0.12	+0.04	
Q	-0.89	-086		-0.99	-1.02	

Van der Waals corrections.

One of the most significant problems with DFT is the inability of standard functionals to describe long-range electron correlations (also known as dispersion forces or van der Waals forces). Dispersion forces originate from the response of electrons in one region to instantaneous charge density fluctuations in another. The main term of such interaction is dipole-induced dipole, which gives rise to the well known $-1/r_6$ dependence with the interatomic distance. Standard functionals do not describe these forces because instantaneous density fluctuations are not considered, and they consider only local properties to calculate the exchange correlation-energy. Many different DFT -based methods have been developed to try to fix this problem. The most simple approach is to add an additional energy term which accounts for the missing long range attraction:

$$E_{disp} = -\sum_{A,B} \frac{C_6^{AB}}{R_{AB}^6}, \tag{2.24}$$

where the dispersion coefficients C_6^{AB} depend on the elemental pairs A and B. Although this correction scheme looks very simple, it has also several short comings, one of them being that it is not clear how to obtain the C_6 coefficients. One of the most used methods was given by Grimme [19], who calculated the dispersion coefficients from a formula that couples ionization potentials and static polarizabilities of isolated atoms. A problem with this solution is that the coefficients do not depend on the oxidation state or chemical environment of the element, and the error introduced by this approximation can be large. So, thus, other schemes have been developed to

introduce this dependence. In particular, in the method of Tkachencko and Scheffler [23] the dispersion coefficient of an atom in a molecule depends on the effective volume of the atom (when the atoms is "squeezed", its electron cloud becomes less polarizable, leading to a decrease of the C_6 coefficient). After calculating the electronic structure of the system of interest, the electron density of a molecules is divided between the individual atoms, and for each atom, its corresponding density is compared to the density of a free atom. This factor is then used to scale the C_6 coefficient.

2.5 Experimental setup

The experiments have been carried out with the system shown in figure 2.7 in the surface science laboratory (LASUAM) of the Universidad Autónoma de Madrid. The system is called TIREMISU (TIme REsolved MIcroscopy of SUrfaces). The system works in Utra high vacuum (UHV) conditions and it is divided in three chambers: preparation chamber, STM chamber and XPS chamber, that I describe in more detail in the next sections.

2.5.1 Preparation chamber

The preparation chamber contains:

1. A load-lock.
2. A manipulator.
3. A mass spectrometer.
4. A LEED optics.
5. A sputter gun.
6. A molecule evaporator.

The load-lock is a small chamber, like a small cube, with a transfer bar (pumped by a rotatory pump and a turbo pump), used for introducing samples from outside to the preparation chamber without breaking the vacuum in the main system. The preparation chamber is used for cleaning and preparing the sample. The cleaning process consists of cycles of sputtering and annealing. The chamber has a sputter gun, so the sample can be bombarded with Ar^+ ions, and the sample can be heated up with W filaments located on the head of the manipulator. Since this head is electrically isolated from

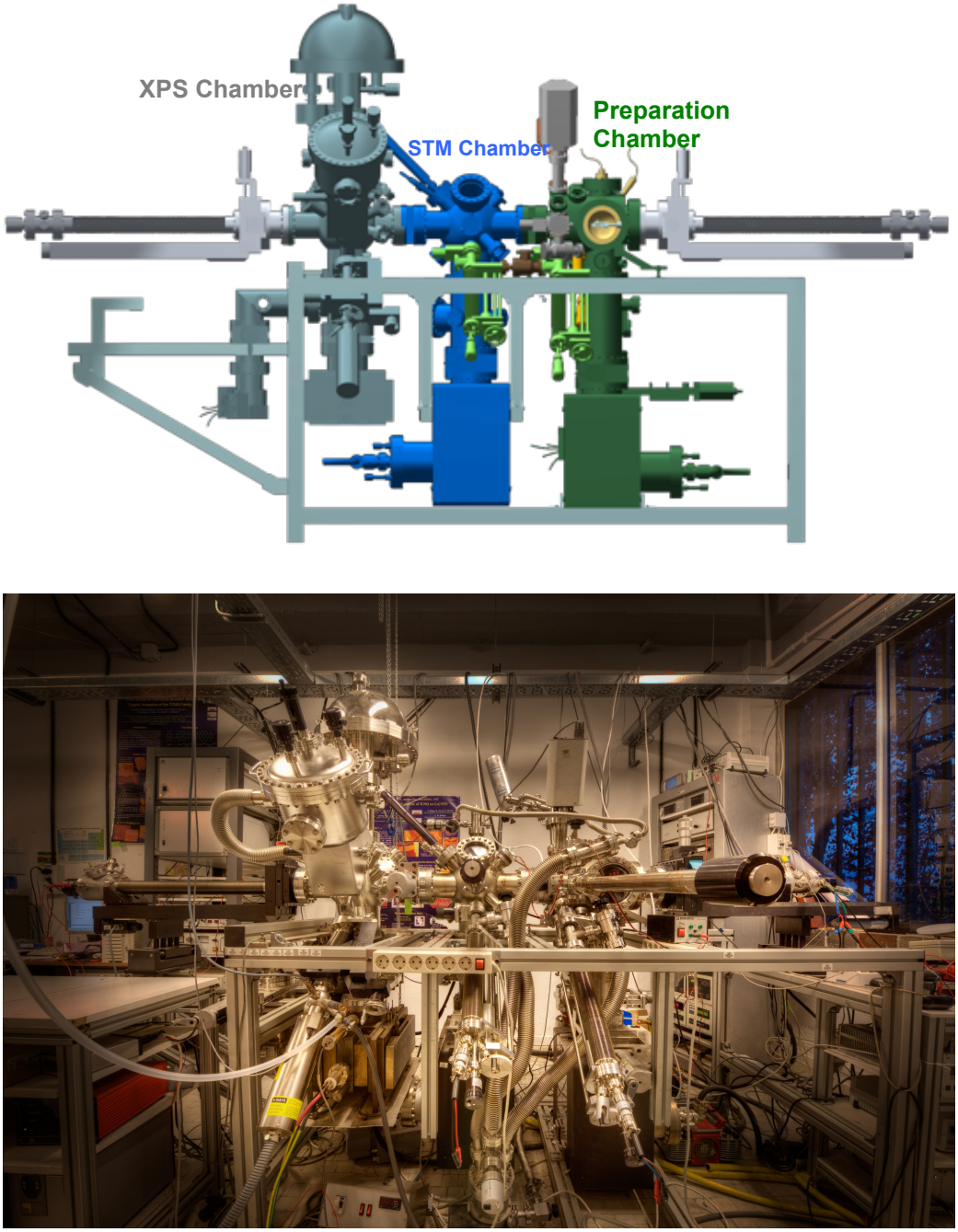

Figure 2.7: *Overview of the TIREMISU system:* ***(a)*** *Preparation chamber (green color), STM Chamber (blue color) and XPS Chamber (gray color).* ***(b)*** *Photo courtesy of José Luis F. Cuñado ©.*

ground, annealing by electron bombardment is also possible. To control the annealing, two thermocouples are located on the head close to the sample. The manipulator is also used as a transfer bar to move samples from the preparation chamber to the STM chamber.

For deposition in this chamber we have one molecule evaporator (green light color in figure 2.7), that can be isolated by a valve from the preparation chamber, so we can degas the molecules without contaminating the chamber, or change the molecule powder without braking the vacuum in the preparation chamber. Its vacuum system is the same of the load-lock system. In the preparation chamber the vacuum elements are a rotatory pump, a turbo pump, and an ion pump.

2.5.2 STM chamber

This part of the system, (blue chamber figure 2.7) has different components:

1. A transfer bar.
2. A variable temperature scanning tunneling microscope.
3. A molecule evaporator.
4. A parking.

In this chamber, the vacuum element is an ion pump. As mentioned before, the sample is introduced in this chamber with the manipulator of the preparation chamber, as shown in figure 2.8. With the transfer bar, the sample can be mounted facing down in the STM. This microscope is a commercial Aarhus STM from Specs company.

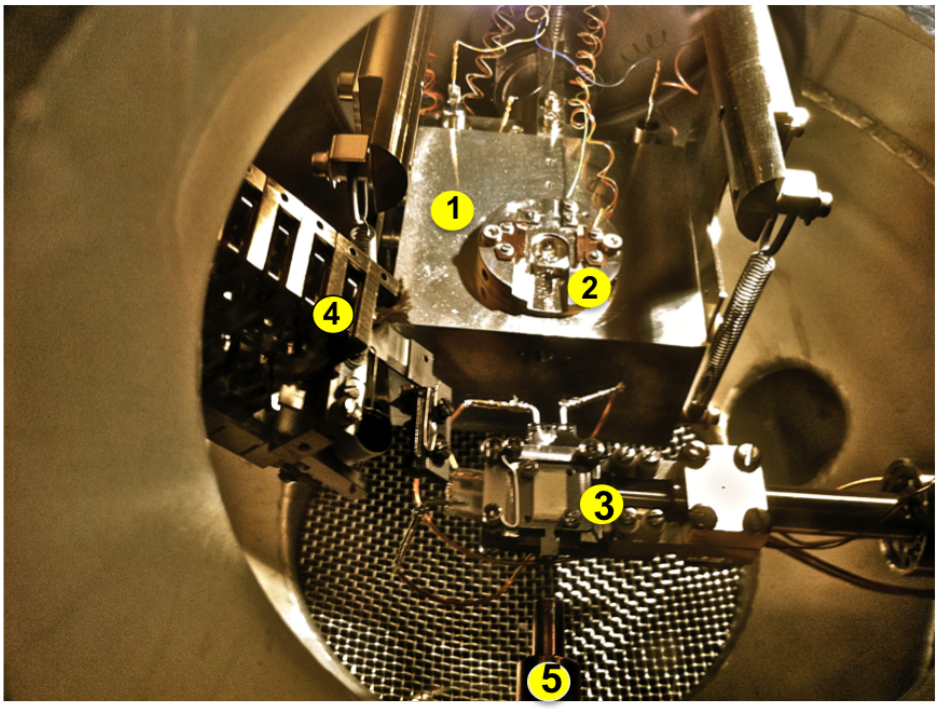

Figure 2.8: *Photograph of the interior of the STM chamber. 1. Aluminium block of the STM; 2. the place where the sample holder is mounted for STM measurements: it is normally held down on the STM top by two copper clamp;, 3. Head of the manipulator of the preparation chamber; 4. Parking; and 5. Transfer bar.*

In this STM the tip is connected to ground and the sample is connected to the bias voltage. The tip is usually made of tungsten, and it is mounted on a piezolectric system. Figure 2.9 shows a schematics of the piezo scanner. The sample is fixed on the STM by two copper clamps.

The movement of the tip consists of two modes: **approach**, and **scan**. In the approach mode the tip goes to the sample until reaching the tunneling regime. This movement is realized by a linear motor, called the inchworm, consisting of a piezoelectric tube fitted around a ceramic rod. The inchworm is divided in three sections, with the corresponding electrodes attached. The middle section controls the elongation of the tube while the upper and lower sections clamp or unclamp the piezo tube to the rod. By applying a sequence of voltages to the electrodes, the rod can be moved up or down. All the approach sequence is done by the electronics. To prevent tip collisions the motor stops at a preset value of the tunnel current.

For the scan mode the tip is mounted on a piezoelectric 4-fold segmented scanner tube connected to the ceramic rod. This piezo tube has a single

common electrode on the inside and four electrodes on its outside, which control the tip movement in the X-Y directions. This is achieved by applying asymmetric voltages, to contract and expand the piezo elements, to opposite electrodes on the outer section of the scanner tube. The Z direction is controlled by a feedback system which keeps the tip-sample distance constant by applying a bias voltage to the inner electrode, causing an expansion or contraction of the whole tube scanner along the Z direction.

Important advantages of this compact design are a fast approach between tip and sample, a very high mechanical stability, and a very fast scan speed. The tip is very stable and usually it is not necessary to replace it for a long time. The tip is always at room temperature while the bulk of the microscope can be cooled down with liquid nitrogen. The measurement temperature range used in this thesis goes from 100 K to room temperature.

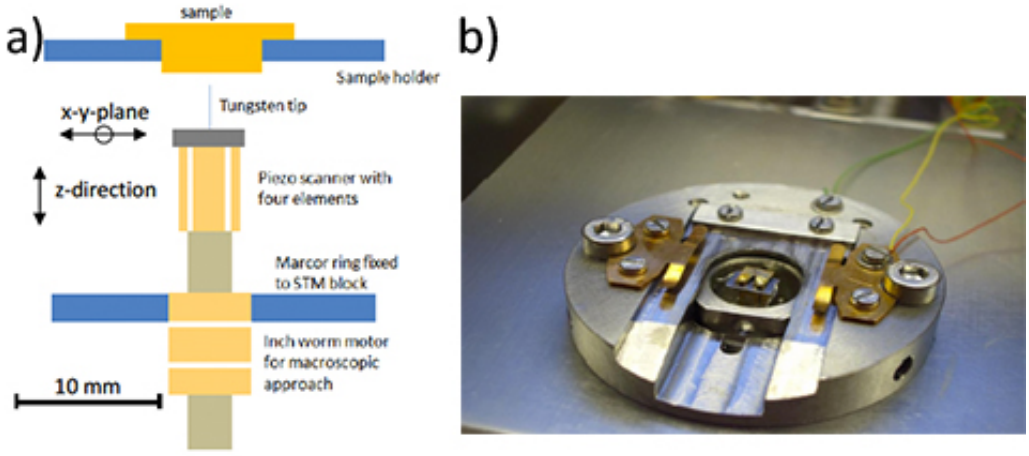

Figure 2.9: *a) Scheme of the Aarhus STM. b) The head of the STM. The tip is in the center of the head pointing up. The sample is mounted facing down held by two copper clamps.*

Since the STM aluminum block has an optical access, the molecules can be deposited directly onto the sample when it is placed on the STM, using a molecule evaporator directed to the microscope (green light color in figure 2.7), which allows to deposit the molecules with the substrate held at different temperatures. Hence, different experiments can be studied depositing the molecules with the sample held at low temperature and then continue

measuring at any temperature between 100 K and room temperature. The vacuum system for the molecule evaporator is the same than for the other evaporator in the preparation chamber. The last component is the parking, in which six samples can be stored and also annealed.

2.5.3 XPS chamber

The XPS chamber was incorporated in the system during my thesis. The components of this chamber are:

1. A variable temperature manipulator.
2. The X-ray source.
3. A monochromator.
4. An hemispherical electron energy analyzer.

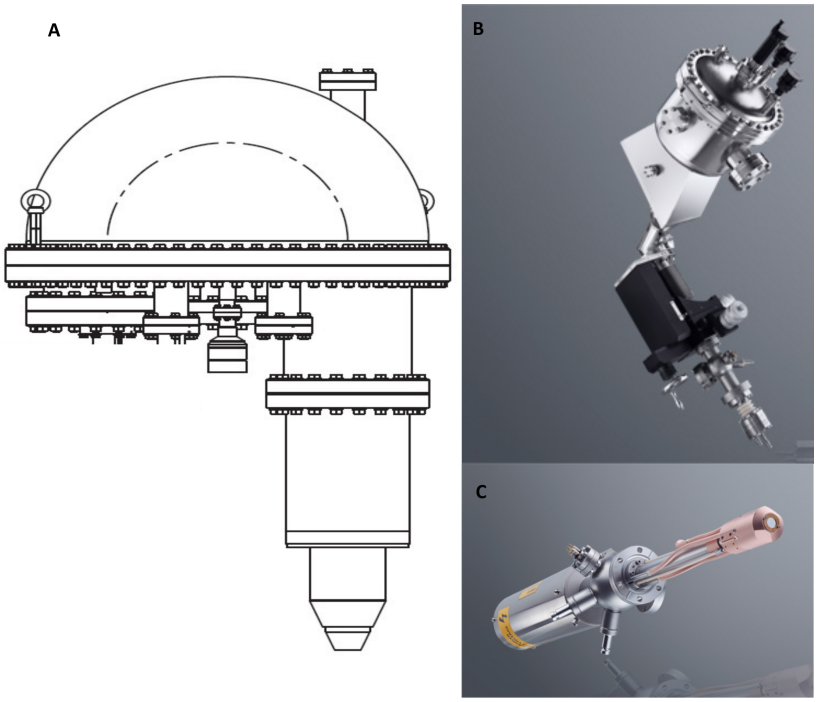

Figure 2.10: *a) The hemispherical energy analyzer commercial from SPECS (PHOIBOS 150 with 5 channeltron). b) Ellipsoidal quartz cystal monochromator from SPECS (FOCUS 500). c) X-ray source, also from SPECS (XR 50 M); this source has two target: Al Kα and Ag Lα.*

The sample transfer from the STM chamber to this chamber can be done with the manipulator. This manipulator is similar to the existing in the preparation chamber, but in this one the sample can be cooled down to liquid nitrogen temperature.

This chamber has a commercial X-ray source (Fig. 2.10) from SPECS, XR 50 M, that has two anodes, which implies that two different photon energies can be selected; one of the targets is Aluminum, which emits $K\alpha$ radiation with a photon energy of 1486.6 eV, and the second anode is Ag, which emits $L\alpha$ radiation with a photon energy of 2984 eV. To generate the X-ray beam, the anode (target) is bombarded by electrons coming from a filament. Due to the high voltage difference (15 KV, high voltage) between the filament and the anode, the electrons are accelerated towards the anode. The atoms of the anode are excited so an ionization process of electron core levels occurs and the anode emits x-ray radiation. Due to these collisions the anode can overheat, so it is necessary to cool it down with water to avoid damages in the anode material.

The radiation from the X-ray source goes to the ellipsoidal quartz single crystal monochromator where it is reflected and focused to the sample. This monochromator is also commercial from SPECS, model FOCUS 500, and reduces the line width of the x-ray source. The monochromator works according to Bragg's Law of X-ray diffraction:

$$n\lambda = 2d\sin\theta \tag{2.25}$$

The monochromator can reduce the line width of the x-ray source. Due to the small source size the monochromator resolution is limited by the rocking curve width of the quartz crystals to 160 mV. In our case, the reference sample was $3d_{5/2}$ of silver sample, and the full width at half maximum intensity is 0.8 eV.

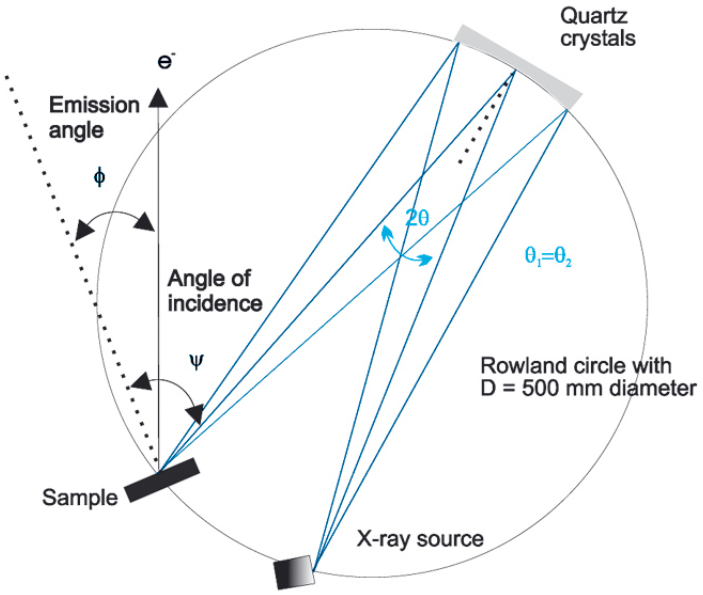

Figure 2.11: *Path of the X-ray radiation, from the source, to the sample, through the monochromator.*

When the radiation hits the sample, the electrons ejected outside the sample are collected by an hemispherical electron energy analyzer, PHOIBOS 150, also commercial from SPECS. The first part of this detector is a lens system, the lens tubes, that defines the analysis area and angular acceptance by imaging the emitted particles onto the entrance slit of the analyzer. In addition, the electrons are retarded in the lens for subsequent energy analysis. The second part is the energy analyzer, which consists of two hemispherical spheres (inner and outer concentric hemispheres) that act as an energy filter. The electrons that leave the analyzer enter in the detector which can be of different types: channeltron, CCD detector, delay-line detector and spin detector. In our case, it consists of 5 channeltrons.

In summary, this unique TIREMISU system is a very powerful tool, that allows to inspect the same sample with atomic resolution by STM and, very important to provide electronic information by XPS of exactly the same sample. So, it is possible to do a very complete study about what is happening to the molecules absorbed on a metal substrate, both at low (100 K) and room temperature. For example, if the system has different structure at low

temperature and room temperature, it is possible to study these two different situations in both the STM and XPS chambers. Usually, the measurements were carried out first with STM, then with XPS, and after that again with STM to check if the radiation has somehow changed the molecule. In some cases, radiation damage can be prevented by carrying out the XPS measurements at low temperature.

3

Donor and acceptor molecules on solid surfaces

In this chapter we will discuss the adsorption and assembly of some donors and acceptors molecules on solid surfaces. We will report the properties of the individual components: two electron acceptor molecules (TCNE, TCNQ) and one electron donor molecule (TTF), when absorbed separately on a Ag(111) substrate. In the next chapter, we will study the self-assembly of combined donor-acceptors systems on Ag(111).

3.1 Introduction

In the last decades organic chemistry has had a huge importance in the development of new organic electronic devices: organic-light emitting diodes (OLEDs), photovoltaic solar cells and organic field effect transistors (FETs) [24–27]. Most of these systems are composed of donor and/or acceptor molecules deposited on solid substrates, which has prompted the study of the growth of organic thin films on solid surfaces. Some of the reported systems have been, for example, in the case of acceptor molecules, fullerenes (C60, C70, PCBM) [28], TCNQ [29, 30] and his derivatives, like F4-TCNQ [31], TCPQ [32], and in the case of donor molecules, pentacene [33], TTF and his derivates [34–36], etc.

Figure 3.1 shows the electronic affinity and the ionization potential of the different molecules used in this chapter, and the work-functions of some representative substrates.

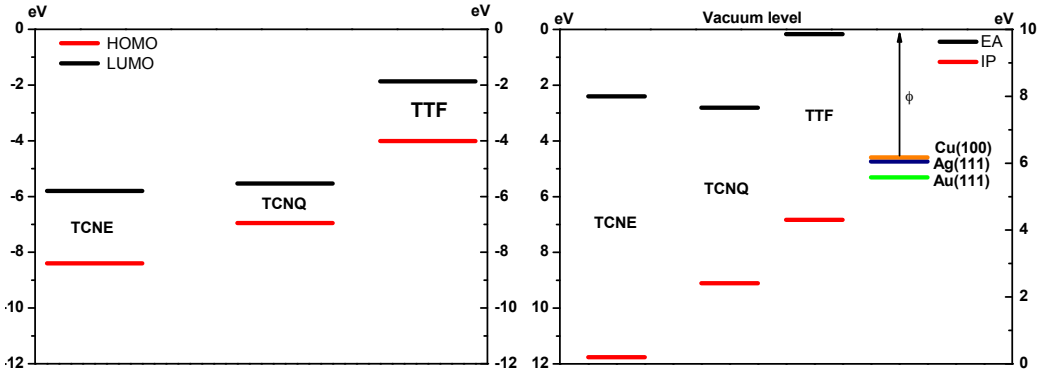

Figure 3.1: *a) Calculated HOMO and LOMO levels for TCNE, TCNQ, and TTF. b) Their electron affinities and ionization potentials: TCNQ ($E_A = 2.81eV$, $I_p = 9.11eV$) [37–40], TCNE ($E_A = 2.4eV$, $I_p = 11.76eV$) [41–44], and TTF ($E_A = 0.17eV$, $I_p = 6.83eV$) [45–47]. The work-functions of some representative metals are also plotted: $\phi Au_{111} = 5.31eV$, $\phi Cu_{100} = 4.59eV$, $\phi Ag_{111} = 4.74eV$ [48–51].*

3.2 Description of the TCNE molecule

Tetracyanoethylene (TCNE, C_6N_4), more correctly ethenetetracarbonitrile, is a clear colored organic compound first synthesized in 1957 at E. I. du Pont de Nemours and Co. by the copper-catalyzed thermolysis of dibromomalonitrile [52]. This molecule belongs to the cyanocarbons group, and it is one of the most versatile organic compounds, used in many different reactions [53–56]. It is a strong electron acceptor with a large electron affinity (the values reported in the literature encompass a broad uncertainty ranging, from 1.7 eV to 3.17 eV [41–43]) and an ionization potential of $\sim$ 11.76 eV [44].

This molecule, planar and symmetric, can be viewed as an ethylene molecule with the four hydrogen atom replaced with cyano groups (Figure 3.2a). These cyano groups have low energy π^* orbitals, and the presence of four such groups, with their π systems linked (conjugated) to the central C=C double bond, gives rise to an excellent acceptor. Figure 3.2b shows the calculated electrostatic potential projected onto a charge density isosurface; this electrostatic potential is color coded, going from red (more negative) to blue (more positive). This reveals that there is a negative potential around the nitrogen atoms, and a positive one close to the central C=C molecule. Figures 3.2c and 3.2d show the frontier molecular orbitals in gas phase, Highest Occupied Molecular Orbital (HOMO) and Lowest Unoccupied Molecular

Orbital (LUMO) respectively.

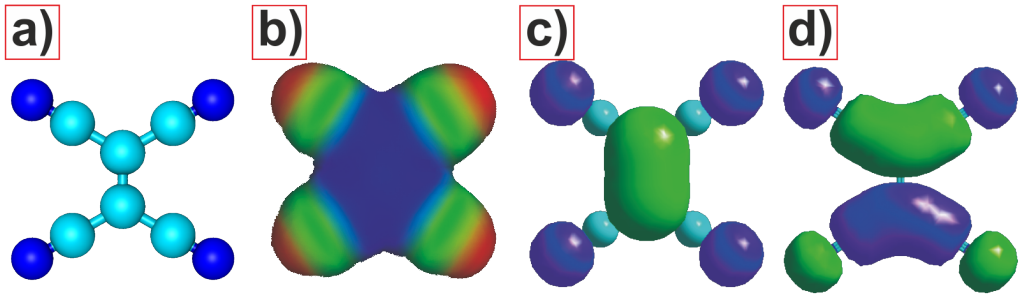

Figure 3.2: *a) Chemical structure of TCNE; dark blue spheres are nitrogen atoms, light blue spheres are carbon atoms, b) the electrostatic potential projected onto a charge density isosurface (blue and red color means positive and negative potential, respectively). Frontier molecular orbital of TCNE in gas-phase c) HOMO, and d) LUMO.*

On the other hand, some of the compounds $M(TCNE)_x$, where M is a paramagnetic transition-metal ion, form an important group of ferromagnets with many potential applications, since some of them (in particular V(TCNE)) have a relatively high curie temperature of up to 400 K. Thus, TCNE can play an important role in molecule-based room-temperature magnets (molecular magnets) and spin-injections devices [57, 58].

The adsorption of TCNE on noble-metal surfaces has been extensively investigated: for example on copper (100) [59], (111) [60], silver(100) [61, 62] and gold(111) [63], showing different molecule-molecule and molecule-substrate interactions. On the other hand, some examples of studied thin film organic magnets include V(TCNE) on Ag(100) [64], on nickel [65], glass, and NaCl [66], Co(TCNE) on gold [67, 68], Ni(TCNE) on gold [69], etc

Experimental

These molecules are very volatile; they were evaporated at room temperature from a glass crucible refrigerated by cooling water. During sublimation the sample was placed in the STM, which allows both deposition on the metallic substrates and STM imaging to be carried out in the temperature range of 100 K to 300 K.

3.2.1 TCNE on Au(111)

One of the main goals of our work is to build donor-acceptor charge transfer complexes on metal surface. For this reason we need a substrate where the interaction molecule-substrate is rather weak. Previous studies have shown that TCNE has a strong chemical interaction with copper [63], so we started with a less reactive substrate.

In the first experiments, we have used a Au(111) substrate, as shown in figure 3.3. When the molecule was deposited at room temperature, the sample surface looks clean, even if the STM images are acquired at 180 K, implying that TCNE molecules do not adsorb on Au(111) at room temperature. Figure 3.3a, Figure 3.3b and Figure 3.3c show representative STM images recorded at 173 K after depositing 0.7 ML of TCNE on Au(111) at 173 K. The molecules form well-ordered islands. The lengths of the unit cell vectors are $b_1 = 5.8(\pm 0.8)$ Å, $b_2 = 5.8(\pm 0.8)$ Å, and $\gamma = 110^0$, where γ is the angle formed by $\boldsymbol{b_1}$ and $\boldsymbol{b_2}$. The herringbone reconstruction of Au(111) is visible through the layer of molecules, suggesting that the Au-TCNE interaction is rather weak.

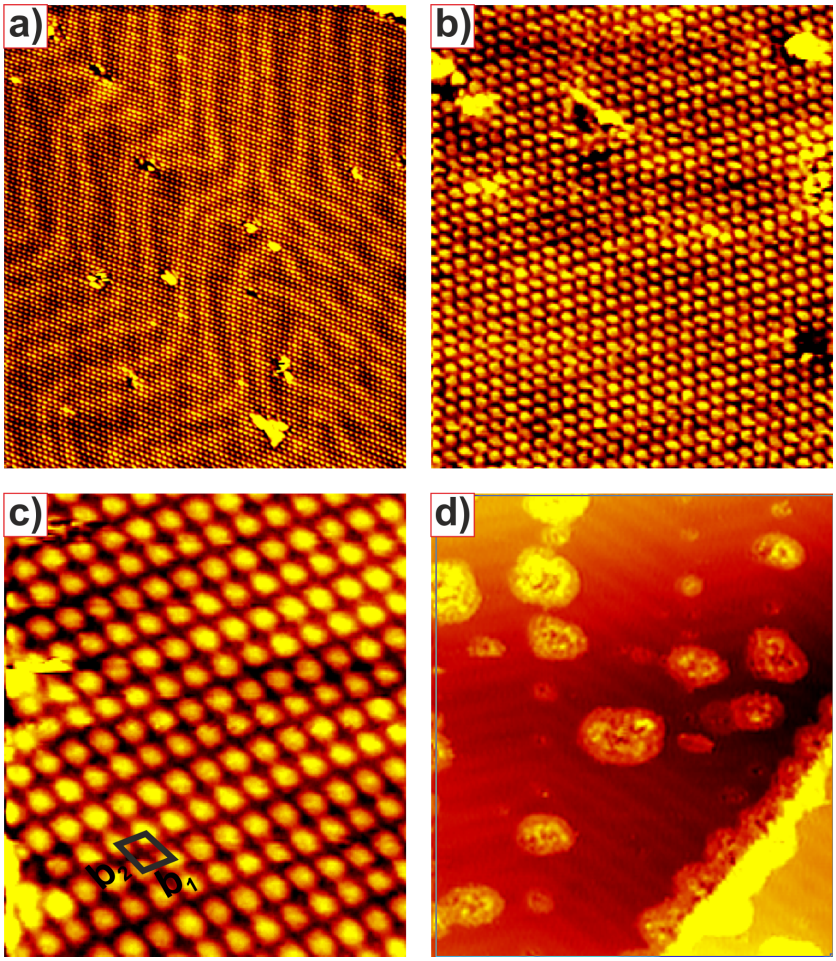

Figure 3.3: *a,b,c) STM image of 0.7ML of TCNE on Au(111); the molecules were sublimated at 173 K and the images were acquired also at 173 K. The reconstructed Au(111) surface with his characteristic herringbone pattern is still visible under the TCNE layer. d) STM image (taken at 175 K) after annealing the sample at RT: the ordered islands disappear. The image shows the clean gold surface with some remaining clusters, probably due to the desorption of TCNE. a) 489 Å × 564 Å; -0.10 nA, -1.8 V. b) 147 Å × 169 Å; 0.20 nA, 0.60 V. c) 68 Å × 79 Å; -0.16 nA, -2,43 V. d) 489 Å × 564 Å; -0.22 nA, -1.7 V.*

After annealing at room temperature the molecular self-assembled islands disappear, as shown in figure 3.3d (the STM image was taken at 175 K), although some irregular clusters remain on the surface. In addition, XPS measurements show that the nitrogen peak has disappeared completely. We can conclude that the molecule was desorbed and/or decomposed from the gold surface after annealing to room temperature, so this substrate does not

seem appropriate for building donor-acceptor networks with the TCNE as the acceptor molecule. We can observe the different behavior of the same molecule on gold (weak interaction) and on copper (strong interaction), which shows the important role of the substrate in the molecular adsorption process.

3.2.2 TCNE on Ag(111)

In this section, we will study the adsorption of TCNE on Ag(111), a substrate where, in principle, an intermediate behavior, when compared to copper and gold, should be expected.

3.2.2.1 Adsorption of TCNE on Ag(111) at low temperature

In the first series of experiments TCNE was deposited on the surface of a Ag(111) single crystal at 130 K. The STM measurements were also taken at the same temperature. Figure 3.4a shows the surface after depositing 0.3 ML. Well-ordered 2D islands are formed. These islands are not connected to the step edges, so it seems that they have started to grow on the terraces. In figure 3.4b it can be observed that these ordered islands can be found in two different orientations, rotated 10^0 with respect to each other. The appearance of the island changes with the bias voltages. The self-assembly seems to have a honeycomb shape with symmetry P6m [70] when topographic STM images were acquired with negative voltage, as shown in figure 3.4c. However, if the bias voltage changes to positive values, the ordered island looks like a Kagome lattice, belonging to the trihexagonal tiling with symmetry P3m1 [70], as shown in the figure 3.4d. Figure 3.5a shows a zoom inside one of the islands, where each protrusion corresponds to one TCNE molecule. The green square is the resulting unit cell with sides $b_1 = 18.9(\pm 1.5)$ Å, $b_2 = 18.9(\pm 1.6)$ Å, and $\gamma = 120^0$. For this unit cell, the matrix describing the epitaxial relationship with the substrate can be written as $\begin{pmatrix} b_1 \\ b_2 \end{pmatrix} = \begin{pmatrix} 7 & 5 \\ -5 & 2 \end{pmatrix} \begin{pmatrix} a_1 \\ a_2 \end{pmatrix}$. The unit cell directions forms $\pm 5^0$ with the secondary high symmetry axis, in agreement with the experimental results. Thus, the arrangement of the molecules leads to a chiral structure, as shown in the figure 3.4b.

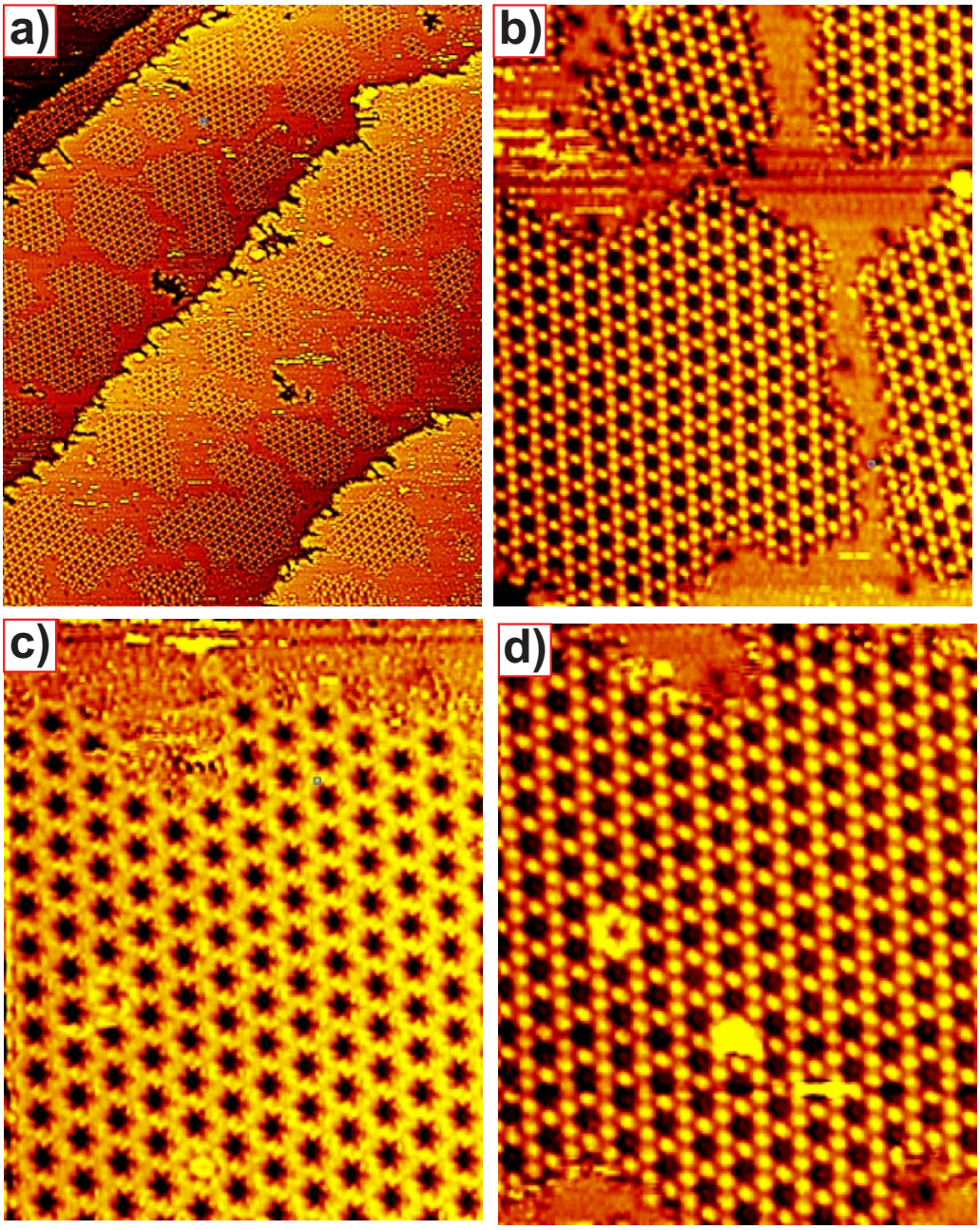

Figure 3.4: *a) Large scale STM image taken after depositing TCNE on Ag(111) at 130 K (all the images were acquired at 130 K). b) STM image showing the two possible orientations of the islands. c,d) STM images of the same TCNE island taken with negative and positive bias voltage, respectively. a) 978 Å × 1227 Å; 0.3 nA, 1.7 V. b) 293 Å × 368 Å; 0.26 nA, 1.5 V. c) 196 Å × 245 Å; -0.27 nA -1.3 V. d) 196 Å × 245 Å; 0.27 nA, 1.5 V.*

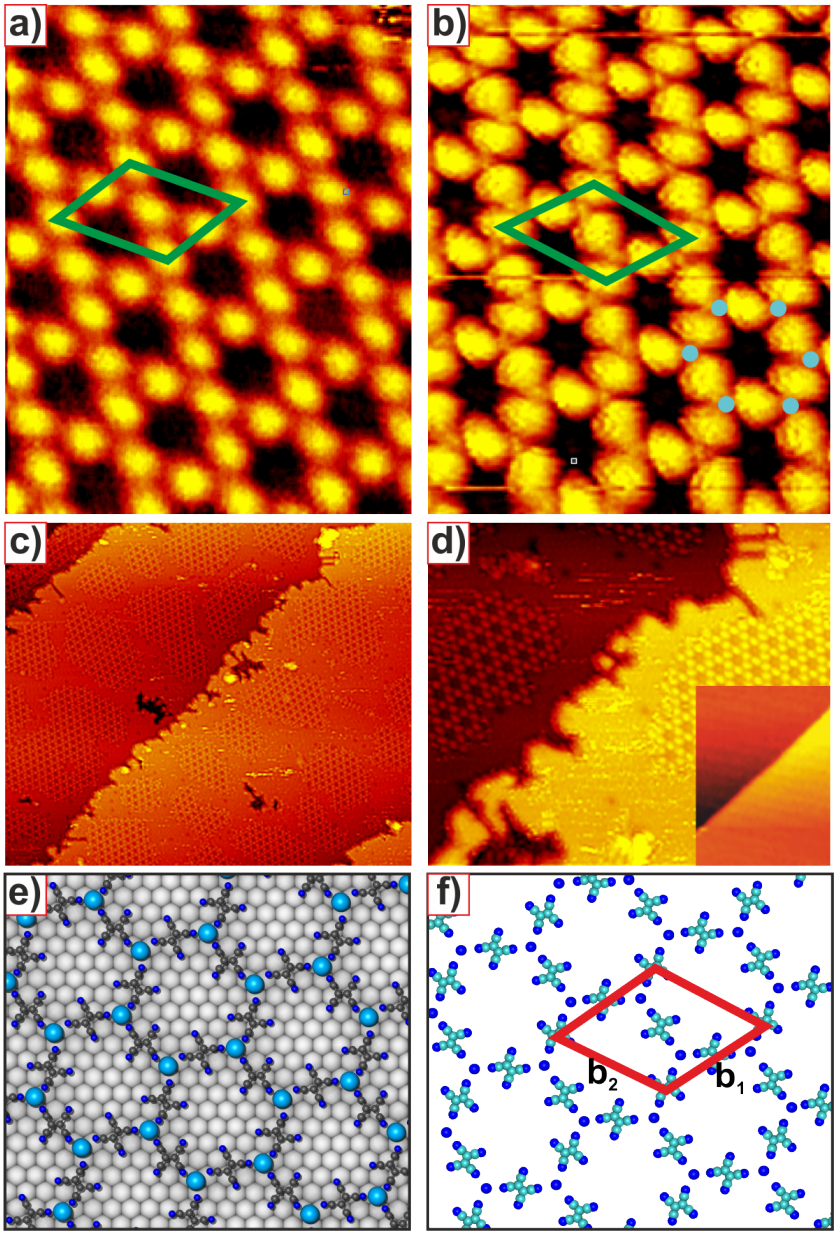

Figure 3.5: *a,b) Close-up images of the TCNE islands. The green square is the resulting unit cell. The blue dots in (b) indicate the position of the silver adatoms. c-d) STM image showing the modification of the steps of the silver substrate after depositing TCNE at low temperature, the inset in (d) shows an STM image, taken at 130 K, of a step in the clean Ag(111) surface. e) The model for the 2D Ag-TCNE coordination network, result of a DFT calculation, for a free standing monolayer. f) A model, result of a DFT calculations, for the Ag-TCNE coordination network (the light blue balls are the silver adatoms). a) 68 Å × 86 Å, 0.240 nA, 1.7 V, b) 68 Å × 86 Å, 0.29 nA, 1.3 V, c) 928 Å × 785 Å, 0.3 nA, 1.7 V, d) 330 Å × 281 Å; 0.31 nA, 1.7 V. Inset d) 334 Å × 447 Å; -0.7 nA, -2.4 V.*

Figure 3.5b shows a high resolution STM image where some structures with spherical shape can be observed between the molecules (for clarity, the position of some of them have been marked with blue circles). We think that these structures are Ag adatoms coming from the Ag surface that are forming a Ag-TCNE coordination networks with the TCNE molecules. Actually, STM images of the step edges of the surface (figure 3.5c and figure 3.5d) show that they do not look straight as in the clean silver clean surface. On the contrary, the step edges are completely irregular, with some gulfs, like etched; and there are some holes even on the terraces. Step etching and adsorbate induced modification of metal surfaces have been observed for oxygen, sulfur, or organic molecules containing electronegative units (e.g., benzoic acid, carboxylic or anhydride groups) [71–74]. Very recently, step etching of the Cu(100) surface after room temperature deposition of F4-TCNQ (tetrafluoro-tetracyanoquinodimethane) has also been reported [75]. In many cases (including the last one), step etching leads to surface faceting, where the molecule-substrate interaction can stabilize high Miller index surfaces [73]. In our experiments, the STM images strongly indicate that the presence of silver adatoms is due to TCNE-induced step etching; that is, the silver adatoms participating in the Ag-TCNE coordination networks are step edge atoms removed from the steps due to their interaction with the TCNE molecule.

An schematic model for this coordination network is shown in figure 3.5e. In this arrangement, each Ag atom is coordinated with three TCNE molecules, while every molecule is coordinated to two silver adatoms. The network stoichiometry is Ag:TCNE=2:3. To understand the role of the substrate in the arrangement, DFT calculations were carried out for a free standing monolayer of a Ag-TCNE coordination network with a similar geometry (figure 3.5f). The lattice parameter for the optimized structure is 18.4 Å, in good agreement with the experimental results. Thus, it seems that the substrate, besides providing the silver adatoms, only determines the possible orientations of the islands. DFT calculations were also carried out for the model shown in figure 3.5e (including the silver substrate). The results will be discussed later.

Nucleation process. Even for low coverages and low temperature (130 K), the molecules could not be found in isolated form on the terraces. The sequence of STM images shown in figure 3.6a-d shows changes in size and shape of the TCNE islands even at this temperature. The area corresponding to the clean surface has a fuzzy appearance due to the presence of diffusing molecules. At the same time, TCNE islands are continuously changing shape and size, maintaining the honeycomb structure. Figure 3.6f shows the minimum building block that can be observed (marked with the smaller blue circle

in figure 3.6e) contributing to the self-assembly of the islands. It consists of three TCNE molecules around one silver adatom. However, the apparently most stable unit is the hexagonal motif (as shown in figure 3.6f, black circle).

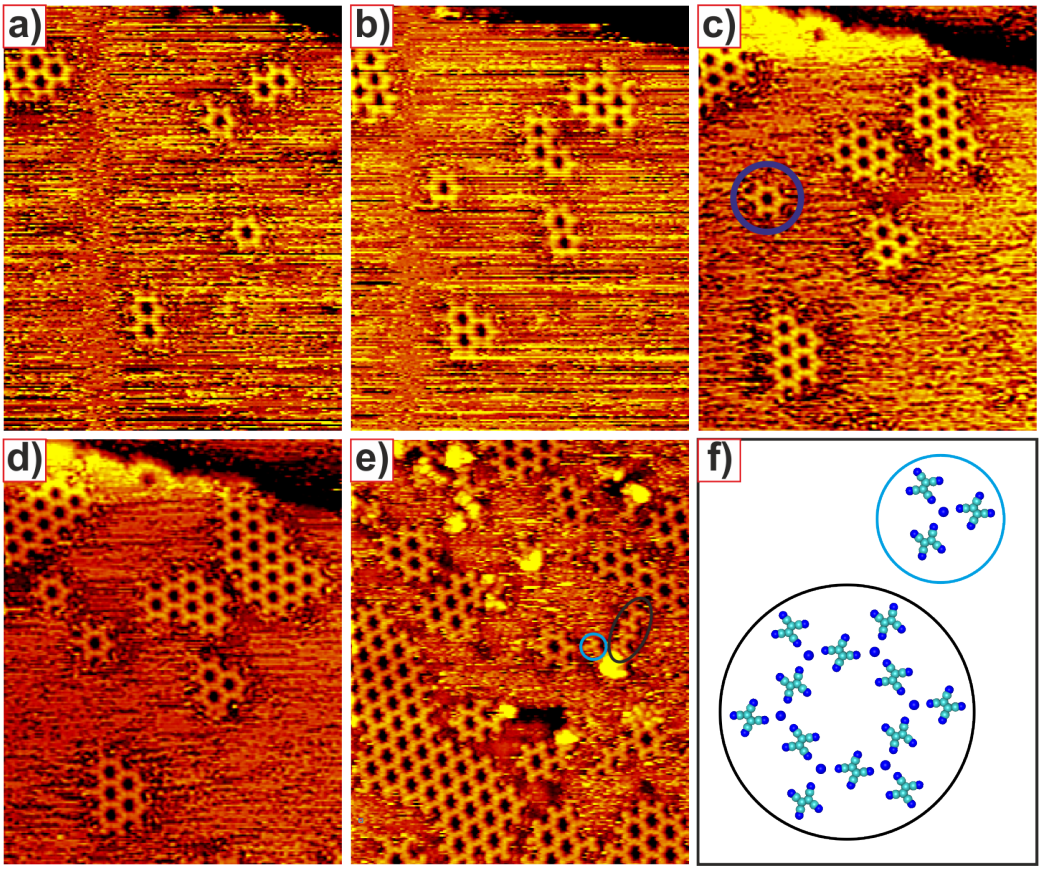

Figure 3.6: *a-d) Sequence of STM images, taken every 30 s, of 0.1 ML of TCNE grown at 133 K on Ag(111) and imaged at the same temperature. Even at this temperature the molecules are very mobile. e) Another STM image where the minimum stable building block can be observed (marked by the blue circle). f) A model for the most stable building blocks participating in the islands growth. a-d) 293 Å × 368 Å; -0.18 nA, -1.35 V. e) 293 Å × 368 Å; -0.16 nA, -2.09 V.*

According to these results, the following model can be proposed for the nucleation and growth of the Ag-TCNE coordination network: At 130 K the TCNE molecules are still very mobile. When they reach a step, the cyano groups do not only interact with the silver terrace atoms, but also with the silver atoms at the step edges. Most probably, the diffusing TCNE molecules are able to pull out some atoms from the steps, which diffuse over the surface

and interact with the TCNE molecules to form the LT coordination network.

3.2.2.2 Adsorption of TCNE on Ag(111) at room temperature

In another series of experiments the molecule was deposited with the silver substrate held at room temperature. The STM images, shown in figure 3.7, were recorded either at room temperature, either at low temperature (close to 170 K), but no change with the temperature measurement could be observed. After depositing 0.3 ML of TCNE on the silver surface, the molecules also form well-ordered islands with a honeycomb symmetry, like at low temperature, but with a different motif and unit cell. Also, islands with two different orientations can be found on the silver surface, as shown in figure 3.7a-b. The red rhomboid in figure 3.7d marks the unit cell for one of the two orientations, with sides $b_1 = 23.3(\pm 1.1)$ Å, $b_2 = 23.3(\pm 1.2)$ Å, and $\gamma = 120^0$. For this arrangement, the matrix describing the epitaxial relationship with the substrate can be written as $\begin{pmatrix} b_1 \\ b_2 \end{pmatrix} = \begin{pmatrix} 10 & 5 \\ -5 & 5 \end{pmatrix} \begin{pmatrix} a_1 \\ a_2 \end{pmatrix}$.

The orientation of this unit cell vectors differs 10^0 with respect to the high symmetry axis of the silver substrate, leading to a chiral arrangement of the molecules and explaining the two types of islands found on the surface. Like at low temperature, the appearance of the arrangement depends on the bias voltage (figure 3.7b-c), the shape of the island in one case is consisting by hexagon and in the other case this network is building by spheres.

Also in this case a zoom inside the island (figure 3.7d) seems to indicate the presence of silver adatoms (some of them are marked with blue circles) participating in the assembly of the TCNE molecules, giving rise to a new Ag-TCNE coordination network. A model for this structure is shown in figure 3.7e. In this case, each Ag adatom is coordinated with three molecules, but every molecule is coordinated to three silver adatoms and the network stoichiometry is Ag:TCNE=1:1 (in the low temperature case it was 2:3). The larger amount of silver atoms can be explained by noting that at room temperature the probability of step etching increases, the population of silver adatoms on the surface increases accordingly, and a new coordination network with a higher Ag:TCNE ratio is formed. Note, however, that the appearance of the step edges is different from the low temperature case. Now they look more straight, and are fully covered with molecules, as shown in figure 3.7a, which can be explained by a self-healing process; due to the more effective atomic diffusion along the steps, they can recover their original shape. Based on this model, DFT calculations for a free standing monolayer were carried out. The blue rhombus in figure 3.7f represents the resulting unit cell, with a

lattice parameters of 23.2 Å, in good agreement with the experimental value.

The room temperature arrangement can also be obtained by depositing the molecules at low temperature, and then increasing the temperature up to room temperature. This transition, however, is irreversible: once the room temperature arrangement is obtained, lowering the temperature does not modify the situation. Also, we found some intermediate temperature at which the low temperature phase coexists with the room temperature phase. We will discuss this transition state later in more detail.

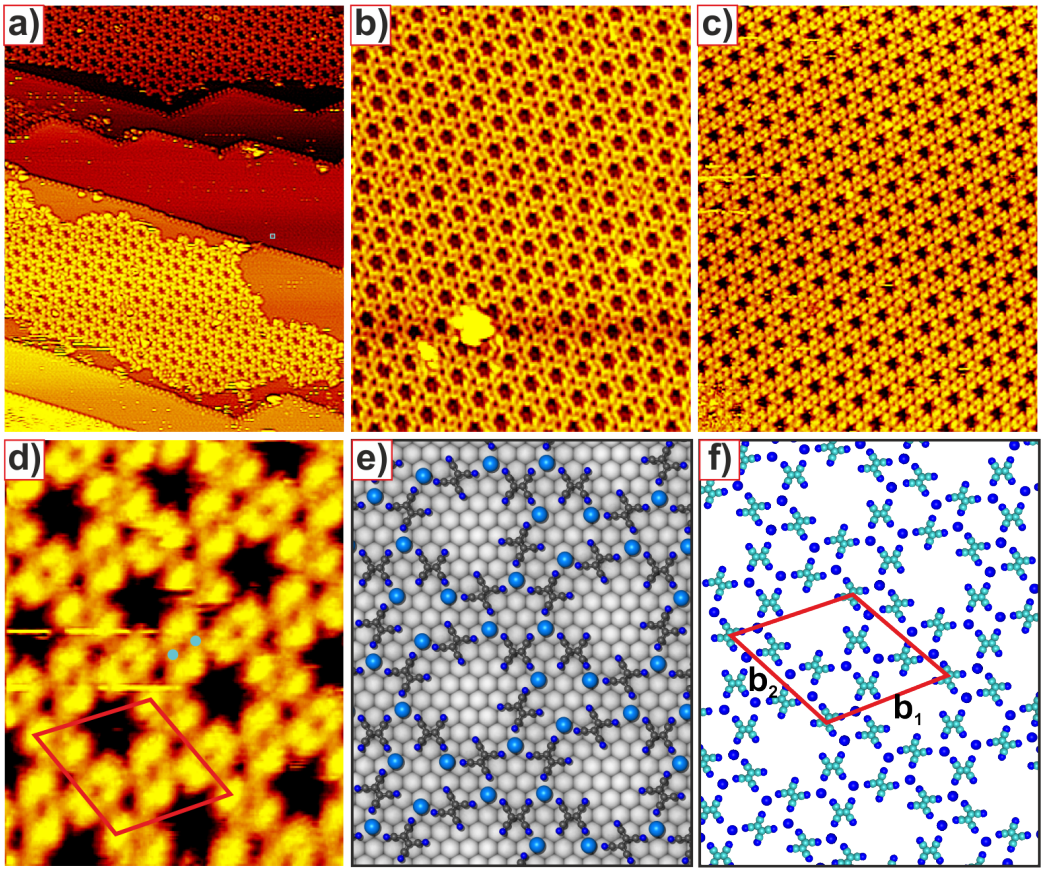

Figure 3.7: *STM images of TCNE grown at room temperature on Ag(111), a,d) STM image acquired at 170 K. b,c) STM images with two different voltages, measured at room temperature. d) Close-up image of a TCNE island, where the silver adatoms can be clearly seen (the blue dots indicate the positions of some of the silver adatoms, while the red rhombus is the unit cell. e) A model for the RT arrangement, result of a DFT calculation (the blue spheres are the silver adatoms). f) A 2D model of the TCNE arrangement at room temperature. a) 489 Å × 614 Å; -0.32 nA, -2.08 V. b) 293 Å × 368 Å; -0.36 nA, -2.2 V. c) 293 Å × 368 Å; -0.25 nA, -1.2 V. d) 68 Å × 86 Å; -0.19 nA, -1.2 V.*

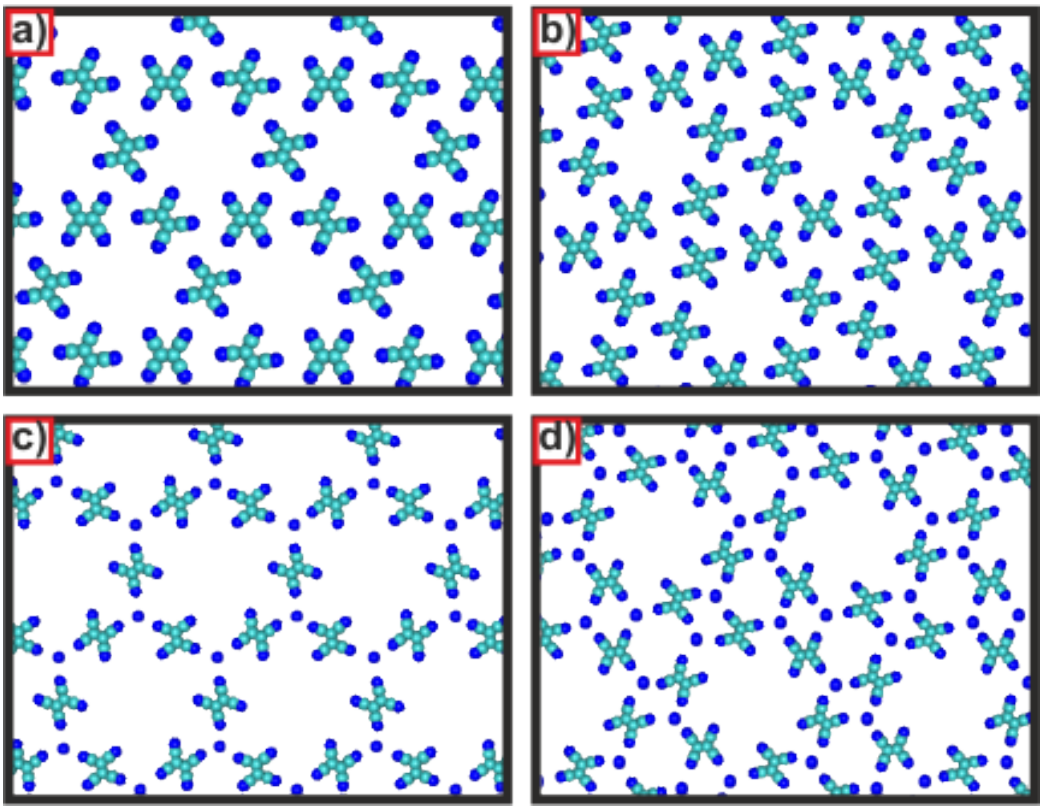

Figure 3.8: *Two different models, without (a,b) and with (c,d) silver adatoms, results of DFT calculations, for the LT (a,c) and RT (b,d) arrangements of TCNE on Ag(111).*

Note that it is possible to build TCNE self-assembled structures with similar geometries to those shown in figures 3.5f and figure 3.7f without Ag adatoms (figure 3.8a-b). DFT calculations for a free standing monolayer were also carried out for these networks. In the low temperature arrangement, the lattice parameter turns out to be 14.9 Å which is significantly lower than the experimental value (18.4 Å). On the other hand, the theoretical lattice parameters for the room temperature self-assembly is 20.8 Å which is also too small when compared with the experimental value (23.3 Å). This is an additional confirmation of the participation of silver atoms in the TCNE arrangement.

The participation of substrate adatoms in the formation of metal organic coordination networks has been previously reported, especially in the case of copper substrates [76, 77]. Their presence as a 2D gas on the surface is due to the continuous evaporation from the atomic steps, and their concentration strongly depends on temperature but also on the surface orientation. Thus,

they have been observed to form part of metal-organic complexes at 300 K on Cu(100) but only at 425 K on Cu(111) [78]. In the case of Au(111), it has been proposed that the adatoms may originate from the lifting of the herring-bone reconstruction. However, the extent of the presence of silver adatoms on a silver crystal is not clear. Although their participation in metal-organic coordination networks like hybrid chains with silver adatoms have been proposed, (in cases where the molecules contains C-I or C-Br bonds, this kind of reactions have been used on copper [79, 80], silver [81, 82], and gold [83] substrates), the activation barrier for atom detachment from a step has been estimated to be 0.71 eV [84], which makes diffusion along the step edges the dominant mechanism explaining step fluctuations on this surface, even at room temperature. Another possibility, suggested in the case of TCNQ on Ag(111)[85], that would explain the existence of silver adatoms is the rearrangement of substrate atoms due to the strong interaction with the cyano groups of the molecule, in a similar way to what has been reported for TCNE and TCNQ on Cu(100) [30, 59]. In our case, however, we can conclude that the presence of silver adatoms is due to the TCNE-induced step etching. Up to now, the most common functional groups normally used to form the ligand-metal bonds have been the carboxylate, pirydil and carbonitrile groups. Within the last family, dicarbonitrile-polyphenyls [86], TCNQ [87–89], and F4-TCNQ [90] have been employed. However, to our knowledge, no extended purely 2D network has been reported using TCNE, and only the bottom-up fabrication by atomic manipulation of small V-TCNE clusters on Ag(100) has been reported [64]. This could be interesting because TCNE is one of the smallest molecules involved in metal organic coordination networks (together with the carboxylic acid $C_20_4H_2$) [91], and therefore able to provide a rather short metal-to-metal distance (between 7 and 10 Å in the TCNE-derivatives bulk metal organic magnets) [92].

Molecular self-assembly of TCNE on Ag(111) at high coverage

While at low temperature only one phase was found, at room temperature other types of arrangements were found for higher coverages. Due to the complexity of these networks we will not discuss them in detail. After room temperature deposition, as shown in figure 3.9 (STM images taken at 300 K), the molecules formed well-ordered islands with a more compact hexagonal arrangement. Around the islands some fuzzy noise can be observed, due to the mobility of the molecules. The unit cell vectors of this new structure measure $b_1 = 31.7(\pm 1.5)$ Å, $b_2 = 31.7(\pm 1.4)$ Å, and $\gamma = 120^0$. Also in this case the network seems to include some silver adatoms, as shown in figure 3.9b (some of them are marked by a black circle), although we could not

figure out a specific molecular model for this assembly.

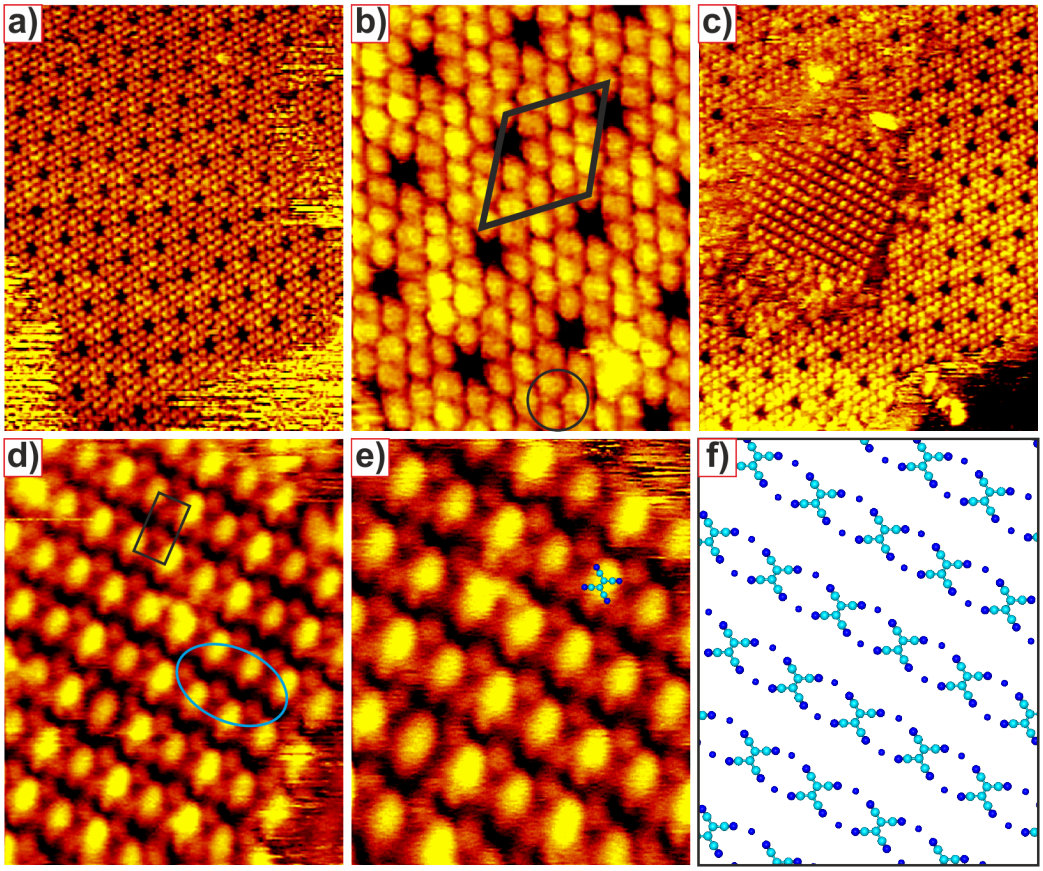

Figure 3.9: *STM images taken after room temperature deposition of TCNE on Ag(111) (all the images were acquired at room temperature). a,b) The more compact hexagonal network. c-e) Rectangular network of TCNE with silver adatoms. f) A model of this rectangular structure. a) 293 Å × 368 Å; -0.37 nA, -1.9 V b) 98 Å × 123 Å; -0.08 nA, -0.8 V. c) 293 Å × 368 Å; -0.08 nA, -0.8 V. d) 68 Å × 86 Å; -0.1 nA, -1 V. e) 49 Å × 61 Å; -0.1 nA, -0.8 V.*

Occasionally inside these islands, another type of arrangement with a different order can be found, as shown in figure 3.9c. This new assembly has a rectangular unit cell, with sides $b_1 = 8.0(\pm 0.9)$ Å, $b_2 = 11.3(\pm 0.8)$ Å, and $\gamma = 90^0$. This structure is also composed of molecules and silver adatoms. In figures 3.9d and figure 3.9e the TCNE molecule is the elongated bright protusion, and it is surrounded by four smaller round protrusions, However, not always the four protrusions appear, which seems to indicate that they are not a part of the intrinsic structure of TCNE and could be silver adatoms.

A model for this structure is shown in figure 3.9f. DFT calculations for this free standing 2D layer give $b_1 = 8.6$ Å, and $b_2 = 10.0$ Å, very close to the experimental results (a very similar arrangement has been reported for TCNE on Cu(100) [63], where the small protrusions around the elongated protrusions correspond to the copper atoms and hence the islands built a metal-organic coordination network with the copper substrate). Between the rectangular island and the hexagonal one there is an area where the molecule are diffusing on the surface and whose size is continuously changing since the molecules are attaching and detaching of the island all the time.

Close to the Monolayer

For larger coverages, a new type of closed-packed island of TCNE molecules appears, initially coexisting with the hexagonal phase, as shown in figure 3.10a (STM images taken at 150 K). In this case there is no free space between the new kind of island and the room temperature phase, as shown in figure 3.10b. Increasing the deposition time, the hexagonal phase starts to disappear and these new ordered islands form big domains with sizes of hundreds of nanometers. The molecules seem to be arranged in parallel rows with an intermolecular distance $b_2 = 7.2(\pm 1.1)$ Å. Although the apparent structure changes with the bias voltage, as shown in figure 3.10c and figure 3.10d. Close-up images allow to find out the unit cell of this assembly, shown in figure 3.10d. The lattice parameter in the direction perpendicular to the rows is $b_1 = 47.6(\pm 0.6)$ Å. The unit cell contains then 5 molecules, although not equally spaced; two different distances can be observed: while the rows labeled A-A' and B-A are separated 7 Å, the other rows (A'-B, B-C and C-B) are separated 11.2 Å. This pattern is similar to the structure observed when TCNE is deposited on Ag(100) [61, 62], where the molecule is in one row are rotated 90^0 with respect to the next one.

Notice that the distance of 11.2 Å (B-C cell) is similar to the inter row distance in the structure shown in figure 3.9e . Maybe this structure is the first stage of the closed-packed phase shown in figure 3.10d when the molecules covered all the space inside the compact hexagonal phase, further increase of the molecular density must be accompanied by a phase transformation.

Upon further increase of the coverage, this closed packed molecular structure continues growing until a new more compact structure starts to appear, as shown in figure 3.10e and figure 3.10f. The unit cell vectors for this new phase measure $b_1 = 7.6(\pm 0.9)$ Å, $b_2 = 7.8(\pm 1)$ Å, and $\gamma = 90^0$. This island is the more compact phase for TCNE molecules on Ag(111) we could find. A possible model for this structure is shown in figure 3.10g, where DFT calculations give a lattice parameter of $b_1 = 7.9$ Å and $b_2 = 8.0$ Å.

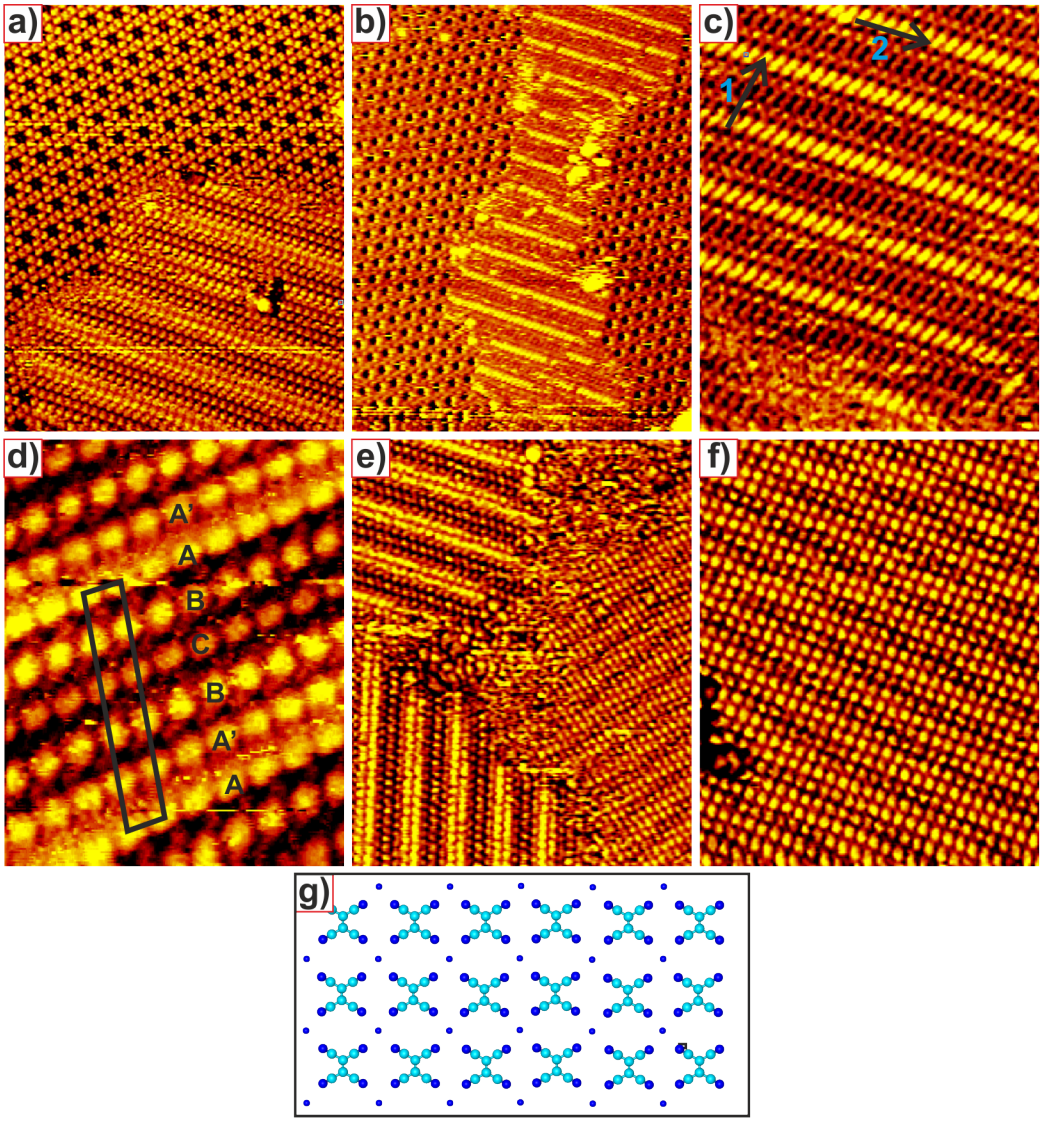

Figure 3.10: *STM images taken after increasing the coverage of TCNE on Ag(111) at room temperature (the STM images were taken at 150 K). a-b) Large STM images of a self-assembled domain of TCNE; they show an hexagonal RT TCNE islands with a new rhomboid phase developing inside. c-d) Topographic images showing a zoom inside this new phase, where it is possible to observe the molecular arrangement. e-f) Increasing further the dosage of TCNE, a still more compact square phase can be observed. g) A model for this compact structure. a) 293 Å × 368 Å; -0.25 nA, -1.5 V. b) 489 Å × 614 Å; -0.13 nA, -2.6 V. c) 196 Å × 245 Å; -0.32 nA, -2.3 V. d) 68 Å × 86 Å; -0.09 nA, -0.6 V. e) 293 Å × 368 Å; -0.12 nA, -0.8 V. f) 196 Å × 245 Å; -0.32 nA, -2.3 V.*

3.2.2.3 TCNE on Ag(111) at intermediate temperatures

As mentioned in the introduction, the room temperature arrangement can be obtained by depositing the molecule at low temperature (130 K) and then annealing the system up to room temperature. After showing the different types of phases that can be found depending on the temperature and coverage, in this subsection we will discuss the self-assembly of the TCNE on Ag(111) at intermediates temperatures. Figure 3.11 shows STM images taken after depositing the molecules at 150 K and increasing slowly the temperature up to 200 K. Three types of assemblies are observed to coexist at this temperature: the usual low temperature phase, the room temperature phase and a new intermediate phase.

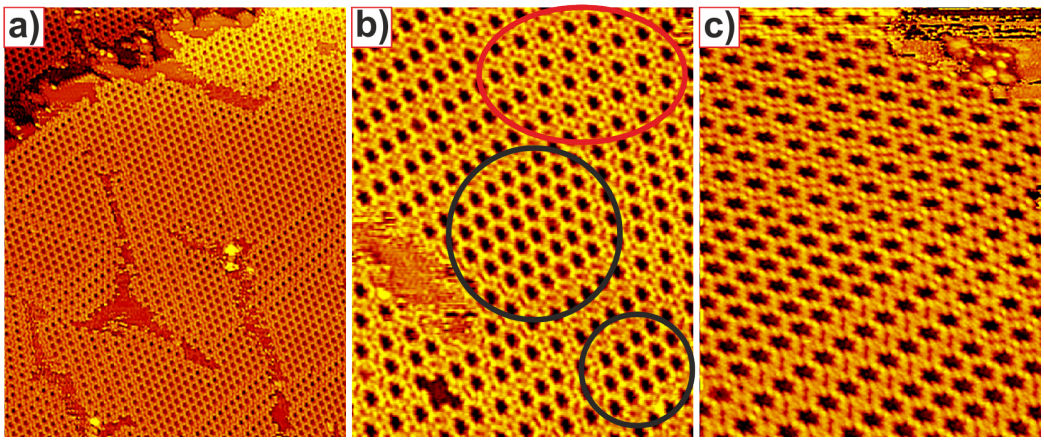

Figure 3.11: *Topography STM images, taken close to 200 K, of self-assembled TCNE island on Ag(111). The molecules were deposited at 150 K, and the temperature was slowly increased. The images show the coexistence of the low temperature phase and the room temperature phase, while a new intermediate phase is also present. a) 685 Å × 859 Å; -0.52 nA, -1.7 V. b) 293 Å × 368 Å; -0.36 nA, -1.5 V. c) 196 Å × 245 Å; -0.4 nA, -0.99 V.*

Figure 3.11b shows the coexistence of the three phases (the blacks circles marked the low temperature phase, the red ellipse indicated the room temperature island phase, and finally surrounding these islands the new intermediate phase can be found). This transition phase can be considered a mixture of the other two; that is, in one direction it consists of chains of molecules with the structure of the low temperature island, but in the other directions these chains assembly together like in the room temperature phase. The step edges also look like in an intermediate state (figure 3.11a): part of

them have big gulfs and look like very irregular, like after LT deposition, but at the same time other parts of the steps edges look much more straight and fully covered by molecules, like after RT deposition.

3.2.2.4 Electronic structure of TCNE on Ag(111): XPS measurements and DFT calculations

To study the electronic structure and possible charge transfer effects when the molecule is adsorbed on the surface, XPS measurements were carried out. In this case, some radiation damage could be observed after X-ray irradiation at room temperature, this damage was observed with the STM, where the islands disappear and the sample are completely dirty. For that reason, all the XPS measurements reported were carried out here with the sample at 80 K (after irradiation, the sample was measured again in the STM and no change in the surface could be observed).

Figure 3.12a and figure 3.12b show the C1s and N1s core levels corresponding to the low temperature phase (top position), the room temperature phase (middle position) and the clean Ag surface (bottom spectra). In both the LT and RT structures the N1s peaks appears at 398.2 eV (remember that two broad peaks appearing at $\sim$ 398.5 and 393.0 eV for the clean Ag surface are due to bulk plasmon losses)[93]. It has been reported that, for neutral TCNE, the N1s peak appears around 400.2 eV [65, 67, 94]. On the contrary, for TCNE salts, where the TCNE molecule is negatively charged, the N1s peak appears around 398.8 eV, which is closer to the experimentally found binding energies.

The main C1s peak can be located around 285.4 eV. Again, for the neutral molecule, the C peak appears at 287.7 eV [67], while for TCNE salts the binding energy is around 285.9 eV [65, 67], once again closer to the experimental value. This value is also closer to that found in TCNQ on Cu(100) [95]. Figure 3.12c shows that the carbon region spectrum can be deconvoluted into two main peaks and a broader one representing a shake-up satellite. These two peaks are located at 285.5 eV, and 285.1 eV. A Mulliken population analysis (see below) of the electronic densities on every carbon atoms leads to two different groups of atoms: the four carbon atoms in the cyano groups hold a positive charge of 0.161 e, while the other two carbon atoms, connected by a double bond, have a negative charge of -0.161 e. Since a positive charge on an atom increases the binding energy, the carbon close to the cyano group would thus be expected to appear on the high binding energy side of the spectra (285.5 eV). The experimental area ratio between the two components, 4:2, is quantitatively consistent with the expected radio.

Thus, the analysis of the nitrogen and carbon core levels suggest that

the TCNE molecule is negatively charged when adsorbed on the silver surface. Another proof of this charge transfer from the substrate to the TCNE molecule is provided by work-function measurements, as shown in figure 3.12d for samples with different coverages. The experimental work-function of Ag(111) is 4.74 eV, in good agreement with the values reported in the literature [48, 49], and increases in approximately a linear way when increasing the TCNE coverage. For coverages over a monolayer the work-function saturates at a value of ~ 5.7 eV, and the work-function of the metal substrate can thus increased ~ 1 eV by depositing TCNE molecules.

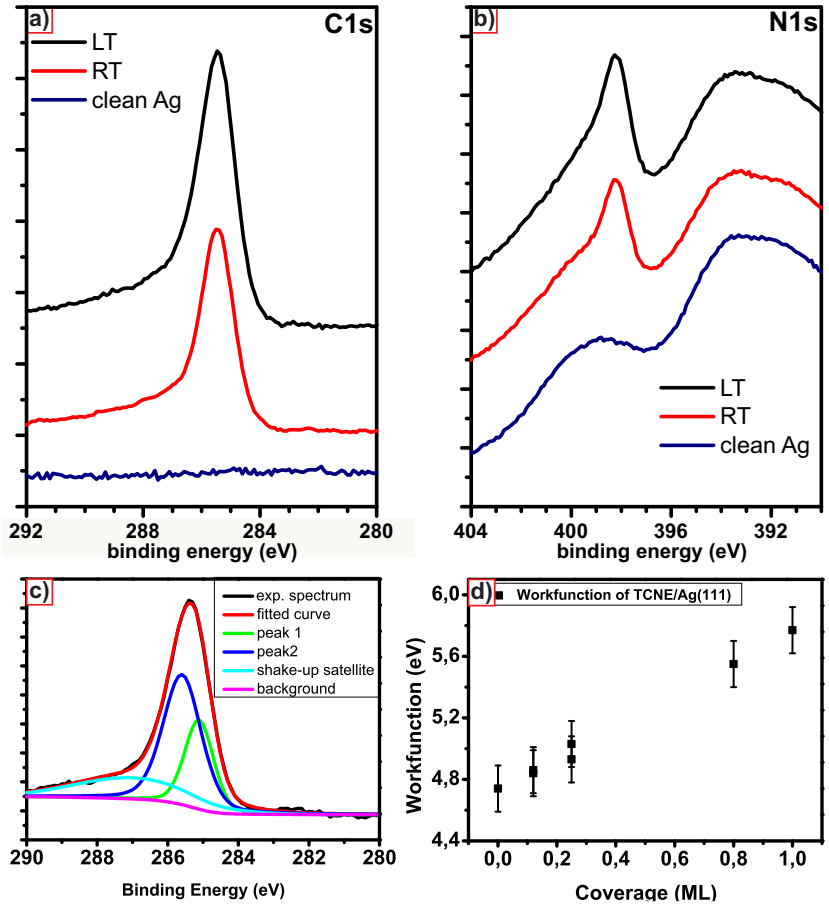

Figure 3.12: *XPS spectra of TCNE/Ag(111) taken at 80 K. The intensity of all the spectra have been normalized to the intensity of the $Ag3d_{5/2}$ peak. a-b) C1s and N1s core levels measured after low temperature and room temperature deposition. The spectra has been displaced vertically for clarity. c) An example of the deconvolution of the C1s XPS spectrum. d) The work-function of TCNE/Ag(111) systems as a function of the TCNE coverage.*

In conclusion, the XPS results confirm the existence of an electron transfer from the substrate to the TCNE molecules, as evidenced by the shift of the core levels and the increase of the work-function. Similar charge transfer has been observed for TCNE adsorbed on polycrystalline silver [96], Cu(111) [97], Cu(100) [59], and Ag(100) [62].

To gain insight into these results, we have performed DFT calculations of a TCNE molecule on the Ag(111) surface. Of all the tested possibilities, the minimum energy configuration is shown in figure 3.13. The TCNE molecule is slightly bent, with the N atoms closer to the silver surface (by 0.30 Å) than the central C atoms. At the same time, the Ag atoms directly below the N atoms are slightly pulled up (0.29 Å higher than the ideal surface termination).

This situation is very similar to what has been reported for TCNE adsorbed on Cu(100) [59] or TCNQ on Cu(100) [30]. In there, the acceptor molecules strongly modify the copper surface, in such a way that the highest copper atoms act as bridges between the TCNE molecules. In our case the calculations also indicate that the molecule gets ~ 0.88 e from the silver substrate. We have also performed DFT calculations of the LT and RT networks (figures 3.5e and 3.7e). When the TCNE molecule is coordinated to the silver adatoms, the total charge on the TCNE molecule is approximately the same (-0.86 e for the LT phase and -1.15 e for the RT phase). These results seem to indicate that a strong electron acceptor, such as TCNE, on the silver surface gets negatively charged (with approximately 1 e), irrespectively of the formation or not of a Ag-TCNE coordination network with silver adatoms. In the absence of such network, the molecule takes all the charge from the silver substrate. If the coordination network exists, TCNE takes part of the electron from the substrate and part from the silver adatom. In addition, the results indicate that the charge on the silver adatoms is -0.45 e in both cases.

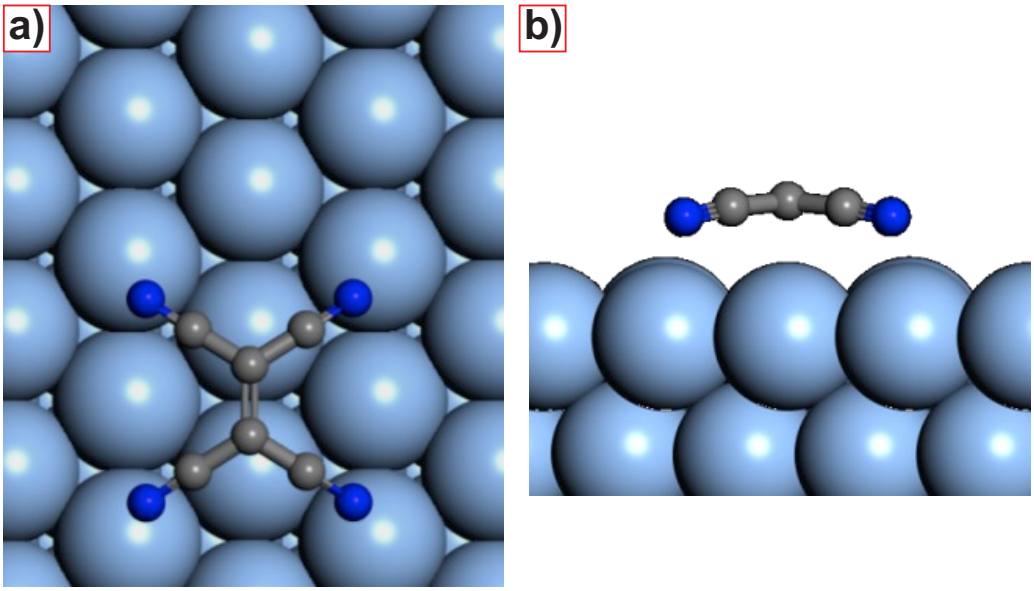

Figure 3.13: *Results of DFT calculations showing the optimized conformation of an isolated TCNE molecule on the Ag(111) surface. a) Top view, b) side view.*

3.3 Description of the TCNQ molecule

Tetracyanoquinodimethane (TCNQ), discovered in the 60's by L. M. Melby and coworkers [98], is one of the strongest organic electron acceptors with a large electron affinity of 2.81 eV [37, 38] and an ionization potential of $\sim$ 9.1 eV [39, 40]. TCNQ has long been regarded as a prime candidate for organic/inorganic charge transfer compounds and it has received great attention since it forms charge-transfer salts with high electrical conductivity, a discovery that has been very important in the development of organic electronics [99, 100]. In the last years, the adsorption and the assembly on metal surfaces like gold [101], silver [102], copper [30], and graphene [29, 103] has been reported. In some cases the electronic structure of TCNQ is strongly perturbed by the surface electrons. For example, in the copper case, TCNQ takes two electrons from the substrate, the cyano groups interact very strongly with the copper atoms, and this makes the molecule to bend slightly and some copper atoms to move up close to the nitrogen atoms. Actually, this rearrangement of the copper surface seems to drive the self-assembly of the TCNQ molecules [30]. On the contrary, in the case of gold or graphene, the interaction between molecule and substrate is rather weak [101, 103].

Figure 3.14a shows the chemical structure of TCNQ. It has a central

quinoid carbon ring, which is connected to four hydrogen atoms and four cyano terminations groups or two dicyanomethylene groups. Figure 3.14b and figure 3.14c show the frontier orbitals, HOMO and LUMO, respectively, of TCNQ in gas phase. A clear difference between these two states is the node that appears in the center of the molecule in the LUMO case. Also, STM simulated images are shown in figure 3.14d and figure 3.14e (this adsorption models was first relaxed in gas phase with the semiempirical PM3 method, the original program code stems from Oliver Gröning and Roman Fasel at the EMPA in Saint Gallen, Switzerland) [104].

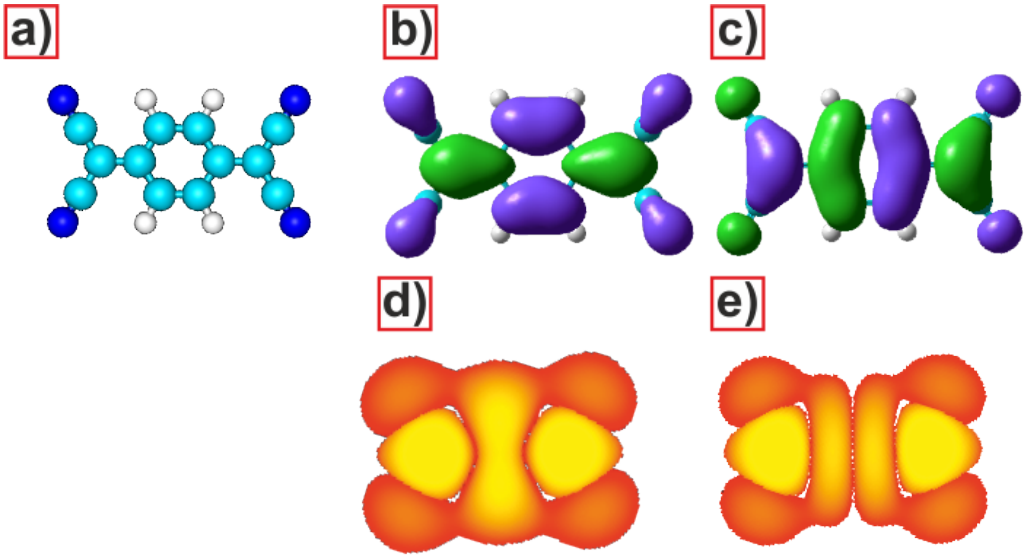

Figure 3.14: *a) Chemical structure of TCNQ (dark blue spheres are nitrogen atoms, light blue spheres are carbon atoms and white spheres are hydrogen atoms. Frontier molecular orbital of TCNQ in gas-phase: b) HOMO and c) LUMO. Simulated STM images of the d) HOMO, e) LUMO.*

As mentioned before, TCNQ is a good electron acceptor that can easily take up to two electrons. One extra negative charge is delocalized in one of the two dicyanomethylene groups and causes bond changes (bond $\boldsymbol{B_3}$ goes from double bond to single bond character, as shown in figure 3.15) and an partial aromatization of the central quinoid ring (which has some influence on the flexibility of the molecule and thus on the adsorption geometry). A second electron is hosted in the other dicyanomethylene group and completes the aromatization process.

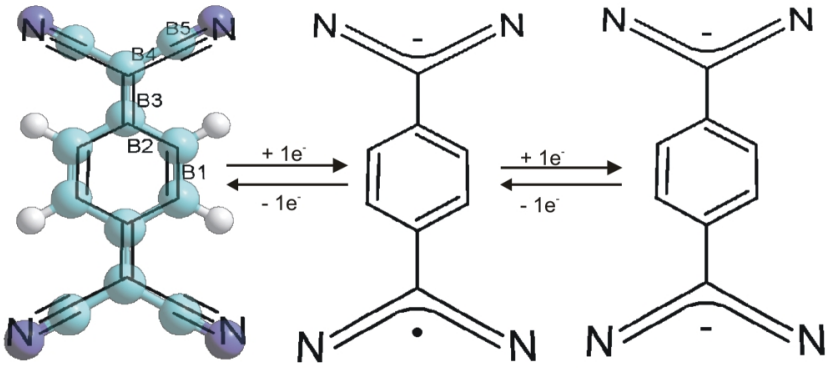

Figure 3.15: *Scheme of the chemical structure of $TCNQ^0$, $TCNQ^{-1}$ and $TCNQ^{-2}$. When the neutral TCNQ accepts one electron an extra negative charge is delocalized in one of the two dicyanomethylene groups and causes bond changes, where ($\boldsymbol{B_3}$) goes from double bond to single bond, and a partial aromatization of the central quinoid ring. A second electon is hosted in the other dicyanomethylene group and completes the aromatization process.*

3.3.1 TCNQ on Ag(111)

Experimental. The images taken at 77.8 K were measured in a commercial low temperature Omicron STM in collaboration with *Koen Lauwaet* from IMDEA-Nanoscience. The molecules were sublimated at 350 K from a glass crucible.

In this subsection we will discuss the adsorption of TCNQ on Ag(111). Figure 3.16 shows STM images, acquired at two different temperatures: a) 77.8 K, and b) 300 K, after depositing a submonolayer amount of TCNQ on the Ag(111) surface held at room temperature. As shown in figure 3.16a some disordered clusters appear on the surface; an around these agglomerations, 1D, rather irregular chains are formed. A model for the self-assembly of these chains is shown in figure 3.16c. As illustrated in figure 3.16d for a dimer of molecules, it is based on the interaction between the negatively charged cyano groups of one molecule and the positively charged hydrogens atoms in the central ring of the next one, forming so-called weak hydrogen bonds. In this case, however, the interaction with the substrate deviates the relative position from the gas-phase minimum energy configuration. This is the main bonding motif for self-assembled monolayers of TCNQ on the Au(111) surface [101], where the interactions molecule-substrate is weak. A similar interaction has also been reported on Cu(100) along one of the self-assembly directions [30].

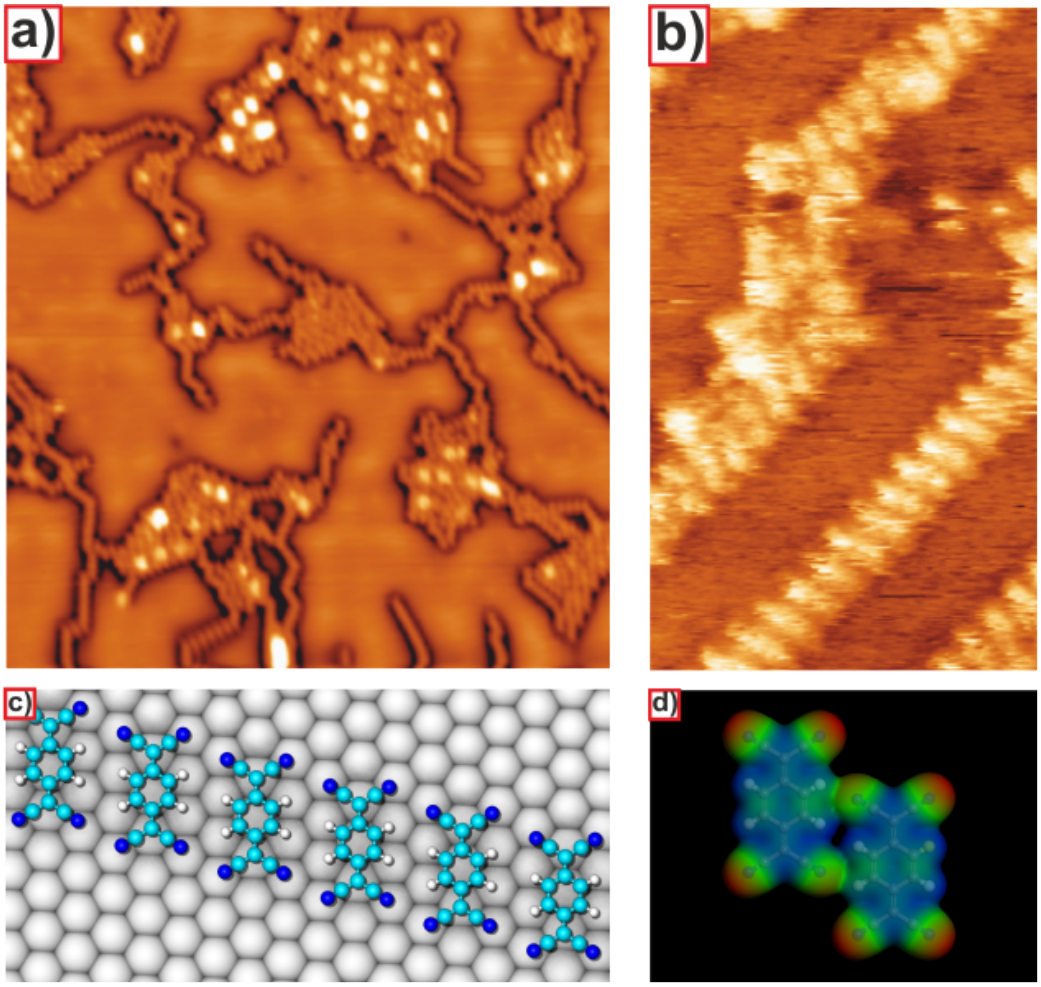

Figure 3.16: *STM images after depositing a submonolayer amount of TCNQ on Ag(111). a) This large STM image shows the molecules are assembled like chains taken at 77.8 K. b) STM images of the inset of the chain phase taken at 300 K. c) Model of the chains on the Ag(111) surface. d) Calculated minimum energy configuration for two parallel, coplanar, TCNQ molecules. A charge density isosurface, color-coded according to the electrostatic potential (red color means negative charge and blue means positive charge) is also drawn. a) 546 Å × 598 Å; -0.3 nA, -0.6 V. b) 85 Å × 139 Å; -0.45 nA, -1.5 V.*

Increasing the coverage, the chains phase still appears on the surface but coexisting with two closed-packed phases, shown in figure 3.17a. These two molecular structures continue growing upon the completion of the TCNQ monolayer. In **Phase I** (marked with a dark circles in figure 3.17a), the molecules are well-ordered with a rhomboid unit cell (marked in black in fig-

ure 3.17b) with sides $b_1 = 11.4(\pm 0.8)$ Å, $b_2 = 7.2(\pm 0.8)$ Å, and $\gamma = 70^0$. The matrix describing the epitaxial relationship with the substrate can be written as $\begin{pmatrix} b_1 \\ b_2 \end{pmatrix} = \begin{pmatrix} -1 & 2 \\ 3 & 4 \end{pmatrix} \begin{pmatrix} a_1 \\ a_2 \end{pmatrix}$. Which gives $b_1 = 10.6$ Å and $b_2 = 7.8$ Å and the angle between them is 65.2^0, in good agreement with the experimental results. A model for this arrangement is shown in figure 3.17c (which is the result of a DFT calculation). Note that this structure is different enough from the self-assembly of a 2D free-standing layer of TCNQ molecules with a similar geometry (figure 3.17d, notice that the relative position of the N atoms). In both cases, the lateral arrangement of molecules along the b_2 directions can be explained by the formation of the C≡N$\cdots$H-C hydrogen bonds. For the free standing monolayer, due to the negative charge around the nitrogen atoms, the molecules are rotated along the vertical direction to minimize the repulsive N-N interaction and maximize the electrostatic attractive interaction between one N atom and the C atom of the dicyano group of the upper molecule. On the contrary, on the Ag(111) surface the molecules rotate to maximize the N-Ag interaction, which is enough to compensate for the greater N-N repulsion. The charge in every TCNQ molecule is -0.52 e.

The growth of this phase on Ag(111) has already been reported [85] (and a similar self-assembled has been observed on Cu(100) [30]). Actually, it has been suggested that Ag substrate atoms may play a role to stabilize this structure [85], although we did not find any experimental evidence for the existence of these intermediate Ag atoms (according to the DFT results, the maximum difference between the vertical positions of the last layer of the silver atoms is 0.22 Å).

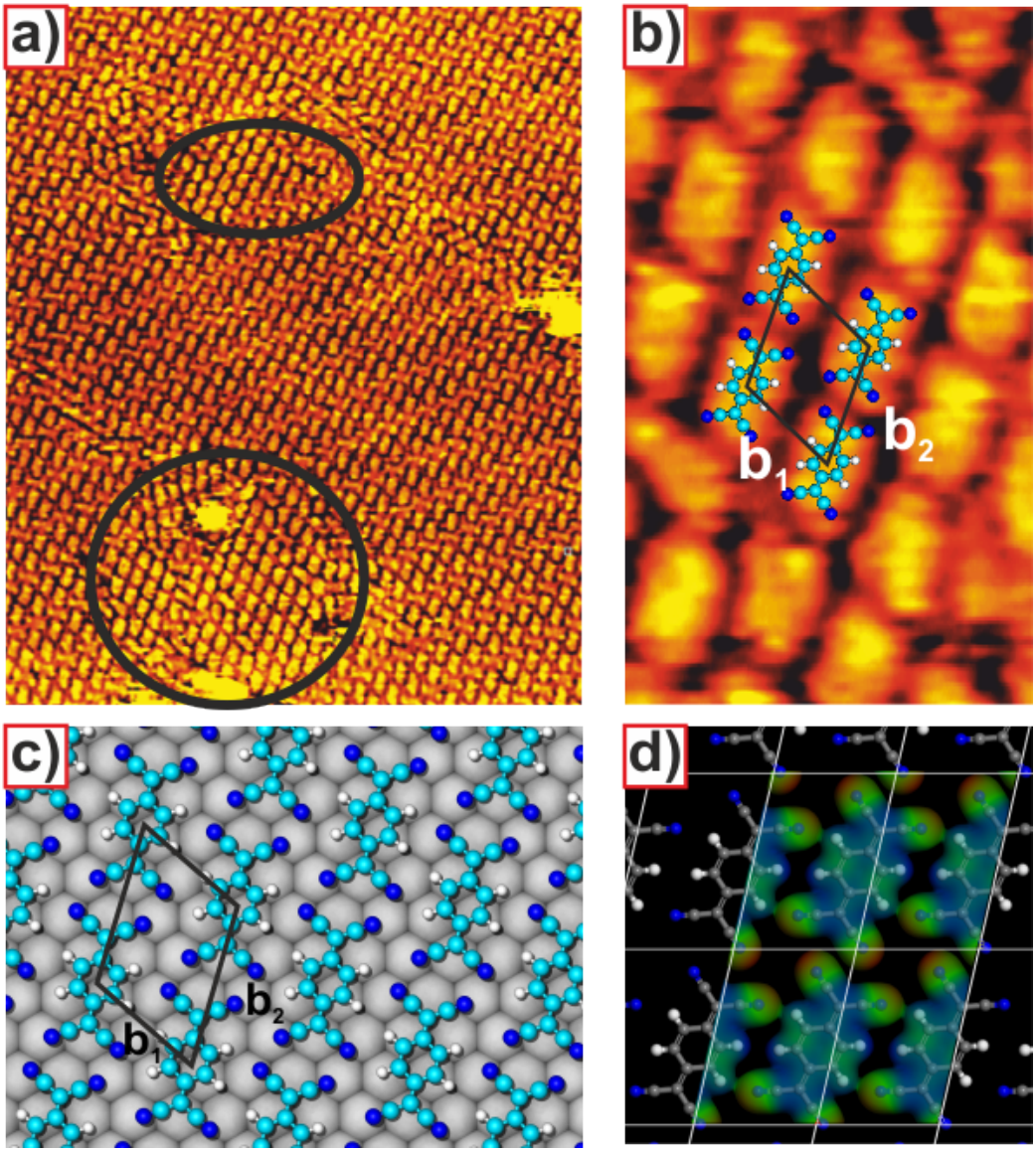

Figure 3.17: *STM images of TCNQ molecule on Ag(111) taken at room temperature. a) Increasing the coverage, two closed-packed phases are coexisting: phase I (marked by dark circles) and phase II. b) A close-up image into phase I. c) Schematic model for phase I. d) A model of the free-standing monolayer and overlaying the electrostatic potential projected onto a charge density isosurface of the TCNQ in gas phases. a) 278 Å × 336 Å; -0.31 nA, -0.67 V. b) 32 Å × 55 Å; -0.31 nA, -0.67 V*

The other phase, **Phase II** is shown in figure 3.18a. The unit cell contains three molecules, one of them rotated by 90^0 with respect to the other two.

Similar network has been reported for TCNQ on Cu(111) [105, 106]. Figure 3.18b shows a close-up STM image of this phase with an schematic model of the molecular arrangement superimposed. The sides of the unit cell (marked by the purple rectangle) measure $b_1 = 20.9(\pm 0.7)$ Å, $b_2 = 12.6(\pm 0.9)$ Å, and $\gamma = 85^0$. For this assembly, the matrix describing the epitaxial relationship with the substrate can be written as $\begin{pmatrix} b_1 \\ b_2 \end{pmatrix} = \begin{pmatrix} 8 & 2 \\ 2 & 5 \end{pmatrix} \begin{pmatrix} a_1 \\ a_2 \end{pmatrix}$ which gives $b_1 = 21.2$ Å, $b_2 = 12.8$ Å, and $\gamma = 83^0$. A model for this arrangement is shown in figure 3.18c. For this model, DFT calculations indicate that the silver surface is strongly buckled, with a maximum difference in height of the atoms in the last layer of up to 1.3 Å (figure 3.18e). For this configuration we could not find a stable free-standing monolayer, so it seems that the substrate silver atoms play a crucial role in stabilizing this structure. An alternative model is shown in figure 3.18d and figure 3.18f. In here there is one silver adatom per unit cell, with the result that the surface distortion is much smaller. For this configuration there is a stable free-standing layer, with lattice parameters $b_1 = 21.55$ Å, $b_2 = 13.09$ Å, and $\gamma = 80.4^0$ very close to the experimental values. In the first model, the charge every TCNQ molecules is -0.66 e, while in the second model it is -1.13 e. At the present time, we can not decide which of the two models is the correct one.

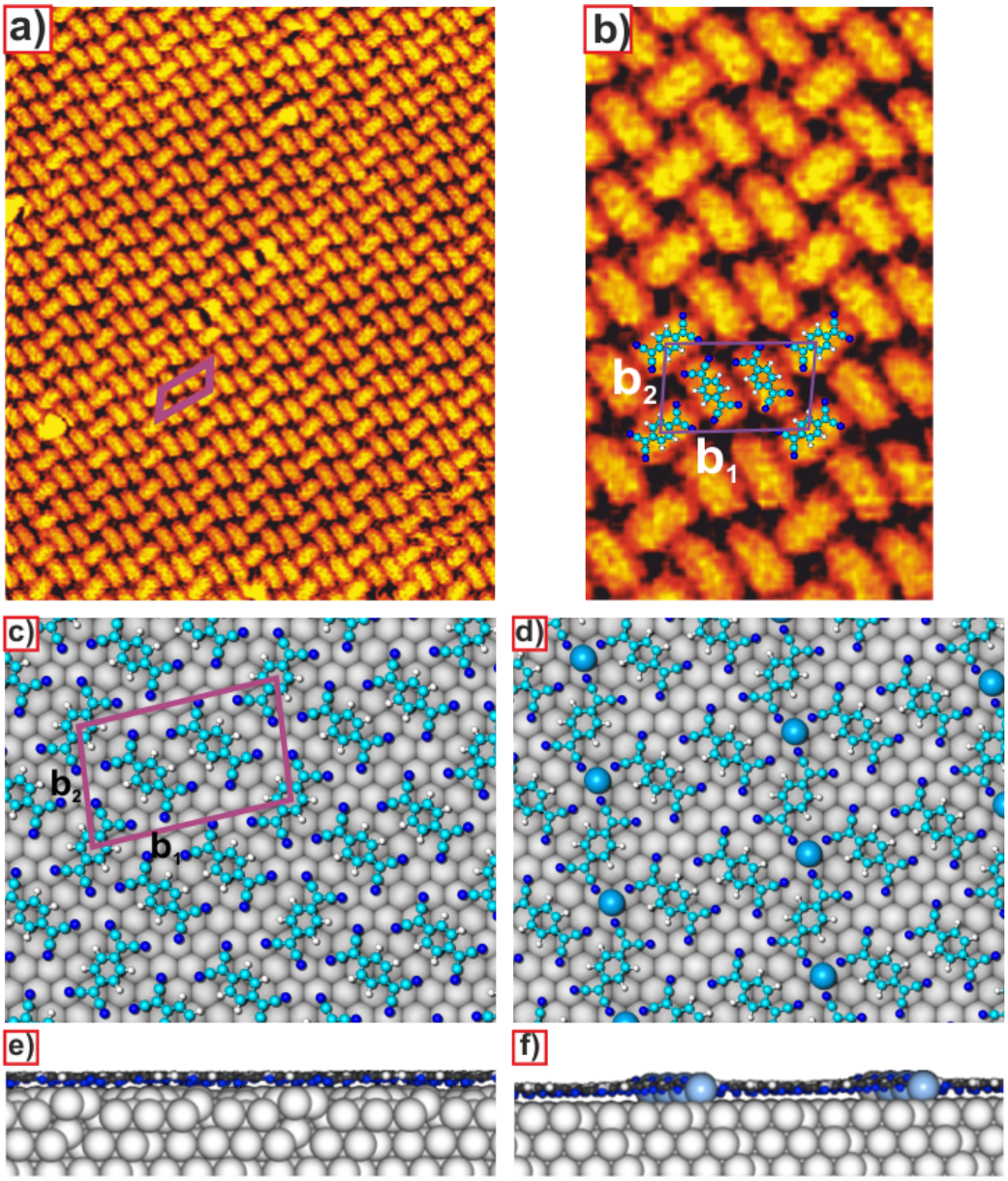

Figure 3.18: *a,b) STM images, taken at room temperature, of TCNQ on Ag(111), phase II. In (b) the molecular model was superimposed. c-e) Top and side view of two possible models for the structure of phase II. The blue atoms in (d) are silver adatoms. a) 185 Å × 224 Å; -0.13 nA, -0.57 V. b) 50 Å × 82 Å; -0.13 nA, -0.57V.*

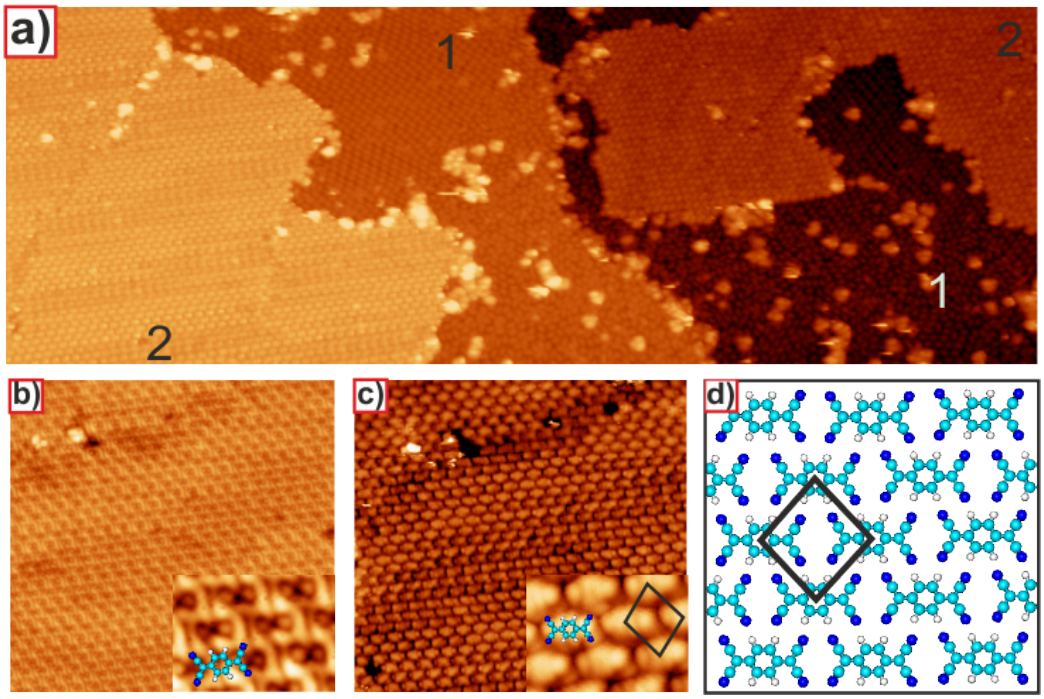

Figure 3.19: *a) Large scale STM image, acquired at 77.8 K, showing two monolayers of TCNQ on Ag(111) (number 1 and 2 denote the first and second layer, respectively. b-c) Sequence of STM images taken at different bias voltages. The inset in (b), taken at positive voltage, resembles the LUMO of the molecule. A TCNQ molecule is superimposed in each inset. d) Model for the free-standing monolayer of TCNQ molecules. a) 1083 Å × 407 Å; -15 pA, -1 V. b) 218 Å × 210 Å; 10 pA, 1.1 V. c) 218 Å × 210 Å; 10 pA, 0.4 V.*

Both phases still coexist until completion of the monolayer, as it can be observed in figure 3.19a, taken at 77.8 K, that shows a bilayer of TCNQ molecules on the silver surface. The second layer (number 2 in the figure) also forms well-ordered islands, but it exhibits a different arrangement than the first monolayer (denoted by number 1). The molecular self-assembly in the second layer can be obtained from the analysis of high resolution STM images. Figure 3.19c shows the unit cell, with sides $b_1 = 9.6(\pm 0.7)$ Å, $b_2 = 9.1(\pm 0.9)$ Å, and $\gamma = 100^0$. A very similar arrangement has been reported for TCNQ on Au(111) [101] and on graphene/Ir(111) [103], substrates where also the interaction molecule-substrate is very weak. A 2D model for this network with the optimized geometry obtained from a DFT calculation is shown in figure 3.19d, where the lattice parameter are $b_1 = b_2 = 8.9$ Å and $\gamma = 84^0$. In this network the self-assembled structure is stabilized also via C≡N$\cdots$H-C hydrogen bonds. Note that the relative position between two molecules differs

somewhat from the optimized structure for a single dimer (figure 3.16d), but in this case the symmetric arrangement allows for a more compact assembly.

Topographic STM images taken at different bias voltages, allow to obtain intramolecular resolution and identify the frontier molecular orbitals, as shown figure 3.19b and figure 3.19c (in both insets a TCNQ molecule was superimposed to show the molecular orientation). For positive voltages, corresponding to the unoccupied molecular orbitals, the STM images (figure 3.19b) resembles the calculated LUMO for an isolated TCNQ molecule (figure 3.14e) with a clear node at the center of the molecule. It can be observed also the overlap between neighboring molecules, which can be explained as the formation of a spatially extended intermolecular orbital.

3.3.2 XPS results and DFT calculations of TCNQ on Ag(111)

As in the previous cases, we will use XPS measurements to investigate the charge state of the TCNQ molecule (figure 3.20). Table 3.1 shows measured binding energies reported in the literature for the N1s core level on different substrate. For bulk (neutral) TCNQ, the nitrogen 1s core level exhibits a single peak at 399.6 eV [30, 107] and for TCNQ on gr/Ir(111), where the interaction molecule-substrate is weak, the binding energy is 399.3 eV [108]. In our experiments, the main peak of nitrogen appears at a 398.28 eV, almost the same that in the case of TCNE, (as mentioned before, in the XPS spectra of the clean Ag surface taken in the N1s region the two peaks appearing at $\sim$ 398.5 and 393.0 eV are due to bulk plasmon losses) [93]). This value is similar to the value reported for TCNQ salts [109–111] and TCNQ on gr/Ru(0001) [108], where TCNQ is negatively charged, which is an indication of a negative charge transfer from the substrate to the molecule.

The XPS spectrrum taken in the C1s-region is shown in figure 3.20b. In this case the spectrum can be deconvoluted into two peaks at 285.86 eV and 284.65 eV. This values are similar to the ones reported for neutral TCNQ powder, where C1s peaks appear at 285.2 eV (quinoid ring) and 286.5 eV (cyano ring) [30, 107, 110, 112, 113]. Actually a peak around 284.65 eV is characteristic feature of molecules containing benzene rings [114, 115]. In order to identify these two peaks, a Mulliken population analysis of the electron density, obtained from DFT calculations (see below) of a TCNQ molecule adsorbed on the silver surface was performed. Two groups of C atoms with similar charges can be identified in this way. The four carbon atoms in the cyano groups with two carbon atoms which connect the cyano group with the main body of the molecule hold a positive charge of 0.15 e,

Table 3.1: *N1s binding energy for TCNQ*

sample	N 1s (eV)
TCNQ(bulk) [30, 107]	399.6
TCNQ on gr/Ir(111) [108]	399.3
TCNQ multilayer on Au(111) [85]	399.1
TCNQ on Au(111) [85]	398.7
TCNQ on Cu(100) [30]	398.7
LiTCNQ [111]	398.6
CuTCNQ [111]	398.6
$Cu(TCNQ)_2$ [111]	398.6
$k^+(TCNQ)^-$ [109]	398.6
TCNQ on gr/Ru(0001) [108]	398.3
TCNQ on Ag(111) [85]	398.2
TCNQ on Ag(111) [this work]	398.3
TCNE on Ag(111) [this work]	398.2

while the remaining 6 carbon atoms have a similar negative charge, -0.26 e. Since a positive charge on an atom increases the binding energy, the C1s core levels of the C atoms in the cyano groups correspond to the higher binding energy component. The experimental area ratio between the two components, 1:1, is qualitatively consistent with the Mulliken analysis.This is another evidence that supports the existence of electron transfer from the substrate to the TCNQ molecules. Similar situations have been reported for TCNQ molecule on Cu(100) [30, 95, 102] and Ag(111) [85].

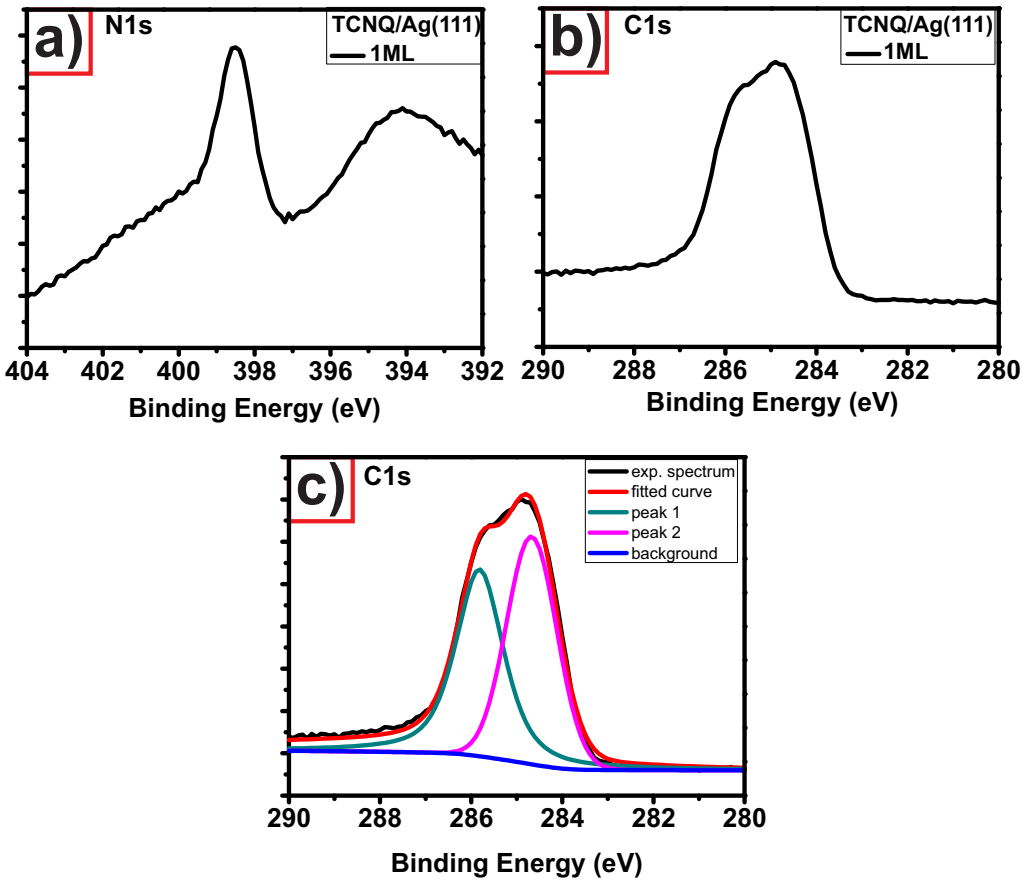

Figure 3.20: *XPS spectra of 1 ML of TCNQ on Ag(111): a) nitrogen 1s core level; and b) carbon 1s core level . c) The C1s XPS spectrum showing the deconvolution into two components.*

Another evidence of this charge transfer is the increase of the work-function, that changes from 4.74 eV for the clean Ag(111) surface to 5.36 eV after depositing one monolayer of TCNQ. These two results (core levels shifts and work-function increase) strongly suggest the existence of charge transfer from the silver substrate to the TCNQ molecules.

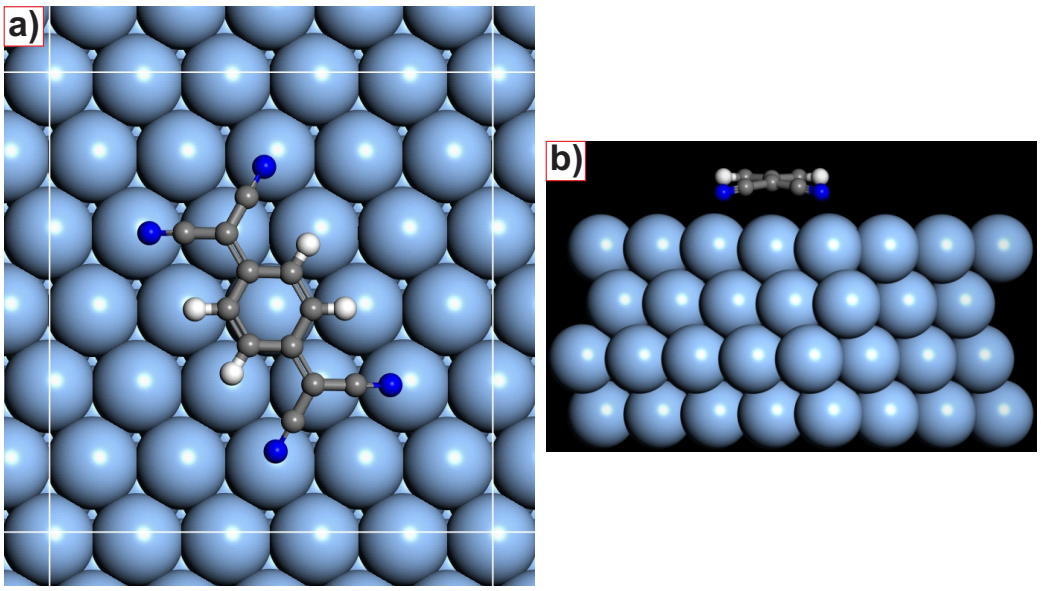

Figure 3.21: *Results of DFT calculations showing the optimized conformation of an isolated TCNQ molecule on the Ag(111) surface: a) top view, b) side view.*

As mentioned before, we have performed DFT calculations of a TCNQ molecule on the Ag(111) surface. Of all the tested possibilities, the minimum energy configuration is shown in figure 3.21. The TCNQ molecule is slightly bent, with the N atoms closer to the silver surface than the central C atoms. This situation is very similar to that observed when TCNE is adsorbed on Cu(100) [59] or TCNQ on Cu(100) [30]. In there, the acceptor molecules strongly modify the copper surface, in such a way that the highest copper atoms act as bridges between the TCNE or TCNQ molecules. In our case the calculations indicate that the molecule gets $\sim$ 0.99 e from the silver substrate, which is in agreement with the experimental results.

3.4 Description of the TTF molecule

Tetrathiafulvalene (TTF) is a well-known donor molecule [116, 117]. It was discovered almost at the same time by Wudl in 1970 [118], by Hüning [119] and by Coffen in 1971 [120]. Studies about this donor and its derivatives have been reported in thousands of papers; it is probably the most famous electron donor molecule [121]. Also, the adsorption and assembly on noble-metal surfaces has been investigated on different substrates like gold (111) [122–124], copper (100) [125], silver and copper (111) [126], gold and silver

(110) [127–129].

This molecule TTF ($C_6S_4H_4$) is a non-aromatic π donor with a ionization potential of 6.83 eV [45, 46] and with a electron affinity of 0.17 eV [47]. TTF is formed by two dithiolylidene rings connected by carbon atoms, as shown in figure 3.22b. The redox transformation is shown in figure 3.22a: these two species are thermodynamically stable and the TTF can be oxidized to the cation radical $\mathbf{TTF^{+1}}$ and dication $\mathbf{TTF^{+2}}$, a reversibly process within a very accessible potential window. This potential can be tuned by the attachment of electron-donating and electron-withdrawing substituents and for that reason some derivatives of this molecule is tried to functionalizing the TTF core. Figure 3.22c and figure 3.22d also show the frontier molecular orbitals, HOMO and LUMO, respectively.

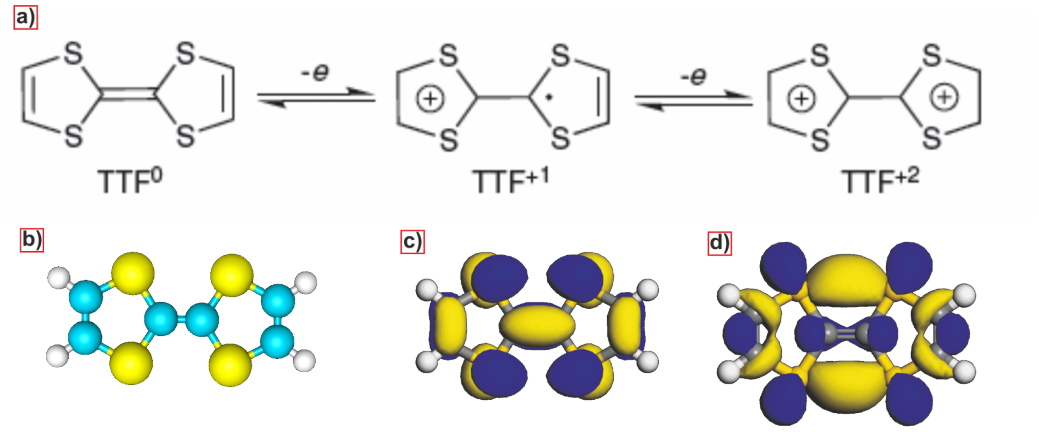

Figure 3.22: *a) Scheme of the redox transformation of TTF. b) Chemical structure of TTF (yellow spheres are sulfur atoms, light blue spheres are carbon atoms and white spheres are hydrogen atoms). Frontier molecular orbitals of TTF: c) HOMO, and d) LUMO.*

3.4.1 TTF on Ag(111)

In this section we will report a series of experiments aimed to study the adsorption of TTF on the Ag(111) surface at different coverages. The molecules were deposited from a glass crucible at room temperature on a silver substrate also held at room temperature. At this temperature the TTF molecules are very mobile on the silver surfaces, so the STM images shown in this section were measured at 150 K, but even at this temperature the molecules are free to move on the surface. Figure 3.23 shows representative STM images taken after depositing different amounts of TTF. From the early stages, the step

edges are fully covered, as shown in figure 3.23a. Figure 3.23a shows a STM image after depositing low coverage and the terrace of the silver surface looks clean. After increasing the amount of TTF, as shown in figure 3.23b, the step edges continue fully covered, but the only proof of a higher coverage is the noise in the STM images created by the mobility of the molecules. Only a few images could be acquired showing individual, still molecules (figure 3.23c). The molecules found in isolated form show a ring-like appearance. A similar shape has been observed when adsorbed on Au(111), where a repulsive interaction between the molecules at low coverages has been reported [122, 123].

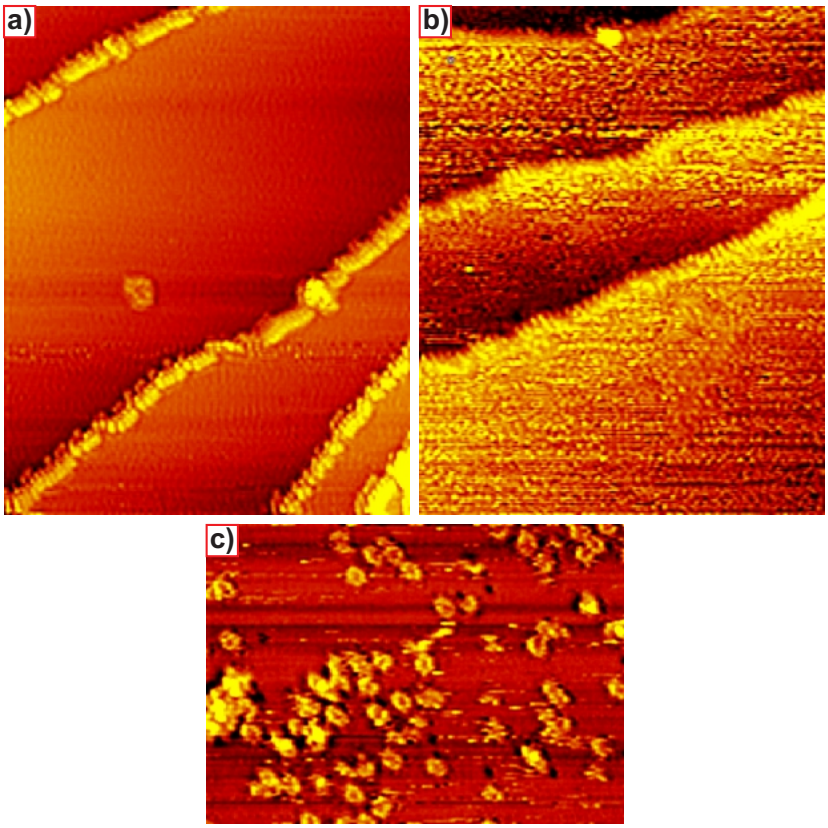

Figure 3.23: *a-b) STM images of TTF on Ag(111) taken at 170 K with different coverages. At low coverages, the molecules nucleate at the step edges. When increasing the coverage, the only evidence of the presence of the molecules is the noise in the STM images. c) STM image of isolated TTF molecules absorbed on the Ag(111) surface. a) 489 Å × 614 Å; -0.32 nA, -1.5 V. b) 293 Å × 368 Å; -0.45 nA, -0.8 V. c) 487 Å × 384 Å; -0.4 nA, -4.2 V*

After annealing the sample at 350 K during 10 minutes, the STM images acquired at 170 K, reveal the presence of well-ordered island, as shown in figure 3.24, while the adsorption of the TTF at room temperature have not been observed island. The borders of the islands are not very regular, but all the islands are attached to the step edges (fully covered), which seems to indicate that the nucleation of the islands starts at the step edges and not on the terraces. Inside the islands there are some bright lines can be seen (as shown in the inset figure 3.24a), which are actually domain grain boundaries.

Figure 3.24b and 3.24c illustrate in more detail the self-assembly inside the island. The long axis of the molecule is oriented along the high symmetry directions of the silver surface, so it could be possible other orientation of the molecules along to the other two high symmetry axis but in our experiments it can not be observed (some TTF molecular models are superimposed on the STM image to clarify the dimensions). The black square in figure 3.24c shows a (centered) unit cell; it has a rectangular symmetry, with sides $b_1 = 10.4(\pm 0.9)$ Å and $b_2 = 10.7(\pm 0.7)$ Å, and $\gamma = 90^0$. A model of this arrangement is shown in figure 3.24d. The matrix describing the epitaxial relationship with the substrate can be written as $\begin{pmatrix} b_1 \\ b_2 \end{pmatrix} = \begin{pmatrix} 4 & 2 \\ 0 & 4 \end{pmatrix} \begin{pmatrix} a_1 \\ a_2 \end{pmatrix}$. A model of this arrangement is shown in figure 3.24d.

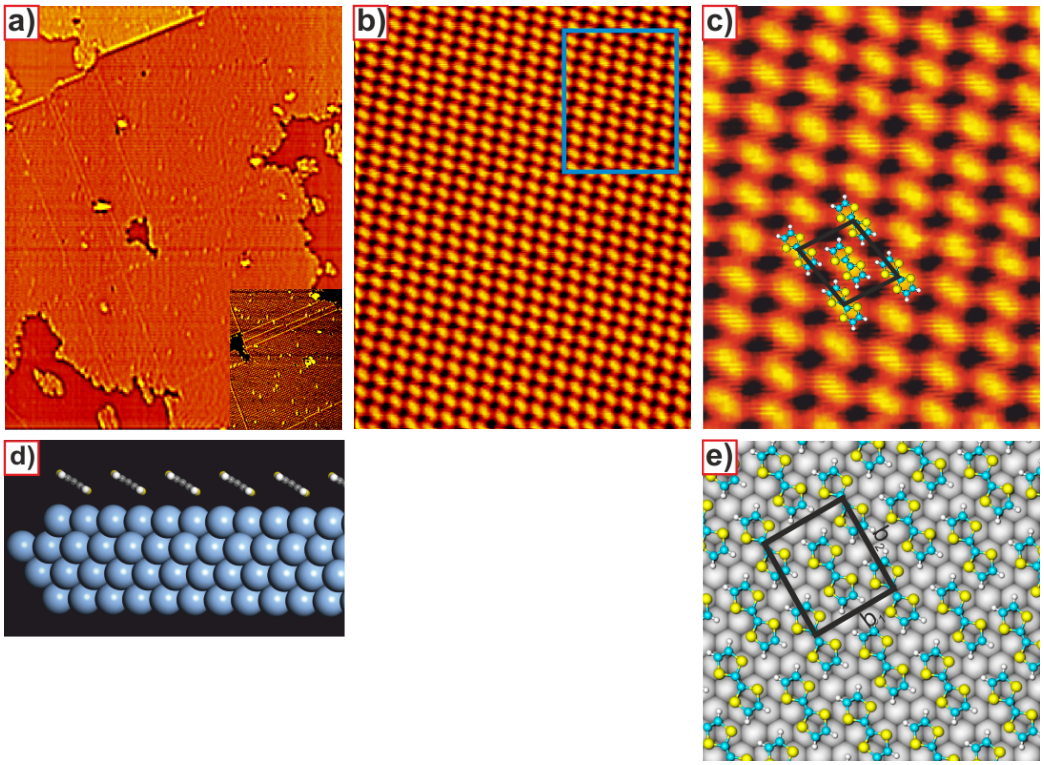

Figure 3.24: *a-c) STM images of TTF on Ag(111), taken at 130 K, after annealing at 350 K. a) Large island have been observed, inside this island bright lines appears along the island, it could be some defects. b) The blue square marked the zoom of the island used for the next image. The black square in (c) indicate a centered unit cell of the 2D assembly, with a molecular model superimposed. d-e) side and top view of DFT calculations taken into account the silver substrate. a) 978 Å × 1227 Å; -0.56 nA, -1.7 V. inset a) 489 Å × 614 Å. b) 147 Å × 184 Å; -0.380 nA, -0.32 V. c) 49 Å × 61 Å; -0.380 nA, -0.32 V.*

DFT calculations for this structure indicate that the molecules are not flat on the surface. A side view of the optimized conformation (figure 3.24d) shows that the molecular plane forms an angle of 30.5^0 with respect to the surface, due to the fact that commensurablility with the substrate puts the molecules too close together. DFT calculations for a free standing monolayer (figure 3.24e) show that for the molecules to be completely planar the lattice parameters should be $b_1 = 11.44$ Å (which is ~ 1 Å larger than the experimental value) and $b_2 = 10.59$ Å. The estimated charge transfer in this case is 0.10 e per molecule. A similar tilted arrangement has been proposed for TTF on Cu(100) and seems to be related to the relatively strong intermolecular van der Waals interaction between relative to the molecule-substrate

interaction [125].

Figure 3.25 shows STM images, taken at 130 K, after annealing the TTF islands (two different coverages) at 400 K during 10 minutes. The well-ordered islands disappear, and new islands with line shape appear on the surface. The directions of these lines coincide with the high symmetry directions of the silver surface. These molecular chains are easily manipulated with the STM tip, indicating that they are only weakly bound to the substrate. We will show later that these chains are not composed of just intact, TTF molecules and these chains could be a kind of polymer maybe with some silver adatoms, like other examples reported in the literature [80, 82, 83]. After annealing at higher temperature (500 K), the molecules are completely desorbed from the substrate.

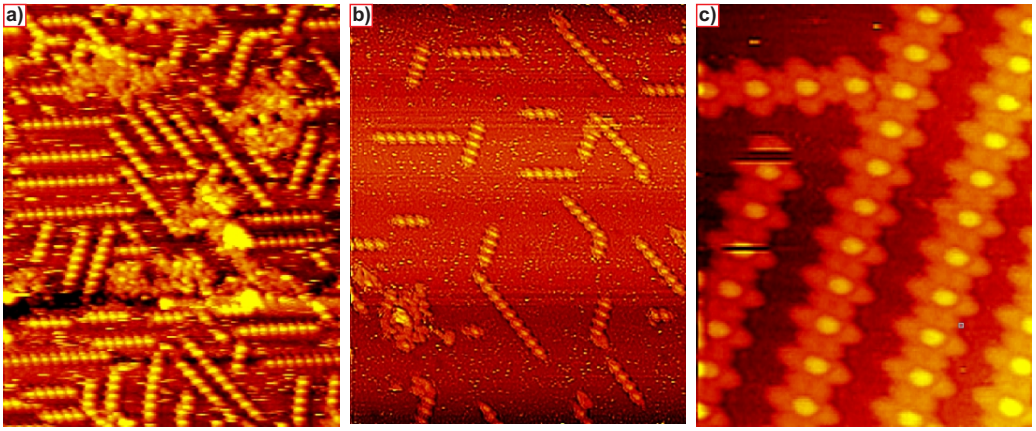

Figure 3.25: *STM images, taken at 130 K, of two different coverages of TTF on Ag(111) after annealing at 400 K. These molecular chains can be easily manipulated on the surface with the STM tip. a) 489 AA × 614 Å; -0.24 nA, -2.66 V. b) 489 Å × 614 Å; 0.44 nA, 0.31 V. c) 98 Å × 123 Å; -0.16 nA, -1.8 V.*

3.4.2 XPS results and DFT calculations of TTF on Ag(111)

In this section, we will try to elucidate the behavior of the TTF molecule on the silver surface and the changes observed in the STM images upon annealing. The XPS measurements reported in this section (figure 3.27) were carried out with the sample at 80 K trying to avoid radiation damage during the experiment.

First to all, since the STM results show that after room temperature deposition the molecules remain isolated, DFT calculations were carried out

to find the optimum conformation of a TTF molecule on the Ag(111) surface. As shown in figure 3.26a the TTF molecule is adsorbed almost flat on the surface, with a slight tilt of 8.5^0 of the molecular plane with respect to the silver surface. The tilt is due to the fact that the adsorption geometry is not symmetrical, with two of the S atoms close to on-top position, which leaves the other two S atoms close to hollow sites (a similar adsorption geometry has been reported for TTF on Au(111) [36]). The calculations for this structure also indicate that the molecule is slightly positively charged, donating 0.13 e to the silver substrate. For TTF on Au(111) the molecular charge is larger, around 0.6 e [36], which is probably related to the larger work-function of the gold.

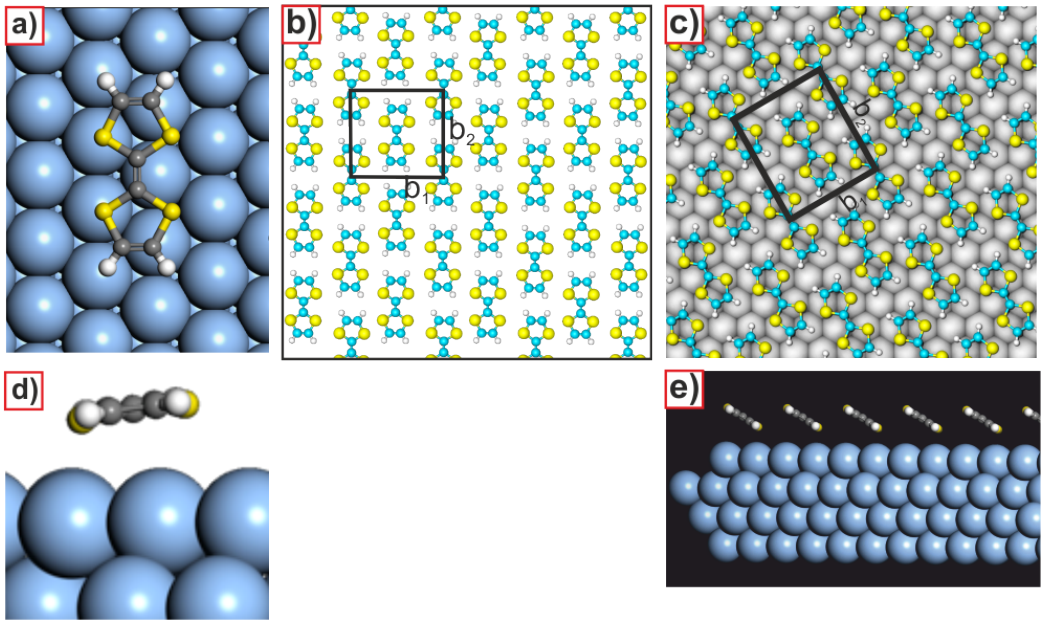

Figure 3.26: *Theoretical calculations of the possible islands of TTF molecules where b_1, b_2 are the vectors of the cell. a,d) Results of DFT calculations showing the optimized conformation of an isolated TTF molecule on the Ag(111) top and side view, respectively. b) Results of DFT calculations showing the optimized structure of a free standing monolayer of TTF molecules, in this case the cell is marked by this blue square. c-e) Top and side view of DFT calculations when the Ag(111) substrate is taken into account. The corresponding cell is demarcated by this black square.*

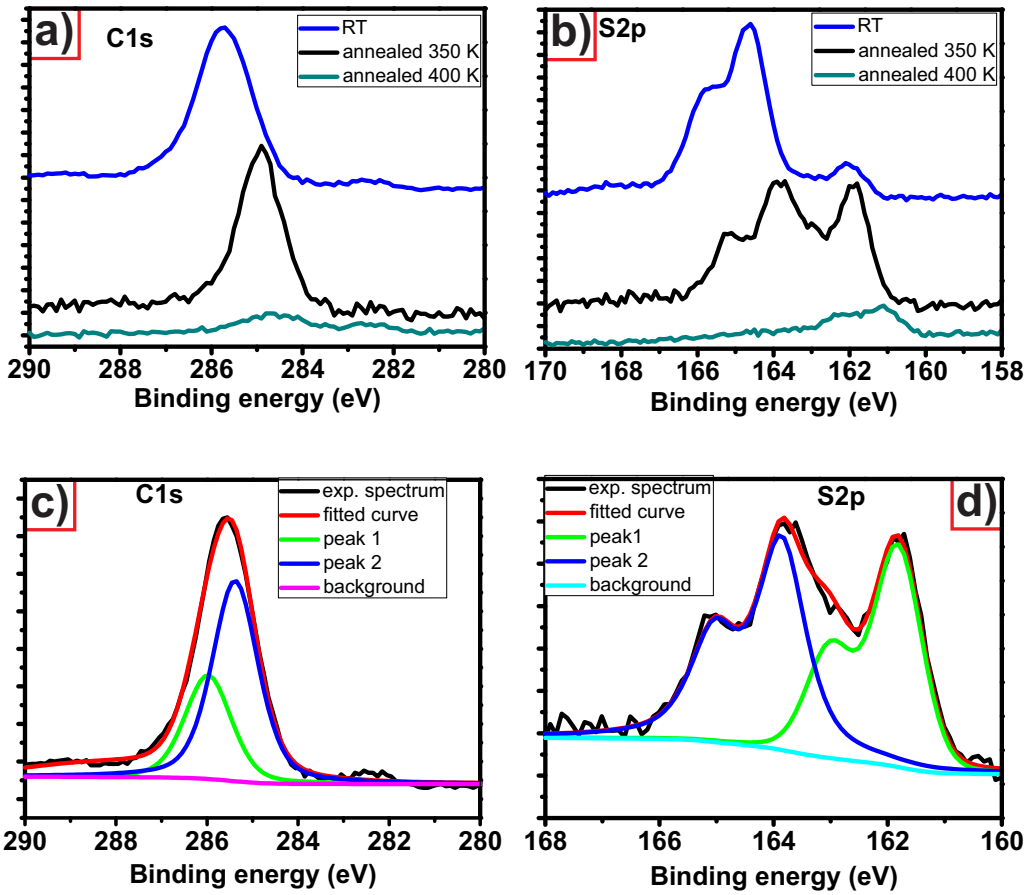

Figure 3.27: *a,b) C1s and S2p XPS spectra of TTF on Ag(111) after toom temperature deposition and after annealing to 350 K and 400 K. with the deconvolution peaks. c,d) An example of deconvolution of the C1s and S2p spectra. All the measurements were performed at 80 K.*

Figure 3.27b shows the sulfur 2p spectrum (this peak is split into $2p_{1/2}$ and $2p_{3/2}$ components due to the spin-orbit coupling). In agreement with the DFT results that show that isolated molecules are almost planar on the silver substrate, after room temperature deposition, and the four S atoms hold a very similar charge (-0.15 e). Only one doublet sulfur peak (the $2p_{3/2}$ component appears at 164.47 eV) is measured, since the four S atoms in this configuration are almost equivalent (the small peak close to 161.8 eV could be due to the presence of some molecules adsorbed slightly tilted). On the other hand, when the system is annealed to 350 K, the STM images show ordered island where the molecule are significantly tilted (according to the DFT calculations), and two doublet sulfur peaks with the same intensity

should be expected, which is actually the case, the 2 main peaks appearing at 163.80 eV and 161.80 eV. The higher binding energy value is similar to the value measured in systems with a direct sulfur-gold and sulfur-silver interactions, as found for thiol-based on gold, silver films [130] and on Au(111) [131] and thiophene molecules on Au(111) [132], and should then correspond to the sulfur atoms closer to the surface (a similar value has been reported for TTF molecules on graphene [133]). Figure 3.27d shows an example of the deconvolution peaks with the peak corresponding to the sulfur atoms close to the surface appearing at lower binding energy.

After annealing the sample at 400 K, the intensity of the peak is strongly reduced, and one of the two sulfur peaks disappears, while the other appears at a also different binding energy. This seems to indicate decomposition and/or desorption of the TTF molecule.

With respect to the C peak, the maximum of the C1s core level (figure 3.27a) can be located at 285.57 eV, 284.84 eV and 284.47 eV for samples grown at room temperature, and after annealing at 350 K and 400 K, respectively; that is, the peak shifts to lower binding energy when increasing the temperature. The shift between RT and 350 K could be due to the tilt of the molecule, that decreases the screening effect from the metal substrate. After annealing to 400 K (when the molecular chains appear), the intensity decreases dramatically, probably because the molecule desorb and/or decompose from the surface).

Let's consider the room temperature spectrum. This peak can be deconvoluted into two peaks, 285.28 and 285.97 eV, as shown in figure 3.27c. A Muliken population analysis of the electronic densities, obtained from DFT calculations, on every carbon atom, leads to two different groups. The four carbon atoms close to the hydrogen terminations have -0,004 e. The other two carbon atoms located on the molecular center and connected by double bound exhibit a positive charge, 0,126 e. Since a negative charge on an atom decreases the binding energy, the carbon close to the hydrogen terminations, should appear on the low binding energy of the spectra. The experimental area ratio between these two components, 4:2, is qualitatively consistent with this interpretation.

We have also estimated the relationship between the areas of the carbon and sulfur peaks. Since the molecule consists of 6 carbon atoms and 4 sulfur atoms, the theoretical ratio C:S ratio is 1.5. Taking into account the area of the elements and the sensitivity factor of each elements [134, 135], the experimental ratio between the areas should be $1.3(\pm 0.1)$, which is actually the case at all the temperatures, even after annealing at 400 K. Thus, although the XPS and STM images indicate significative changes and probably partial desorption, on the surface the relative amount of S and C atoms still remains

the same.

We also measured the work-function of the TTF/Ag(111) system in the different cases. The results are given in the table 3.2. In the case of room temperature deposition, the work-function decreases below to the work-function of the clean silver surface, which can be related to a combination of the so-called "Pillow effect" [136] and the dipole induced by the (small) charge transfer from the molecule to the substrate. A similar decrease has been observed for TTF on Au(111) [36]. However, when the system was annealed the molecules are not isolated and they self-assemble in ordered islands with the molecules tilted with respect to the surface. It can be expected that the work-function changes. If the work-function increases as a result of the fact that the number of molecules per unit area increases too and also the sulfur peak shifts to lower binding energy, 163.5 eV. So, The electronic dipole induce by this tilting could be the responsible for the observed increase in the work-function.

Table 3.2: *Worfunction of TTF on Ag(111)*

s	Worfunction (eV)
Ag(111)	4.74
Low Θ at RT	4.54
High Θ at RT	4.5
350 K	5.1

3.5 Conclusions

In this chapter, we have reported the different assemblies of different charge acceptor (TCNE, TCNQ) and an charge donor (TTF) molecule on metallic substrates.

In the case of the TCNE, we have observed the important role played by the substrate-molecule interaction. When the molecule was deposited on Au(111) directly with the substrate held at room temperature, well ordered islands were found. However, after annealing to room temperature, the molecules desorb from the surface.

For the silver substrate, upon deposition of TCNE on Ag(111) at 160 and 300 K two different Ag-TCNE coordination networks, with different stochiometries are formed. Contrary to previous reports, the silver adatoms come from the molecule induced step etching of the silver step edges. It is worthy to note that if deposition were done at room temperature, the

molecule induced step etching would be hard to guess, since at this temperature the steps practically recover the equilibrium room temperature phase. Also, XPS measurements and DFT calculations show that there is a significant charge transfer from the substrate to the molecule ($\sim$ 1 e), in agreement with the acceptor character for TCNE.

The growth of TCNQ on Ag(111) shows the existence of three different self-assembling process at the same time, and the participation of silver adatoms can not be definitely excluded. Again, the interaction between molecule and surface is very strong (unlike on Au(111)) with an appreciable charge transfer from the substrate to the molecule ($\sim$ 1 eV). On the other hand, in the case of a bilayer of TCNQ on Ag(111), the second layer is strongly decoupled from the substrate, and the molecular self-assembly is very similar to the case of TCNQ on Au(111). Due to this weak interaction, the molecule keeps practically neutral and the electronic properties of TCNQ layer almost unaltered.

Finally, the donor TTF molecules adsorbs in two possible configurations on the Ag(111) surface. After room temperature deposition the molecule is adsorbed almost planar on the surface, although their mobility is still very high. After annealing to 350 K, the molecules formed well-ordered islands in which the TTF is slightly tilted with respect to the surface. After annealing to 400 K, the molecules formed new islands with line shape, although these chains may not be composed of just intact TTF molecules as it can be corroborate with XPS measurements where the intensity of the peak decreases dramatically. In this case, and in agreement with its donor character the TTF molecules are slightly positively charge ($\sim$ 0.1 e).

4

Charge transfer complexes on Ag(111)

In this chapter we will discuss the adsorption and the assembly of combined donor-acceptor molecules on Ag(111). Two different systems will be described: TCNE-TTF and TCNQ-TTF.

4.1 Introduction

In the last years there has been great interest in the study of organic charge-transfer (CT) complexes [137, 138]. These complexes are molecular compounds mixing two species with different electron affinities: an electron donor (D, small ionization potential) and an electron acceptor (A, large electron affinity). In these compounds a partial charge is transferred from the HOMO of the donor to the LUMO of the acceptor molecule. Charge transfer processes between D-A complexes and metallic electrodes are at the heart of novel organic optoelectronic devices with interesting electrical and optical properties such as solar cells, OLEDs, to name a few [24–27, 139].

The first organic compound exhibiting metallic electrical conductivity [100], TTF-TCNQ, was discovered in 1973 [140]. It was formed from the electron donor tetrathiafulvalene (TTF) and the electron acceptor tetracyanoquinodimethane (TCNQ) [141, 142]. This salt crystallizes in a one-dimensionally stacked polymer, consisting of segregated stacks of cations and anions of the donors and the acceptors. The organic crystal forms by anisotropic non-covalent interactions between TTF and TCNQ. The TTF-

TCNQ crystal is monoclinic with lattice constants: a = 1.23 nm, b = 0.38 nm, c = 1.85 nm and build-up from similar stacks of the donor and acceptor molecule parallel to the short b axis. In this b directions the "ring double bond" overlap of molecular planes is characteristic of both molecule stacking, as shown in figure 4.1. The a direction corresponds to alternate rows of between donor and acceptor molecules. The charge transfer from TTF to TCNQ, 0.6 e, leads to a large metallic conductivity along the rows, and to a large resistive anisotropy [116]. The metallic behavior of the compound is due to: **i** the formation of bands through the π-overlapping of the molecular components, and **ii** the partial occupation of these bands at the Fermi level. The molecular packing maximizes the overlapping integral and, consequently, the amount of charge that can be delocalized along the stacks. The free carriers are generated in both π-stacked rows due to charge transfer between TTF and TCNQ (from the HOMO of the donor to the LUMO of the acceptor). This transferred charge is delocalised along the b direction of the crystal resulting in a quasi one-dimensional electron dispersion as it has been both described by theoretical DFT calculations [142, 143] and observed experimentally [144]. The discovery of this charge transfer complex opened up the field of molecular organic conductors.

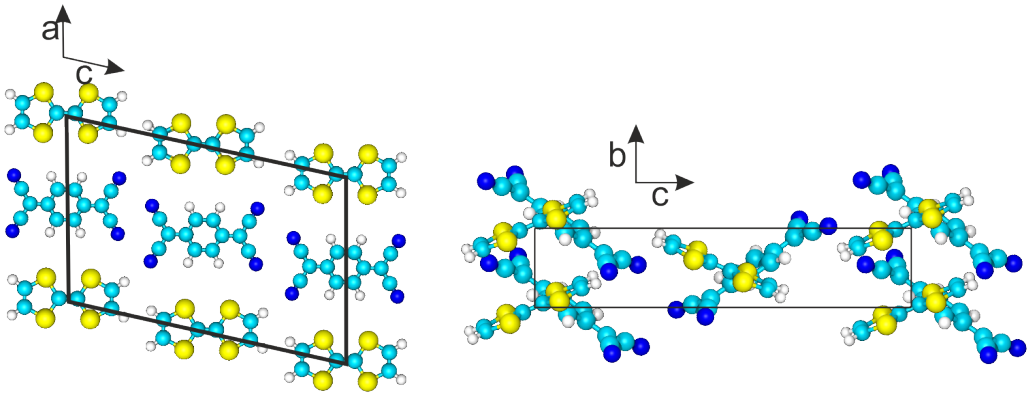

Figure 4.1: *Crystal structure of the TCNQ-TTF complex showing the a,b,c directions. (left side) view along onto the ac directions, (right side) view along the bc directions.*

TTF cations and TCNQ anions, stabilized by H-bonds [145]. This mixture is an organic conductor, but it is not a superconductor. The first organic molecule that is a superconductor, Tetramethyl-tetraselenafulvalene-phosphorus hexafluoride ($TMTSF_2PF_6$), was discovered in 1980 [146]. Charge transfer salts with superconducting capabilities were not achieved for several

years after the synthesis of TTF-TCNQ.

Although the growth of thin films of TTF-TCNQ on different substrates, like graphene [147] and Au(111) [122, 148] (see figure 4.1) has been reported, also DFT calculations [149], in contrast with the existing exhaustive study of the bulk properties of charge transfer solids [143, 150, 151], very little is known about the thin-film behavior. The transition from bulk D-A complexes to ultra-thin films of monolayer thickness deposited on metals introduces a new phenomenology related to the organic-inorganic interface. Effects like hybridization, CT with the surface and molecular level alignment become factors that may govern the electronic transport. Hence, the adsorption of an ultra-thin D-A on a metal opens a new field of research for the potential application of CT complexes as devices int he nanoscale. So, in this field it is very important to understand the organic-inorganic interface, the donor-acceptor layer effect on the metal surface. One of the few studies about the interface of TTF-TCNQ mixture has found that the interface retains its metallic character due to the charge transfer between the two molecules [152].

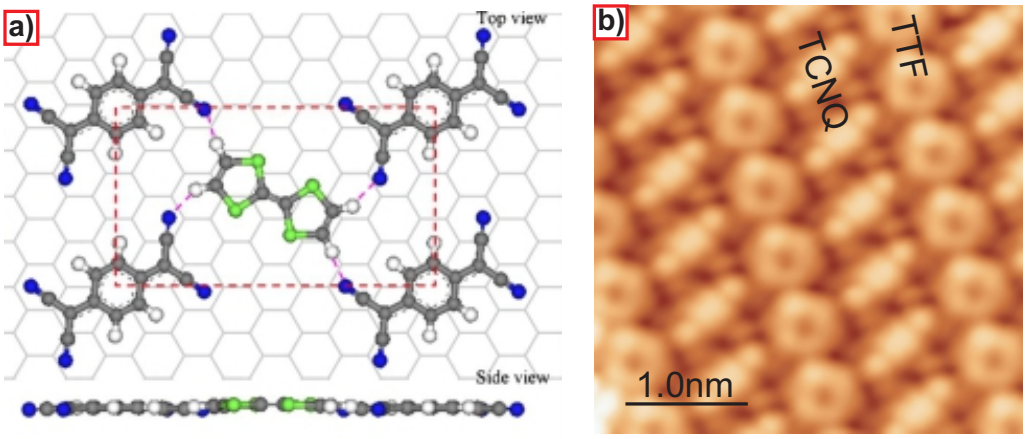

Figure 4.2: *a) Top and side view of the proposed model of TCNQ-TTF adsorbed on graphene (image taken from Ref [147]). b) STM image of the TCNQ-TTF complex on Au(111), (the stoichiometry ratio is 1:1); (image taken from the [122]).*

The metal/organic interfaces are a subject of increasing interest in the condensed matter community. Besides TCNQ-TTF, a large number of different charge transfer complexes have been reported, for example, TCNE-TTF [153–155], PCBM-exTTF [156], TTF-TNAP [157], (BEDT-TTF)-($SF_5CH_2CF_2SO_3$) [158] and TMTSF-TCNQ [159], among others mixtures with porphyrin or phthalocyanines [160–165].

4.2 TCNQ-TTF on Ag(111)

In the first part of this chapter, we have studied the mixed adsorption of TCNQ-TTF on Ag(111). When TCNQ and TTF are deposited at room temperature on Ag(111) they form spontaneously different mixed phases (figure 4.3). Naturally, the molecular arrangement inside these phases depends on the stoichiometry ratio of the donor and acceptor molecules (but not on the order of deposition). An excess of enough TTF leads to the formation of a mixed phase with stoichiometry 1(TCNQ):2(TTF); increasing the TCNQ concentration leads to the formation of the mixed phases: 1(TCNQ):1(TTF), 2(TCNQ):1(TTF) and 4(TCNQ):1(TTF). In the next section, we will study in more detail these structures: the arrangement of the molecules inside the islands and their electronics structure.

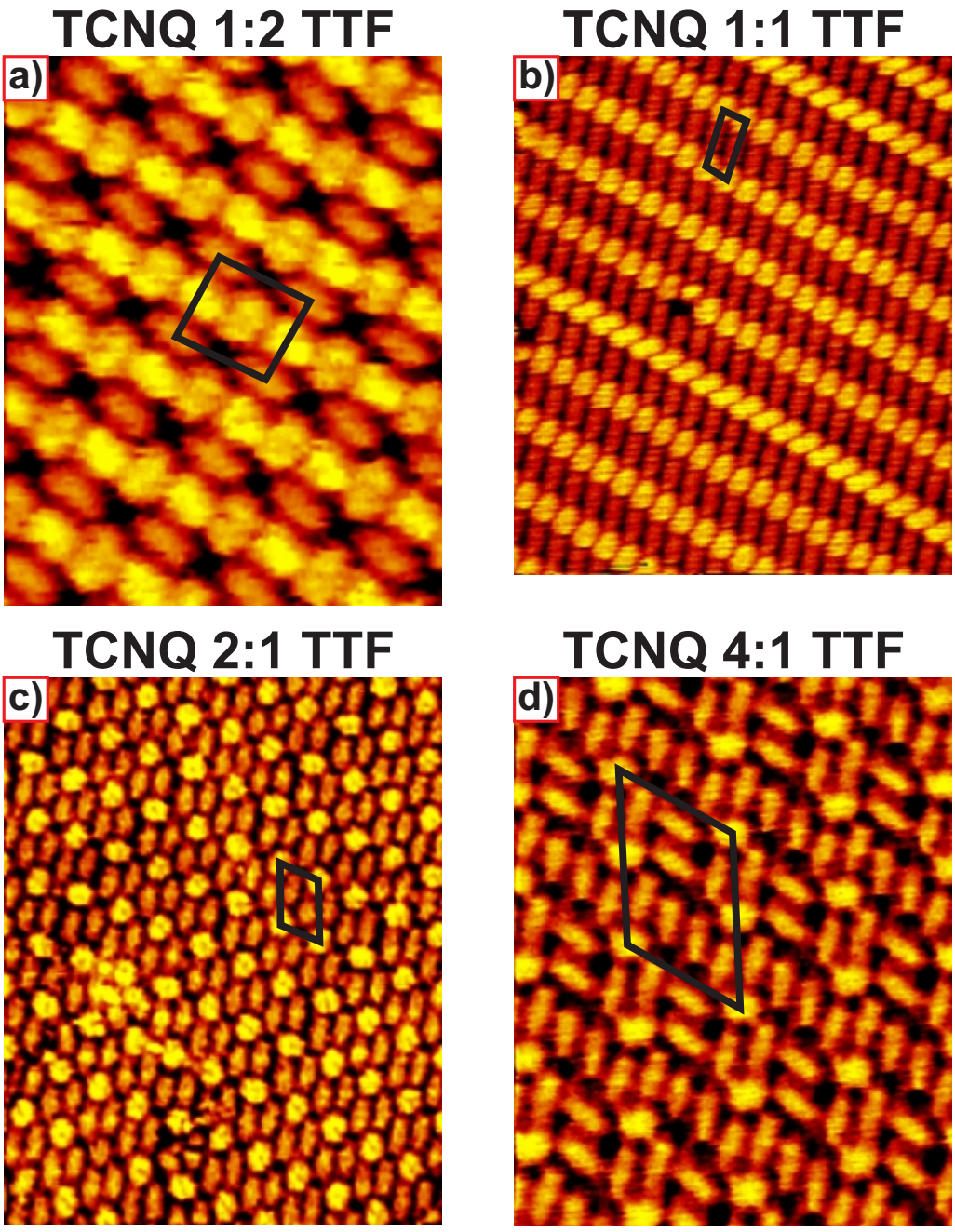

Figure 4.3: *STM images of the different phases of mixed TCNQ-TTF on Ag(111) with the following stoichiometry relation: a) 1:2. b) 1:1. c) 2:1. d) 4:1. a) 68 Å × 86 Å; -0.18 nA, -0.71 V. b) 129 Å × 154 Å; -0.29 nA, -0.67 V. c) 147 Å × 184 Å; -0.34 nA, -0.14 V. d) 98 Å × 123 Å; -0.35 nA, -0.76 V.*

4.2.1 TCNQ 1:2 TTF

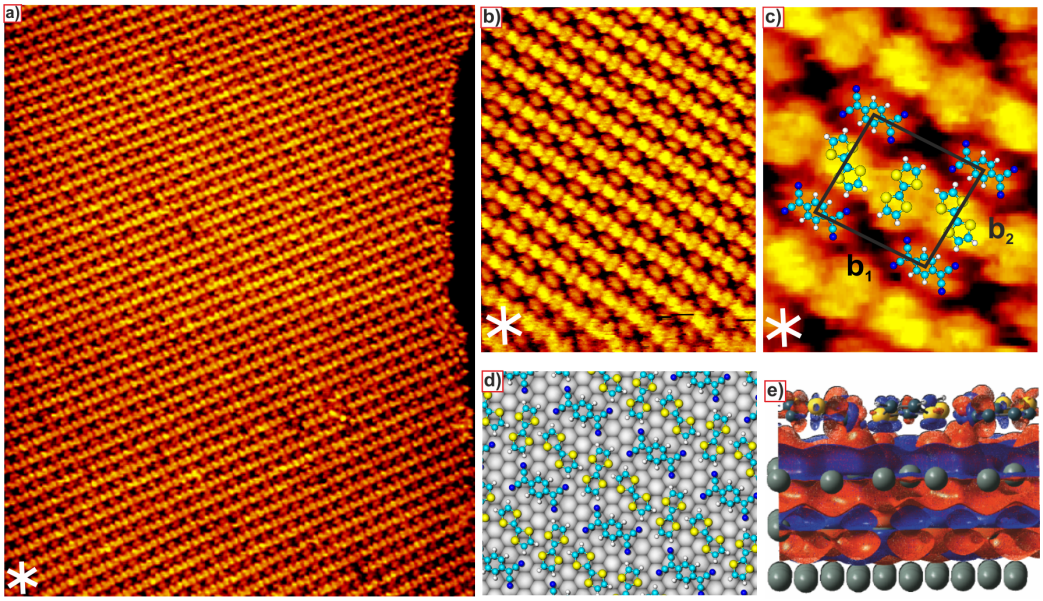

Figure 4.4: *Large STM images of a self-assemble domain of the mixed of TCNE 1:2 TTF on Ag(111) taken at 120 K. c) The self-assembly model of the mixed island above the STM image, the black square indicate the corresponding unit cell. d) DFT calculations taking into account the silver substrate. e) Induced charge density. Blue and red mean a defect and an excess of electrons, respectively. The adsorption only significantly affects the outermost layers of the substrate. a) 488 Å × 613 Å; -0.2 nA, -0.74 V. b) 147 Å × 184 Å; -0.18 nA, -0.71 V. c) 34 Å × 45 Å; -0.18 nA, -0.71 V.*

Figure 4.4a and figure 4.4b show representative STM images (recorded at 120 K) after depositing TCNQ and TTF on Ag(111) at room temperature. Ordered islands that extended over hundreds of angstroms onto the substrate form spontaneously on the surface. As shown in figure 4.4b, we can easily identify two different rows. The structure seems to be composed of alternate parallel rows of the two molecules, where one row (bright) is composed of TTF molecules and the other (dark) of TCNQ molecules. In the TTF row the molecules alternate between two different orientations. A closer look at the STM images (figure 4.4c) reveals the internal structure of the island. The unit cell of this structure contains one TCNQ molecule and two TTF molecules, as shown in figure 4.4c; the sides of this cell are $b_1 = 13.9(\pm 0.6)$ Å, $b_2 = 14.0(\pm 0.8)$ Å, and $\gamma = 90^0$. The proposed model (actually, the final

result of a DFT calculations, see below) is shown in figure 4.4d. The matrix describing the epitaxial relationship with the substrate can be written as $\begin{pmatrix} b_1 \\ b_2 \end{pmatrix} = \begin{pmatrix} 0 & 5 \\ 6 & 3 \end{pmatrix} \begin{pmatrix} a_1 \\ a_2 \end{pmatrix}$.

The lattice parameters for this model measure $\boldsymbol{b_1} = 14.67$ Å, and $\boldsymbol{b_2} = 15.25$ Å, in good agreement with the experimental values. The observed arrangement can be explained by the formation of S$\cdots$H-C hydrogen bonds between TTF molecules, while TTF and TCNQ are connected by C$\equiv$N$\cdots$H-C and S$\cdots$H-C hydrogen bonds.

As mentioned in chapter 2, the theoretical calculations for the mixed TCNQ-TTF phases presented in this chapter were made by *the group of Fernando Martín* from the Universidad Autónoma de Madrid. In order to estimate atomic charges, topological analyses of the electron density were carried out based on Bader's atoms-in-molecules (AIM) theory by using the Bader analysis program [166–168]. However, for a better comparison with the results in the previous chapter, we have also performed a Mulliken population analysis. In general, both results are very similar, and follow almost exactly the same trend when comparing different phases.

Table 4.1 shows the results of both methods (the Bader results in parenthesis) for the partial charges of the three molecules in the unit cell, the two TTF molecules (edge and central denote the position in the unit cell marked in figure 4.4c), and the TCNQ molecule. Both TTF hold a small positive charge (around 0.24 e), confirming their donor character. On the other hand, the acceptor TCNQ molecule takes -1.10 e from its environment (that is, -0.24 e from each TTF molecule and -0.62 e from the silver substrate). However, calculated charge density difference isosurfaces (blue and red mean a defect and an excess of electrons, respectively) show that the charge transfer from TTF to TCNQ takes place through the substrate, and not directly between the molecules as shown in figure 4.4e; that is, TTF donates charge to TCNQ via the Ag surface.

We can compare these results with the partial charges of the molecules in a free-standing layer of TTF-TCNQ with exactly the same geometry but without the silver substrate. In this case, TCNQ holds a negative charge of -0.83 e, with each TTF molecule donating 0.42 e. Thus, the presence of the silver substrate increases slightly the acceptor character of TCNQ and decreases "the donating effort" of TTF, since TCNQ can take the electrons more easily from the silver substrate. This can be easily explained because the difference between the electron affinity of TCNQ (2.81 eV), and the work-function of Ag(111) (4.74 eV) is smaller than the difference between the electron affinity of TCNQ and the ionization potential of TTF (6.83 eV).

Table 4.1: *Partial charge of the different molecules on the Ag(111) in the mixed phase TCNQ-TTF, 1:2 stoichiometry (where $\Delta q < 0$ corresponds of a gain of electrons and $\Delta q > 0$ indicates a loss of electrons). Both Mulliken and Bader (in parenthesis) results are given. Results are also given for a free-standing layer with exactly the same geometry but wihouth the silver substrate.*

	$Q(gas\ phase)$ (e-)	$Q(Ag(111))$ (e-)
Ag		+0.62 (+1.06)
TTF (Edge)	+0.42 (+0.36)	+0.24 (+0.14)
TTF (Central)	+0.43 (+0.45)	+0.23 (+0.24)
TCNQ	-0.83 (-0.81)	-1.10 (-1.44)

We have also estimated the adsorption energy per molecule as the difference between the total energy of the system and the sum of the total energies of the free relaxed molecules and the surface as

$$E_{ad} = E_{(TCNQ+TTF/Ag)} - [E_{Ag} + (E_{TCNQ} + E_{TTF}] \tag{4.1}$$

For this phase with 1 TCNQ and 2 TTF the adsorption energy is $E_{ad} = -2.49eV/molec.$

4.2.2 TCNQ 1:1 TTF

Figure 4.5a shows a STM image, acquired at 120 K, of a new mixed TCNQ-TTF phase obtained by depositing additional TCNQ molecules with the substrate held at room temperature during the deposition. Again, the molecules form well-ordered islands. Figure 4.5b and figure 4.5c show close-up STM images of this phase, which seems to be composed of parallel rows of TTF (bright) and TCNQ (dark) molecules. In this case, the unit cell contains one TCNQ and one TTF molecule, as shown in figure 4.5c. There are two types of TTF rows, in which the orientation of the TTF molecules differs by $\sim 35^0$. In the following we will consider only the unit cell shown in figure 4.5c. The sides of this cell are $b_1 = 7.5(\pm 0.8)$ Å, $b_2 = 19.2(\pm 0.9)$ Å, and $\gamma = 100^0$. A model for this structure is proposed in figure 4.5d. In this model the TCNQ molecules interact with the TTF molecules through the formation of S$\cdots$H-C hydrogen bonds, and one another by the formation of C$\equiv$N$\cdots$H-C hydrogen bonds. For this arrangement, the matrix describing the epitaxial relationship with the substrate can be written as $\begin{pmatrix} b_1 \\ b_2 \end{pmatrix} = \begin{pmatrix} 2 & -1 \\ 4 & 8 \end{pmatrix} \begin{pmatrix} a_1 \\ a_2 \end{pmatrix}$. Theoretical calculations was carried out and similar value was obtained. The values of the molecular charges obtained from the DFT calculations are shown in Ta-

ble 4.2. In this case TTF holds a positive charge of +0.42 e, while TCNQ is negatively charge with -1.02 e (that is, 0.6 e of every TCNQ molecule are coming from the silver substrate). Figure 4.5e shows a plot of a charge density difference isosurface. Also in this case the results of the theoretical calculations indicate that charge transfer takes place through the substrate and not directly between molecules. The adsorption energy for this arrangement is -2.27 eV/molec. The formation of a 1:1 TCNQ-TTF phase has been already reported on Au(111) [122, 148, 169] with the same arrangement and similar unit cell. In this case the TCNQ gains charge directly (one electron) from the TTF, due to the interaction with the surface is mainly dominated by the TTF molecule and the interaction between TCNQ and the substrate is weak.

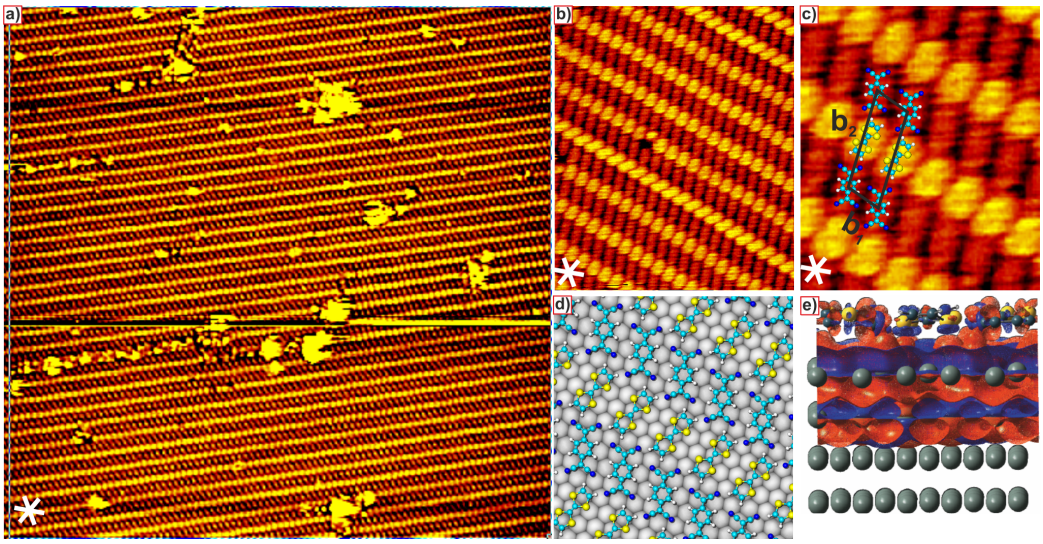

Figure 4.5: *Topogpahic STM images of a self-assemble domain of the mixed of TCNQ 1:1 TTF on Ag(111) deposited at RT and acquired at 120K. c) The self-assembly model of the mixed island above the STM image, the black square indicate the corresponding unit cell. d) DFT calculations taking into account the silver substrate. e) Induced charge density. Blue and red mean a defect and an excess of electrons, respectively. a) 681 Å × 662 Å; -0.2 nA, -0.71 V. b) 147 Å × 184 Å; -0.29 nA, -0.67 V. c) 43 Å × 51 Å; -0.29 nA, -0.67 V.*

For comparison, the partial charges for a free-standing layer of TCNQ 1:1 TTF with the same geometry has also been calculated. In this case the charge transfer from TTF to TCNQ is $\sim$ 0.6 e. Again, the presence of the silver substrate increases the acceptor character of TCNQ, which now takes $\sim$ 0.42 e from TTF and 0.6 e- from the silver substrate.

Table 4.2: *Partial charge of the TCNQ and TTF on the Ag(111) in the mixed phase TCNQ-TTF, 1:1 stoichiometry. Again both mulliken and Bader (in parenthesis) results are given. Also for a free-standing layer with the exactly same geometry.*

	$Q(gas\ phase)$ (e-)	$Q(Ag(111))$ (e-)
Ag		+0.6 (+1.12)
TTF	+0.67	+.42 (+0.3)
TCNQ	-0.67	-1.02 (-1.42)

It is worthy to note that the charge transfer calculated for the free-standing layer coincides with the charge transfer in the bulk compound, even though the geometry is rather different. As mentioned before, in bulk the molecules from separate rows stabilized by π-π interactions, and the TCNQ molecules in one row are rotated 58.5^0 with respect to the TTF molecules in the neighboring rows [170]. In here, the molecules are almost planar on the silver surface. This seems to be in agreement with the results of Beltrán et al. [149], that indicate that the amount of charge transfer, related to the different $\varepsilon HOMO(TTF) - \varepsilon LUMO(TCNQ)$, should not depend very much of the details of the TTF/TCNQ interface geometry, as long as it is metallic.

4.2.3 TCNQ 2:1 TTF

After increasing the TCNQ concentration, a new phase of the TCNQ-TTF mixture was obtained, as shown in figure 4.6. Again, the molecular domains extend over hundreds of angstroms on the silver surface. Some defects in the domains can be observed in the image as large hollows. Figure 4.6b and figure 4.6c show close-up images of this mixed phase. The bright protrusions are the TTF molecules, and each molecule is surrounded by six TCNQ molecules. In this case the acceptor TCNQ forms zig-zag rows that interact by C≡N$\cdots$H-C hydrogen bonds with one another and through $S\cdots$H-C bonds with the TTF molecules. The sides of the unit cell are $b_1 = 13.6(\pm 0.6)$ Å, $b_2 = 17.2(\pm 0.7)$ Å, and $\gamma = 80^0$. Figure 4.6d shows a model for this mixed phase, where the unit cell contains two TCNQ molecules and one TTF molecule. For this assembly, the matrix describing the epitaxial relationship with the substrate can be written as $\begin{pmatrix} b_1 \\ b_2 \end{pmatrix} = \begin{pmatrix} 4 & -1 \\ 7 & 6 \end{pmatrix} \begin{pmatrix} a_1 \\ a_2 \end{pmatrix}$. Again the theoretical calculations was carried out with the experimental unit cell by relaxed structure of a TTF-TCNQ layer which results in $b_1 = 13.45$ Å and $b_2 = 17.85$ Å, in good agreement with the experimental values. The results of the DFT calculations concerning the charge transfer are shown in Table 4.3.

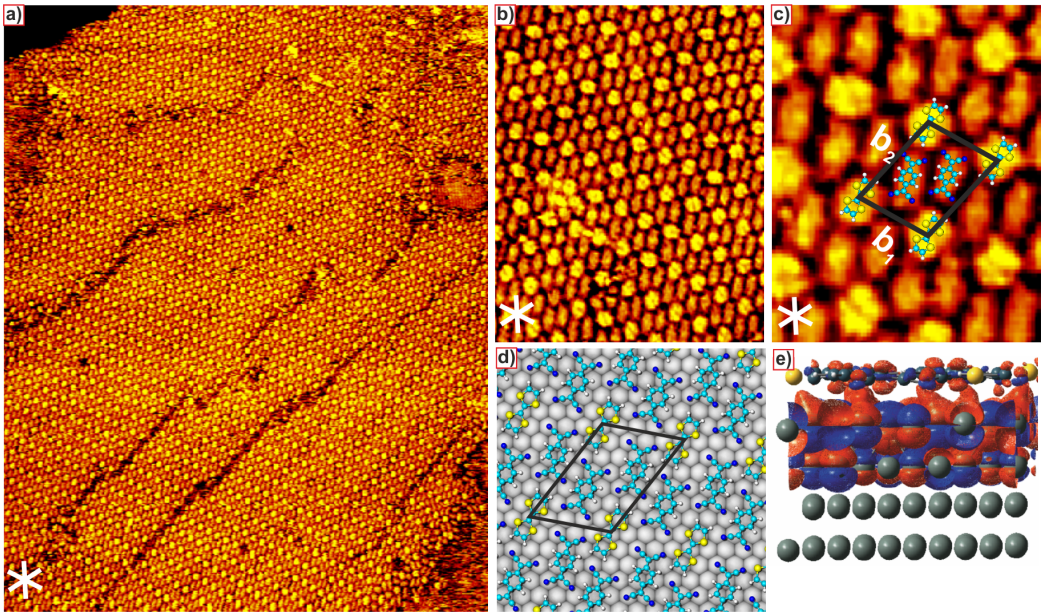

Figure 4.6: *Large STM images of a self-assembly domain of the mixed of TCNQ 2:1 TTF on Ag(111) deposited at RT and acquired at 120 K. c) The self-assembly model of the mixed island above the STM image, the black square indicate the corresponding unit cell. d) DFT calculations taking into account the silver substrate. e) Induced charge density. Blue and red mean a defect and an excess of electrons, respectively. a) 681 Å × 662 Å; -0.2 nA, -0.71 V. b) 147 Å × 184 Å; -0.34 nA, -0.14 V. c) 49 Å × 61 Å; -0.34 nA, -0.14 V.*

Table 4.3: *Partial charge of the different molecules on the Ag(111) in the mixed phase TCNQ-TTF, 2:1 stoichiometry (where $\Delta q < 0$ corresponds of a gain of electrons and $\Delta q > 0$ indicates a loss of electrons). Both Mulliken and Bader (in parenthesis) results are given. Results are also given for a free-standing layer with exactly the same geometry but wihouth the silver substrate.*

	Q*gas phase* (e-)	Q*Ag*(111) (e-)
Ag		+1.32 (+2.2)
TTF	+0.92	+0.51 (+0.37)
TCNQ (up)	-0.47	-0.93 (-1.30)
TCNQ (down)	-0.45	-0.94 (-1.27)

TTF donates +0.51 electrons to the silver substrate. The two types of TCNQ hold a with similar charge (-0.9 e), so in this case 0.66 e in each TCNQ are coming form the silver surface. As in the previous cases, charge density

difference isosurfaces (figure 4.6e) show that the charge transfer takes place through the substrate, and not directly between molecules. The adsorption energy for this arrangement is -3.05 eV/molec.

4.2.4 TCNQ 4:1 TTF

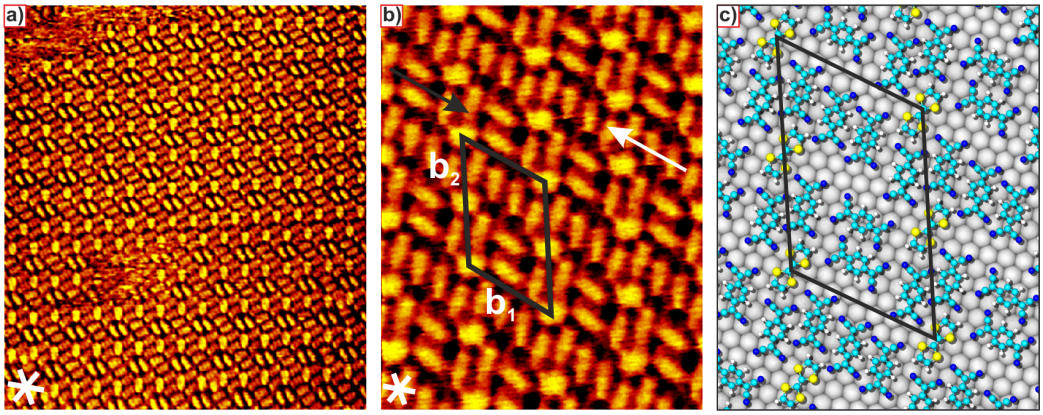

Figure 4.7: *a) Large STM image of a self-assemble domain of the mixed of TCNQ 4:1 TTF on Ag(111) deposited at RT and acquired at the same temperature. b) Zoom of TCNQ-TTF with 4:1 stoichiometry. c) Proposed structural model indicating the epitaxial relationship with respect to the silver surface. a) 291 Å × 325 Å; -0.52 nA, -0.45 V. b) 98 Å × 123 Å; -0.35 nA, -0.76 V.*

Figure 4.7a shows a large STM image of a new self-assembled mixed TCNQ-TTF phase obtained after further increasing the dosage of TCNQ. A close-up image is shown in figure 4.7b. This phase can be view as composed of two types of rows of TCNQ molecules with TTF molecules between the rows. The first type has a zig-zag shape (marked with white arrow) and is very similar to those found in the mixture TCNQ-TTF with 2:1 stoichiometry. The other row, marked with black arrow, is made by alternating couples of TCNQ molecules rotated 90^0 with respect to the next pair of TCNQ molecules. Every TTF molecules is surrounded by six TTF molecules, as in the 2:1 TCNQ-TTF phase. The unit cell contains 8 TCNQ and 2 TTF molecules, and the sides of this cell are $b_1 = 27.1(\pm 0.8)$ Å, $b_2 = 39.9(\pm 0.9)$ Å, and $\gamma = 120^0$. Figure 4.7c shows a model for this arrangement, the matrix describing the epitaxial relationship with the substrate can be written as $\begin{pmatrix} b_1 \\ b_2 \end{pmatrix} = \begin{pmatrix} 7 & -3 \\ 4 & 14 \end{pmatrix} \begin{pmatrix} a_1 \\ a_2 \end{pmatrix}$. Due to the size of this new unit cell, theoretical calculations for this mixtures have not been carried out.

4.3 TCNE-TTF on Ag(111)

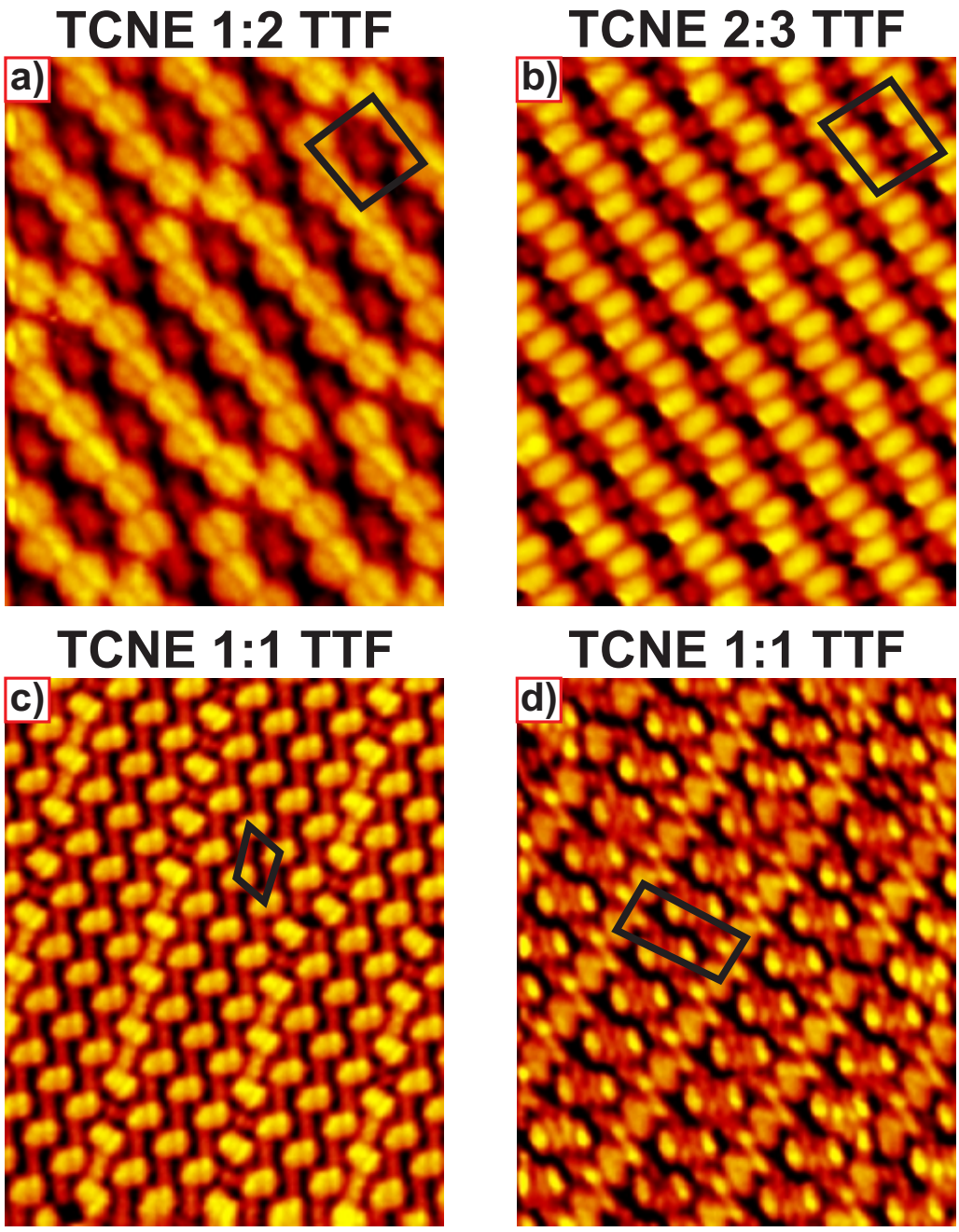

Figure 4.8: *STM images of different domains of mixed TCNE-TTF on Ag(111) with the following stoichiometry relation: a) 1:2. b) 2:3. c) 1:1. d) 1:1 with silver adatoms. a) 68 Å × 86 Å; 0.68 nA, 0.31 V. b) 98 Å × 123 Å; 0.55 nA, 0.30 V. c) 98 Å × 123 Å; -0.3 nA, -0.11 V. d) 98 Å × 123 Å; -0.53nA, -1.53V.*

In the next series of experiments, we have studied the mixed adsorption of TCNE-TTF on Ag(111). First of all, we have checked that the order of deposition of the acceptor and donor molecules does not play an important role. So, the acceptor can be deposited before or after the donor molecule and the self-assembly of the TTF-TCNE structures does not change. To avoid confusions, all the experiments shown in this section have been realized by depositing first the donor molecule TTF and then the acceptor TCNE. When TTF and TCNE are deposited on Ag(111) at room temperature they form spontaneously different mixed phases with molecular arrangements whose structure depends only on the ratio of both molecules on the surface. Figure 4.8 shows all the different phases that can be found. An enough excess of TTF reveals the formation of a mixed phase with stoichiometry (TCNE)1:2(TTF); after increasing the TCNE concentration, another mixed phases appear: (TCNE)2:3(TTF), (TCNE)1:1(TTF) and another different phase with 1:1 stoichiometry but with the participation of silver adatoms. In every case, the arrangement of the molecules inside this phases lead to chiral structures (see below).

4.3.1 TCNE 1:2 TTF

Figure 4.9 shows STM images, taken at 125 K, of the mixed phase 1:2 (TCNE:TTF) on Ag(111). The substrate was kept at room temperature during molecular deposition. The molecular domains extend over hundreds of angstroms over the substrate. The molecules seem to form chains spontaneously, although the size of each singular chain is different due to defects in the arrangement. Figure 4.9a shows two possible configurations of the chains (black and blue) with orientations that differ 10^0 respect to the high symmetry directions of the silver surface. The chains are built by connecting either the upper part of the following chain with the center of previous chain, or connecting the lower part of the next chain with the center of the chain, in the other case. However, the axis of the isolated chains (marked in black and blue arcs in figure 4.9a and black arcs in figure 4.9 d) are oriented along the high symmetry directions of the silver surface. Figure 4.9b shows a zoom inside the mixed island, where the singular chain is consisting by two semicircle, which each semicircle is made of 5 TTF molecule and two TCNE molecules inside the chain, on the upper/lower part of the chain is around three TCNE molecules. This size of the chain (5 TTF) is the more common but also it can be found with 4-6 TTF molecules.

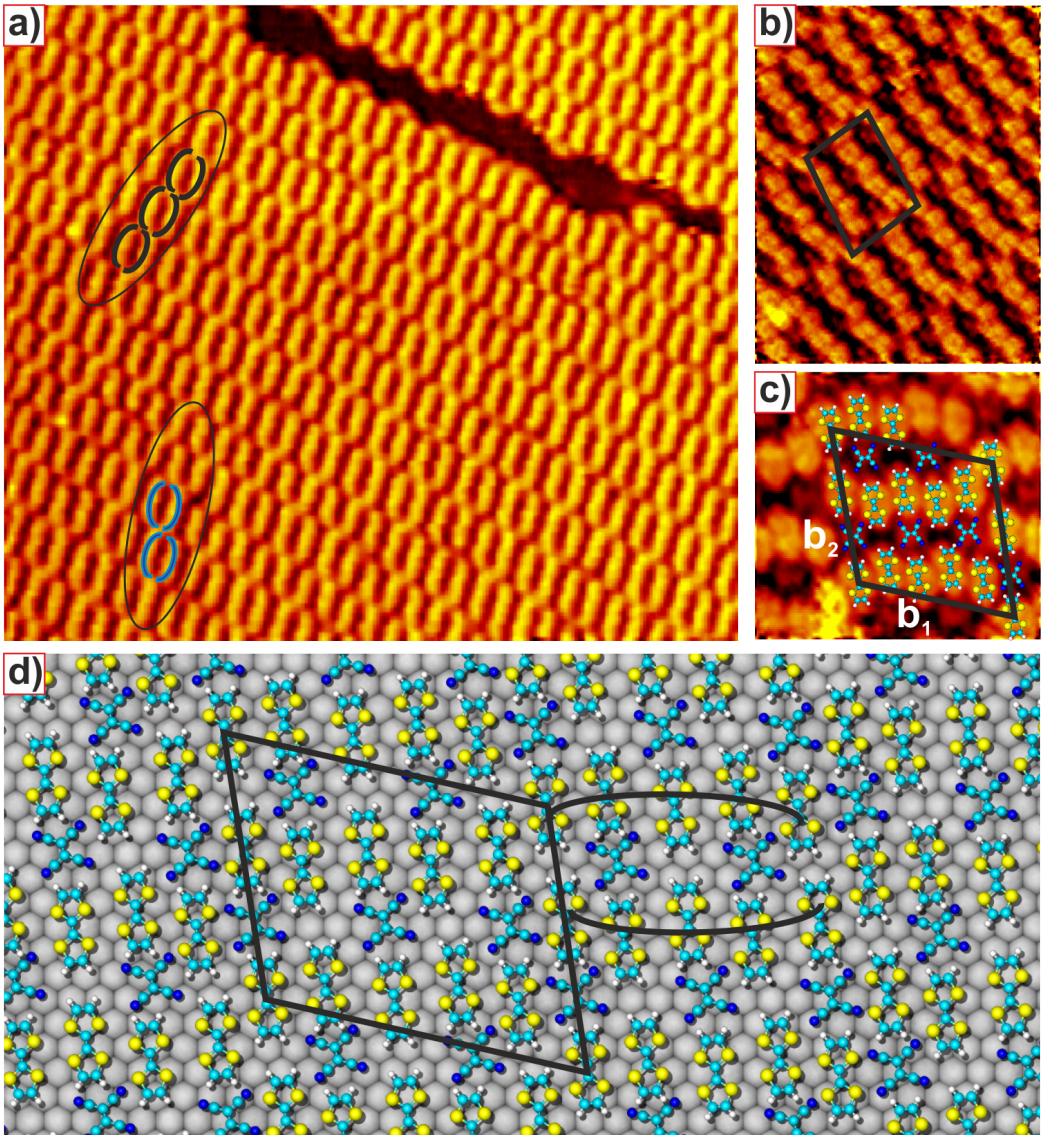

Figure 4.9: *a-c) STM images, taken at 125 K, of a self-assembled domain of the mixed TCNE 1:2 TTF phase on Ag(111). a) The two ellipses mark the two possible direction of the chains. c) A close-up STM image with the molecular structures superimposed. The black square indicate the unit cell. d) Proposed structural model indicating the epitaxial relationship with respect to the silver surface. a) 489 Å × 423 Å; -0.45 nA, -0.78 V. b) 98 Å × 123 Å; -0.38 nA, -0.48 V. c) 55 Å × 51 Å; -0.93 nA, -0.48 V.*

Figure 4.9c shows a zoom inside this island with a model of the unit cell superimposed. The unit cell of this structure contains five TCNE and

ten TTF molecules, with sides $b_1 = 34(\pm 0.9)$ Å, $b_2 = 29.6(\pm 0.8)$ Å, and $\gamma = 110^0$. For this assembly, the matrix describing the epitaxial relationship with the substrate can be written as $\begin{pmatrix} b_1 \\ b_2 \end{pmatrix} = \begin{pmatrix} 10 & -3 \\ 4 & 11 \end{pmatrix} \begin{pmatrix} a_1 \\ a_2 \end{pmatrix}$. Figure 4.9d shows a model of this mixed phase.

The TTF molecules form *zig-zag* chained structures uniformly over the surface. The interaction between TTF molecules is dominated by S$\cdots$H-C hydrogen bonds. This self-assembly is very similar to what has been reported on Au(111) for a coverage of 0.5ML [36, 122, 171]. In the upper part of the figure 4.9c has drawn three TTF molecules, where the center molecule is connected to the other molecules from its hydrogen atoms to the sulfur atoms of its neighboring. Hence the hydrogen bonds of this molecule are full. On the other hand, each TCNE molecule is surrounded by six TTF molecules, where the TTF upper and lower are connected by hydrogen bonds to the neighbors TTF. The other 4 TTF are interacted with TCNE by C$\equiv$N$\cdots$H-C hydrogen bonds. This bonds constitutes part of the driving force behind the mixed phase formation.

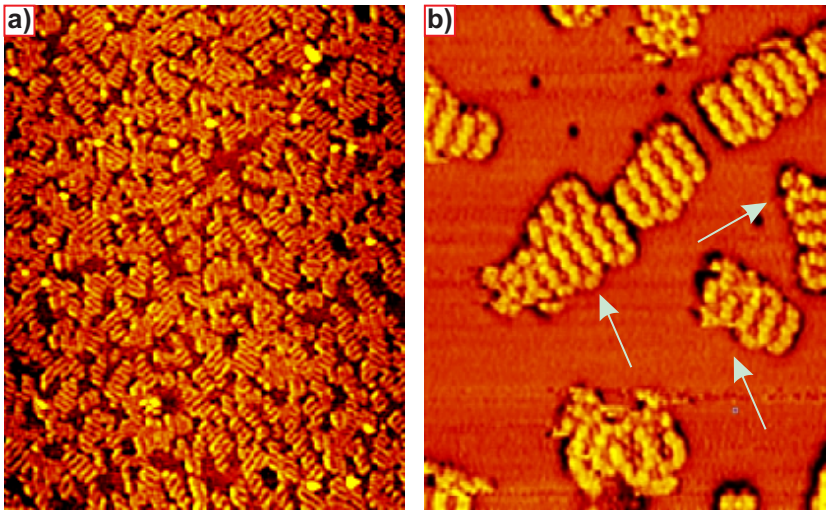

Figure 4.10: *Large STM images of early stages of the mixed TCNE 1:2 TTF on Ag(111) when the TCNE are deposited directly to the STM at 125 K and imaged at the same temperature. a) 978 Å × 1227 Å; -0.53 nA, -0.67 V. b) 293 Å × 368 Å; -0.49 nA, -0.74 V.*

Low temperature (125 K) deposition of TCNE onto TTF molecules on Ag(111) results in the formation of small islands, as shown in figure 4.10. That have the same appearance than the large chains but in this case they

consists of only one link: at this temperature the molecules have enough mobility to form the TCNE-TTF mixture, but not enough energy to build the large chains. In figure 4.10 it can be observed also the three possible orientations of the chains (marked by white arrow) for this arrangement, which also coincide with the high symmetry axis of the silver surface. Moreover, these small islands can be converted into large domains like those shown in figure 4.9a by increasing the temperature up to room temperature. In addition, these self-assemblies are the early stages of the mixed TCNE 1:2 TTF.

4.3.2 TCNE 2:3 TTF

Figure 4.11 presents an STM image, acquired at 150 K, of a mixed TCNE-TTF phase, obtained by depositing additional TCNE molecules. The substrate was kept at room temperature during molecular deposition. The molecules form spontaneously mixed domain. Figure 4.11a shows a typical overview STM image revealing highly ordered domains composed of alternating long bright rows of TTF and dark rows of TCNE. The rows can be found oriented in six different directions. The ordering along the TTF rows is very similar to the chain order and it is dominated by S$\cdots$H-C hydrogen bonds. The molecules are located in three different heights, as shown in the figure marked by this circle. It is like a stair of three steps and it is connected to the next by the upper molecule with the following bottom molecule. Moreover, the neighboring rows are closer, figure 4.11b marked by ellipsoid, in where the upper molecule in one row are always close to the bottom molecule in the other row. This arrangement avoid the formation of TCNE rows and these molecules are connected by pairs of TCNE inside this mixed. This self-assembly can be observed with more details in the high resolution STM image shown in figure 4.11c. From the STM image a model of the planar self-assembled mixed phase can be tentatively suggested where the acceptors and donors molecules interact and form a hydrogen bonds network by short range C$\equiv$N$\cdots$H-C connections. In this case the unit cell consists of two TCNE and three TTF molecules, with $b_1 = 16.3(\pm 0.8)$ Å, $b_2 = 18.8(\pm 0.6)$ Å, and $\gamma = 70^0$. For this assembly, the matrix describing the epitaxial relationship with the substrate can be written as $\begin{pmatrix} b_1 \\ b_2 \end{pmatrix} = \begin{pmatrix} 6 & 5 \\ -1 & 6 \end{pmatrix} \begin{pmatrix} a_1 \\ a_2 \end{pmatrix}$. The orientation of this unit cell is not along the high symmetry axis of the silver substrate allowing the formation of this mixed phase in 6 different orientations (figure 4.12a) (three of them can be seen in figure 4.11a). Some of them,V and VI, can be seen in figure 4.12c and figure 4.12d. They are chiral between them.

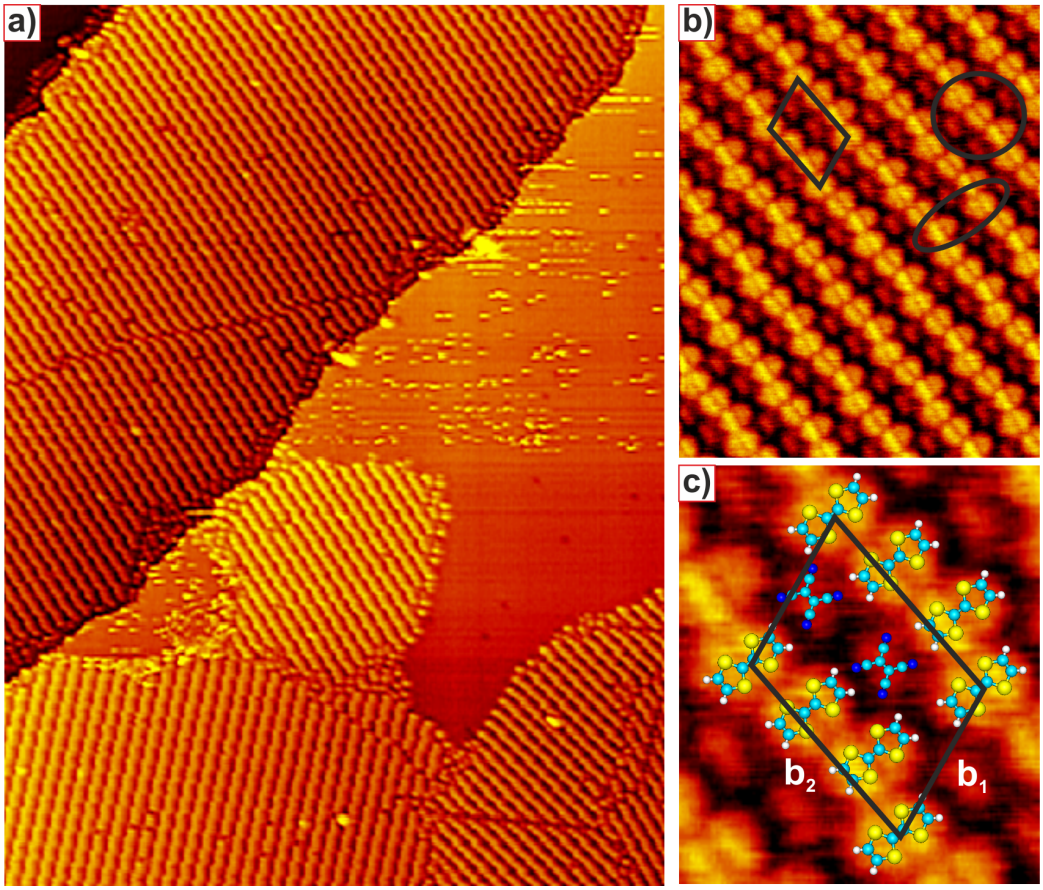

Figure 4.11: *STM images, taken at 150 K, of a molecular self-assembled domain of the mixed TCNE 2:3 TTF on Ag(111) at RT. c) STM image of the mixed domain is presented with the model superimposed to illustrate the surface unit cell. a) 692 Å × 924 Å; 0.44 nA, 0.78 V. b) 98 Å × 123 Å; -0.3 nA, -0.08 V. c) 33 AA × 39 Å, -0.3 nA; -0.08 V.*

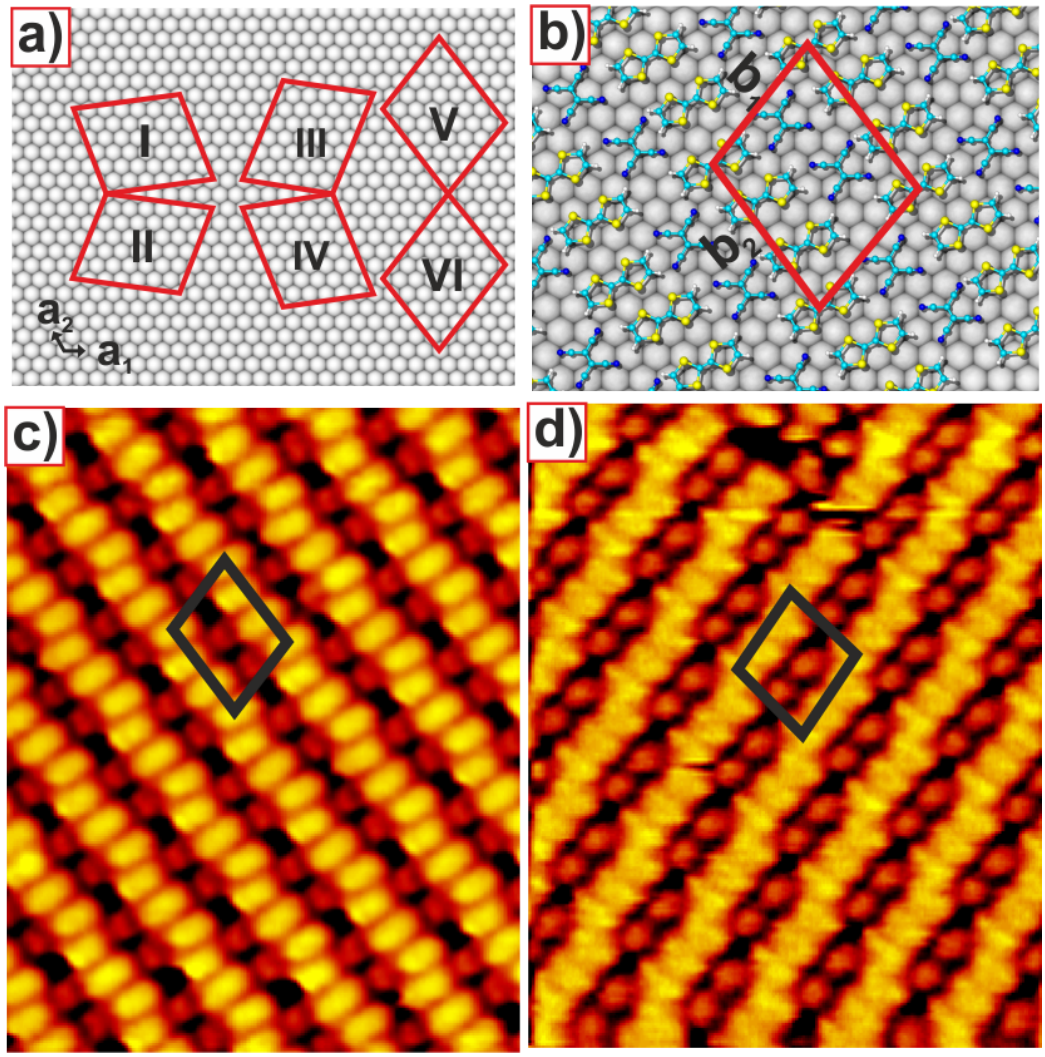

Figure 4.12:
The six different possible orientations of the experimentally measured unit cell on Ag(111) for the 2:3 TCNE-TTF mixed phase. b) Proposed structural model indicating the epitaxial relationship with respect to the silver surface. c-d) STM image for two orientations of this acceptor-donor networks, V and VI, respectively. c) 98 Å × 123 Å; 0.55 nA, 0.30 V. d) 98 Å × 123 Å; -0.34 nA, -0.35 V.

4.3.3 TCNE 1:1 TTF

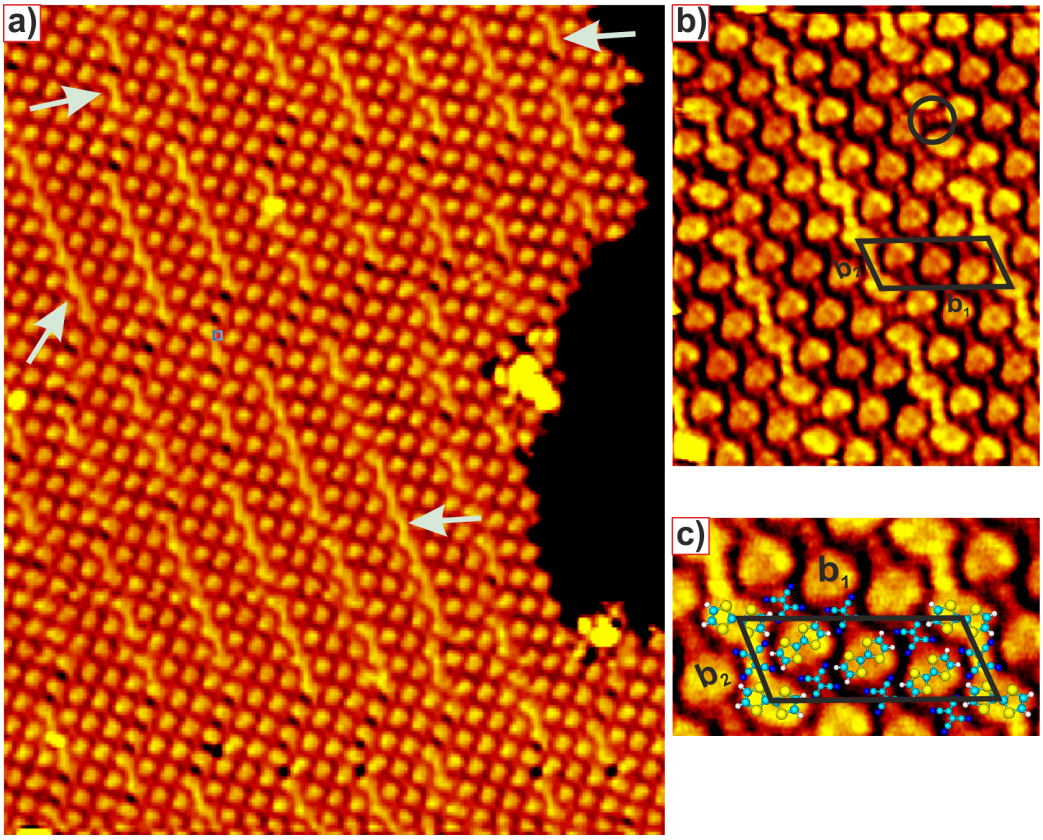

Figure 4.13: *a) Large STM image of a supramolecular phase of mixed TCNE 1:1 TTF on Ag(111) taken at 133 K. The bright rows consists of TCNE and TTF molecules, where TTF are slightly rotated with respect to the TTF inside the other part of the island. b) Self-assembled mixed phase of TCNE-TTF on Ag(111). c) Zoom inside the mixed island with the model of the unit cell superimposed, the black square indicate the unit cell. a) 293 Å × 368 Å; -0.49 nA, -0.99 V. b) 98 Å × 123 Å, -0.43 nA, -0.99 V. c) 59 Å × 34 Å, -0.43 nA, -0.99 V.*

Increasing a bit more the TCNE dosage on the surface, the "row islands" disappear and a new arrangement of this mixed phase is observed, as shown in figure 4.13. In this large topographic image can be found bright protrusions (marked by white arrow) with different lengths and some ordered between them. Figure 4.13b shows this self-assembled inside this bright protrusions where it can be observed three rows between them. A close-up of this mixed phase shown in figure 4.13c, where the bright rows are made of alternate

TCNE and TTF molecules, with this resolution can be understood why in the large images these rows have different lengths. Figure 4.13b shows a defect (marked by this black circle), where the TCNE molecule are rotated 90^0 respect to the other TCNE on the rows but the TTF always has the same orientation. As consequence of that the global appearance looks like a discontinuous bright rows. On the other hand, The other rows are also made of alternate TTF and TCNE molecules, but the donor molecules are rotated 60^0 with respect to the other TTF inside the bright rows. In addition, the arrangement between TCNE-TTF molecule are different than the other mixed phase. In the other cases the TCNE can be found in the head-on position of the TTF molecule. Here the TCNE is positioned at the head-on position but also at the side of the TTF and the molecular coordination are changed. In order to know which is the trigger in this mixed phase. It has been reported that TTF with $\sim$ 0.8 ML on Au(111) induces 2D TTF-island, where the molecules pack densely in a parquet-like structure where adjacent molecules are rotated also 60^0 [36, 122]. Moreover, it has been reported that the phase transformation of the 2D metal-organic coordination networks driven by in-plane compression of trispyridylbenzene (TPyB) with copper on Au(111) [172]. So, the molecular coordination could be depend on the stoichiometry and the density of the molecules inside the island. We estimated the molecular density on the different TCNE-TTF domains:

Table 4.4

TCNE-TTF domain	molecular density ($1/\text{Å}^2$)
1:2	0.34
2:3	0.36
1:1	0.37

The donor-acceptor network with more molecular density per Å as the 1:1. As a consequence of this results with the stoichiometry changes and the pack densely of TTF on Au(111) with higher coverage. It can be explained the changes in the molecular coordination for this mixture 1:1 TCNE-TTF, where some TTF are rotated 60^0 respect to others. Again, as the other phases, the self-assembled structure is stabilized via S$\cdots$H-C hydrogen bonds between TTF molecules and via C$\equiv$N$\cdots$H-C hydrogen bonds between acceptor and donor molecules.

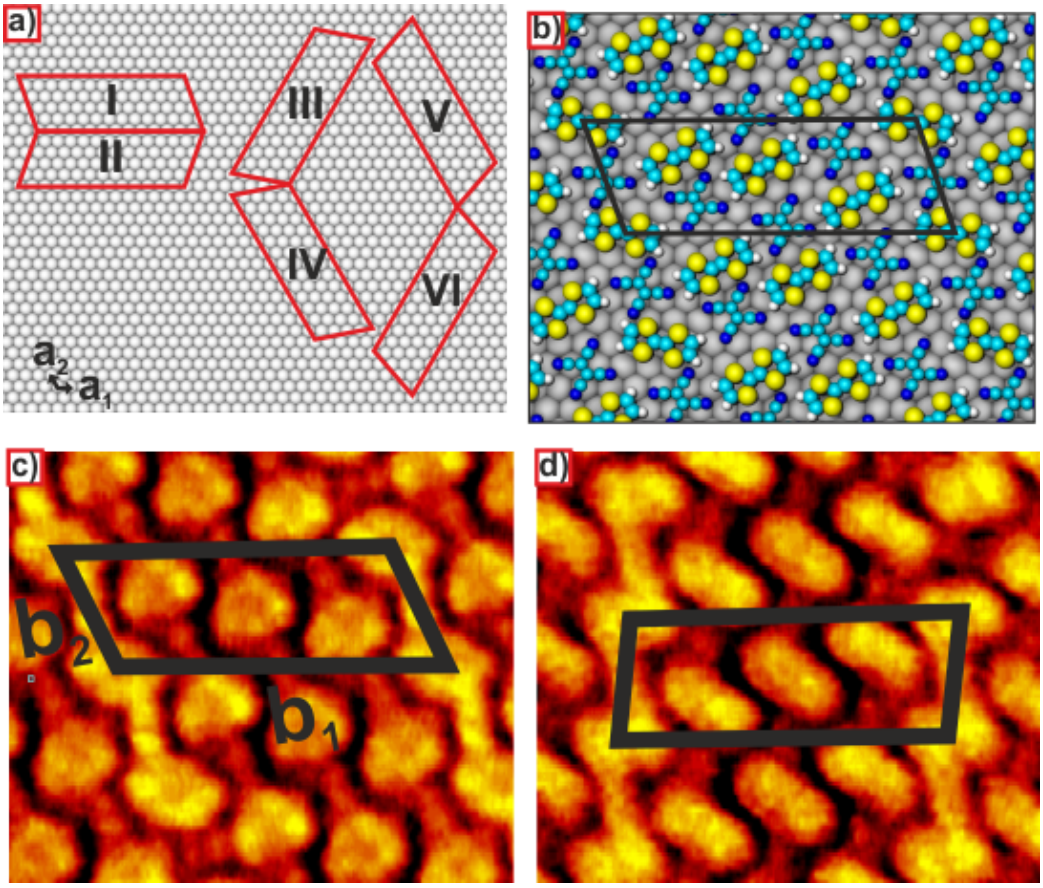

Figure 4.14: *The six different possible orientations of the experimentally measured unit cell on Ag(111) for the 1:1 TCNE-TTF mixed phase. b) Proposed structural model indicating the epitaxial relationship with respect to the silver surface c-d) STM images for two orientations of this acceptor-donor networks, I and II, respectively. c) 53 Å × 45 Å; -0.26 nA, -0.35 V. d) 53 Å × 45 Å, -0.43 nA, -0.99 V.*

In this case the unit cell consists of four TCNE and four TTF molecules and one of the side orientation is along the high symmetry axis of the silver substrate however the molecules inside the unit cell is slightly tilted respect to the silver axis. Allowing the formation of this mixed phase in 6 different orientations as shown in figure 4.14a. Figure 4.14c and figure 4.14d present two of this possible directions. The sides of this unit cell are $b_1 = 35.8(\pm 1)$ Å, $b_2 = 13.1(\pm 0.7)$ Å, and $\gamma = 110^0$. A model for this structure is proposed in figure 4.14b, the matrix describing the epitaxial relationship with the substrate can be written as $\begin{pmatrix} b_1 \\ b_2 \end{pmatrix} = \begin{pmatrix} 13 & 0 \\ 1 & 5 \end{pmatrix} \begin{pmatrix} a_1 \\ a_2 \end{pmatrix}$.

4.3.4 TCNE 1:1 TTF with silver adatoms

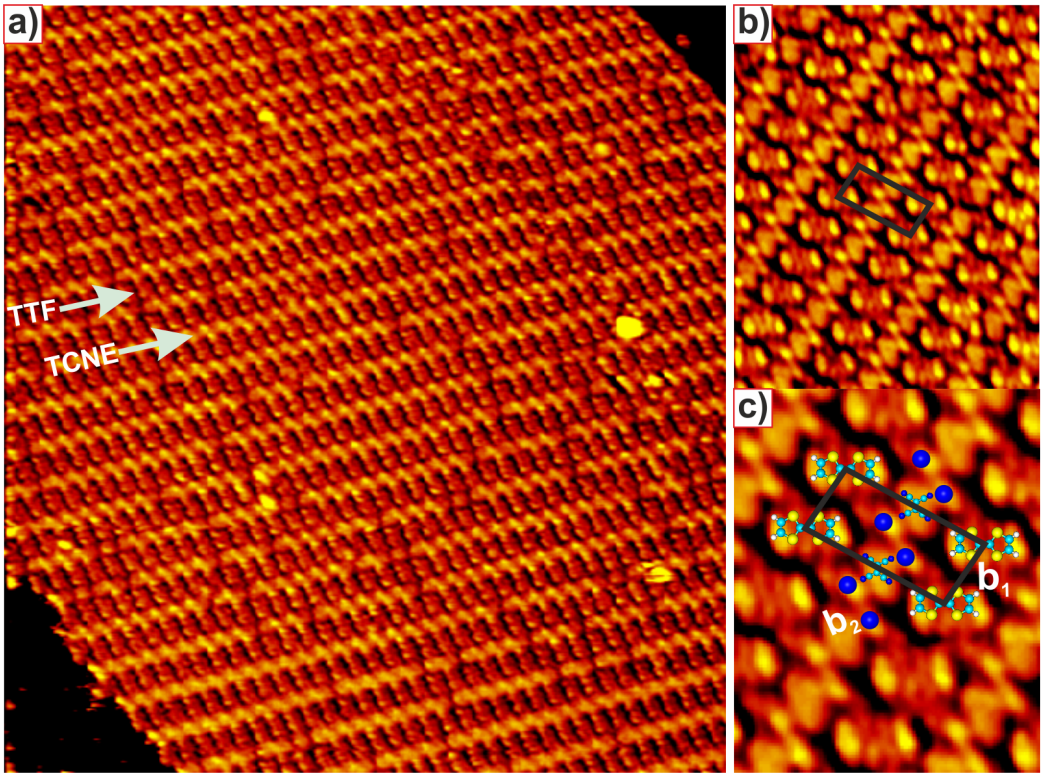

Figure 4.15: *A typical overview STM topography image of TCNE and TTF rows taken at 150 K. b) STM image of an ordered TCNE-TTF with silver adatoms on Ag(111). c) Zoom inside the 1:1 mixed domain with intramolecular resolution with the unit cell model superimposed. a) 489 Å × 519 Å; -0.3 nA, -1.74 V. b) 98 Å × 123 Å, -0.53 nA, -1.53 V. c) 49 Å × 60 Å, -0.53 nA, -1.53 V.*

When the TCNE dosage on the surface is further increase, again a different mixed structure is obtained. Figure 4.15a shows a large scale image where the molecules seem to be arranged in parallel rows, marked by white arrow. At first sight, this self-assembly looks like the TCNE 1:1 TTF phase, since it is composed of alternating rows of acceptor and donor molecules. This structure is similar that TCNQ 1:1 TTF observed on Ag(111), as shown in previous section, and also it has been reported on Au(111) [148, 169]. However a zoom inside this arrangement (figure 4.15b and figure 4.15c) shows that the islands are not only made of TCNE and TTF molecules, but there are also silver adatoms participating in the phase structure. This new rows are formed by alternating one TCNE and two silver adatoms. Different phenomena are

involved in this new mixed phase:

1. The molecular coordination again had changed and the TCNE are positioned at the head-on position of the TTF molecule like the 1:2 and 2:3 stoichiometries.

2. The molecular density inside the unit cell, taking into account the silver adatoms, is 0.18 ($1/\text{Å}^2$) which is much lower than the other networks.

3. An increment of TCNE dosage respect to the other networks and the strong acceptor character of the molecule could lead to the presence of silver adatoms, as shown for pure TCNE islands.

As a consequence of them the mechanism of the new mixed phased can be explained. Figure 4.15c shows a zoom with intramolecular resolution where a molecular model of the unit cell was superimposed. This unit cell contains one TCNE molecule, one TTF molecule and two silver adatoms. In this networks the self-assembled structure can be described by S$\cdots$H-C hydrogen bonds between TTF molecules, two cyano groups of acceptor molecule are connected to two the silver adatoms (as we explained in the previous chapter, a similar interactions has been shown after depositing just TCNE islands on the silver surface), the other two cyano groups are interact with the TTF molecules by C$\equiv$N$\cdots$H-C hydrogen bonds. Finally, in the figure 4.15c it can be observed that some sulfur atoms are assembled with the silver adatoms.

The sides of this unit cell are $b_1 = 23.2(\pm 1)$ Å, $b_2 = 13.5(\pm 0.6)$Å, and $\gamma = 90^0$. A model for this structure is proposed in figure 4.16b, the matrix describing the epitaxial relationship with the substrate can be written as $\begin{pmatrix} b_1 \\ b_2 \end{pmatrix} = \begin{pmatrix} 5 & 4 \\ -5 & 4 \end{pmatrix} \begin{pmatrix} a_1 \\ a_2 \end{pmatrix}$. With these values, six different orientations of this phase on Ag(111) should exist, as shown in figure 4.16a. Figure 4.16c and figure 4.16d shows two of this domains.

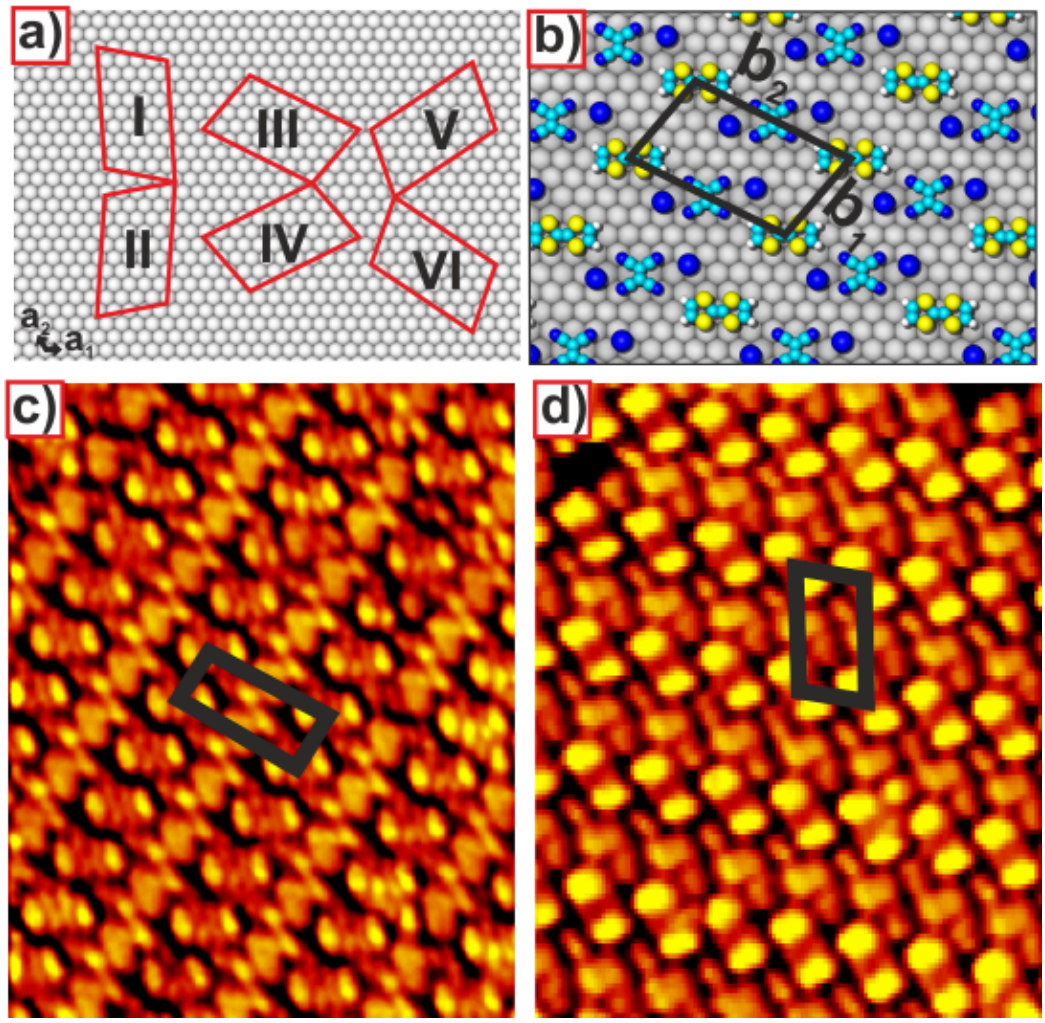

Figure 4.16:
The six different possible orientations of the experimentally measured unit cell on Ag(111) for the 1:1 TCNE-TTF mixed phase with two silver adatoms. b) Proposed structural model indicating the epitaxial relationship with respect to the silver surface. c-d) STM images for two orientations of this acceptor-donor networks, III and I, respectively. c) 98 Å × 123 Å; -0.53 nA, -0.15 V. d) 98 Å × 123 Å; -0.46 nA, -0.59 V.

Figure 4.17 shows a four STM images that was taken at four different bias voltages. STM simulated images was carried out for different orbitals of the molecule. Figure 4.17 also shows this adsorption models that was first relaxed in gas phase with the semiempirical PM3 method, (the original program code stems from Oliver Gröning and Roman Fasel at the EMPA in

Saint Gallen, Switzerland). The experimental results and these simulations are very similar, although all the voltages of the STM are positive.

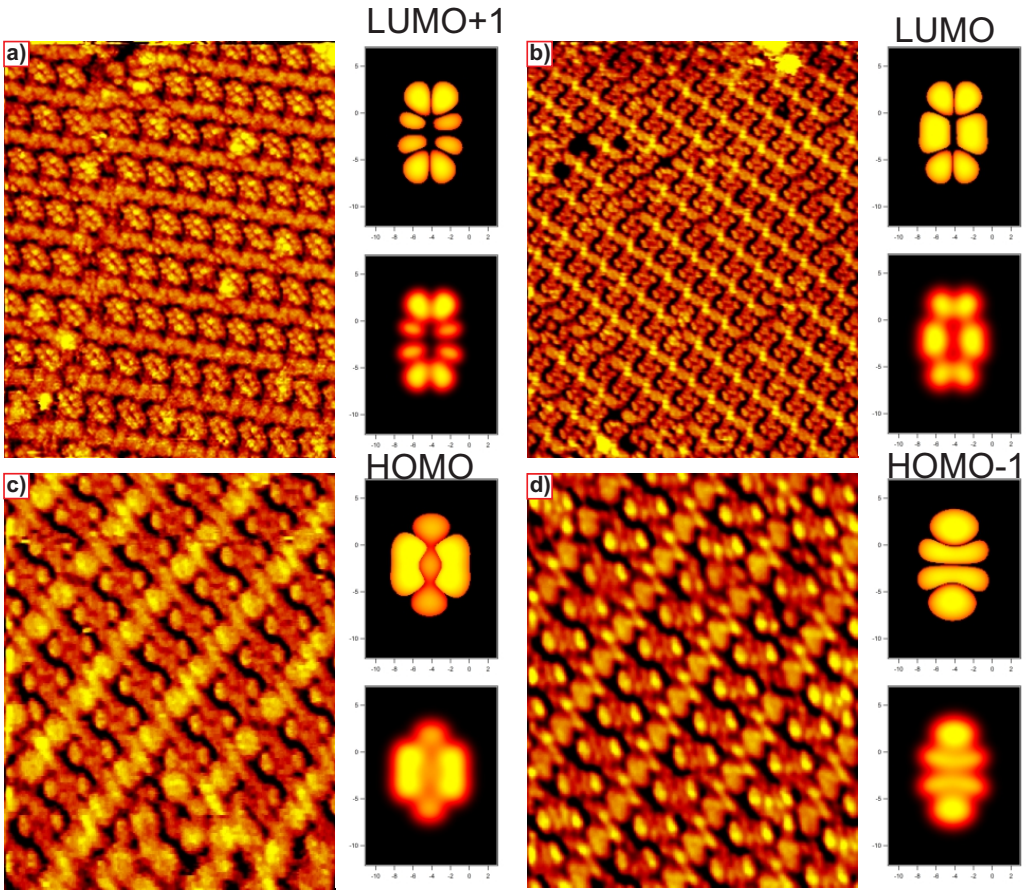

Figure 4.17: *STM images of TCNE-TTF mixed phased with 1:1 stoichiometry on Ag(111) taken at four different bias voltages and imaged at 150 K. At the right side of all the images, in the upper part has been drawn different orbitals of the donor molecule and below is the simulated STM images of TTF molecule. a) 147 Å × 184 Å; -0.55 nA, -0.524 V, b) 196 Å × 245 Å; -0.37 nA, -0.71 V. c) 98 Å × 123 Å; -0.16 nA, -0.76 V. d) 98 Å × 123 Å, -0.53 nA, -1.53 V .*

No new mixed phased has been observed upon further increase of the TCNE dosage. On the contrary, due to this excess of TCNE, the acceptor starts to growth on the pure TCNE islands at room temperature. Figure 4.18 shows the coexistence of last phase (mixture 1:1 with silver adatoms) with the pure TCNE islands. Similar behavior has been reported with the mixture of $F_{16}CuPc$ and Pentacene on Au(111) [165]. In addition, after

this ratio stoichiometry the system are saturated and it can not form more mixture acceptor-donor phases.

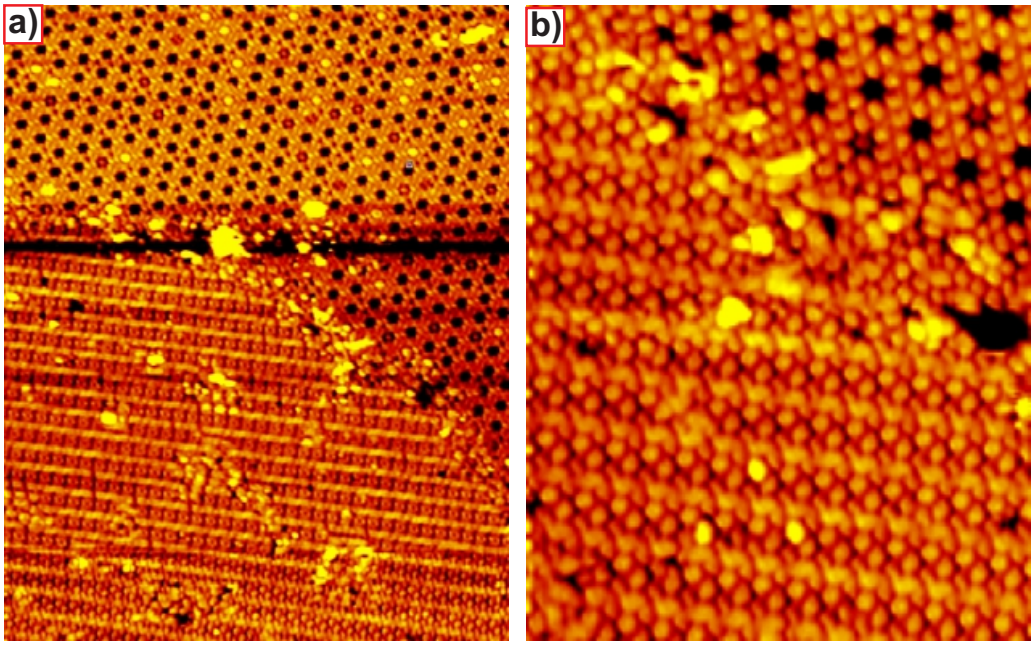

Figure 4.18:
A typical overview STM topography image taken at 180 K. After increase the dosage of TCNE on Ag(111). Coexist the pure TCNE islands and TCNE-TTF mixed with silver adatoms with 1:1 stoichiometry. a)489 Å × 614 AA, -0.31 nA, -0.34 V, b) 196 Å × 245 Å, -0.36 nA, -2.2 V.

4.3.5 Mixed adsorption of TCNE and TTF annealed on Ag(111)

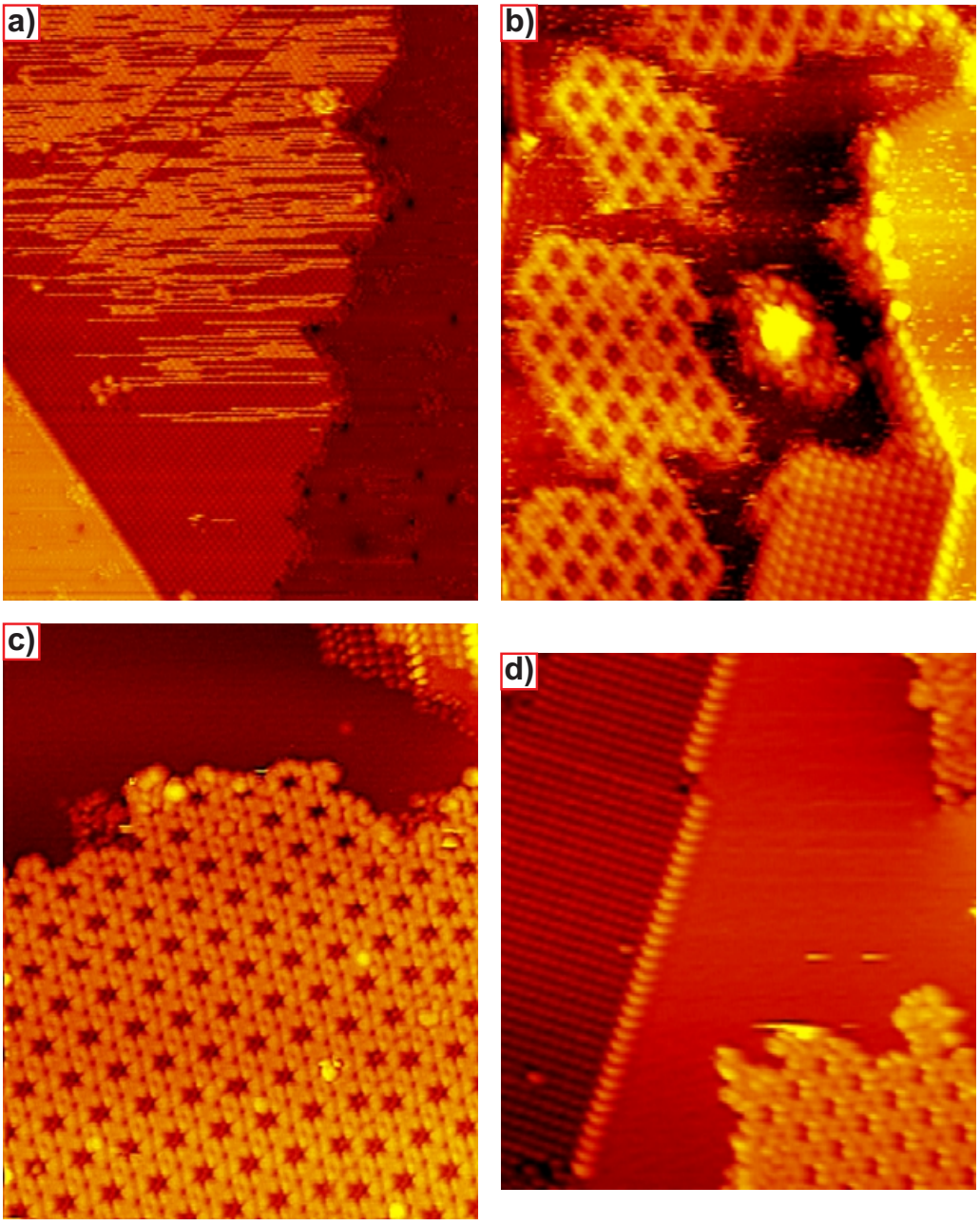

Figure 4.19: *Large STM image of TTF annealed at 350 K and then TCNE was deposited on Ag(111) at 100 K and imaged at the same temperature. a) Well TTF annealed order island and on top some TCNE molecules. b) STM images taken at 120 K where TCNE low temperature islands appear with TTF annealed island. c-d) Topographic STM image, after annealing the sample at room temperature and imaged at 120 K. Coexist TTF annealead islands with TCNE room temperature islands. a) 488 Å × 613 Å; -0.69 nA, -1.8 V. b) 195 Å × 245 Å; -0.47 nA, -1.44 V. c) 195 Å × 245 Å; -0.35 nA, -1.48 V. d) 247 Å × 280 Å; -0.31 nA, -1.36 V.*

To clarify a bit more that the molecule TTF molecule are adsorbed almost planar when it is mixed with the TCNE molecule. In this series of experiments, the donor, TTF, was evaporated on Ag(111) with the sample at room temperature. After annealing at 350 K during 10 minutes the molecules form well order islands where the TTF are slightly tilted, as described in the chapter 3. Then, the acceptor, TCNE, was deposited directly to the STM at 100 K at the same temperature. The STM images (figure 4.19a) show some noise and mobility above the TTF islands. Increasing slowly the temperature a few kelvins, pure acceptor islands start to growth on the silver substrate in the low temperature ordering as described in the chapter 3, and this phase coexist with the TTF islands; that is, in this case TTF and TCNE do not mix, even after increasing slowly the temperature up to room temperature (figure 4.19c and figure 4.19d) where it can be observed the pure TCNE island with the pure TTF annealed island. So, the slightly tilted TTF molecules are more stable inside the pure donor island forming a mixture with the acceptor. Further increase of the temperature to promote intermixing on the system is not possible because the TCNE molecules desorb at 350 K, almost the same temperature at which pure TTF islands are formed.

4.3.6 Electronic structure of TCNQ-TTF compounds on Ag(111)

In order to obtain more information on the electronic properties of the adsorbed acceptor-donor systems on the Ag(111) surface, XPS measurements were carried out. Both core-level shifts and changes in the work-function of the various systems have been tracked trough the various changes in stoichiometry.

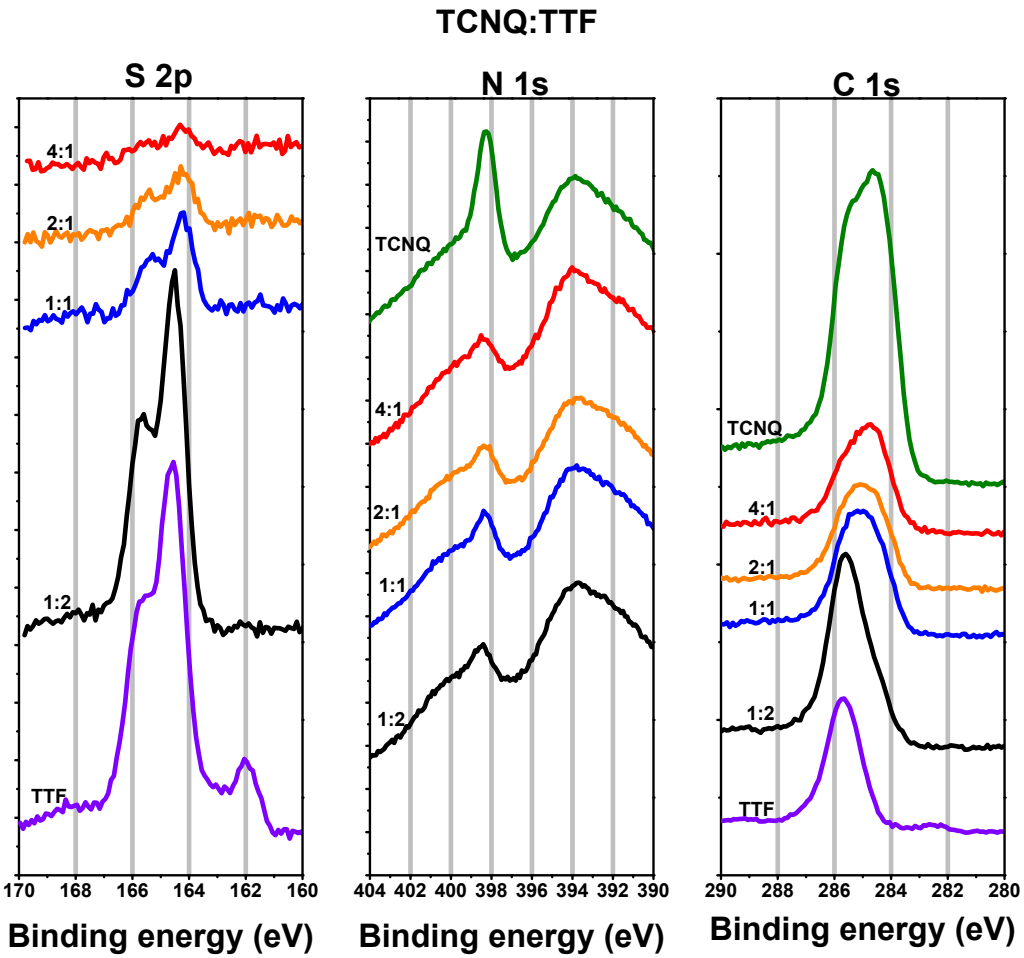

Figure 4.20: *S2p, N1s and C1s region of the XPS spectra taken on the different TCNQ-TTF networks. The spectra corresponding to the pure TTF and TNCQ layers are also included. The spectra are displaced vertically for clarity. The stoichiometry ratios indicated for every spectra correspond to the majority phase observed in the STM images.*

Figure 4.20 shows a high resolution spectra of the various regions of interest (S2p, N1s, and C1s core levels) for the different TCNQ-TTF (figure 4.20) and TCNE-TTF (figure 4.23) compounds on Ag(111). As mentioned in the previous chapter, the nitrogen region of study, figure 4.20, overlaps with features stemming from plasmon loss peaks of the Ag(111) surface, thereby masking part of the nitrogen peak [93]. For each element a different behavior is found. For the S2p component, figure 4.20, present in the TTF molecules, a single doublet is observed, indicating that the molecule is adsorbed almost

planar on the silver surface, in agreement with the theoretical calculations of the previous chapter. Furthermore, a shift in binding energy of the S2p doublet is observed with changing stoichiometry, decreasing the apparent binding energy with increasing TCNQ content. For the C resonance, figure 4.20, a shift in the same direction is observed, while the peak shape seems to evolve smoothly from the shape corresponding to pure TTF to the shape corresponding to pure TCNQ. For the nitrogen resonance a smaller shift to lower binding energies is also observed. To quantify these shifts in more detail, figure 4.21 shows the binding energies of the core levels of both donor and acceptor molecules obtained by fitting the spectra of figure 4.20.The apparent core-level binding energy of the TCNQ seems indeed to remain constant for all observed stoichiometries, while the core-level of the TTF molecules is lowered. Also in this figure 4.20 shows the theoretical position of this mixed phases.

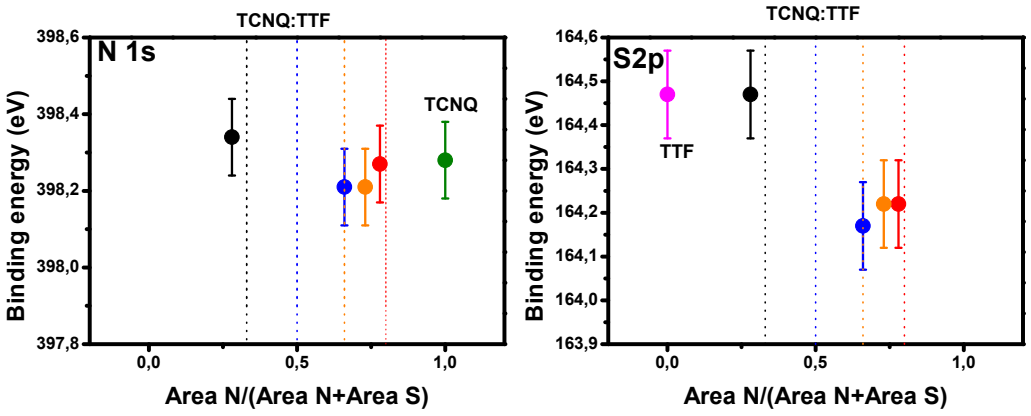

Figure 4.21: *The evolution of the sulfur and nitrogen core levels binding energies as a function of the area of the relative amount of TCNQ and TTF molecules (measured as the ration between the area of N1s peak and the sum of the areas of the N1s peak and the S2p peak). The vertical dashed lines correspond to the stoichiometry phases TCNQ:TTF 1:2, 1:1, 2:1, and 4:1.*

These results are seemingly contradicting the theoretical results relative to the partial charges on the TTF and TCNQ molecules for the different phases, where it is calculated that the TTF molecules donate more charge (becoming more positive) upon increasing the number of TCNQ neighbors (see table 4.5 and figure 4.22). In a first approximation, one would expect that the oxidation of the donor molecules would shift the core levels to higher binding energies, since it should be harder to remove additional electrons.

Table 4.5: *Summary of tje calculated partial charges on the TCNQ and TTF molecules for all the different mixed phases TCNQ-TTF on gas phase and on Ag(111), where* $\Delta q_{bader} < 0$ *corresponds of a gain of electrons and* $\Delta q_{bader} > 0$ *indicates a loss of electrons*

TCNQ:TTF/ Ag(111)	Q(e)				
	TTF	1:2	1:1	2:1	TCNQ
TTF (edge)		+0.24			
TTF (central)		+0.23			
TTF	+0.10		+0.42	+0.51	
TCNQ (up)				-0.93	
TCNQ (down)				-0.94	
TCNQ		-1.10	-1.02		-0.99

TCNQ:TTF (gas phase)	Q(e)				
	TTF	1:2	1:1	2:1	TCNQ
TTF (edge)		+0.42			
TTF (central)		+0.43			
TTF			+0.67	+0.92	
TCNQ (up)				-0.47	
TCNQ (down)				-0.45	
TCNQ		-0.83	-0.67		

However, not only the change in the number of valence electrons of a molecule dictates the core level shift of its constituent atoms. Additionally, and easily overlooked, is that the screening of the atom by its external environment plays a crucial role [173]. As shown in [173] and [164], this screening effect is able to mask the shift of the core level induced by the change in molecular valence electrons, and can even lead to a shift in the opposite direction. As shown in [173], the expected core level shift is given by an addition of both effects, and they can be treated separately.

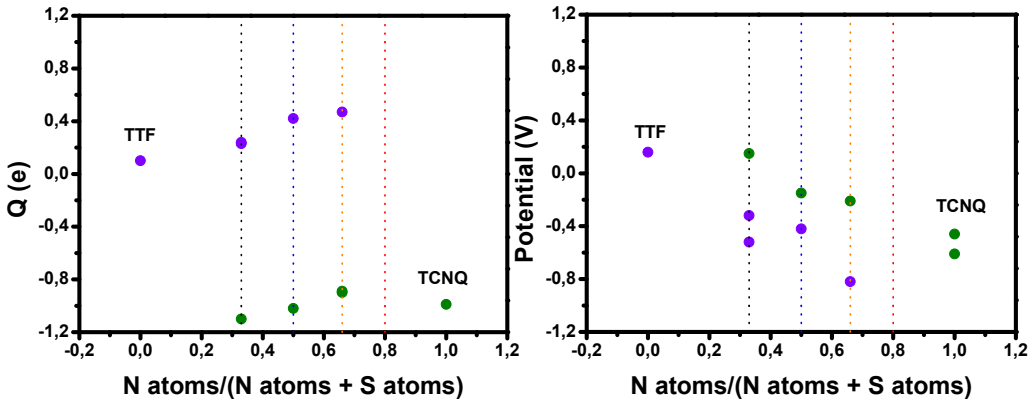

Figure 4.22: *Calculated partial charges of the TTF and TCNQ molecules for every one of the different mixed phases. b) potential that feels one molecule (TTF or TCNQ) due to the partial charge of the surrounding molecules for the different phases.*

To first approximation, we can conclude the potential a molecule "feels" due to the charge in the neighboring molecules. The results, assuming point charges localized in the geometric centers of the molecules and considering only first neighbors, are shown in figure 4.22. For both molecules, the potential becomes more negative as the TCNQ content increases, which makes sense because the charge of the TCNQ molecules, negative, is greater than the charge in the TTF molecules (positive). A more negative potential, implies a decrease in binding energy, due to the electrostatic repulsion. Although it is difficult to translate both effects (molecular charge and potential) into core level shifts [173], we can see that the effect of the potential is in agreement with the experimental results, and apparently, the dominant effect. In addition, this should explain why the core level shift when increasing the TCNQ content is larger for S2p than for N1s, since the charge in the potential for TTF when going to pure TTF to TTF 1:2 TCNQ is larger than the change in potential for TCNQ when going from TTF 2:1 TCNQ to pure TCNQ.

It is useful to compare the results about the partial charges with those calculated for free-standing layers with exactly the same geometry. In this case, as the TCNQ content increases, the TTF charge (positive) increases and the TCNQ charge (negative) decreases. On Ag(111), the TTF charge increases with TCNQ content, but the TCNQ charge remains approximately constant and equal to -1 e.

4.3.7 Electronic structure of TCNE-TTF compounds on Ag(111)

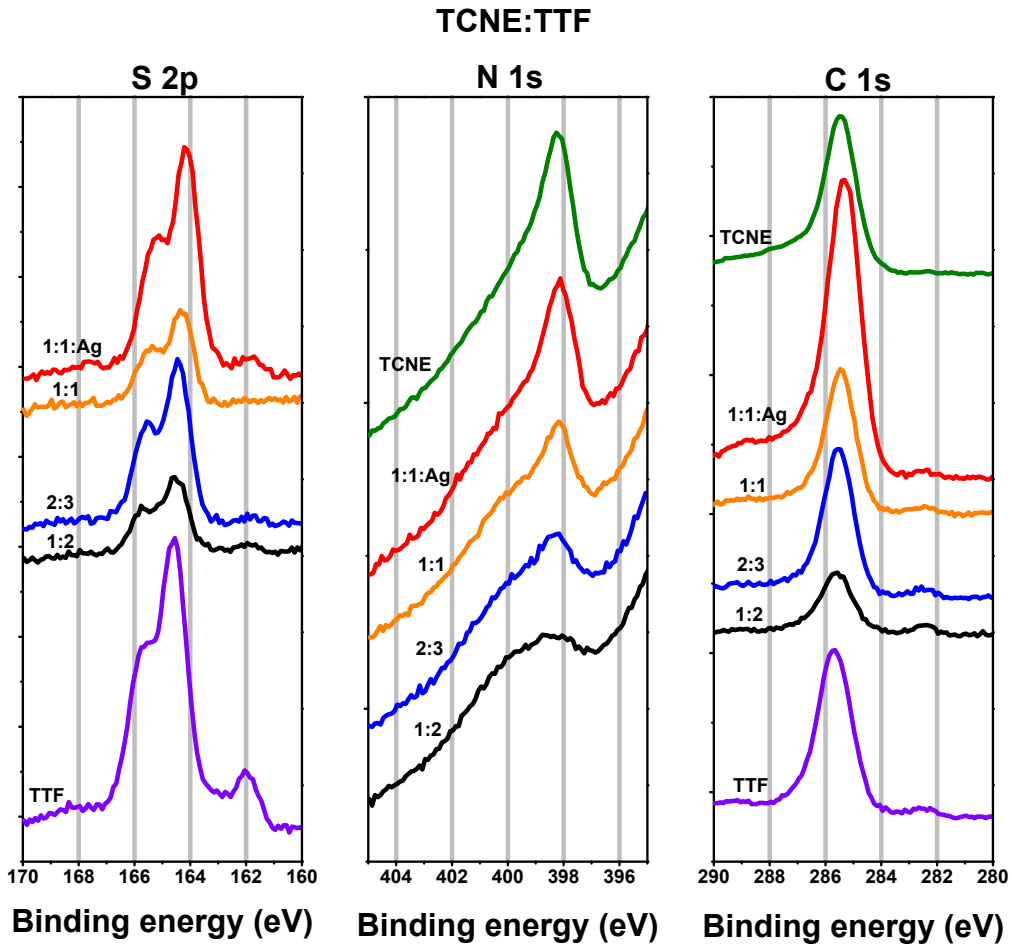

Figure 4.23: *S2p, N1s and C1s region of the XPS spectra taken on the different TCNE-TTF networks. The spectra corresponding to the pure TTF and TCNE layer are also included. The spectra are displaced vertically for clarity. the stoichiometry ratios indicated for every spectra correspond to the majority phase observed in the STM images.*

The XPS results for the mixed TCNE-TTF phases are shown in figure 4.23. Although smaller, the S2p core level shows a decrease in binding energy when increasing the TCNE content, while the N1s binding energy remains approximately constant as shown in figure 4.24. Unfortunately, we do not have

theoretical results concerning charge transfer for these systems. However, since the charge transfer for TCNE (-0.88 e) and TCNQ (-0.99 e) are very similar, we should expect the behavior of the potential to follow the same trend than for the TCNQ-TTF system.

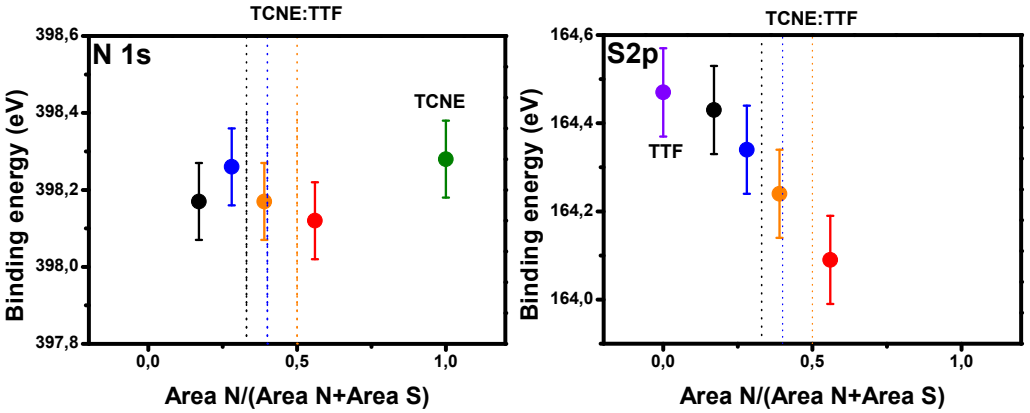

Figure 4.24: *The evolution of the sulfur and nitrogen core levels binding energies as a function of the relative amount of TCNE and TTF molecules (measured as the ration between the area of the N1s peak and the sum of the areas of the N1s peak and the S2p peak). The vertical dashed lines correspond to the stoichiometry phases TCNE-TTF 1:2, 2:3, and 1:1.*

For the TCNE-TTF system we have also measured the work-function as a function of the TCNE content. While the adsorption of a pure TTF layer causes a small decrease with respect to the work-function of the clean surface (- 0.25 eV), TCNE increases the work-function by 0.96 eV. Figure 4.25 shows that the variation for the mixed layers does not follow a simple lineal relationship with the TCNE content, as it should be if the partial charge on the molecules would not depend on the stoichiometry ratio. In any case, the variation between the two extreme values of the work-function depends smoothly on the TCNE content and, in principle, an appropriate combination of TTF and TCNE with the right stoichiometry would allow to build an interface with a previously required work-function.

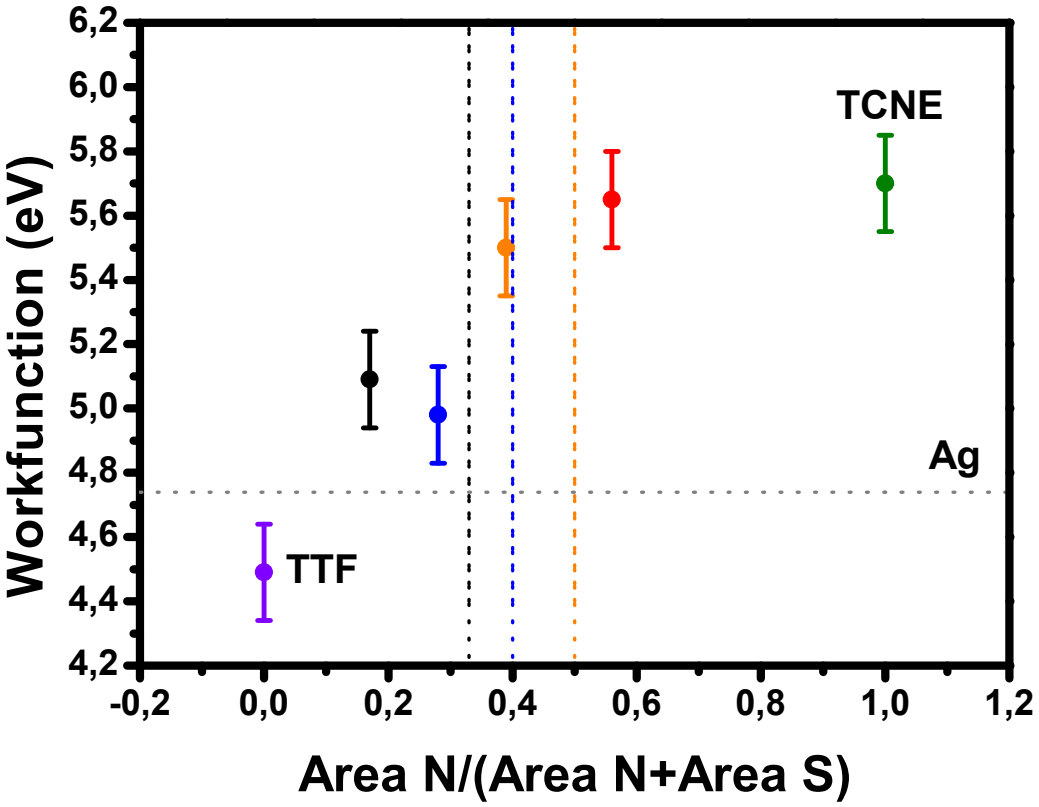

Figure 4.25: *Work-function of the different TCNE-TTF phases as a function of the TCNE content. The horizontal line is the worfuction of the Ag(111) surface.*

4.4 Conclusions

In this chapter we have studied the adsorption, the structural and electronic properties of two mixed acceptor-donor systems (TCNQ-TTF and TCNE-TTF) on Ag(111). In both cases, after deposition at room temperature, and depending on the stoichiometry, the molecules form spontaneously mixed phases, some of them not known in bulk phase. The metal surface allows us to expand the variety of such Donor-Acceptor networks.

In the case of TCNQ-TTF, increasing the TCNQ dosage on the systems, four different phases have been observed with TCNQ:TTF stoichiometries: 1:2, 1:1, 2:1, and 4:1, respectively and each leading to different levels of charge transfer. TCNQ, being a strong electron acceptors, holds in every case a negative charge close to 1 e. However, the charge on the TTF molecules, being

positive, seems to increase with the TCNQ content. At the same time, and contrary to expectations, both C1s and S2p core levels shift to lower binding energy with excess of TCNQ, while the N 1s core level does not shift appreciably due to the strong interaction with the substrate. These results show that for these mixed systems, the core level shifts do not only depend on the charge state of the molecule. Actually, simple calculations show that the effect of the potential created by the nearby molecules (for both TCNQ and TTF, more negative when increasing the TCNQ content) shifts the core levels in the opposite direction, an effect that can actually overcome the effect of the molecular charge.

In the case of TCNE-TTF also four different acceptor-donor phases have been reported: 1:2 , 2:3 , 1:1, and 1:1 with silver adatoms. The last phase show the strong character of the acceptor, as when the TCNE molecules was deposited on Ag(111) when silver adatoms are incorporated to the mixed phase. The XPS measurements show similar results than for the TCNQ-TTF case, and we can expect the potential the molecules feel to follow the same trend than for that system. In addition, we have also shown that the surface work-function can be controlled by adjusting the ration of TCNE and TCNQ molecules.

In summary, the STM, XPS measurements, with support of DFT calculations, show that controlling the stoichiometry ratio in these complexes allow us to tune both the structural and the electronic properties of a donor-acceptor system.

5

DCNQI and DCNQI-Fe on metal substrates

5.1 Introduction

In this chapter we have studied the adsorption and the assembly of dicyano-p-quinonediimine (DCNQI) on Cu(100) and Ag(111). Also, the adsorption and the assembly of DCNQI molecules with Fe atoms on Ag(111) and the formation of a Fe-DCNQI coordination network are discusssed.

5.2 DCNQI

5.2.1 The molecule

DCNQI is an electron acceptor belonging to the TCNQ family which forms a large number of charge transfer and coordination compounds exhibiting metallic conductivity [174–177]. This acceptor molecule (figure 5.1), planar in gas phase, consists of a quinoid carbon ring and two cyanoimine groups (=N-CN). It has two stable configurations: the trans-form, that has the cyanoimine groups pointing towards opposite sides of the molecular main axis, and the cis-form, where both cyanoimine groups point towards the same side of the molecule.

Isomerization takes place when one of this cyanoimine group changes from one side to the other side of the molecular axis. The isomerization

mechanism can be **i)** an inversion, **ii)** a rotation or **iii)** an intermediate mechanism [178]. In the first case the cyano group moves in the plane of the molecule (as determined by the C ring) and rotates 180^0 degrees around the N atom, while in the second case the cyano group moves out of the plane of the molecular axis until it lies again within the main plane.

The stereochemistry of DCNQI and its derivatives has been thoroughly investigated [176, 179]. For the parent compound, trans/cis configurations are easily interconverted in solution (with an activation energy $E_a =\sim 0.5eV$), although the trans-isomer is slightly preferred (80:20) [179], since the dipole moments are reduced in this configuration [179]. Theoretical calculations reveal that isomerization takes place via inversion of the cyano group around the imine nitrogen atom, with a gas phase activation energy of 0.63 eV, that it was previously reported [176] (our own calculations give $E_a =\sim 0.66eV$).

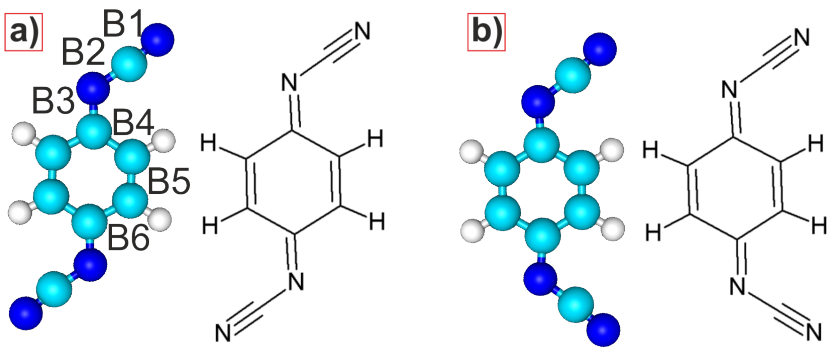

Figure 5.1: *Chemical structure of the DCNQI molecule (dark blue=nitrogen atoms, light blue=carbon atoms, white=hydrogen atoms) a) Trans configuration of the molecule; b) Cis configuration.*

We have carried out DFT calculations of DCNQI in gas phase for different charge states. The results are schematically shown in figure 5.2. When the molecule is in the neutral state (zero charge), the energy barrier for isomerization is 0.66 eV very similar to the experimental value measured in solution, and the transition takes place by inversion of the cyano group. When the molecule accepts one electron, $(DCNQI)^{1-}$, the transition state reveals that the isomerization take places by a mixture of inversion and rotation, with an energy barrier (0.63 eV) very similar to that of the neutral molecule. In the last case, when the molecule accepts two electrons, $(DCNQI)^{2-}$, the energy barrier is much lower, 0.26 eV, and isomerization takes place by rotation of the cyano group around the imine nitrogen atom. This is possible because in the dianion state there is a significant electron redistribution (figure 5.3):

the quinoid ring becomes aromatic and the double bond B3 takes a single bond character allowing the rotation of the cyanoimine group. In all cases the cis-isomer is always slightly higher in energy than the trans-isomer.

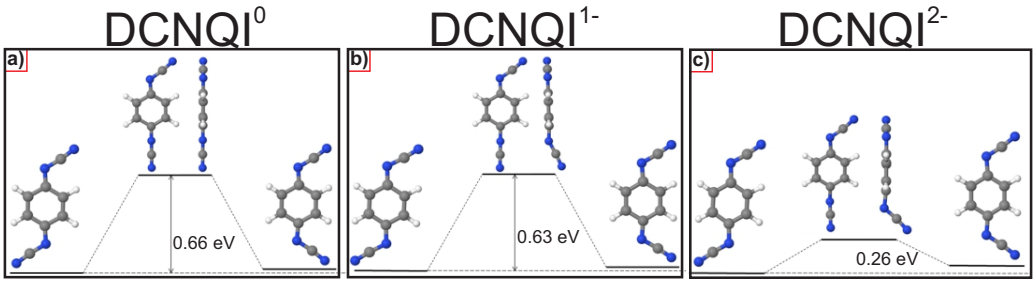

Figure 5.2: *Results of gas phase calculations showing the transition state (center) and the energy barrier from the trans-isomer (left) to the cis-isomer (right), for three charge states: a) DCNQI in neutral state:*$(DCNQI)^0$*. b) the anion* $(DCNQI)^{1-}$*. c) the dianion* $(DCNQI)^{2-}$*.*

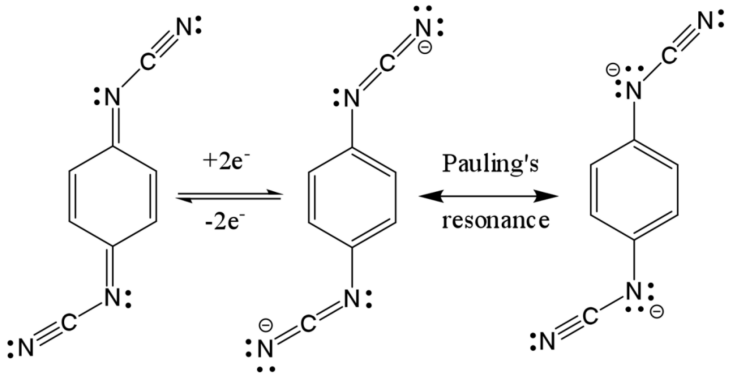

Figure 5.3: *Scheme of the changes in the electron distribution in the trans-form of DCNQI when it accepts two electron: the quionid ring becomes aromatic and the double bond connecting the ring with the cyanoimine group (*$\boldsymbol{B_3}$*) changes from double bond to single bond, allowing the rotation of the cyano group around the imine nitrogen atom.*

5.3 DCNQI on metal substrates

5.3.1 Introduction: Isomerization on metal surfaces

In the last years, there has been much interest in the realization of molecular switches for the development of new technologies with possible applications in molecular electronics. For a molecule to act as a switch, it is required the existence of at least two stable switching states with different physical/chemical properties (for instance, a change in conductance), where the switching process can be controlled by an external influence. In addition, if the molecules are to be integrated in an electronic circuit, they need to be deposited on a substrate.

Cis-trans isomerization reactions have been recently proposed as models for the action of molecular-scale switches [180]. Molecules like azobenzene derivatives have two stable isomers: a nearly planar trans-form and a non-planar cis-form. However, adsorption on a surface may change the molecule properties. For example, when deposited on Cu(110) only the trans-isomer can be found due to the strong interaction between the substrate and the molecule [181]. So far, successful switching experiments have been performed only on Au(111), where the isomerization reaction has been triggered by light irradiation [182–187], thermal activation [185, 188, 189], and the tunneling current [190] or the electric field [191, 192] from the tip of a scanning tunneling microscope. It thus appears that minimizing surface-molecule interaction should promote the isomerization reaction. Also, other types of molecules have been used for isomerization mechanism on Au(111), as imine derivates [193]. For that reason, the more reactive substrates are usually avoided for successful molecular switches, and inert surfaces with weak molecular-substrate interactions should be the only ones in which isomerization reactions triggered by external influences could be expected to take place. However, it might also be happen that molecule-surface interactions could, in some cases, bring the molecular conformation closer to the transition state, thereby facilitating the progress of the reaction. In any case, to exploit isomerization reactions as switching processes, it is important to study how the molecules are absorbed on the substrate and the interaction of the surface with the molecules. More studies are thus needed to correlate molecule-surface interactions and isomerization reactions.

In this chapter, we are going to study the thermal isomerization process of DCNQI when deposited on two different substrates: Cu(100) and Ag(111). We will show that this molecule undergoes a thermally induced isomerization reaction which is actually facilitated by the molecule-substrate interactions.

Experimental

DCNQI was deposited by sublimation from a glass crucible, kept between 320 K and 340 K, onto the sample when it was already placed on the STM. As mentioned in chapter 2, in this way the sample could be held at any temperature between 100 K and room temperature, both during sublimation and for subsequent STM measurements.

5.3.2 DCNQI on Cu(100) *

After depositing 0.03 ML of DCNQI on Cu(100) at 145 K, the STM images (taken at the same temperature), show that disordered clusters of molecules appear on the copper terraces. These clusters disappear close to 235 K and the molecules starts to form well-ordered islands with an internal square symmetry (figure 5.4a and figure 5.4b). The molecular network so formed is rather open, which means that relatively strong directional interactions are controlling the assembly. The unit cell for this arrangement, which we call the LT phase, can be described by the epitaxial relationship $\boldsymbol{b_1} = 3\boldsymbol{a_1} + 4\boldsymbol{a_2}$ and $\boldsymbol{b_2} = -4\boldsymbol{a_1} + 3\boldsymbol{a_2}$. In the figure 5.4d shown the results of the DFT calculations when the Cu(100) substrate is taken into account.

To understand this arrangement, DFT calculations were carried out for a free standing monolayer. The results (figure 5.4c) show that a very similar molecular network can be obtained for the trans configuration of the molecule. Such configuration enables the formation of hydrogen bonds that would not be possible for the cis configuration. Moreover close-up images show that the shape of the molecule in the STM images is spindle-like, with a center of symmetry, that is absent in the cis configuration. The binding energy per molecule inside the free standing monolayer can be defined as

$$E_{bind} = \frac{-(E_{net} - nE_{mol})}{n} \tag{5.1}$$

where E_{net} is the total energy of the unit cell for a free-standing DCNQI monolayer, n is the number of molecules in the unit cell, and E_{mol} is the energy of an isolated DCNQI molecule. In this case the binding energy per molecule amounts to 0.61 eV.

*These results have been partially described in Christian Urban's Thesis [95], so we will give here a summary of the most relevant conclusions.

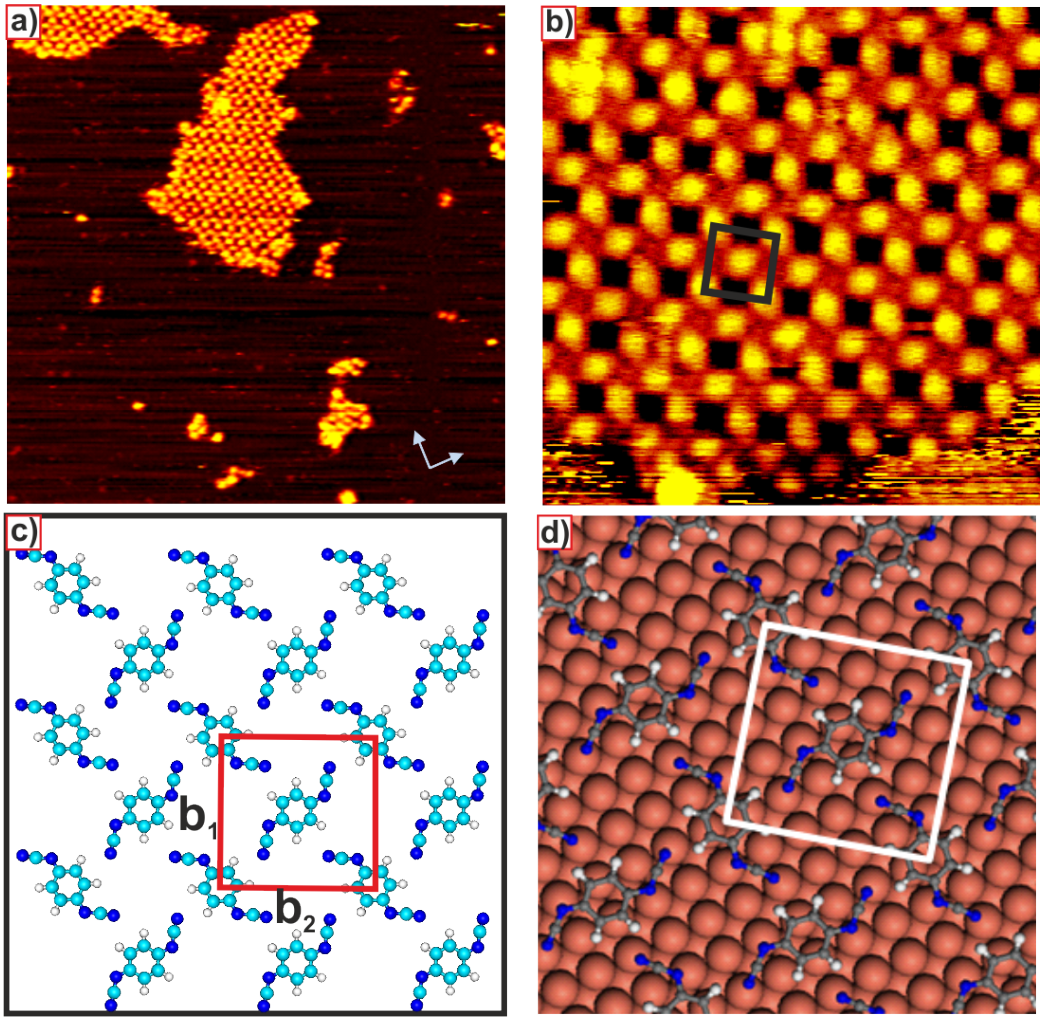

Figure 5.4: *a,b) STM images (taken at 255 K) of islands of DCNQI molecules on the Cu(100) surface after depositing 0.03 ML at 145 K. c) The results of DFT calculations showing the minimum energy configuration of a 2 dimensional free standing monolayer of DCNQI molecules in the trans configuration. The binding energy per molecule inside the free-standing DCNQI layers, and the lattice parameters are* $\Delta\ E = 0.61$ *eV,* $a = 12.99$ *Å,* $b = 12.86$ *Å. d) Proposed model for the low temperature phase of DCNQI on Cu(100). The white square indicate the unit cell of the 2D assembly. a) 512 Å × 610 Å; -0.23 nA, -1.79 V. b) 113 Å × 95 Å; -0.21 nA, -1.0 V.*

DCNQI has also been evaporated with the copper single crystal held at room temperature. Figure 5.5a and figure 5.5b show the results after depositing 0.23 ML. In this case the molecules also form ordered islands but with a

different internal order than for low temperature deposition. The structure of the islands is more compact. The unit cell in this case, that we can call the RT phase, can be described by the epitaxial relationship $\boldsymbol{b_1} = 6\boldsymbol{a_2}$ and $\boldsymbol{b_2} = 6\boldsymbol{a_1}$. In the figure 5.5d shown the results of the DFT calculations when the Cu(100) substrate is taken into account. The appearance of the molecules is also different: they show a croissant shape and, therefore, lack a center of symmetry, reminding strongly of the molecular shape of the cis-isomer. Actually, DFT calculations for a free standing monolayer show that this arrangement can be explained by the formation of hydrogen bonds between molecules in the cis configuration (figure 5.5c). Moreover, assuming that the molecules are in the cis configuration also explains the asymmetric shape of the molecules in the STM images. The theoretical lattice parameters for this square network are $b_1 = b_2 = 15.78$ Å, which are very close to the experimental value (15.3 Å). After trying different geometries, this turns out to be the most stable network that can be obtained for a 2D free-standing layer of DCNQI molecules, either in the cis or in the trans configuration with a binding energy per molecule of 0.72 eV. If there is any possible isomerization, once the molecules are part of this cis network, the process become irreversible (the islands in figure 5.5a and figure 5.5b are stable at least until 400 K).

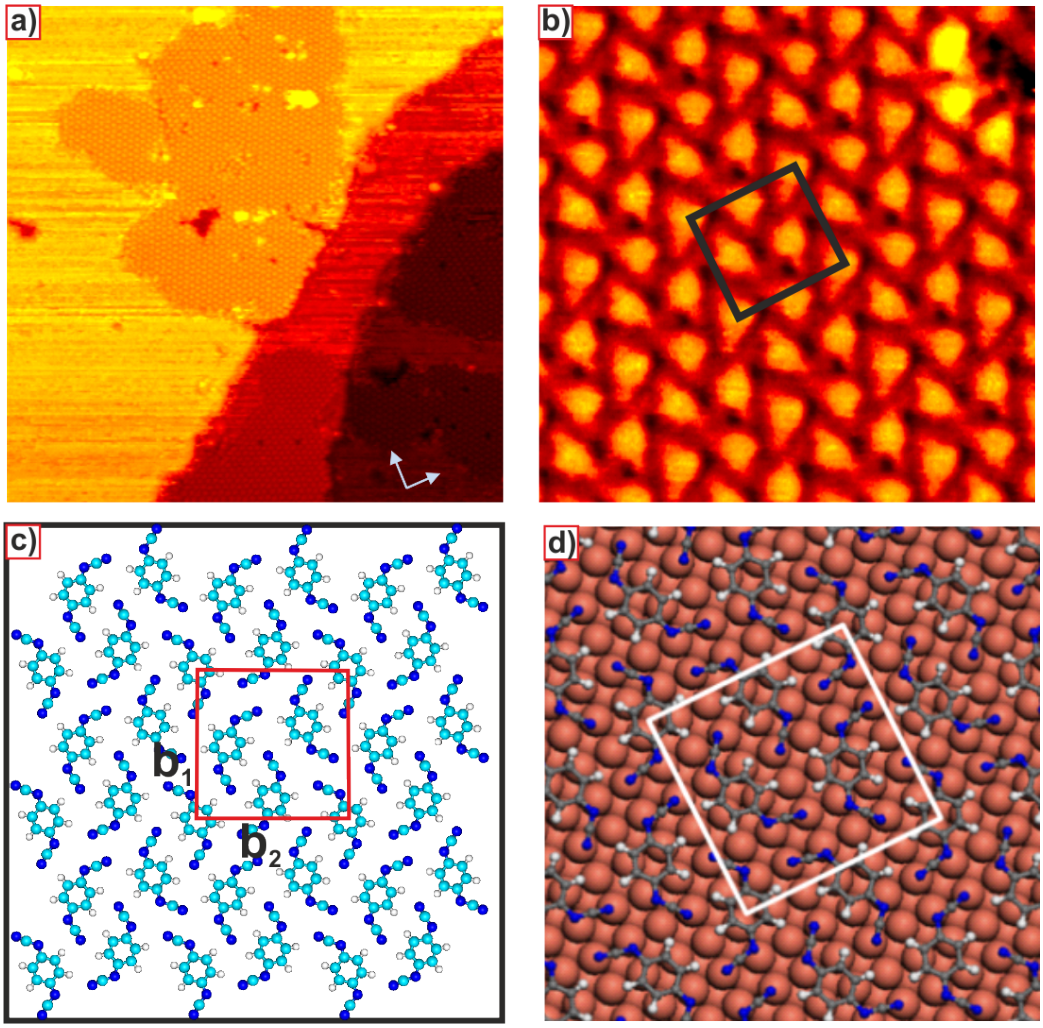

Figure 5.5: *a,b) STM images (taken at room temperature) of islands of DCNQI molecules on Cu(100) after depositing 0.23 ML at room temperature. c) The results of DFT calculations showing the minimum energy configuration of a 2 dimensional free standing monolayer of DCNQI molecules in the cis configuration. The binding energy per molecule inside the free-standing DCNQI layers, and the lattice parameters are* $\Delta E = 0.72$ *eV,* $a = 15.79$ *Å,* $b = 15.71$ *Å. d) The proposed model for the room temperature phase. The white square indicate the unit cell of the 2D assembly. a) 625 Å × 745 Å; -0.43 nA, -1.24 V. b) 75 Å × 75 Å, -0.48 nA, -1.24 V.*

The RT-phase can also be obtained by depositing directly with the substrate at low temperature and annealing the system to room temperature. Around $\sim$ 245 K the molecules reorganize into the RT-phase. Initially both

phases coexist on the copper surface (figure 5.12a), until the transition from the LT-phase to the RT-phase is complete (figure 5.12d). These RT-phase islands are stable at least up to $\sim$ 440 K.

The fact that isomerization takes place at 245 K means that the energy barrier is much lower than 0.66 eV (the gas phase value) [179]. We have performed DFT calculations of the minimum energy conformation of a DCNQI molecule on the Cu(100) surface, both for the trans and cis isomers. The results (figure 5.6a and figure 5.6c), show an isolated DCNQI molecule absorbed with the quinoid ring parallel to the copper surface. The cyano groups, on the other hand, are bent downwards. The surface is distorted, with the Cu atoms close to the N atoms lifted 0.16 Å from the ideal surface termination. Actually, similar molecular and surface distortions have been reported in the case of TCNQ on Cu(100)[30]. As in that case, there is a considerable charge transfer from the substrate to the molecule, which here amounts to $\sim$ 1.6 e. As a consequence of the electronic redistribution, the lengths of the molecular bond also experiment significant changes (see table 5.1):

Table 5.1: *Bond lengths (in Å) of the neutral DCNQI molecule ($(DCNQI)^0$), in the dianion state $(DCNQI)^{-2}$, and adsorbed on the Cu(100) surface*

Bond	$(DCNQI)^0$	$(DCNQI)^{2-}$	DCNQI/Cu(100)	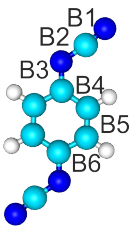
B_1	1.18	1.19	1.20	
B_2	1.32	1.30	1.29	
B_3	1.32	1.38	1.40	
B_4	1.45	1.43	1.42	
B_5	1.36	1.39	1.41	
B_6	1.45	1.42	1.42	

The phenyl ring becomes almost aromatic, and bond $\boldsymbol{B_3}$ increases appreciably its length, acquiring a marked single bond character and facilitating the rotation of the cyano group. As should be expected, all these changes are very similar to what happens to the doubly charged DCNQI molecule in gas phase. In the case of doubly charged DCNQI in gas phase, the lengthening of bond $\boldsymbol{B_3}$ facilitates the rotation of the cyano group, and the calculated energy barrier for isomerization decreases down to a value of 0.26 eV. When the molecule is adsorbed on the surface, the calculation of the energy barrier is much more complicated, because if we assume that isomerization takes place while the molecule is diffusing on the surface, the exact initial and final states are not exactly known. We have explored different possibilities, and found that, in every case, the energy barrier is much lower than for the

neutral isolated molecule. For example, in the case shown in figure 5.6, the barrier for going from trans (left) to cis (right) is only 0.17 eV.

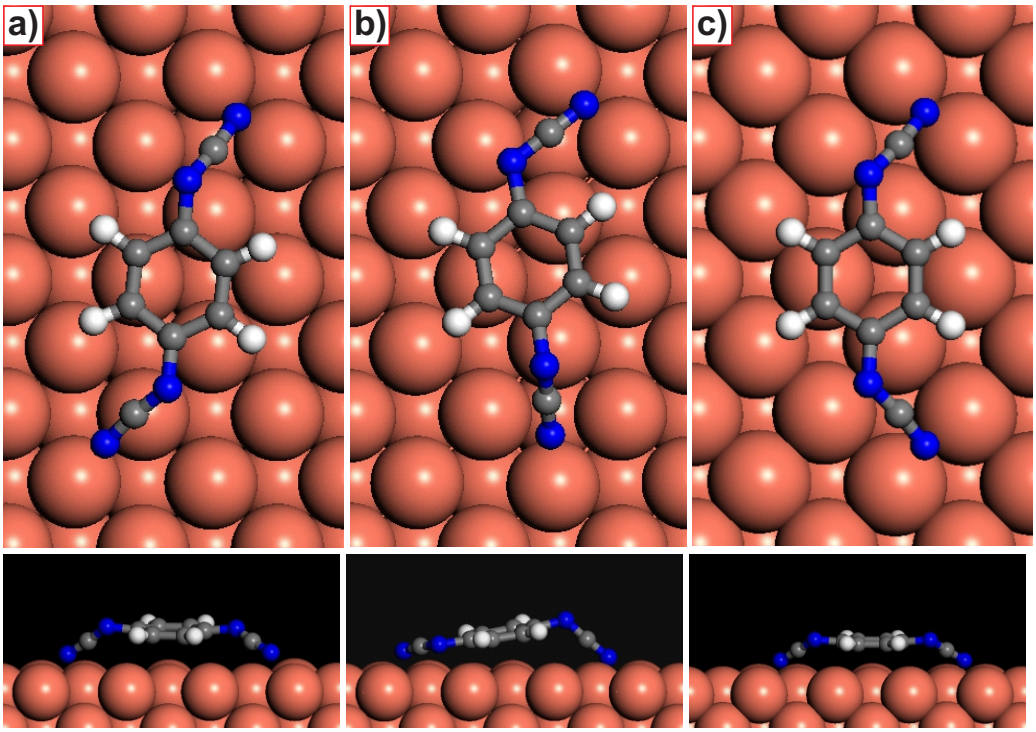

Figure 5.6: *Top and side view of a) a local minimum structure of the trans-DCNQI molecule, c) a local minimum structure of cis-DCNQI, and b) corresponding transition state of the isomerization from a) to c).*

Thus, the results show that, in this case, charge transfer can modify the molecular bond configuration, facilitating the rotation of specific chemical bonds and decreasing isomerization barriers. This, in turn, can also modify the islands structure on the substrate. In summary, we have demonstrated, for the DCNQI/Cu(100) system, the causal connection among the strong molecule-surface interaction, charge transfer, the isomerization reaction and the surface islands structure, being an example of crucial interface effects in organic devices architecture.

5.3.3 DCNQI on Ag(111)

To study how specific to the particular system are the results obtained in the previous section, we have also investigated the adsorption behavior of DCNQI on Ag(111).

In the first series of experiments DCNQI was evaporated onto the surface of the Ag(111) single crystal at 100 K (the STM images were measured at $\sim$ 150 K). In this case, even at this temperature the molecules form ordered compact islands. These islands have a shape of large fringes strongly elongated along one direction, like 1D ribbons, as shown in figure 5.7. The orientation of the long side of the islands for an angle of $30^0(\pm 5^0)$, marked with the black arrow in figure 5.7b, and $40^0(\pm 5^0)$, marked with the blue arrow in figure 5.7b, with the high symmetry axis of the silver crystal.

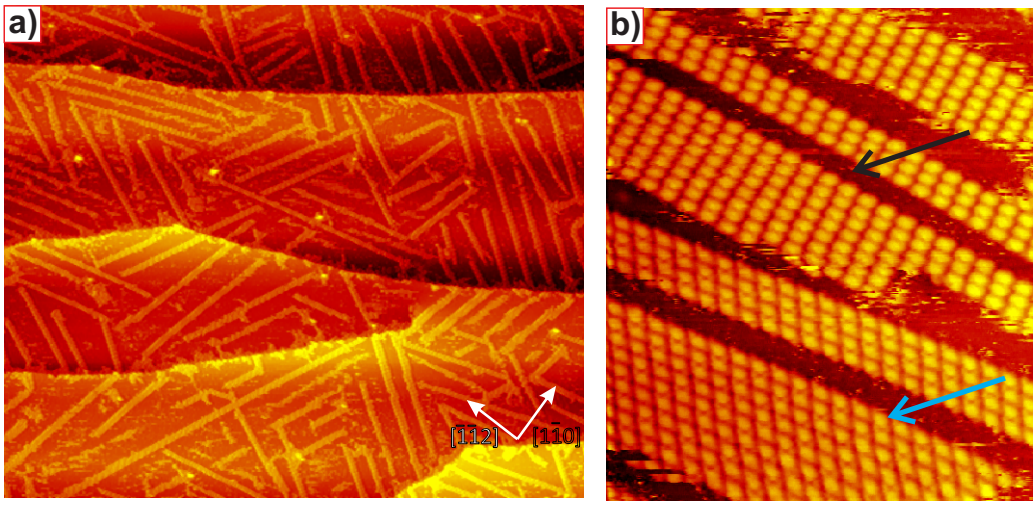

Figure 5.7: *a,b) STM images (taken at 150 K) of DCNQI on Ag(111) after depositing 0.3 ML at 100 K. In (b) it can be observed that there are two types of ordered islands, where the unit cell can be rhomboidal (blue arrow) or rectangular (black arrow). a) 1972 Å × 1673 Å; -0.8 nA, -2 V. b) 198 Å × 229 Å; -0.63 nA, -1.79 V.*

Two types of molecular arrangements are found inside the islands (figure 5.7b). In the first type (marked with a blue arrow), the molecules are ordered with a rhomboidal unit cell, as indicated in figure 5.8a with a black square. The sides of this unit cell measure $b_1 = 7.6(\pm 1.3)$ Å and $b_2 = 10.3(\pm 0.9)$ Å, and $\gamma = 115^0$. These measurements are compatible with a commensurate structure described by the epitaxial relationship $\begin{pmatrix} b_1 \\ b_2 \end{pmatrix} = \begin{pmatrix} 1 & 3 \\ 3 & -1 \end{pmatrix} \begin{pmatrix} a_1 \\ a_2 \end{pmatrix}$ as shown in figure 5.8b. This rhomboidal order can be explained with the help of DFT calculations for a DCNQI free-standing monolayer of DCNQI molecules in the trans-configuration with a similar arrangement is obtained (figure 5.8c), and connected through hydrogen bonds. The lengths of the theoretical lattice parameters are $b_1 = 7.7$ Å, and $b_2 = 10.0$ Å in good

agreement with the experimental values. In this case the binding energy per molecule amounts to 0.66 eV.

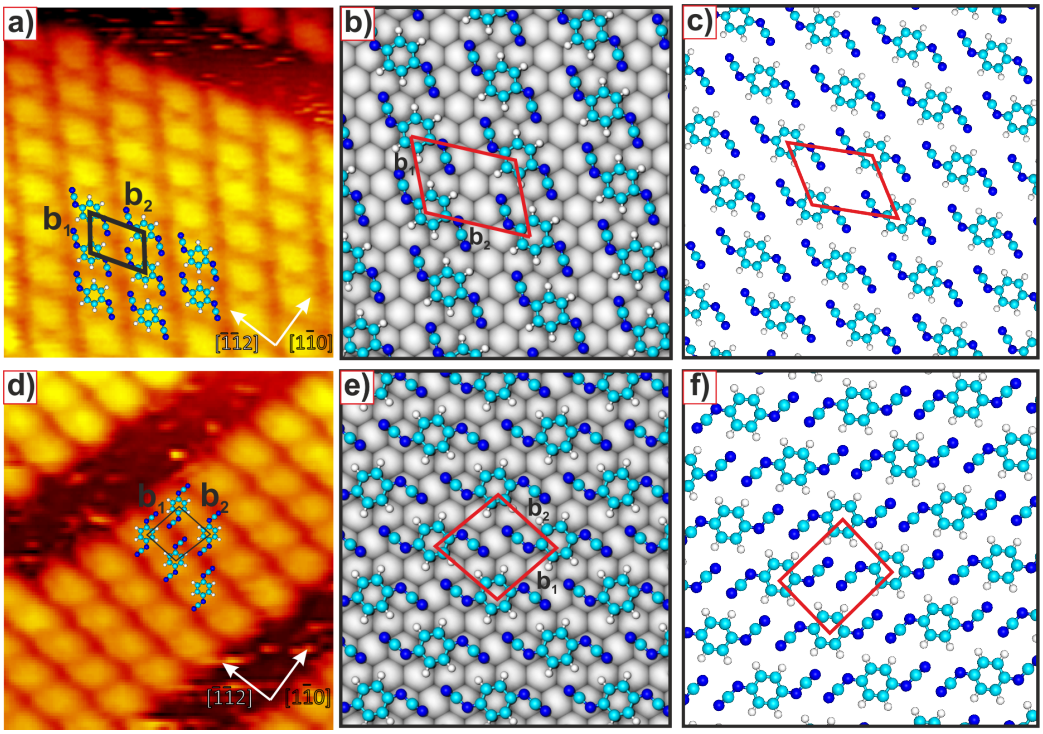

Figure 5.8: *a,d) STM images (taken at 180 K), of the internal structure of the two types of islands observed after depositing DCNQI on Ag(111) at 100 K. b,e) Proposed models, and c,f) Results of DFT calculations for a 2D networks for a free standing monolayer of the two types of LT DCNQI islands (the black squares indicate the unit cell of the 2D assembly): a-c) with a rhomboidal unit cell (black square); d-f) with a rectangular unit cell. In both cases the molecules are in the trans configuration. a) 60 Å × 65 Å; -0.63 nA, -1.79 V. d) 60 Å ×65 Å; -0.44 nA, -2.38 V. c) 0.48 eV; $a = 7.73$ Å, $b = 9.98$ Å. f) 0.48 eV; $a = 8.08$ Å, $b = 6.73$ Å.*

We have made theoretical calculations using the semi-empirical PM3 method to understand the interaction between two DCNQI molecules as a functions of their relative position. The results are shown in figure 5.9: these calculations assume that one molecule is in the origin of coordinates and maps the energy of a second, coplanar molecule as a function of its position. Energy minima are thus the locations in which a second molecule might be expected to be placed. The position of the four minima in figure 5.9 correspond well with the experimental observations and the results of the DFT calculations for the global network, thus showing that the structure can be

simply explained by pairwise interactions.

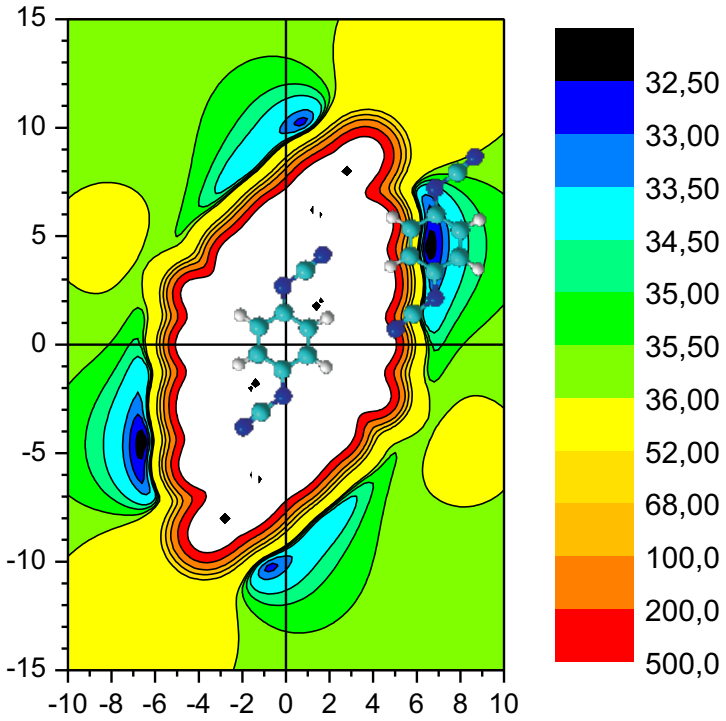

Figure 5.9: *Results of theoretical calculations, using the semi-empirical PM3 method, showing the energy of a pair of molecules as a function of their relative position. Only the nodes can therefore be taken into account for the coordinates of a second molecule. This maps reveals four positions very close to a minima of the map (blue areas) are potential binding sites.*

Islands with a second type of arrangement were also found at low temperature (marked with a black arrow in figure 5.7b). In this case the molecules are ordered with an almost square unit cell, with sides $b_1 = 8.3(\pm 0.8)$ Å, $b_2 = 7.1(\pm 0.6)$ Å, and $\gamma = 95^0$ (figure 5.8d and figure 5.8e). For this ordering, the matrix can be written as $\begin{pmatrix} b_1 \\ b_2 \end{pmatrix} = \begin{pmatrix} 3 & 2 \\ -1 & 2 \end{pmatrix} \begin{pmatrix} a_1 \\ a_2 \end{pmatrix}$. DFT calculations of a free-standing monolayer with this geometry also find a local energy minima close to this arrangement, with theoretical lattice parameters $b_1 = 8.08$ Å, and $b_2 = 6.73$ Å. The calculated binding energy per molecule is 0.67 eV. The fact that both low temperature phases are very close in energy explains the coexistence of both structures. Note that for the rectangular lattice the lateral positions of the molecules do not correspond to the local minima represented in figure 5.9 for pairwise interactions, implying the possible influence

of collective effects.

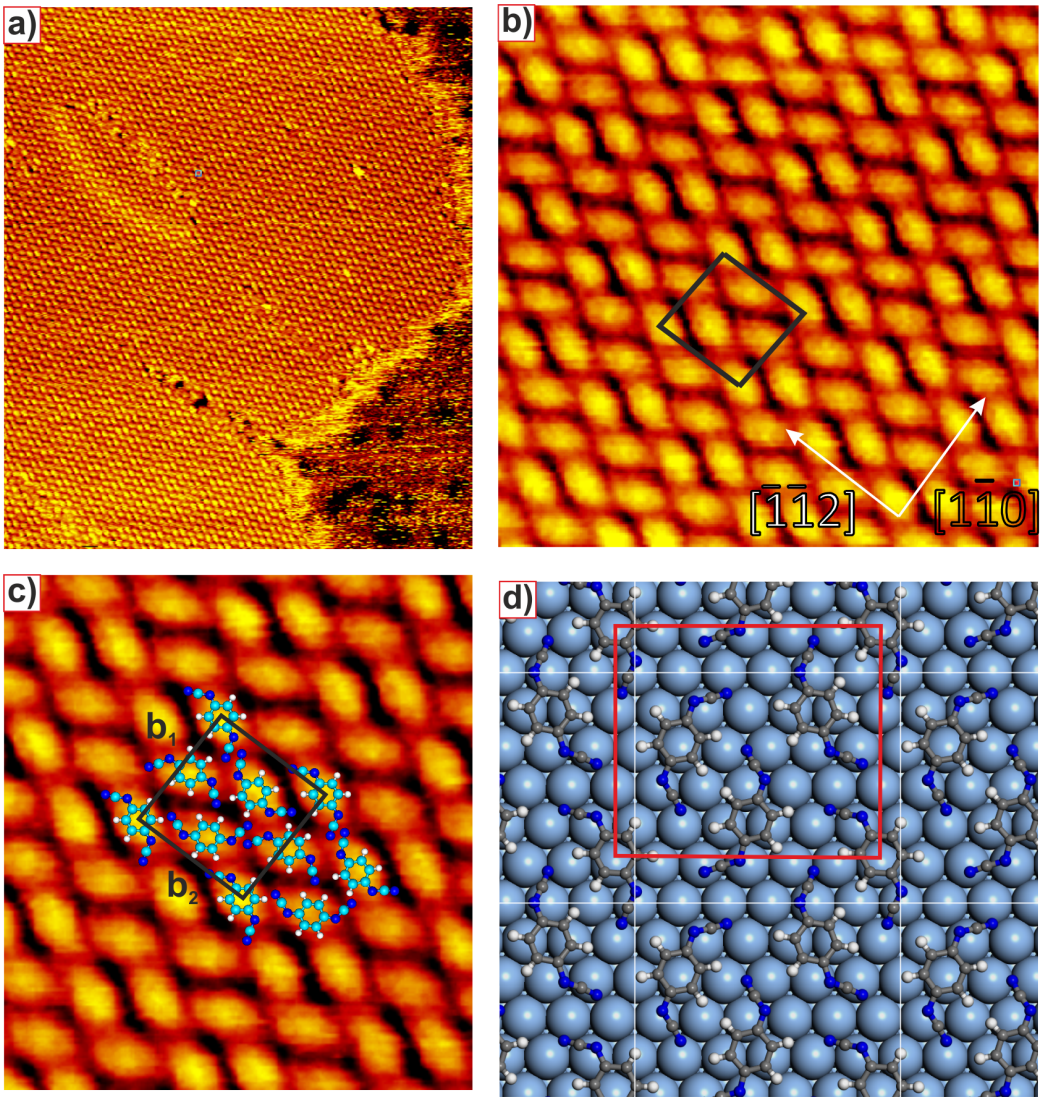

Figure 5.10: *a,b,c) STM images of the Ag(111) surface after depositing almost 0.9 ML of DCNQI at room temperature. The images were taken at room temperature. The black squares in b) and c) indicate the unit cell of the 2D assembly. The white arrows in b) indicate the substrate directions. d) Proposed model for the 2D assembly of DCNQI molecules on Ag(111) after room temperature deposition, indicating the epitaxial relationship with respect to the siver surface. The red square is the resulting unit cell. a) 496 Å × 573 Å; -0.61 nA, -0.99 V. b) 89 Å × 90 Å; -0.69 nA, -1.3 V. c) 60 Å ×65 Å; -0.69 nA, -1.3 V.*

In a second series of experiments, DCNQI was deposited at room temper-

ature on the silver substrate. Figure 5.10 shows a set of increasing resolution STM images of the Ag(111) surface almost completely covered by DCNQI molecules. The darker yellow part in the images in figure 5.10a is the silver surface, and has a fuzzy appearance due to the presence of diffusing DCNQI molecules. The molecules are ordered with an rectangular unit cell, with sides $b_1 = 16.1(\pm 1.3)$ Å, and $b_2 = 14.7(\pm 0.9)$ Å long, parallel, respectively, to the $[1\bar{1}0]$ and $[\overline{11}2]$ directions of the silver surface. Close-up STM images (figure 5.10b and figure 5.10c) are consistent with the DCNQI molecules being flat on the surface, all of them in the cis configuration, held together by a mixture of hydrogen bonds and van der Waals interactions. A model of this arrangement is shown in figure 5.10c. In this case the lattice can be described by the epitaxial relationship $\begin{pmatrix} b_1 \\ b_2 \end{pmatrix} = \begin{pmatrix} 6 & 0 \\ 3 & 6 \end{pmatrix} \begin{pmatrix} a_1 \\ a_2 \end{pmatrix}$.

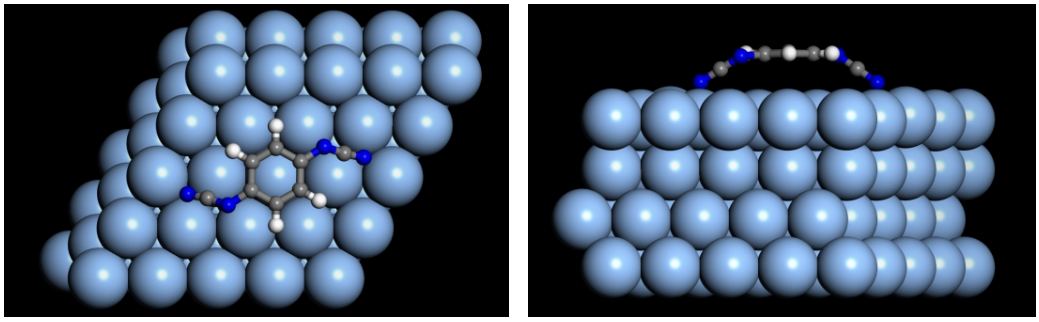

Figure 5.11: *Top and side view of local minimum structure of the trans-DCNQI molecule. The calculated charge transfer is 0.91 e.*

If there is any possible isomerization, once the molecules are part of this cis network, the process becomes irreversible (the islands in figure 5.10a are stable at least until 400 K). Note that the molecular arrangement within the island at room temperature on Ag(111) is very similar to the observed on Cu(100), and then can be understood with the model shown in figure 5.5c (only the lattice parameters are slightly different, if we assume the molecular network to be commensurate with the surface lattice). As in the case on Cu(100), the RT phase can be obtained by annealing to RT the LT phase. In this case the transition takes places at lower temperature (210 K). Again, DFT calculations show that the isomerization process is facilitated by the charge transfer form the substrate to the molecule. When the molecule is adsorbed on the silver surface (figure 5.11 shows the calculated configuration of an isolated trans-isomer), it accepts almost one electron (~ 0.91 e), which, as mentioned previously, changes the bond configuration (see table

5.2) facilitates the rotation of the cyano-imine group, decreasing the trans-cis isomerization energy barrier. Also, like in the case of Cu(100) this isomerization process is not reversible after the molecule changes to the cis-isomer and forms part of a cis-island.

Table 5.2: *Summary of bond lengths (in Å) of the neutral DCNQI molecule ($(DCNQI)^0$), in the dianion state $(DCNQI)^{-2}$, and adsorbed on the Cu(100) and Ag(111) surface.*

Bond	$(DCNQI)^0$	$(DCNQI)^{2-}$	DCNQI/ Cu(100)	DCNQI/ Ag(111)	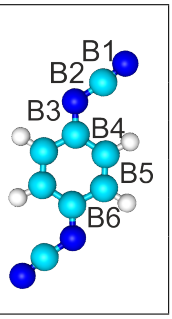
B_1	1.18	1.19	1.20	1.22	
B_2	1.32	1.30	1.29	1.26	
B_3	1.32	1.38	1.40	1.40	
B_4	1.45	1.43	1.42	1.41	
B_5	1.36	1.39	1.41	1.39	
B_6	1.45	1.42	1.42	1.41	

5.3.4 Transition from trans-island to cis-island on both substrates

Although both on Cu(100) and Ag(111) charge transfer from the substrate facilitates the isomerization reaction, there are some differences between the two systems.

For the copper surface, both types of islands (cis and trans configurations) coexist at the transition temperature (245 K, figure 5.12). After depositing DCNQI at low temperature the LT trans-phase can be observed. Close to the transition temperature, the LT phase becomes unstable and LT islands dissolve over time. At the same time the formation of RT islands takes place. Thus, the transition from one configuration to the other is not direct, but occurs by detachment of the molecules from the trans-LT phase to a 2D gas, isomerization, and attachment of cis-molecules to the RT phase islands. The isomerization reaction thus take place while the molecules are freely diffusing over the terraces, and not when they are attached to the islands.

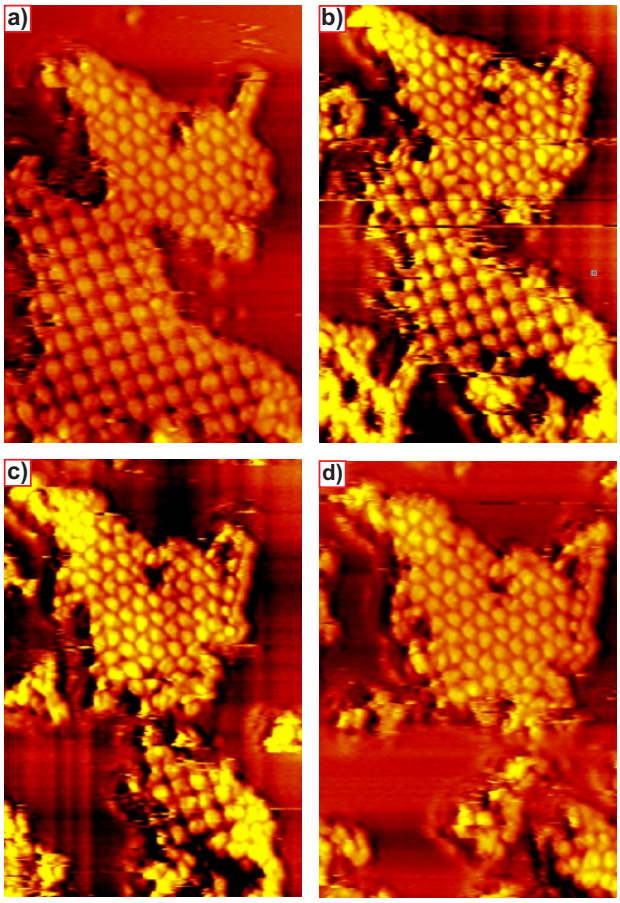

Figure 5.12: *Sequence of STM images of DCNQI on Cu(100) taken at 245 K. The STM images have been measured on the same area of the surface every 60 s. The images show how the LT island disappear while at the same time when the RT appears. a-d) 200 Å × 220 Å; -0.22 nA, -1.67 V.*

For the silver substrate, we could not observe coexistence of trans and cis-islands. In this case after depositing the molecules at low temperature and increasing slowly the temperature, close to the transition temperature (at 210 K) the LT islands disappear and a new type of ordered island can be observed (figure 5.13a and figure 5.13b). These islands are probably a mixture of both molecule isomers, although due to the lack of the resolution we could not propose a concrete model for this arrangement. Anyway, it seems that in this case the molecules do not need to escape from the island for isomerization to take place. Increasing further the temperature (250 K), this intermediate phase island changes, transforming slowly in the RT phase through a series of intermediate steps (figure 5.13c and 5.13d).

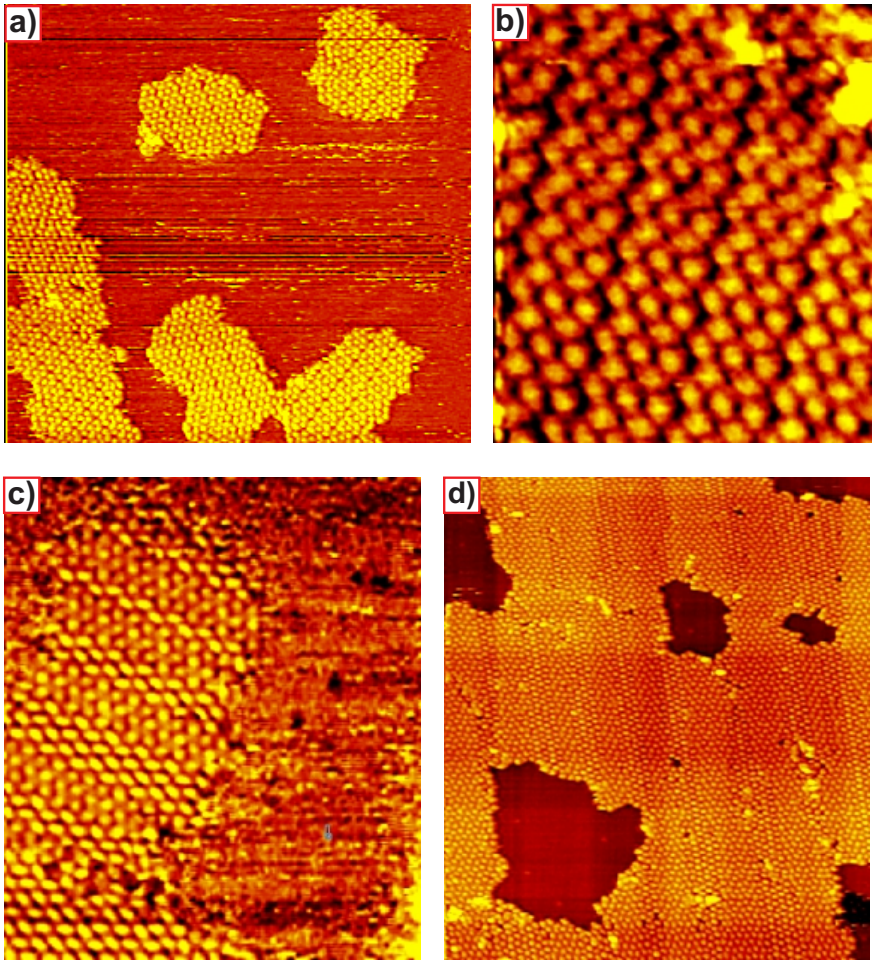

Figure 5.13: *a,b) STM images of the intermediate DCNQI islands on Ag(111) at 210 K. c,d) STM images of DCNQI on Ag(111) after increasing slowly the temperature taken at 250 K. a) 200 Å × 220 Å; -0.22 nA, -1.67 V. b) 200 Å × 220 Å; -0.22 nA, -1.67 V. c) 198 Å × 229 Å; -0.48 nA, -1 V. d) 496 Å × 562 Å; -0.43 nA, -1.37 V.*

To conclude, the transition from the LT phase (trans-island) to the RT phase (cis-island) takes place in a different way on Cu(100) and Ag(111). In the case of copper, the transition occurs when the molecules detach from the trans-island and are diffusing freely on the surface. In the case of the silver this process is not clear, since islands with both cis and trans isomers may exist on the surface, so it is possible that the isomerization reaction can take place inside the island: the molecules change gradually (in an ordered way) to the new configuration , until the island is composed entirely of cis

molecules.

5.3.5 Conclusions

In this section, we have studied the isomerization reaction of DCNQI on Cu(100) and Ag(111). In both cases, after low temperature deposition, the molecules assemble on the surface in the trans-configuration, but when the temperature is increased, an isomerization reaction takes places, and at room temperature all the molecules are in the cis-configuration. In both substrates, the transition is not reversible, since the RT islands are much more stable than the LT islands. We have shown that isomerization takes place at a lower temperature than in solution because, being DCNQI an electron acceptor, the charge transfer from the substrate causes a reorganization of the electronic structure of the molecule, facilitating the rotation of the cyano-group around the imine N atom.

Charge transfer at the organic/metal interface has long been recognized as an important parameter that may modify the energy level alignment and then the charge injection barriers, affecting the functionality of the electronic devices. However, it has been shown that charge transfer may also have other consequences both on the molecule and/or the metal surface, causing, for example, molecular distortion or substrate mediated self-assembly and allowing chemical reactions not present in solution. Here we have shown that, in some cases (DCNQI adsorbed on Cu and Ag), charge transfer modifies the molecular bond configuration, thus facilitating the rotation of the cyano-imine group and decreasing the trans-cis isomerization barrier. This, in turn, modifies the internal islands structure.

5.4 A coordination network: DCNQI-Fe on Ag(111)

5.4.1 Introduction: 2D coordination networks

Coordination chemistry started at the end of the 19th and beginnings of the 20th century [194], and it has been studied intensively ever since, because traditional bulk coordination compounds have very interesting properties, with many applications in catalysis, gas storage and separation, magnetism .... Over the last decades, supramolecular coordinations networks (or metallo-supramolecular) has attracted also wide interest. More recently, the fabrication of two dimensional coordination networks on solid surfaces has increased the number of properties and extended the fields of applications. These metal-ligand coordination networks are promising tools candidates for the

design and fabrication of nanostructured surfaces through the formation of self-assembled nanometer-scale periodic networks (2D) [87, 195–198]. These advances constitute a significant promise for different areas of tecnhological relevance, including catalysis, gas storage, molecular electronics, molecular magnetism, sensor design, or molecular switches and motors [199–202].

Coordination bonds share specifity and directionality with hydrogen bonds and, being stronger than hydrogen bonds, which makes for more robust networks, do not suffer from the irreversibility inherent to covalent networks, which makes possible the preparation of large areas of well-ordered arrays of molecules, in some cases covering multiple surface terraces [203]. However, the presence of the surface makes these compounds inherently different from their bulk counterparts, since the interaction molecule-surface or metal ligand-surface may compete with both molecule-molecule and molecule-ligand interaction. Thus, while the structure of some of the 2D coordination compounds are very similar to certain crystallographic planes already present in well-known bulk systems, other coordination numbers and geometries are completely new.

In the last years, different chemical groups (carboxylic, carbonitrile, pyridyl groups) have been used to build these 2D metal-organic coordination networks, with different reactive metals atoms (Mn, Cu, Co, Fe, Zn, Ce, Gd) and on different substrates (copper, silver, gold) [204–207]. The group most commonly used has been the carboxylic one, which, after deprotonating and changing into a carboxylate group, has been shown to make coordination bonds with different metal ions (Cu, Fe, Co, Mn, Cs) on Cu(100) [76, 208–211], Cu(110) [212] and Au(111) [213]. Another functional groups that have been reported are the carbonitrile- and hydroxyl-terminated polyphenyl linkers codeposited with Co and Fe atoms on Ag(111) [214–216], Cu(100) [217], Cu(111) [218, 219]. And the coordination of the pyridyl group with Cu and Fe atoms on copper [220] and silver [196, 221] substrates has also been reported. However, in spite of all these previous works, many questions remain open about the nature of such coordination bond when a metal surface is involved.

In this section we are also going to study the formation of a 2D Fe-DCNQI metal-organic coordination network. Most of the reported bulk (3D) coordination compounds of DCNQI use different monovalent metals, with the general formula $(DCNQI)_2M^+$, but also with Cu, which seems to have a mixed valency. To our knowledge, however, there are no reports of surface coordination networks with DCNQI as the ligand. Previously, thin films of a DCNQI derivative, 2,5-dimethyl-N,N'-dicyanoquinonediimine (DMe-DCNQI), have been grown on Ag(111) by vapor deposition [222]. In these layers the molecules adsorb parallel to the surface, with a high

degree of lateral order. In addition, films of $Cu(DMe-DCNQI)_2$ and $Na(DMe-DCNQI)_2$ (several nanometers thick) were prepared by subsequent evaporation of DMe-DCNQI and metal counterions on a cold silver substrate and by annealing to room temperature [222]. Ordered structures were also observed on Cu(110) [223] and Ag(110) [224].

In this chapter, we will show that, after depositing DCNQI and Fe on Ag(111), a 2D coordination network is formed. The structural and electronic properties of this network have been studied by X-Ray photoelectron spectroscopy and scanning tunneling microscopy.

5.4.2 STM results of DCNQI-Fe on Ag(111)

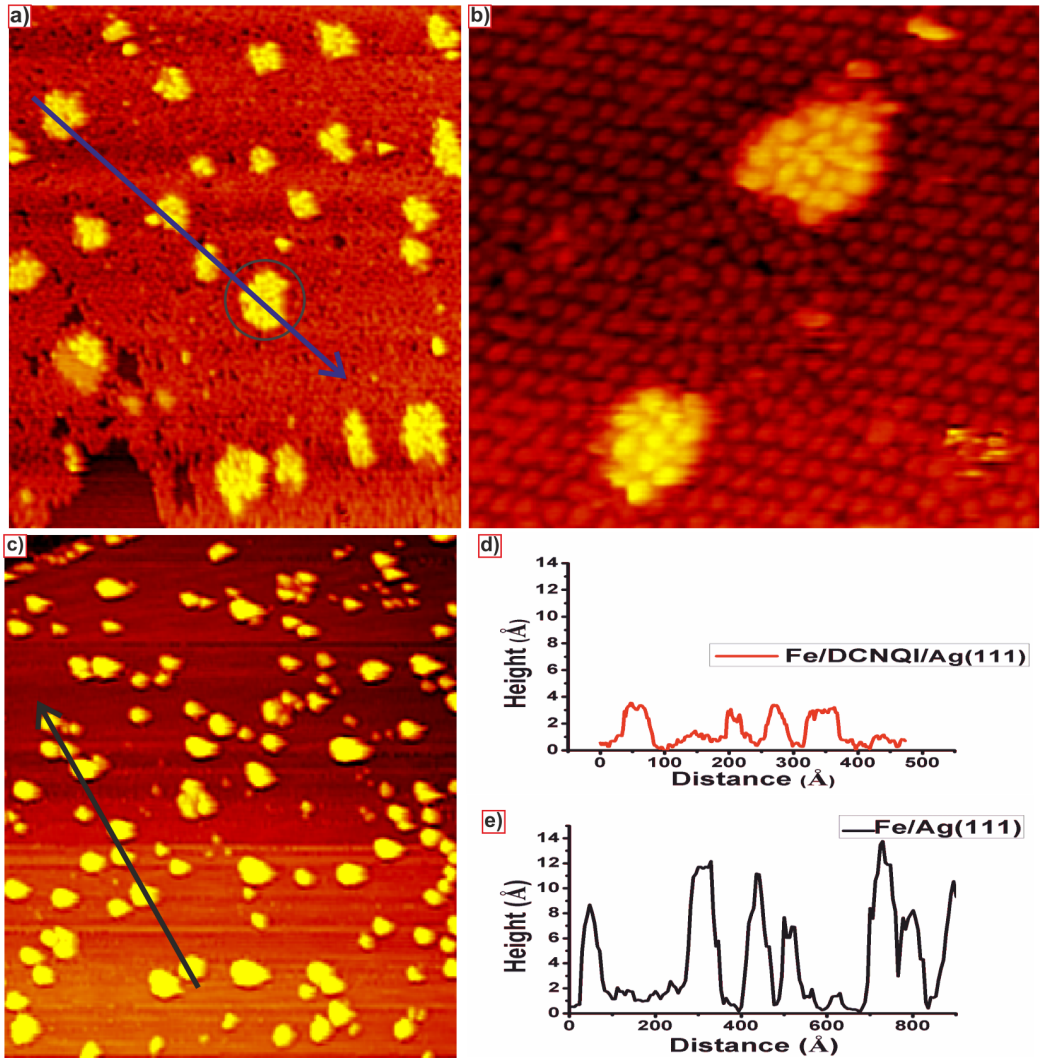

Figure 5.14: *a,b) STM images taken after depositing 0.1 ML of Fe on 1 ML of DCNQI/Ag(111) at room temperature. c) STM image taken after depositing 0.1ML of Fe on Ag(111) at room temperature. d,e) Height profile along the lines drawn in images a) and c). The arrows indicate the direction of the measurement. a) 496 Å × 573 Å; -0.18 nA, -1.53 V, b) 195 Å × 179 Å; -0.22 nA, -1.13 V. c) 1488 Å × 1719 Å; -0.59 nA, -2.02 V.*

To build the coordination network, the molecule DCNQI was first deposited on the silver surface at room temperature, obtaining the RT phase described

in the previous section, with the molecule in the cis-configuration. After depositing 0.1 ML of Fe (Fe was sublimated from an iron rod using an Omicron EFM 3 electron-beam evaporator) at room temperature on this surface, a number of islands (with a density of $\sim 1.3 \times 10^{-16}/m^2$ and a height around 3 Å) appear on the surface. A closer look (see the island circled in blue in figure 5.14a and 5.14b) show that these islands have two different levels: a rather unstructured one with a height of 1.8 Å over the silver surface, and second one that appears to be a molecular layer with a height of 1.2 Å, as shown in the profile graph in figure 5.14e. The space between the islands is covered by the original hydrogen-bonded DCNQI layer, although somewhat distorted, especially close to the islands. Apparently, the iron atoms have diffused over the silver surface to form monoatomic height islands which have been covered by DCNQI molecules. Notice that this situation is different to the case of Fe on the clean Ag(111) surface, as shown in figure 5.14c. Here the iron atoms fully cover the step edges and after that the iron grows in the Volmer-Weber mode, forming three-dimensional Fe clusters several layers high [225]. For a coverage of 0.1 ML, the average height of the cluster is 12($\pm$1.5) Å, as shown in the height profile in figure 5.14d. It seems that the DCNQI layer act as a surfactant, preventing the growth of 3D islands and promoting 2D growth [226–228].

After annealing to 380 K, a number of patches with a different order appear embedded within the DCNQI layer (some of them are marked with a circle in figure 5.15a). A closer look (figure 5.15c) reveals that the new structure seems to be composed of Fe atoms forming an hexagonal lattice connected by DCNQI molecules, in such a way that two Fe atoms are connected by two DCNQI molecules (every Fe atom is connected to 4 DCNQI molecules) forming a set of parallel 1D chains (a model for this structure is shown in figure 5.15d). The hexagonal lattice can be described by the epitaxial relationship $\begin{pmatrix} b_1 \\ b_2 \end{pmatrix} = \begin{pmatrix} 3 & -1 \\ 1 & 4 \end{pmatrix} \begin{pmatrix} a_1 \\ a_2 \end{pmatrix}$. A model for this structure is shown in figure 5.15d. Notice that two types of interactions are taken place in this arrangement: one is the Fe-DCNQI coordination bond that allows the formation of the chains; the other is the interaction between chains, mainly through the formation of C=N-C$\cdots$H-C hydrogen bonds, i.e., one nitrogen belonging to the imine group of one molecule in one chain is connected to the hydrogen of the adjacent molecule in the other chain.

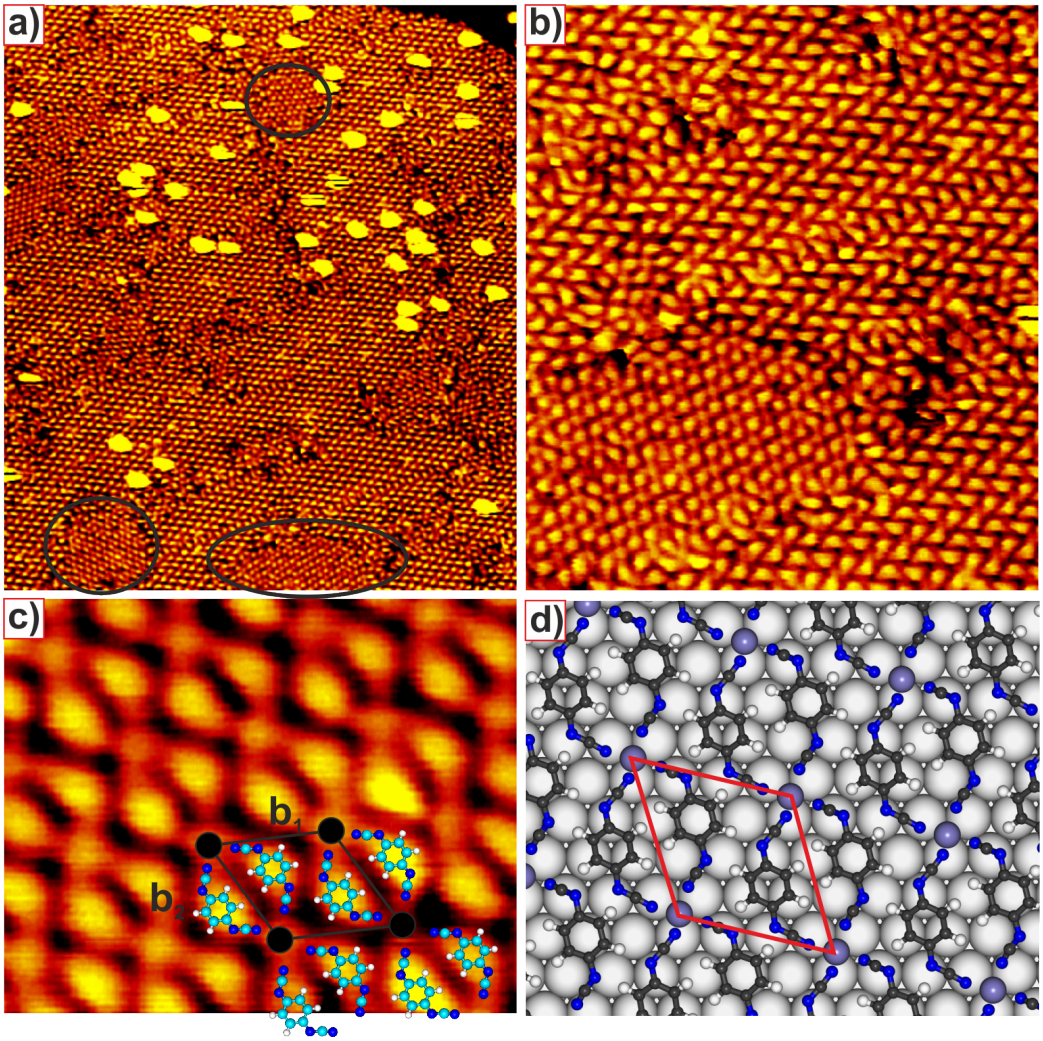

Figure 5.15:
a,b,c) STM images taken after annealing the Fe/DCNQI/Ag(111) system to 380 K (the measurements were made at room temperature. d) Proposed structural model. a) 496 Å × 565 Å; 0.43 nA, 1.13 V. b) 198 Å × 229 Å; 0.43 nA, 1.13 V. c) 50 Å × 40 Å; 0.41 nA, 1.13 V.

There are several interesting things about this structure. First, although DCNQI-Me salts (where Me can be Cu, which seems to have a mixed valence, or a monovalent metal) have been reported [179], to our knowledge there are no bulk DCNQI-Fe coordination compounds. Also, the reported DCNQI salts, where the molecule is always in the trans-configuration, crystallize in the group I41/a [229, 230]. In there, the metal ions are arranged like a string

of pearls, and each metal ion is surrounded by four DCNQI ligands whereby four stacks of ligands are produced. That is, although in these compounds the metals atoms are also four-fold coordinated, they form a square lattice, not hexagonal like here.

5.4.3 Electronic structure of the coordination network: XPS measurements of DCNQI-Fe on Ag(111)

In order to shed some light into the nature of the Fe-DCNQI layer, XPS spectra have been measured during the different stages of growth. Figure 5.16 shows the N1s, and Fe2p core levels of a) the clean Ag(111) surface; b) after depositing a submonolayer amount of DCNQI; c) after depositing 0.1 ML Fe on this molecular layer; and d) after annealing to 380 K. Regarding the N1s spectra, the two broad peaks appearing at $\sim$ 398.5 and 393.0 eV in the clean Ag surface are due to bulk plasmon losses [93]. After depositing DCNQI, a small new feature appears at $\sim$ 398.5 eV, which is consistent with the N1s binding energy measured after depositing DMe-DCNQI on Ag(111) [222] or Ag(110) [224]. To our knowledge, there are no XPS data of bulk DCNQI related compounds. For $TCNQ^0$ the N 1s peak appears at 399.6 eV [30]. In our experiments the binding energy is significantly smaller, and actually it is closer to the N1s binding energy measured on $Cu(TCNQ)^-$ salts, 398.7 eV [231], suggesting that DCNQI is negatively charged, in good agreement with the results in section 5.3.3. The position of this peak does not change after Fe deposition or even after annealing. The C 1s core level is composed of two contributions at 284.7 and 286.1 eV, with an area ratio of $\sim 3:1$, which would correspond to the C atoms of the C ring and the C atoms from the cyano groups, respectively. Once again, this peak does not change appreciably after Fe deposition. The Fe peak, on the other hand, does change after annealing at 380 K. On the freshly deposited sample, the main Fe 2p peak appears at $\sim$ 707 eV, which is characteristic of metallic iron, Fe^0 [232, 233]. After annealing, the peak appears just as a broad feature centered around 709.5 eV, i.e., close to the position of Fe^{+2} [232, 233]. This is similar to the reported Fe2p binding energy in Fe-Terephtalic acid coordination networks on Cu(100) [208].

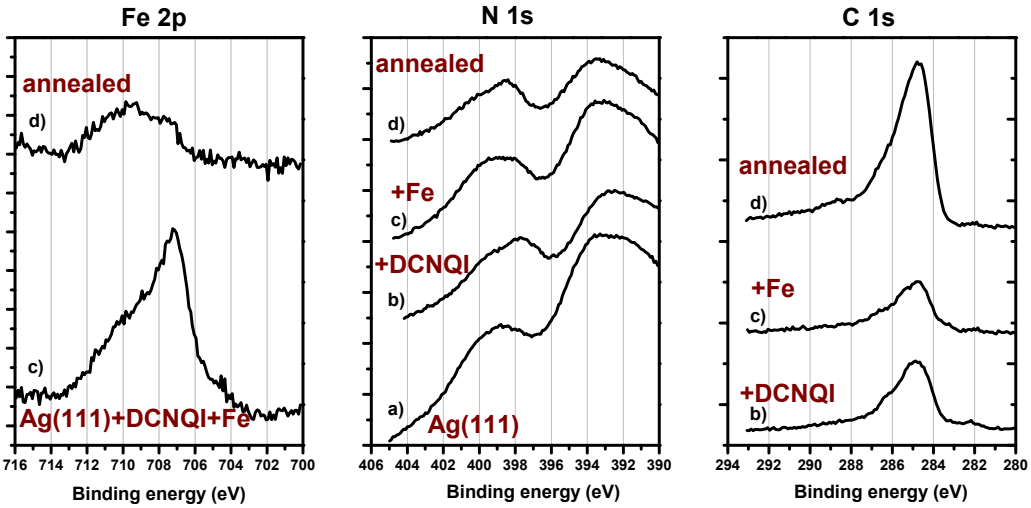

Figure 5.16: *Fe2p, N1s and C1s region of the XPS spectra taken a) on a clean Ag(111) surface; b) after DCNQI deposition; c) after Fe deposition on the DCNQI layer; d) after annealing to 380 K the Fe-DCNQI/Ag(111) system.*

Trying to understand the XPS results, figure 5.17a shows the calculated DFT optimized geometry of an isolated DCNQI molecule, in the cis conformation, on the Ag(111) surface. As in the case of the trans molecule (figure 5.11), there is a strong molecular distortion: the molecule is far from being planar, with the N atoms very close to the surface, the torsion angle between the cyano bonds and the central carbon ring being around 32^0. As mentioned before, this distortion is facilitated by the charge transfer from the metal to the molecule (~ 0.89 e), which makes the central C ring aromatic and makes the bond B3 single bond-like.

To simulate the DCNQI layer, we have considered the model in figure 5.10d. The results are shown in figure 5.17b. Now the C rings are almost parallel to the silver surface but, despite the formation of hydrogen bonds between the cyano groups and the H atoms of neighboring molecules, the molecules are also distorted, with the terminal N atoms very close to the surface. The total charge on the molecules is 0.67 e, slightly smaller than for the isolated molecules.

The results for the Fe-DCNQI/Ag(111) system are shown in figure 5.17c. Since two DCNQI molecules are connected to the same Fe atoms, the carbon rings are no longer parallel to the surface, in order to avoid the H-H repulsion between neighboring molecules. The total charge on the DCNQI molecule is -0.59 e, only slightly smaller than for the DCNQI layer, which explains why the N1s peak binding energy remains approximately the same after formation

of the coordination network. The calculations give an estimated charge of +0.53 e for the Fe atoms, in accordance with the XPS results.

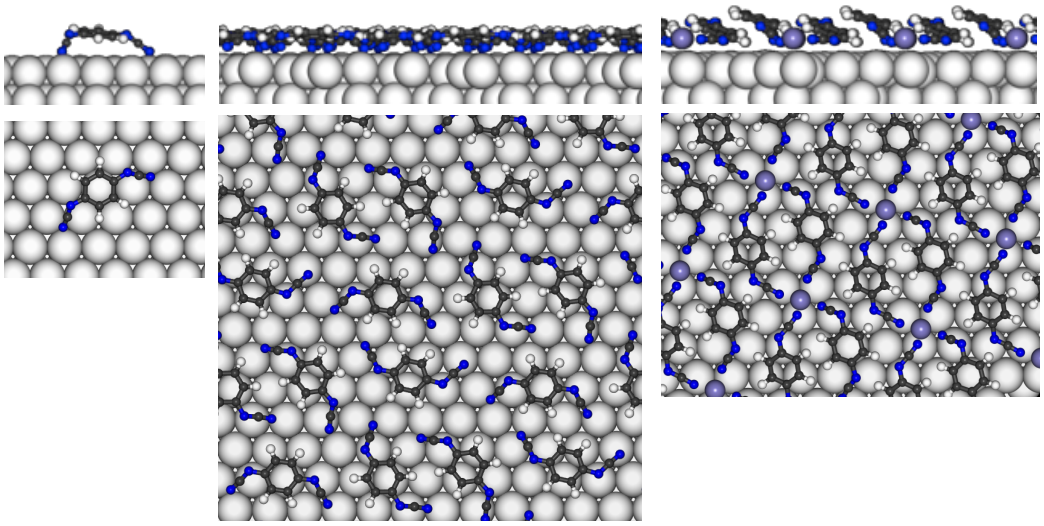

Figure 5.17: *Results of the DFT calculations showing top and side views of a) an isolated cis-molecule on the Ag(111) surface; b) the DCNQI hydrogen bonded network; c) the Fe-DCNQI coordination network.*

The picture that comes out from these calculations is the following. DCNQI is a strong electron acceptor, and, upon deposition on Ag(111), takes 0.89 e from the surface. This charge transfer comes with a pronounced molecular distortion, where the external N atoms come very close to the surface. When the coverage increases, the molecules form a hydrogen bonded network, which decreases slightly (-0.67 e). These changes are more significant upon the formation of the Fe-DCNQI coordination network (the charge of a DCNQI molecules is -0.53 e), since now the N atoms are involved in the coordination bond with the Fe atoms. On the other hand, the Fe atoms get a positive partial charge of 0.53 e. Notice that for a free-standing Fe-DCNQI coordination network the charge of the Fe atoms is practically the same (+0.48 e), but the DCNQI molecules hold only a partial charge of -0.24 e. It is then the interaction with the silver atoms the responsible for the increase in the charge of DCNQI, but without affecting significantly to the Fe-DCNQI coordination bond. In the table 5.3 shown a summary of the different charges.

Table 5.3

	Q(DCNQI)	Q(Fe)
DCNQI/Ag(111)	-0.89	
2D DCNQI/Ag(111)	-0.67	
2D Fe-DCNQI/Ag(111)	-0.53	+0.53
2D Fe-DCNQI	-0.24	+0.48

5.4.4 A disordered coordination network DCNQI-Fe on Ag(111)

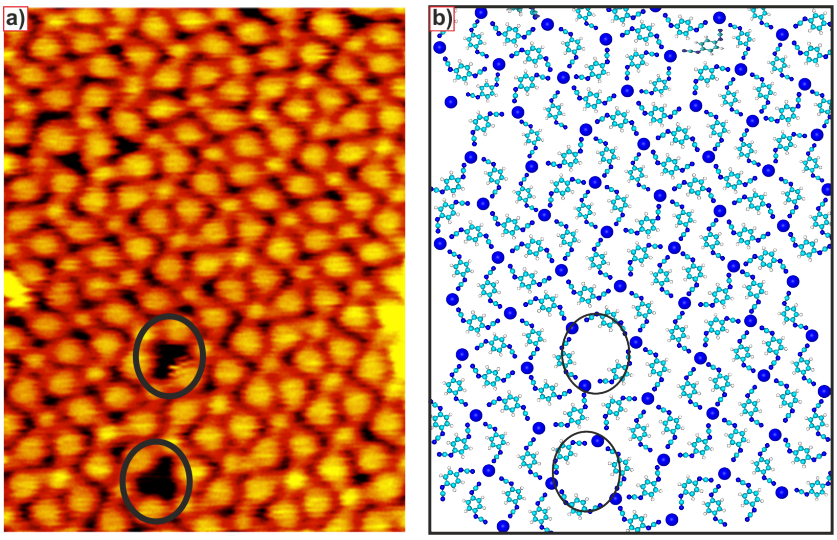

Figure 5.18: *a) STM image of a region of the Fe-DCNQI system after annealing to 320 K. b) Structural scheme of the image shown in (a). a) 77 Å × 80 Å; -0.26 nA, -0.52 V.*

When the subtraste was annealed at a slightly lower temperature (320 K), the structure shown in 5.15c and figure 5.15d does not appear. Instead, in some regions of the Fe-DCNQI layer a different motif, like that shown in Figure 5.18a, can be observed. In this case, the Fe atoms form exactly the same hexagonal lattice than before, but the arrangement of the DCNQI molecules is completely different. While the Fe coordination number is still 4, that is, every Fe atom is connected to four DCNQI molecules, now these are arranged in an apparent random way, and the resulting system is not periodic at all. A scheme of this random coordination is shown in figure 5.18b, where

the black dots represent the iron atoms and the molecules are coordinated as in the adjacent STM images. In spite of this disorder the Fe atoms are forming an hexagonal lattice. Similar disordered coordination network have been reported, like 1,3,5-tris(pyridin-4-ylethynyl)benzene on Cu(111) [220], also molecule with terminal carbonitrile functional groups coordinated with cerium or gadolinium on Ag(111) [234], but in this case the rare earths are also disordered.

5.4.5 Conclusions

Metal ligand coordination interactions are generally more rigid and directional than hydrogen bonds and therefore are employed to supramolecular systems in order to synthesize more robust structures. General design principles follow the coordination chemistry of metal ions having specific coordination geometry (tetrahedral, square, octahedral, etc.) and the choice of molecules representing adequate functional groups. For example, the coordination geometry of the metal atoms changes due to the spatial confinement on surfaces and the substrate actively influences the adsorbates from geometrical arrangements to chemical modifications.

In this section, we have studied a 2D coordination network, DCNQI-Fe on Ag(111) formed by depositing a submonolayer amount of Fe on top of a layer of DCNQI. It is worthy to mention that the DCNQI layer act as a surfactant, preventing the growth of the iron in 3D islands. After annealing to 320 K, a disorder coordination networks appears; in this configuration the iron atoms are forming an hexagonal lattice, and the DCNQI molecules are coordinated to the iron atoms, in such a way that one molecule is bonded to two iron atoms and every atom is coordinated with four molecules. The arrangement of the molecules, however, is rather disordered. After increasing the temperature a new coordination network is formed, where the iron atoms are forming an identical hexagonal lattice, the DCNQI molecules are ordered to form a set of parallel 1D chains. These 1D chains are connected together by C=N-C$\cdots$H-C hydrogen bonds, allowing the formation of a 2D coordination network. Moreover, we found that depositing the molecule and the iron metal on the Ag(111), the metal keeps metallic behavior, but we found that the iron metal shifts to oxidation state after annealing this system when the coordination network DCNQI-Fe is obtained. The charge of the Fe atoms in this coordination network is ~ 0.5 e.

6
General Conclusions

The subject of the present doctoral thesis has been the investigation, using variable temperature STM and XPS, and the results of DFT calculations, of the structural and electronic properties of three different organic electron acceptor molecules (TCNE, TCNQ, and DCNQI) and one organic electron donor molecule (TTF) deposited on metal substrates (Cu(100), Ag(111), Au(111)).

In the following, we summarize some of the more relevant results obtained in this thesis:

For all the studied systems, charge transfer at the organic/metal interface plays an important role since may modify the energy level alignment and then the charge injection barriers. Also, charge transfer has other consequences that have been reported, such as molecular distortion or substrate mediated self-assembly. In particular, the strong interaction of TCNE with the Ag(111) substrate promotes the presence of silver adatoms on the surface to form Ag-TCNE coordination networks. TCNQ has also a strong interaction with the silver substrate and the presence of the silver adatoms cannot be definitively ruled out. However, the second layer shows only a weak interaction, and the molecule are decoupled from the substrate. In these two systems, the amount of charge from the substrate to the molecule is close to 1 e. On the other hand TTF can be adsorbed in two different configurations: almost planar, after room temperature deposition, or tilted with respect to the surface, after annealing the sample at 350 K. although it is

a donor molecule, it holds on a small positive charged, 0.1 e. In addition, we have shown that, in the case of DCNQI on Cu(100) and Ag(111), charge transfer decreases the energy barrier between the trans- and cis-isomers of the molecule, with the consequence of the activation of an isomerization reaction by thermal energy below room temperature.

In the mixed donor-acceptor systems, TTF-TCNQ and TTF-TCNE on Ag(111), several phases with different stoichiometries have been studied, each one leading to a different levels of charge transfer. In this case charge transfer takes place through the metal substrate, that acts as an intermediary between the donor and acceptor. These results show that for these mixed systems, the core level shifts in photoemission experiments do not only depend on the charge state of the molecule but also on the environment. A simple calculations shows that the effect of the potential created by the nearby molecules (for both TCNQ and TTF, more negative when increasing the TCNQ content) shifts the core levels to lower binding energies, an effect that can actually overcome the effect of the molecular charge.

Finally, the fabrication of an Fe-DCNQI coordination network has been reported. Actually, two different networks appear on the surface: ordered one and a disordered self-assembly; although in both case the iron atoms form an hexagonal lattice. In addition, we have shown that the iron atoms changes his metallic character to oxidized state.

In summary, the results presented in this thesis shows the important role that charge transfers plays at the metal-organic interface. These investigations shows also the power of combining different experimental techniques, like VT-STM and XPS, in an unique system, with theoretical calculations to understand the structural and electronic properties of the metal-organic systems.

7
Conclusiones generales

El tema de la presente tesis doctoral ha sido la investigación, usando un microscopía de efecto túnel (STM) de temperatura variable, espectroscopía de fotoemisión (XPS), y los resultados de los cálculos teóricos (DFT), de las propiedas estructurales y electrónicas de tres moléculas orgánicas aceptoras de electrones diferentes (TCNE, TCNQ, y DCNQI) y una molécula orgánica donora de electrones (TTF) depositadas sobre substratos metálicos (Cu(100), Ag(111), y Au(111)).

Seguidamente, resumimos alguno de los resultados más relevantes obtenidos en esta tesis:

Para todo los sistemas estudiados, la transferencia de carga en la interfase orgánica/metal juega un papel importante puesto que puede modificar el alineamiento de los nivel de energéticos y por tanto las barrera de inyección de carga. Pero además, la transferencia de carga tiene otras consecuencias que han sido relatadas, como la distorsión molecular o un papel activo del substrato en el auto-ensamblado molecular. En particular, la fuerte interacción del TCNE con el substrato Ag(111) promueve la presencia de adátomos de plata sobre la superficie que dan lugar a la formación de redes de coordinación Ag-TCNE. El TCNQ también tiene una fuerte interacción con el substrato de plata, y la presencia de los adátomos de plata no pueden ser descartada. Sin embargo, la segunda capa muestra una débil interacción, y las moléculas están desacopladas del substrato. En estos dos sistemas, la cantidad de carga desde el substrato a la molécula es cerca de 1 e. Por otra parte, el TTF puede estar en dos configuraciones diferentes sobre la superficie: casi plana, después de depositar a temperatura ambiente, o ligeramente inclinada con respecto al

substrato, después de calentar la muestra a 350 K. Aunque es una molécula donora, solo está ligeramente cargada positivamente, 0.1 e. Además, hemos mostrado que, en el caso del DCNQI en Cu(100) y Ag(111), la transferencia de carga decrece la barrera de energía entre los isomeros trans- y cis- de la molécula, con la consecuencia de la activación de una reacción de isomerización por energía térmica por debajo de temperatura ambiente.

En los sistemas de mezclas donores-aceptores, TTF-TCNQ y TTF-TCNE sobre la Ag(111), hemos estudiado distintas fases con diferentes estequiometrías, cada una de ellos conduciendo a diferentes niveles de transferencia de carga. En este caso la transferencia de carga tiene lugar a tráves del substrato metálico, el cuál actúa como intermediario entre el donor y el aceptor. Estos resultados muestran que para estos sistemas de mezclas, el desplazamiento de los niveles de energía de los átomos en los experimentos de fotoemisión no solo dependen del estado de carga de la molécula pero también de su entorno. Un simple cálculo muestra que el efecto del potencial creado por las moléculas próximas (tanto para el TCNQ como para el TTF, es más negativo cuando el contenido de TCNQ aumenta) desplaza los niveles de los átomos a energías de ligadura más bajas, un efecto que actualmente supera el efecto de la carga molecular.

Finalmente, ha sido demostrado la fabricación de una red de coordinación Fe-DCNQI. En realidad, dos redes diferentes aparecen sobre la superficie: una ordenada y otra desordenada; aunque en ambos casos los átomos de hierro forman la misma red hexagonal. Además, mostramos que los átomos de hierro cambian su carácter metálico a un estado oxidado.

En resumen, los resultados presentados en esta tesis muestran el papel importante que la transferencia de carga juega en las interfases metal-orgánicas. Estas investigaciones muestran también la potencia de combinar diferentes técnicas experimentales, como el VT-STM y XPS, en un único sistema, con cálculos teóricos, para entender las propiedades estructurales y electrónicas de los sistemas metal-orgánicos.

Bibliography

[1] A. Roth. *Vacuum Technology* (Elsevier Science 1990).

[2] J. O. Hirschfelder, C. F. Curtiss, and R. B. Bird. *Molecular theory of gases and liquids*. Structure of matter series (Wiley-Interscience 1964).

[3] P. Atkins and J. de Paula. *Atkins' Physical Chemistry* (OUP Oxford; 9 edition (19 Nov 2009)).

[4] G. Binning, H. Rohrer, C. Gerber, and E. Weibel. Surface studies by scanning tunneling microscopy. Physical Review Letters **49**, 57 (1982).

[5] G. Binning, H. Rohrer, C. Gerber, and E. Weibel. 7 x 7 reconstruction on Si(111) resolved in real space. Physical Review Letters **50**, 120 (1983).

[6] G. Binning and H. Rohrer. Scanning tunneling microscopy. Surface Science **126**, 236 (1983).

[7] C. Bai. *Scanning tunneling microscopy and its applications* (2000).

[8] J. Bardeen. Tunneling from a many-particle point of view. Physical Review Letters **6**, 57 (1961).

[9] J. Tersoff and D. Hamann. Theory of the scanning tunneling microscope. Physical Review B **31**, 805 (1985).

[10] J. Tersoff and D. Hamann. Theory and applicaction for the scanning tunneling microscope. Physical Review Letters **50**, 1998 (1983).

[11] S. Hufner. *Photoelectron spectroscopy principles and applications* (Springer, 1999).

[12] H. Bubert and H. Jenett. *Surface and thin film analysis: principles, instrumentation, applications* (Wiley-VCH Verlag GmbH 2002).

[13] P. Hohenberg and W. Kohn. Inhomogeneous Electron gas. Physical Review **136**, B864 (1964).

[14] M. Levy. Universal variational functionals of electron densities, first-order density matrices, and natural spin-orbitals and solution of the v-representability problem. Proceedings of the National Academy of Sciences **76**, 6062 (1979).

[15] W. Kohn and L. Sham. Self-consistent equations incluiding exchange and correlation effects. Physical Review **140**, A1133 (1965).

[16] J. Hafner. Ab-initio simulations of materials using VASP: Density-functional theory and beyond. Journal of computational chemistry **29**, 2044 (2008).

[17] J. P. Perdew, K. Burke, and M. Ernzerhof. Generalized gradient approximation made simple. Physical review letters **77**, 3865 (1996).

[18] P. E. Blöchl. Projector augmented-wave method. Physical Review B **50**, 17953 (1994).

[19] S. Grimme. Semiempirical GGA-type density functional constructed with a long-range dispersion correction. Journal of computational chemistry **27**, 1787 (2006).

[20] H. J. Monkhorst and J. D. Pack. Special points for Brillouin-zone integrations. Physical Review B **13**, 5188 (1976).

[21] B. Delley. An all-electron numerical method for solving the local density functional for polyatomic molecules. The Journal of Chemical Physics **92**, 508 (1990).

[22] B. Delley. From molecules to solids with the DMol3 approach. The Journal of Chemical Physics **113**, 7756 (2000).

[23] A. Tkatchenko and M. Scheffler. Accurate molecular Van Der Waals interactions from ground-state electron density and free-atom reference data. Physical Review Letters **102**, 073005 (2009).

[24] S. R. Forrest. The path to ubiquitous and low-cost organic electronic appliances on plastic. Nature **428**, 911 (2004).

[25] M. Granström, K. Petritsch, A. C. Arias, A. Lux, M. R. Andersson, and R. H. Friend. Laminated fabrication of polymeric photovoltaic diodes. Nature **395**, 257 (1998).

[26] N. Koch. Organic electronic devices and their functional interfaces. Chemphyschem: A european journal of chemical physics and physical chemistry **8**, 1438 (2007).

[27] N. R. Armstrong, W. Wang, D. M. Alloway, D. Placencia, E. Ratcliff, and M. Brumbach. Organic/Organic' heterojunctions: organic light emitting diodes and organic photovoltaic devices. Macromolecular rapid communications **30**, 717 (2009).

[28] L. Sánchez, R. Otero, J. M. Gallego, R. Miranda, and N. Martín. Ordering fullerenes at the nanometer scale on solid surfaces. Chemical reviews **109**, 2081 (2009).

[29] M. Garnica, D. Stradi, S. Barja, F. Calleja, C. Díaz, M. Alcamí, N. Martín, A. L. Vázquez de Parga, F. Martín, and R. Miranda. Long-range magnetic order in a purely organic 2D layer adsorbed on epitaxial graphene. Nature Physics **9**, 368 (2013).

[30] T.-C. Tseng, C. Urban, Y. Wang, R. Otero, S. L. Tait, M. Alcamí, D. Ecija, M. Trelka, J. M. Gallego, N. Lin, M. Konuma, U. Starke, A. Nefedov, A. Langner, C. Wöll, M. A. Herranz, F. Martín, N. Martín, K. Kern, and R. Miranda. Charge-transfer-induced structural rearrangements at both sides of organic/metal interfaces. Nature chemistry **2**, 374 (2010).

[31] M. Alonso Garnica. *Electron acceptor molecules deposited on epitaxial graphene studied by means of low temperature scanning tunneling microscopy/spectroscopy.* Ph.D. thesis (2013).

[32] C. Urban, Y. Wang, J. Rodríguez-Fernández, R. García, M. A. Herranz, M. Alcamí, N. Martín, F. Martín, J. M. Gallego, R. Miranda, and R. Otero. Charge transfer-assisted self-limited decyanation reaction of TCNQ-type electron acceptors on Cu(100). Chemical Communications **50**, 833 (2014).

[33] C. B. France, P. G. Schroeder, J. C. Forsythe, and B. A. Parkinson. Scanning tunneling microscopy study of the coverage-dependent structures of pentacene on Au(111). Langmuir **19**, 1274 (2003).

[34] Y. Wang, M. Trelka, I. Preda, A. Vollmer, C. Urban, E. David, M. Alcami, L. Soriano, N. Martin, R. Otero, M. Gallego, and R. Miranda. Growth and structure of self-assembled monolayers of a TTF derivative on Au(111). Journal of Physical Chemistry C **114**, 6503 (2010).

[35] B. Fiedler, E. Rojo-Wiechel, J. Klassen, J. Simon, J. Beck, and M. Sokolowski. Ordered structures of two sulfur containing donor molecules on the Au(111) surface. Surface Science **606**, 1855 (2012).

[36] J. Fraxedas, S. García-Gil, S. Monturet, N. Lorente, I. Fernández Torrente, K. J. Franke, J. I. Pascual, A. Vollmer, R. P. Blum, N. Koch, and P. Ordejón. Modulation of surface charge transfer through competing long-range repulsive versus short-range attractive interactions. Journal of Physical Chemistry C **115**, 18640 (2011).

[37] C. E. Klots, R. N. Compton, and V. F. Raaen. Electronic and ionic properties of molecular TTF and TCNQ. The Journal of Chemical Physics **60**, 1177 (1974).

[38] R. N. Compton and C. D. Cooper. Negative ion properties of tetracyanoquinodimethan: Electron affinity and compound states. The Journal of Chemical Physics **66**, 4325 (1977).

[39] F. Herman, A. R. Williams, and K. H. Johnson. Multiple scattering method based on overlapping atomic spheres with application to the TCNQ molecule. The Journal of Chemical Physics **61**, 3508 (1974).

[40] C. Dahlstrand, K. Yamazaki, K. Kilså, and H. Ottosson. Substituent effects on the electron affinities and ionization energies of tria-, penta-, and heptafulvenes: a computational investigation. The Journal of organic chemistry **75**, 8060 (2010).

[41] L. E. Lyons and L. D. Palmer. A surface ionization source and quadrupole mass filter for photodetachment studies. International Journal of Mass Spectrometry and Ion Physics **16**, 431 (1975).

[42] S. Chowdhury and P. Kebarle. Electron affinities of di- and tetracyanoethylene and cyanobenzenes based on measurements of gas-phase electron-transfer equilibria. Journal of the American Chemical Society **108**, 5453 (1986).

[43] D. Khuseynov, M. T. Fontana, and A. Sanov. Photoelectron spectroscopy and photochemistry of tetracyanoethylene radical anion in the gas phase. Chemical Physics Letters **550**, 15 (2012).

[44] D. J. Knowles and A. J. C. Nicholson. Ionization energies of formic and acetic acid monomers. The Journal of Chemical Physics **60**, 1180 (1974).

[45] E. M. Engler, F. B. Kaufman, D. C. Green, C. E. Klots, and R. N. Compton. Ionization potentials and donor properties of selenium analogs of tetrathiafulvalene. Journal of the American Chemical Society **97**, 2921 (1975).

[46] A. J. Berlinsky, J. F. Carolan, and L. Weiler. Photoelectron spectrum and electronic structure of tetrathiofulvalene (TTF). Canadian Journal of Chemistry **52**, 3373 (1974).

[47] H.-x. Li, R.-h. Zheng, and Q. Shi. Theoretical study on charge carrier mobilities of tetrathiafulvalene derivatives. Physical chemistry chemical physics **13**, 5642 (2011).

[48] A. W. Dweydari and C. H. B. Mee. Oxygen adsorption on the (111) face of silver. Physica Status Solidi (a) **17**, 247 (1973).

[49] A. W. Dweydari and C. H. B. Mee. Work function measurements on (100) and (110) surfaces of silver. Physica Status Solidi (a) **27**, 223 (1975).

[50] H. B. Michaelson. The work function of the elements and its periodicity. Journal of Applied Physics **48**, 4729 (1977).

[51] P. O. Gartland, S. Berge, and B. J. Slagsvold. Photoelectric work function of a copper single crystal for the (100), (110), (111), and (112) faces. Physical Review Letters **28**, 738 (1972).

[52] T. L. Cairns, R. A. Carboni, D. D. Coffman, V. A. Engelhardt, R. E. Heckert, E. L. Little, E. G. McGeer, B. C. Mckusick, W. J. Middleton, R. M. Scribner, C. W. Theobald, and H. E. Winberg. Cyanocarbon chemistry. I. Preparation and reactions of tetracyanoethylene. Journal of the American Chemical Society **80**, 2775 (1958).

[53] A. Fatiadi. New applicatins of Tetracyanoethylene in organic chemistry. Synthesis **1986**, 249 (1986).

[54] A. Fatiadi. Addition and cycloaddition reactions of tetracyanoethylene (TCNE) in organic chemistry. Synthesis **1987**, 749 (1987).

[55] A. Fatiadi. New applications of tetracyanoethyelene in organometallic chemistry. Synthesis **1987**, 959 (1987).

[56] J. S. Miller. Tetracyanoethylene (TCNE): the characteristic geometries and vibrational absorptions of its numerous structures. Angewandte Chemie (International ed. in English) **45**, 2508 (2006).

[57] B. B. Kaul, M. A. Taylor, M. J. Whitton, and G. T. Yee. Beyond TCNE: New building blocks for molecule-based magnets. Synthetic Metals **122**, 471 (2001).

[58] J. W. Raebiger and J. S. Miller. Magnetic ordering in the rare earth molecule-based magnets, Ln(TCNE)3 (Ln = Gd, Dy; TCNE = tetracyanoethylene). Inorganic chemistry **41**, 3308 (2002).

[59] S. Bedwani, D. Wegner, M. Crommie, and A. Rochefort. Strongly reshaped organic-metal interfaces: Tetracyanoethylene on Cu(100). Physical Review Letters **101**, 216105 (2008).

[60] T. Choi, S. Bedwani, A. Rochefort, C.-Y. Chen, A. J. Epstein, and J. A. Gupta. A single molecule Kondo switch: Multistability of tetracyanoethylene on Cu(111). Nano letters **10**, 4175 (2010).

[61] D. Wegner, R. Yamachika, X. Zhang, Y. Wang, M. F. Crommie, and N. Lorente. Adsorption site determination of a molecular monolayer via inelastic tunneling. Nano letters **13**, 2346 (2013).

[62] T. Deilmann, P. Krüger, M. Rohlfing, and D. Wegner. Adsorption and STM imaging of tetracyanoethylene on Ag(001): An ab initio study. Physical Review B **89**, 045405 (2014).

[63] D. Wegner, R. Yamachika, Y. Wang, V. W. Brar, B. M. Bartlett, J. R. Long, and M. F. Crommie. Single-molecule charge transfer and bonding at an organic/inorganic interface: Tetracyanoethylene on noble metals. Nano letters **8**, 131 (2008).

[64] D. Wegner, R. Yamachika, X. Zhang, Y. Wang, T. Baruah, M. Pederson, B. Bartlett, J. Long, and M. Crommie. Tuning molecule-mediated spin coupling in bottom-up-fabricated vanadium-tetracyanoethylene nanostructures. Physical Review Letters **103**, 087205 (2009).

[65] E. Carlegrim, Y. Zhan, F. Li, X. Liu, and M. Fahlman. Characterization of the Ni/V(TCNE)x interface for hybrid spintronics applications. Organic Electronics **11**, 1020 (2010).

[66] K. I. Pokhodnya, A. J. Epstein, and J. S. Miller. Thin-film V[TCNE]x magnets. Advanced materials **12**, 410 (2000).

[67] P. Bhatt and S. Yusuf. Thin films of molecule-based charge transfer complex cobalt tetracyanoethylene: In situ X-ray photoemission study. Surface Science **605**, 1861 (2011).

[68] E. Carlegrim, Y. Zhan, M. de Jong, and M. Fahlman. Electronic structure of thin film cobalt tetracyanoethylene, Co(TCNE)x. Synthetic Metals **161**, 1892 (2011).

[69] P. Bhatt, A. Kanciurzewska, E. Carlegrim, M. Kapilashrami, L. Belova, K. V. Rao, and M. Fahlman. Ferromagnetism above room temperature in nickel-tetracyanoethylene thin films. Journal of Materials Chemistry **19**, 6610 (2009).

[70] B. Grünbaum and G. Shephard. *Tilings and patterns* (W. H. Freeman and company 1986).

[71] F. Besenbacher and J. K. Norskov. Oxigen chemisorption on metal surfaces: general trends for Cu,Ni and Ag. Progress in surface science **44**, 5 (1993).

[72] F. M. Leibsle, S. Haq, B. G. Frederick, M. Bowker, and N. V. Richardson. Molecularly induced step faceting on Cu(110) surfaces. Surface science letters **343**, L1175 (1995).

[73] Q. Chen and N. V. Richardson. Surface facetting induced by adsorbates. Progress in Surface Science **73**, 59 (2003).

[74] J. I. Pascual, J. V. Barth, G. Ceballos, G. Trimarchi, A. De Vita, K. Kern, and H.-P. Rust. Mesoscopic chiral reshaping of the Ag(110) surface induced by the organic molecule PVBA. The Journal of chemical physics **120**, 11367 (2004).

[75] T. Katayama, K. Mukai, S. Yoshimoto, and J. Yoshinobu. Reactive rearrangements of step atoms by adsorption and asymmetric electronic states of tetrafluorotetracyanoquinodimethane on Cu(100). Physical Review B **83**, 153403 (2011).

[76] N. Lin, A. Dmitriev, J. Weckesser, J. V. Barth, and K. Kern. Real-time single-molecule imaging of the formation and dynamics of coordination compounds. Angewandte Chemie International Edition **41**, 4779 (2002).

[77] C. C. Perry, S. Haq, B. G. Frederick, and N. V. Richardson. Face specificity and the role of metal adatoms in molecular reorientation at surfaces. Surface Science **409**, 512 (1998).

[78] J. Barth, J. Weckesser, N. Lin, A. Dmitriev, and K. Kern. Supramolecular architectures and nanostructures at metal surfaces. Applied Physics A: Materials Science & Processing **76**, 645 (2003).

[79] W. Wang, X. Shi, S. Wang, M. A. Van Hove, and N. Lin. Single-molecule resolution of an organometallic intermediate in a surface-supported Ullmann coupling reaction. Journal of the American Chemical Society **133**, 13264 (2011).

[80] R. Gutzler, L. Cardenas, J. Lipton-Duffin, M. El Garah, L. E. Dinca, C. E. Szakacs, C. Fu, M. Gallagher, M. Vondráček, M. Rybachuk, D. F. Perepichka, and F. Rosei. Ullmann-type coupling of brominated tetrathienoanthracene on copper and silver. Nanoscale **6**, 2660 (2014).

[81] K.-H. Chung, B.-G. Koo, H. Kim, J. K. Yoon, J.-H. Kim, Y.-K. Kwon, and S.-J. Kahng. Electronic structures of one-dimensional metal-molecule hybrid chains studied using scanning tunneling microscopy and density functional theory. Physical chemistry chemical physics : PCCP **14**, 7304 (2012).

[82] J. Park, K. Y. Kim, K.-H. Chung, J. K. Yoon, H. Kim, S. Han, and S.-J. Kahng. Interchain interactions mediated by Br adsorbates in arrays of metal-organic hybrid chains on Ag(111). The Journal of Physical Chemistry C **115**, 14834 (2011).

[83] A. Saywell, W. Gren, G. Franc, A. Gourdon, X. Bouju, and L. Grill. Manipulating the conformation of single organometallic chains on Au(111). The Journal of Physical Chemistry C **118**, 1719 (2014).

[84] K. Morgenstern, G. Rosenfeld, E. Laegsgaard, F. Besenbacher, and G. Comsa. Measurement of energies controlling ripening and annealing on metal surfaces. Physical Review Letters **80**, 556 (1998).

[85] C. Wäckerlin, C. Iacovita, D. Chylarecka, P. Fesser, T. A. Jung, and N. Ballav. Assembly of 2D ionic layers by reaction of alkali halides with the organic electrophile 7,7,8,8-tetracyano-p-quinodimethane (TCNQ). Chemical communications **47**, 9146 (2011).

[86] S. Klyatskaya, F. Klappenberger, U. Schlickum, D. Kühne, M. Marschall, J. Reichert, R. Decker, W. Krenner, G. Zoppellaro, H. Brune, J. V. Barth, and M. Ruben. Surface-confined self-assembly of di-carbonitrile polyphenyls. Advanced Functional Materials **21**, 1230 (2011).

[87] T.-C. Tseng, C. Lin, X. Shi, S. Tait, X. Liu, U. Starke, N. Lin, R. Zhang, C. Minot, M. Van Hove, J. Cerdá, and K. Kern. Two-dimensional metal-organic coordination networks of Mn-7,7,8,8-tetracyanoquinodimethane assembled on Cu(100): Structural, electronic, and magnetic properties. Physical Review B **80**, 155458 (2009).

[88] T. R. Umbach, I. Fernández-Torrente, M. Ruby, F. Schulz, C. Lotze, R. Rurali, M. Persson, J. I. Pascual, and K. J. Franke. A typical charge redistribution over a charge-transfer monolayer on a metal. New Journal of Physics **15**, 083048 (2013).

[89] T.-C. Tseng, N. Abdurakhmanova, S. Stepanow, and K. Kern. Hierarchical assembly and reticulation of two-dimensional Mn- and Ni-TCNQ x(x=1, 2, 4) coordination structures on a metal surface. The Journal of Physical Chemistry C **115**, 10211 (2011).

[90] M. N. Faraggi, N. Jiang, N. Gonzalez-Lakunza, A. Langner, S. Stepanow, K. Kern, and A. Arnau. Bonding and charge transfer in metal-organic coordination networks on Au(111) with strong acceptor molecules. The Journal of Physical Chemistry C **116**, 24558 (2012).

[91] R. Otero, J. M. Gallego, A. L. V. de Parga, N. Martín, and R. Miranda. Molecular self-assembly at solid surfaces. Advanced Materials **23**, 5148 (2011).

[92] J. S. Miller. Oliver Kahn Lecture: Composition and structure of the V[TCNE]x (TCNE=tetracyanoethylene) room-temperature, organic-based magnet - A personal perspective. Polyhedron **28**, 1596 (2009).

[93] J. Leiro, E. Minni, and E. Suoninen. Study of plasmon structure in XPS spectra of silver and gold. Journal of Physics F: Metal Physics **13**, 215 (1983).

[94] C. Tengstedt, M. Unge, M. P. de Jong, S. Stafström, W. R. Salaneck, and M. Fahlman. Coulomb interactions in rubidium-doped tetracyanoethylene: A model system for organometallic magnets. Physical Review B **69**, 165208 (2004).

[95] C. Urban. *Structural and chemical effects of charge transfer across metal-organic interfaces*. Ph.D. thesis (2011).

[96] Y. Chou and N. Liang. Surface-enhanced raman scattering from tetracyanoethylene deposited on thin Ag films and charge transfer effects. Chemical physics letters **106**, 472 (1984).

[97] W. Erley and H. Ibach. Spectroscopic evidence for surface anion radical formation of tetracyanoethylene adsorbed on Cu(111) at 100 K: a high-resolution electron energy loss study. The Journal of Physical Chemistry **91**, 2947 (1987).

[98] L. R. Melby, R. J. Harder, W. R. Hertler, W. Mahler, R. E. Benson, and W. E. Mochel. Substituted quinodimethans. II. Anion-radical derivatives and complexes of 7,7,8,8-Tetracyanoquinodimethan. Journal of the American Chemical Society **84**, 3374 (1962).

[99] W. Kaim and M. Moscherosch. The coordination chemistry of TCNE, TCNQ and related polynitrile acceptors. Coordination Chemisty Reviews **129**, 157 (1994).

[100] B. Torrance. The difference between metallic and insultaing salts of tetracyanoquinodimethane (TCNQ): How to desing an organic metal. Accounts of chemical research **12**, 79 (1979).

[101] I. F. Torrente, K. J. Franke, and J. I. Pascual. Structure and electronic configuration of tetracyanoquinodimethane layers on a Au(111) surface. International Journal of Mass Spectrometry **277**, 269 (2008).

[102] T.-C. Tseng. *TCNQ-based Supramolecular Architectures at Metal Surfaces.* Ph.D. thesis (2010).

[103] S. Barja, M. Garnica, J. J. Hinarejos, A. L. Vázquez de Parga, N. Martín, and R. Miranda. Self-organization of electron acceptor molecules on graphene. Chemical communications **46**, 8198 (2010).

[104] O. Gröning and R. Fasel. STM generator software. Empa, Swiss Federal Laboratories for Materials Testing and Research, Switzerland (2004).

[105] S. Barja, D. Stradi, B. Borca, M. Garnica, C. Díaz, J. M. Rodriguez-García, M. Alcamí, A. L. Vázquez de Parga, F. Martín, and R. Miranda. Ordered arrays of metal-organic magnets at surfaces. Journal of physics. Condensed matter: An Institute of Physics journal **25**, 484007 (2013).

[106] M. M. Kamna, T. M. Graham, J. C. Love, and P. S. Weiss. Strong electronic perturbation of the Cu{111} surface by 7,7',8,8'-tetracyanoquinodimethane. Surface science **419**, 12 (1998).

[107] J. M. Lindquist and J. C. Hemminger. High-resolution core level photoelectron spectra of solid TCNQ: determination of molecular orbital spatial distribution from localized shake-up features. the journal of physical chemistry **92**, 1394 (1988).

[108] D. Maccariello, M. Garnica, M. A. Niño, C. Navío, P. Perna, S. Barja, A. L. Vázquez de Parga, and R. Miranda. Spatially resolved, site-dependent charge transfer and induced magnetic moment in TCNQ adsorbed on graphene. Chemistry of Materials **26**, 2883 (2014).

[109] W. D. Grobman, R. A. Pollak, D. E. Eastman, E. T. Maas, and B. A. Scott. Valence electronic sctructure and charge transfer in Tetratiofulvalinium Tetracyanoquinodimethane (TTF-TCNQ) from photoemission spectroscopy. Physical Review Letters **32**, 534 (1974).

[110] M. Higo, T. Futagawa, M. Mitsushio, T. Yoshidome, and Y. Ozono. Adsorption state and morphology of tetracyanoquinodimethane deposited from solution onto the atomically smooth native oxide surface of Al(111) films studied by X-ray photoelectron spectroscopy and atomic force microscopy. The Journal of Physical Chemistry B **107**, 5871 (2003).

[111] J. M. Lindquistt and J. C. Hemminger. High-energy resolution X-ray photoelectron spectroscopy studies of Tetracyanoquinodimethane charge-transfer complexes with copper, nickel, and lithium. Chemistry of Materials **1**, 72 (1989).

[112] J. Giergiel, S. Wells, T. A. Land, and J. C. Hemminger. Growth and chemistry of TCNQ films on nickel (111). Surface **255**, 31 (1991).

[113] S. K. Wells, J. Giergiel, T. A. Land, J. M. Lindquist, and J. C. Hemminger. Beam-induced modifications of TCNQ multilayers. Surface science **257**, 129 (1991).

[114] J. Solomon, R. Madix, and J. Stöhr. Orientation and absolute coverage of benzene, aniline, and phenol on Ag(110) determined by NEXAFS and XPS. Surface Science **255**, 12 (1991).

[115] G. Iucci, V. Carravetta, P. Altamura, M. V. Russo, G. Paolucci, A. Goldoni, and G. Polzonetti. XPS, NEXAFS and theoretical study of phenylacetylene adsorbed on Cu(100). Chemical Physics **302**, 43 (2004).

[116] J. Fraxedas. *Molecular Organic Materials: From Molecules to Crystalline Solids* (Cambridge University Press, Cambridge England, 2006).

[117] N. Martín. Tetrathiafulvalene: The advent of organic metals. Chemical Communications **49**, 7025 (2013).

[118] F. Wudl, G. M. Smith, and E. J. Hufnagel. Bis-1,3-diothiolium chrolide: an unusually stable organic radical cation. Chemical communications 1453 (1970).

[119] S. Hünig, G. Kiesslich, D. Sceutzow, R. Zahrandik, and P. Carsky. Conjugated Radicals. VII. Tetrathiofulvalene and a note on sulfur-containing conjugated radicals. International Journal sulfur chemistry Part C **6**, 109 (1971).

[120] D. L. Coffen, J. Q. Chambers, D. R. Williams, P. E. Garrett, and N. D. Canfield. Tetrathioethylenes. Journal of the American Chemical Society **93**, 2258 (1971).

[121] J. Yamada and T. Sugimoto. *TTF chemistry: Fundamentals and applications of tetrathiafulvalene* (Springer Verlag, Heidelberg, 2004).

[122] I. Torrente. *Local Spectroscopy of bi-molecular assemblies: screening, charge transfer, and magnetism at the molecular scale.* Ph.D. thesis (2008).

[123] I. Fernandez-Torrente, S. Monturet, K. Franke, J. Fraxedas, N. Lorente, and J. Pascual. Long-range repulsive interaction between molecules on a metal surface induced by charge transfer. Physical Review Letters **99**, 176103 (2007).

[124] J. Martínez, E. Abad, C. González, J. Ortega, and F. Flores. Theoretical characterization of the TTF/Au (111) interface: STM imaging, band alignment and charging energy. Organic Electronics **13**, 399 (2012).

[125] Y. Wang, C. Urban, J. Rodríguez-Fernández, J. M. Gallego, R. Otero, N. Martín, R. Miranda, M. Alcamí, and F. Martín. Formation of self-assembled chains of tetrathiafulvalene on a Cu(100) surface. The journal of physical chemistry. A **115**, 13080 (2011).

[126] O. T. Hofmann, G. M. Rangger, and E. Zojer. Reducing the metal work function beyond Pauli pushback: A computational investigation of tetrathiafulvalene and viologen on coinage metal surfaces. The Journal of Physical Chemistry C **112**, 20357 (2008).

[127] B. Martorell Masip. *Organic molecules on metal surfaces: Forecasting structures and spectra.* Ph.D. thesis (2008).

[128] B. Martorell, A. Clotet, and J. Fraxedas. A first principle study of the structural, vibrational and Electronic properties of tetrathiafulvalene adsorbed on Ag(110) and Au(110) surfaces. Journal of computational chemistry **31**, 1842 (2010).

[129] B. Martorell, J. Fraxedas, and A. Clotet. Tetrathia- and tetraselenafulvalene adsorbed on Ag(110): A theoretical study. Surface Science **605**, 187 (2011).

[130] M. Zharnikov and M. Grunze. Spectroscopic characterization of thiol-derived self-assembling monolayers. Journal Physics: Condensed Matter **13**, 11333 (2011).

[131] C. Vericat, M. E. Vela, G. Andreasen, R. C. Salvarezza, L. Vázquez, and J. A. Martín-Gago. Sulfur-substrate interactions in spontaneously formed sulfur adlayers on Au(111). Langmuir **17**, 4919 (2001).

[132] E. Ito, J. Noh, and M. Hara. Different adsorption states between thiophene and α-Bithiophene thin films prepared by self-assembly method. Japanese Journal applied physics **42**, L852 (2003).

[133] D. Choudhury, B. Das, D. D. Sarma, and C. N. R. Rao. XPS evidence for molecular charge-transfer doping of graphene. Chemical Physics Letters **497**, 66 (2010).

[134] J. J.-. Yeh. *Atomic Calculation of Photoionization Cross-sections and Asymmetry Parameters* (Gordon & Breach Science, 1993).

[135] J. J.-. Yeh and I. Lindau. Atomic subshell photoionization cross sections and asymmetry parameters: $1 < Z < 103$. Atomic Data and Nuclear Data Tables **32**, 1 (1985).

[136] H. Vázquez, Y. J. Dappe, J. Ortega, and F. Flores. Energy level alignment at metal/organic semiconductor interfaces: "pillow" effect, induced density of interface states, and charge neutrality level. The Journal of chemical physics **126**, 144703 (2007).

[137] D. Jérome. Organic conductors: From charge density wave TTF-TCNQ to superconducting (TMTSF)2PF6. Chemical reviews **104**, 5565 (2004).

[138] M. Bendikov, F. Wudl, and D. F. Perepichka. Tetrathiafulvalenes, oligoacenenes, and their buckminsterfullerene derivatives: The brick and mortar of organic electronics. Chemical reviews **104**, 4891 (2004).

[139] J. Sworakowski and J. Ulanski. 4 Electrical properties of organic materials. Annual Reports Section "C" (Physical Chemistry) **99**, 87 (2003).

[140] J. Ferraris, D. O. Cowan, V. Waltka, and J. H. Perlstein. Electron transfer in a new highly conducting donor-acceptor complex. Journal of the American Chemical Society **95**, 948 (1973).

[141] T. Nishiguchi, M. Kageshima, N. Ara-Kato, and A. Kawazu. Behavior of charge density waves in a one-dimensional organic conductor visualized by scanning tunneling microscopy. Physical Review Letters **81**, 3187 (1998).

[142] M. Sing, U. Schwingenschlögl, R. Claessen, P. Blaha, J. M. P. Carmelo, L. M. Martelo, P. D. Sacramento, M. Dressel, and C. S. Jacobsen. Electronic structure of the quasi-one-dimensional organic conductor TTF-TCNQ. Physical Review B **68**, 125111 (2003).

[143] J. Fraxedas, Y. J. Lee, I. Jiménez, R. Gago, R. M. Nieminen, P. Ordejón, and E. Canadell. Characterization of the unoccupied and partially occupied states of TTF-TCNQ by XANES and first-principles calculations. Physical Review B **68**, 195115 (2003).

[144] F. Zwick, D. Jérome, G. Margaritondo, M. Onellion, J. Voit, and M. Grioni. Band mapping and quasiparticle suppression in the one-dimensional organic conductor TTF-TCNQ. Physical Review Letters **81**, 2974 (1998).

[145] N. Ara, A. Kawazu, H. Shigekawa, K. Yase, and M. Yoshimura. Structural studies of tetrathiafulvalene-tetracyanoquinodimethane thin films by scanning tunneling microscopy. Applied Physics Letters **66**, 3278 (1995).

[146] D. Jérome, A. Mazaud, M. Ribault, and K. Bechgaard. Superconductivity in a synthetic organic conductor (TMTSF)2PF 6. Journal de Physique Lettres **41**, 95 (1980).

[147] J. T. Sun, Y. H. Lu, W. Chen, Y. P. Feng, and A. T. S. Wee. Linear tuning of charge carriers in graphene by organic molecules and charge-transfer complexes. Physical Review B **81**, 155403 (2010).

[148] N. Gonzalez-Lakunza, I. Fernández-Torrente, K. J. Franke, N. Lorente, A. Arnau, and J. I. Pascual. Formation of dispersive hybrid bands at an organic-metal interface. Physical Review Letters **100**, 156805 (2008).

[149] J. I. Beltrán, F. Flores, J. I. Martínez, and J. Ortega. Energy level alignment in organic-organic heterojunctions: The TTF/TCNQ interface. The Journal of Physical Chemistry C **117**, 3888 (2013).

[150] L. Cano-Cortés, A. Dolfen, J. Merino, J. Behler, B. Delley, K. Reuter, and E. Koch. Spectral broadening due to long-range Coulomb interactions in the molecular metal TTF-TCNQ. The European Physical Journal B **56**, 173 (2007).

[151] S. Ishibashi. First-principles electronic-band calculations on organic conductors. Science and Technology of Advanced Materials **10**, 024311 (2009).

[152] H. Alves, A. S. Molinari, H. Xie, and A. F. Morpurgo. Metallic conduction at organic charge-transfer interfaces. Nature materials **7**, 574 (2008).

[153] D. A. Clemente and A. Marzotto. Structure of two polymorphs of the TTF-TCNE charge-transfer complex and the degree of ionicity. Journal of Materials Chemistry **6**, 941 (1996).

[154] M. Meneghetti and C. Pecile. Partial ionic ground state in the self-dimer mixed stack charge transfer crystal of TTF and TCNE. Synthetic Metals **86**, 2037 (1997).

[155] M. Capdevila-Cortada, J. J. Novoa, J. D. Bell, C. E. Moore, A. L. Rheingold, and J. S. Miller. Unusually long, multicenter, cation(δ+) . . . anion(δ-) bonding observed for several polymorphs of [TTF][TCNE]. Chemistry European journal **17**, 9326 (2011).

[156] R. Otero, D. Ecija, G. Fernandez, J. M. Gallego, L. Sanchez, N. Martín, and R. Miranda. An organic donor/acceptor lateral superlattice at the nanoscale. Nano letters **7**, 2602 (2007).

[157] T. R. Umbach, I. Fernandez-Torrente, J. N. Ladenthin, J. I. Pascual, and K. J. Franke. Enhanced charge transfer in a monolayer of the organic charge transfer complex TTF-TNAP on Au(111). Journal of Physics: Condensed Matter **24**, 354003 (2012).

[158] G. A. Rojas, P. Ganesh, S. J. Kelly, B. G. Sumpter, J. A. Schlueter, and P. Maksymovych. Ionic disproportionation of charge transfer salt driven by surface epitaxy. The Journal of Physical Chemistry C **117**, 19402 (2013).

[159] K. Bechgaard, T. J. Kistenmacher, A. N. Bloch, and D. O. Cowan. The crystal and molecular structure of an organic conductor from 4,4',5,5'-tetramethyl-Δ2,2'-bis-1,3-diselenole and 7,7,8,8-tetracyano-p-quinodimethane [TMTSF-TCNQ]. Acta Crystallographica Section B Structural Crystallography and Crystal Chemistry **33**, 417 (1977).

[160] A. El-Sayed, D. J. Mowbray, J. M. García-Lastra, C. Rogero, E. Goiri, P. Borghetti, A. Turak, B. P. Doyle, M. Dell'Angela, L. Floreano, Y. Wakayama, A. Rubio, J. E. Ortega, and D. G. de Oteyza. Supramolecular environment-dependent electronic properties of metal-organic interfaces. The Journal of Physical Chemistry C **116**, 4780 (2012).

[161] D. G. de Oteyza, A. El-Sayed, J. M. Garcia-Lastra, E. Goiri, T. N. Krauss, A. Turak, E. Barrena, H. Dosch, J. Zegenhagen, A. Rubio, Y. Wakayama, and J. E. Ortega. Copper-phthalocyanine based metal-organic interfaces: the effect of fluorination, the substrate, and its symmetry. The Journal of chemical physics **133**, 214703 (2010).

[162] E. Goiri, M. Matena, A. El-Sayed, J. Lobo-Checa, P. Borghetti, C. Rogero, B. Detlefs, J. Duvernay, J. E. Ortega, and D. G. de Oteyza. Self-assembly of bicomponent molecular monolayers: Adsorption height changes and their consequences. Physical Review Letters **112**, 117602 (2014).

[163] P. Fesser, C. Iacovita, C. Wäckerlin, S. Vijayaraghavan, N. Ballav, K. Howes, J.-P. Gisselbrecht, M. Crobu, C. Boudon, M. Stöhr, T. A. Jung, and F. Diederich. Visualizing the product of a formal cycloaddition of 7,7,8,8-tetracyano-p-quinodimethane (TCNQ) to an acetylene-appended porphyrin by scanning tunneling microscopy on Au(111). Chemistry European journal **17**, 5246 (2011).

[164] A. El-Sayed, P. Borghetti, E. Goiri, C. Rogero, L. Floreano, G. Lovat, D. J. Mowbray, J. L. Cabellos, Y. Wakayama, A. Rubio, J. E. Ortega, and D. G. de Oteyza. Understanding energy-level alignment in donor-acceptor/metal interfaces from core-level shifts. ACS nano **7**, 6914 (2013).

[165] Y. Wakayama, D. G. de Oteyza, J. M. Garcia-Lastra, and D. J. Mowbray. Solid-state reactions in binary molecular assemblies of F16CuPc and pentacene. ACS nano **5**, 581 (2011).

[166] R. F. W. Bader. Atoms in molecules. Accounts of Chemical Research **18**, 9 (1985).

[167] R. F. W. Bader. A quantum theory of molecular structure and its applications. Chemical Reviews **91**, 893 (1991).

[168] R. F. W. Bader. *Atoms in Molecules: A Quantum Theory*. International Ser. of Monogr. on Chem (Oxford University Press, Oxford, 1990).

[169] I. Fernández-Torrente, K. J. Franke, and J. I. Pascual. Vibrational Kondo effect in pure organic charge-transfer assemblies. Physical Review Letters **101**, 217203 (2008).

[170] T. J. Kistenmacher, T. Phillips, and D. O. Cowan. The crystal structure of the 1:1 radical cationâ€“radical anion salt of 2,2'-bis-l,3-dithiole (TTF) and 7,7,8,8-tetracyanoquinodimethane (TCNQ). Acta Crystallographica Section B Structural Crystallography and Crystal Chemistry **30**, 763 (1974).

[171] F. Wennmohs, V. Staemmler, and M. Schindler. Theoretical investigation of weak hydrogen bonds to sulfur. The Journal of Chemical Physics **119**, 3208 (2003).

[172] J. Liu, T. Lin, Z. Shi, F. Xia, L. Dong, P. N. Liu, and N. Lin. Structural transformation of two-dimensional metal-organic coordination networks driven by intrinsic in-plane compression. Journal of the American Chemical Society **133**, 18760 (2011).

[173] J. L. Cabellos, D. J. Mowbray, E. Goiri, A. El-Sayed, L. Floreano, D. G. de Oteyza, C. Rogero, J. E. Ortega, and A. Rubio. Understanding charge transfer in Donor-Acceptor/Metal systems: A combined theoretical and experimental study. The Journal of Physical Chemistry C **116**, 17991 (2012).

[174] S. Hünig. Aromatic/quinoid systems: principles and applications. Pure and applied chemistry **62**, 395 (1990).

[175] N. Martín, J. L. Segura, and C. Seoane. Design and synthesis of TCNQ and DCNQI type electron acceptor molecules as precursors for 'organic metals'. Journal of Materials Chemistry **7**, 1661 (1997).

[176] F. Cossío, P. de la Cruz, A. de la Hoz, F. Langa, N. Martín, P. Prieto, and L. Sánchez. Determination of syn/anti Isomerism in DCNQI Derivatives by 2D Exchange Spectroscopy: Theoretical Underpinning. European Journal of Organic Chemistry **2000**, 2407 (2000).

[177] S. Hünig and P. Erk. DCNQIs new electron acceptors for charge transfer complexes and highly conducting radical anion salts. Advanced Materials **3**, 225 (1991).

[178] J. Galvez and A. Guirado. A theoretical study of topomerization of imine systems: Inversion, Rotation or Mixed mechanisms? Journal of computational chemistry **31**, 520 (2010).

[179] A. Aumüller and S. Hünig. N,N'-Dicyanoquinonediimines-A new class of compounds, I: synthesis and general properties. Liebigs Annalen der Chemie **1986**, 142 (1986).

[180] K. Morgenstern. Switching individual molecules by light and electrons: From isomerisation to chirality flip. Progress in Surface Science **86**, 115 (2011).

[181] J. Miwa, S. Weigelt, H. Gersen, F. Besenbacher, F. Rosei, and T. R. Linderoth. Azobenzene on Cu(110): Adsorption site-dependent diffusion. Journal of the American Chemical Society **128**, 3164 (2006).

[182] A. S. Kumar, T. Ye, T. Takami, B.-C. Yu, A. K. Flatt, J. Tour, and P. S. Weiss. Reversible photo-switching of single azobenzene molecules in controlled nanoscale environments. Nano letters **8**, 1644 (2008).

[183] L.-P. Xu and L.-J. Wan. STM investigation of the photoisomerization of an azobis-(benzo-15-crown-5) molecule and its self-assembly on Au(111). The journal of physical chemistry. B **110**, 3185 (2006).

[184] M. Comstock, N. Levy, A. Kirakosian, J. Cho, F. Lauterwasser, J. Harvey, D. Strubbe, J. Fréchet, D. Trauner, S. Louie, and M. Crommie. Reversible photomechanical switching of individual engineered molecules at a metallic surface. Physical Review Letters **99**, 038301 (2007).

[185] S. Hagen, F. Leyssner, D. Nandi, M. Wolf, and P. Tegeder. Reversible switching of tetra-tert-butyl-azobenzene on a Au(111) surface induced by light and thermal activation. Chemical Physics Letters **444**, 85 (2007).

[186] K. Morgenstern. Isomerization reactions on single adsorbed molecules. Accounts of chemical research **42**, 213 (2009).

[187] K. Morgenstern. Single molecule manipulation. Surface and Interface Analysis **42**, 1634 (2010).

[188] L. Óvári, M. Wolf, and P. Tegeder. Reversible changes in the vibrational structure of tetra-tert-butylazobenzene on a Au(111) surface induced by light and thermal activation. Journal physics Chemical C **111**, 15370 (2007).

[189] D. Rohde, C.-J. Yan, H.-J. Yan, and L.-J. Wan. From a lamellar to hexagonal self-assembly of bis(4,4'-(m,m'-di(dodecyloxy)phenyl)-2,2'-difluoro-1,3,2-dioxaborin) molecules: a trans-to-cis-isomerization-induced structural transition studied with STM. Angewandte Chemie International Edition **45**, 3996 (2006).

[190] M. Alemani, S. Selvanathan, F. Ample, M. Peters, K.-H. Rieder, F. Moresco, C. Joachim, S. Hecht, and L. Grill. Adsorption and switching properties of azobenzene derivatives on different noble metal surfaces: Au(111), Cu(111), and Au(100). Journal of Physical Chemistry C **112**, 10509 (2008).

[191] M. Alemani, M. Peters, S. Hecht, K.-H. Rieder, F. Moresco, and L. Grill. Electric field-induced isomerization of azobenzene by STM. Journal of the American Chemical Society **128**, 14446 (2006).

[192] A. Safiei, J. Henzl, and K. Morgenstern. Isomerization of an azobenzene derivative on a thin insulating layer by inelastically tunneling electrons. Physical Review Letters **104**, 216102 (2010).

[193] J. Mielke, F. Leyssner, M. Koch, S. Meyer, Y. Luo, S. Selvanathan, R. Haag, P. Tegeder, and L. Grill. Imine derivatives on Au(111): evidence for "inverted" thermal isomerization. ACS nano **5**, 2090 (2011).

[194] I. Langmuir. Surface Chemistry. Chemical reviews **XIII**, 147 (1933).

[195] S. Stepanow, N. Lin, and J. V. Barth. Modular assembly of low-dimensional coordination architectures on metal surfaces. Journal of Physics: Condensed Matter **20**, 184002 (2008).

[196] S. L. Tait, A. Langner, N. Lin, R. Chandrasekar, O. Fuhr, M. Ruben, and K. Kern. Assembling isostructural metal-organic coordination architectures on Cu(100), Ag(100) and Ag(111) substrates. Chemphyschem: A european journal of chemical physics and physical chemistry **9**, 2495 (2008).

[197] H. Spillmann, A. Dmitriev, N. Lin, P. Messina, J. V. Barth, and K. Kern. Hierarchical assembly of two-dimensional homochiral nanocavity arrays. Journal of the American Chemical Society **125**, 10725 (2003).

[198] A. Shchyrba, C. Wäckerlin, J. Nowakowski, S. Nowakowska, J. Björk, S. Fatayer, J. Girovsky, T. Nijs, S. C. Martens, A. Kleibert, M. Stöhr, N. Ballav, T. a. Jung, and L. H. Gade. Controlling the dimensionality of on-surface coordination polymers via endo- or exoligation. Journal of the American Chemical Society **136**, 9355 (2014).

[199] M. Kurmoo. Magnetic metal-organic frameworks. Chemical Society reviews **38**, 1353 (2009).

[200] J. Lee, O. K. Farha, J. Roberts, K. A. Scheidt, S. T. Nguyen, and J. T. Hupp. Metal-organic framework materials as catalysts. Chemical Society reviews **38**, 1450 (2009).

[201] R. E. Morris and P. S. Wheatley. Gas storage in nanoporous materials. Angewandte Chemie (International ed. in English) **47**, 4966 (2008).

[202] D. Farrusseng. *Metal-organic frameworks: Applications from catalysis to gas storage* (Wiley-VCH (2011)).

[203] C. S. Kley, J. Čechal, T. Kumagai, F. Schramm, M. Ruben, S. Stepanow, and K. Kern. Highly adaptable two-dimensional metal-organic coordination networks on metal surfaces. Journal of the American Chemical Society **134**, 6072 (2012).

[204] J. V. Barth. Fresh perspectives for surface coordination chemistry. Surface Science **603**, 1533 (2009).

[205] J. V. Barth. Molecular architectonic on metal surfaces. Annual review of physical chemistry **58**, 375 (2007).

[206] N. Lin, S. Stepanow, M. Ruben, and J. V. Barth. Surface-confined supramolecular coordination chemistry. Topics in current chemistry **287**, 1 (2009).

[207] L. Bartels. Tailoring molecular layers at metal surfaces. Nature chemistry **2**, 87 (2010).

[208] S. L. Tait, Y. Wang, G. Costantini, N. Lin, A. Baraldi, F. Esch, L. Petaccia, S. Lizzit, and K. Kern. Metal-organic coordination interactions in Fe-terephthalic acid networks on Cu(100). Journal of the American Chemical Society **130**, 2108 (2008).

[209] A. Dmitriev, H. Spillmann, N. Lin, J. V. Barth, and K. Kern. Modular assembly of two-dimensional metal-organic coordination networks at a metal surface. Angewandte chemie **115**, 2774 (2003).

[210] S. Stepanow, M. Lingenfelder, A. Dmitriev, H. Spillmann, E. Delvigne, N. Lin, X. Deng, C. Cai, J. V. Barth, and K. Kern. Steering molecular organization and host-guest interactions using two-dimensional nanoporous coordination systems. Nature materials **3**, 229 (2004).

[211] P. Gambardella, S. Stepanow, A. Dmitriev, J. Honolka, F. M. F. de Groot, M. Lingenfelder, S. Sen Gupta, D. D. Sarma, P. Bencok, S. Stanescu, S. Clair, S. Pons, N. Lin, A. P. Seitsonen, H. Brune, J. V. Barth, and K. Kern. Supramolecular control of the magnetic anisotropy in two-dimensional high-spin Fe arrays at a metal interface. Nature materials **8**, 189 (2009).

[212] T. Classen, G. Fratesi, G. Costantini, S. Fabris, F. L. Stadler, C. Kim, S. de Gironcoli, S. Baroni, and K. Kern. Templated growth of metal-organic coordination chains at surfaces. Angewandte Chemie (International ed. in English) **44**, 6142 (2005).

[213] S. Clair, S. Pons, S. Fabris, S. Baroni, H. Brune, K. Kern, and J. V. Barth. Monitoring two-dimensional coordination reactions: Directed assembly of co-terephthalate nanosystems on Au(111). The Journal of Physical Chemistry B **110**, 5627 (2006).

[214] U. Schlickum, R. Decker, F. Klappenberger, G. Zoppellaro, S. Klyatskaya, M. Ruben, I. Silanes, A. Arnau, K. Kern, H. Brune, and J. V. Barth. Metal-organic honeycomb nanomeshes with tunable cavity size. Nano letters **7**, 3813 (2007).

[215] D. Kuhne, F. Klappenberger, R. Decker, U. Schlickum, H. Brune, S. Klyatskaya, M. Ruben, and J. V. Barth. High-quality 2D metal-organic coordination network providing giant cavities within mesoscale domains. Journal of the American Chemical Society **131**, 3881 (2009).

[216] M. Bieri, M. Treier, J. Cai, K. Aït-Mansour, P. Ruffieux, O. Gröning, P. Gröning, M. Kastler, R. Rieger, X. Feng, K. Müllen, and R. Fasel. Porous graphenes: two-dimensional polymer synthesis with atomic precision. Chemical communications 6919 (2009).

[217] S. Stepanow, N. Lin, D. Payer, U. Schlickum, F. Klappenberger, G. Zoppellaro, M. Ruben, H. Brune, J. V. Barth, and K. Kern. Surface-assisted assembly of 2D metal-organic networks that exhibit unusual threefold coordination symmetry. Angewandte Chemie **119**, 724 (2007).

[218] M. Marschall, J. Reichert, K. Diller, S. Klyatskaya, M. Ruben, A. Nefedov, C. Wöll, L. N. Kantorovich, F. Klappenberger, and J. V. Barth. Meta-positioning of carbonitrile functional groups induces interfacial edge-on phase of oligophenyl derivatives. The Journal of Physical Chemistry C **118**, 2622 (2014).

[219] J. A. Lipton-Duffin, O. Ivasenko, D. F. Perepichka, and F. Rosei. Synthesis of polyphenylene molecular wires by surface-confined polymerization. Small **5**, 592 (2009).

[220] D. Ecija, S. Vijayaraghavan, W. Auwärter, S. Joshi, K. Seufert, C. Aurisicchio, D. Bonifazi, and J. V. Barth. Two-dimensional short-range disordered crystalline networks from flexible molecular modules. ACS nano **6**, 4258 (2012).

[221] S. Vijayaraghavan, D. Ecija, W. Auwärter, S. Joshi, K. Seufert, M. Drach, D. Nieckarz, P. Szabelski, C. Aurisicchio, D. Bonifazi, and J. V. Barth. Supramolecular assembly of interfacial nanoporous networks with simultaneous expression of metal-organic and organic-bonding motifs. Chemistry European journal **19**, 14143 (2013).

[222] M. Bässler, R. Fink, C. Heske, J. Müller, P. Väterlein, J. U. Von Schütz, and E. Umbach. NEXAFS investigations of highly-ordered ultrathin films of DME-DCNQI on Ag(111). Thin solid films **284-285**, 234 (1996).

[223] H. Kopf, C. Seidel, and H. Fuchs. Low-energy electron diffraction, Scanning tunneling microscopy and X-ray photoemission spectroscopy investigations of DMe-DCNQI on Cu(110). Thin Solid Films **342**, 307 (1999).

[224] C. Seidel, H. Kopf, and H. Fuchs. Growth process and compressed phase of DMe-DCNQI on Ag(110) in the monolayer regime observed by LEED, XPS, and STM. Physical Review B **60**, 14341 (1999).

[225] F. Buchner. *STM investigation of molecular architectures of porphyrinoids on a Ag(111) surface*. Ph.D. thesis, Berlin, Heidelberg (2010).

[226] M. A. Niño, J. Camarero, L. Gómez, J. Ferrón, J. J. de Miguel, and R. Miranda. Surfactant-assisted epitaxial growth and magnetism of Fe films on Cu(111). Journal of Physics: Condensed Matter **20**, 265008 (2008).

[227] M. Passeggi, J. Prieto, R. Miranda, and J. Gallego. Surfactant effect of Pb in the growth of Fe on Cu(111): A kinetic effect. Physical Review B **65**, 035409 (2001).

[228] M. Passeggi, J. Prieto, R. Miranda, and J. Gallego. A scanning tunnelling microscopy view of the surfactant-assisted growth of iron on Cu(111). Surface Science **462**, 45 (2000).

[229] R. Kato, H. Kobayashi, and A. Kobayashi. Crystal and electronic structures of conductive anion-radical salts, (2,5-R1R2-DCNQI)2Cu (DCNQI = N,N'-dicyanoquinonediimine; R1, R2 = CH3, CH3O, Cl, Br). Journal of the American Chemical Society **111**, 5224 (1989).

[230] A. Kobayashi, R. Kato, H. Kobayashi, T. Mori, and H. Inokuchi. The organic π-electron metal system with interaction through mixed-valence metal cation: Electronic and structural properties of radical salts of dicyano-quinodiimine, (DMe-DCNQI)2Cu and (MeCl-DCNQI)2Cu. Solid State Communications **64**, 45 (1987).

[231] R. Heintz, H. Zhao, X. Ouyang, G. Grandinetti, J. Cowen, and K. R. Dunbar. New insight into the nature of Cu (TCNQ): solution routes to two distinct polymorphs and their relationship to crystalline films that display bistable switching behavior. Inorganic Chemistry **38**, 144 (1999).

[232] N. S. McIntyre and D. G. Zetaruk. X-ray photoelectron spectroscopic studies of iron oxides. Analytical Chemistry **49**, 1521 (1977).

[233] K. Wandelt. Photoemission studies of adsorbed oxygen and oxide layers. Surface Science Reports **2**, 1 (1982).

[234] J. I. Urgel, D. Ecija, W. Auwärter, A. C. Papageorgiou, A. P. Seitsonen, S. Vijayaraghavan, S. Joshi, S. Fischer, J. Reichert, and J. V. Barth. Five-vertex lanthanide coordination on surfaces: A route to sophisticated nanoarchitectures and tessellations. The Journal of Physical Chemistry C **118**, 12908 (2014).

List of publications

1. *Effect of Yb concentration on the resistivity and lifetime of CdTe:Ge:Yb co-doped crystals.* N.V. Sochinskii, M. Abellan, J. Rodríguez-Fernández, E. Saucedo, C.M. Ruiz and V. Bermúdez. Applied Physics Letters, **91**, 202112 (2007).

2. *Growth and characterization of CdTe:Ge:Yb.* N.V. Sochinskii, E. Saucedo, M. Abellan, J. Rodríguez-Fernández, P. Hidalgo, J. Piqueras, C.M. Ruiz, V. Bermúdez and E. Diéguez. Journal of Crystal Growth, **310**, 2076-2079 (2008).

3. *Effect of source composition on vapor phase epitaxy of CdZnTe large-area layers.* N. V. Sochinskii, M. Abellan, J. Rodríguez-Fernández, J.L. Plaza, V. Carcelén and E. Diéguez. Journal of Crystal Growth, **310**, 1669-1673 (2008).

4. *Cadmium telluride: a Silicon-compatible optical material as an alternative technolog for building all-optical photonic devices.* A. Martinez, F. Cuesta-Soto, J. García, J. Marti, N.V. Sochinskii, M. Abellan, J. Rodríguez-Fernández, S. Mengali, A. Mercuri, C. Corsi, I. Reid, M. Robertson, S. Neretina, R.A. Hughes, J. Wojcik, J.S. Preston and P. Mascher, Proceedings of SPIE (Silicon Photonics and photonic integrated circuits), **6996**, 699608-1 (2008)

5. *Influence of thermal environments on the growth of bulk cadmium zinc telluride (CZT) single crystals.* V. Carcelén, N. Vijayan, J. Rodríguez-Fernández, P. Hidalgo, J. Piqueras, N. V. Sochinskii, J. M. Perez and E. Diéguez. Journal of Crystal Growth, **311**, 1264-1267 (2009).

6. *Sub-bandgap photoluminescence from as-grown and annealed layers of CdTe.* N. V. Sochinskii, M. Abellán, J. Rodríguez-Fernández, E. Diéguez, J. Franc, P. Hlidek, P. Praus, V. Babentsov. Superlattices and Microstructures, **45**, 228-233 (2009).

7. *Relationship between the Cathodoluminescence Emission and Resistivity in In doped CdZnTe crystals.* J. Rodríguez-Fernández, V. Carcelén, P. Hidalgo, N. Vijayan, J. Piqueras, N. V. Sochinskii, J. M. Perez and E. Diéguez. Journal of Applied Physics, **106**, 044901 (2009).

8. *Development of CdZnTe doped with Bi for gamma radiation detection.* V. Carcelén, J. Rodríguez-Fernández, N. Vijayan, P. Hidalgo, J. Piqueras, N. V. Sochinskii, J. M. Perez and E. Diéguez. CrystEngComm, **12**, 507-510 (2010).

9. *Growth of Bi doped cadmium zinc telluride single crystals by Bridgman Oscillation method and its structural, optical and electrical analyses.* V. Carcelén, P. Hidalgo, J. Rodríguez-Fernández and E. Diéguez. Journal of Applied physics, **107**, 093501 (2010).

10. *Formation of Self-Assembled chains of tetrathiafulvalene on a Cu(100) surface.* Y. Wang, C. Urban, J. Rodríguez-Fernández, J. M. Gallego, R. Otero, N. Martín, R. Miranda, M. Alcami and F. Martín. The Journal of Physical Chemistry A, **115**, 13080-13087 (2011).

11. *Formation of a surface covalent organic framework based on polyester condensation.* A. Marele, R. Mas-Ballesté, L. Terracciano, J. Rodríguez-Fernández, I. Berlanga, S. S. Alexandre, R. Otero, J. M. Gallego, F. Zamora and J. M. Gómez-Rodríguez. Chemical communtications, **48**, 6779-6781 (2012).

12. *Charge transfer-assisted self-limited decyanation reaction of TCNQ-type electron acceptors on Cu(100).* C. Urban, Y. Wang, J. Rodríguez-Fernández, R. García, M. Á. Herranz, M. Alcami, N. Martín, F. Martín, J. M. Gallego, R. Miranda and R. Otero. Chemical Communications, **50**, 833-835 (2014).

AGRADECIMIENTOS

Se podría decir que hacer una tesis es como el “big bang”. Partes de la nada, llegas al caos y al final alcanzas un orden. En mi caso la nada era grande, el caos fue enorme y llegar al orden fue arduo. Sin embargo, estoy orgulloso de mi creación. Siempre llegados a este punto del camino, cuando ya por fin estas cerca de cumplir tu meta, tiendes a mirar atrás y valorar todo lo que ha ocurrido, tanto lo bueno como lo malo, e intentas hacer un balance de todo lo que ha pasado. Mucha gente me ha ayudado en este largo camino, y me gustaría agradecérselo con unas breves palabras. Espero no olvidarme de nadie.

Al profesor Rodolfo Miranda, el cual ha sabido transmitirme el gran entusiasmo que tiene por la ciencia. Cuando todas mis esperanzas estaban agotadas y me planteaba dejar el doctorado, él consiguió volverme a recordar por qué me entusiasmaba la ciencia y sobre todo a valorarme más. También me gustaría agradecer a mi otro director, José María Gallego, por todo lo que me ha enseñado, su predisposición a ayudar en todo momento y su gran paciencia en estos años, en especial durante el tiempo de escritura de esta tesis. A Roberto Otero, al que también considero director de esta tesis, le quiero agradecer su dedicación y paciencia en este tiempo. A todos vosotros os debo todo lo que he aprendido en estos años, muchas gracias por esos consejos y esas intensas charlas sobre ciencia. Me siento muy afortunado de haber podido trabajar con estos grandes científicos y grandes personas.

A mi maestro “Jedi” Christian Urban, que me acogió como su “padawan”. Por todos esos buenos momentos que hemos pasado juntos y todos los buenos consejos que me has dado y me sigues dando. Siempre te estaré eternamente agradecido por tu incondicional ayuda, *Vielen Dank*. A todas las personas, Michaela Häger, Juan Carlos Moreno y Mario Passeggi, que se pasaron por nuestra campana a realizar cortas estancias. También a ese gran refranero belga, Koen Lauwaet, por los buenos momentos juntos y las muchas risas en esa campana. Mucha suerte en tu futuro donde quiera que vayas. Por cierto, aún me debes esa cena..... . A Sara Barja, por todos esos buenos momentos de cafeteo y tu gran apoyo incondicional, incluidas esas "collejas" bien merecidas. A David Écija, por sus buenos consejos y su infatigable apuesta en mí, aunque no hayamos podido trabajar juntos. Puede que en un futuro no muy lejano sea posible, sería un enorme placer.

A todos los compañeros del Laboratorio de superficies que han estado estos años: Marta, Curro, Erika, Manuela, Flavio, Amjad, Cecilia, Antonio, José Luis, Bogdana, Cristina, Marina, Miguel Ángel, Davide y Josefa. Por todos esos buenos momentos juntos tanto en el laboratorio como en los congresos. A toda la savia nueva de TIREMISU por esos grandes momentos que hemos pasado: a Jesús, a Alberto por esos buenos momentos y ayudarme en la “muerte súbita” de mi portátil, y sobre todo a Borjita por ese pepino de portada que te has currado, aunque a veces seas un poco *kamikaze*, eres un crack sigue así. También me gustaría agradecer a todos los jefes del laboratorio por los consejos y muchos buenos momentos vividos: Amadeo, Julio Camarero, Juanjo H. y Daniel.

Gracias al Prof. Dr. Richard Berndt por acogerme en mi estancia en Kiel. Al igual que a toda la gente que trabajaba allí con los que he tenido una muy buena relación y muy

buenos momentos. En especial a Natasha y su marido Maik; Svenja, su novio Michael y sus perritos "pato" y "taxco". Como no también agradecer a mi compañera de piso Jennifer. También me gustaría agradecer al grupo del Dr. Giovanni Costantini por recibirme con los brazos abiertos en Coventry. A toda la gente que pertenecía al grupo en especial: Ada della Pia y Tom White; THANKS guys.

Siempre detrás de una tesis muchas personas se implican para que pueda llegar a buen puerto. Por lo que me gustaría agradecer a todos los técnicos del departamento de Física de la Materia Condensada: Andrés Buendía, Santiago, Juan Benayas, Rosa y José Luis Romera. También me gustará agradecer en especial a Elsa Fuentes por su disposición para ayudar con cualquier papeleo y consulta; al igual que para intercambiarnos recetas y dulces....sin gluten.

A mis colegas por esos buenos momentos durante el "lunch time": Ángel, Laura, Alejandra y sobre todo a Vero compañera de laboratorio en mi corta estancia en el C-IV, gracias por todos esos buenos momentos y sobre todo porque sin tu ayuda no hubiera estado donde estoy.

A todos los compañeros de fatigas y comedia durante mi primer intento de tesis en el IMM, nuestro clan de asturianos en Madrid: Pablo, Chon, Pinhera, Tavo, Ruben. También al resto de gente con los que coincidí allí: Clavero, Granados, Benito, Fuster, Penedo, PG **et al**. Por supuesto a mi gran amigo portugués Rui por esos grandes momentos, sobre todo en el "cafe madrid" y "piolho". Por esas increíbles caipirinhas y francesinhas. A ése "peazo" portugués, Nuno, por esos grandes momentos en las prácticas de electrónica donde nos hemos ayudado y trabajado codo con codo, y sobre todo hemos sufrido juntos esos momentos de estrés de la escritura de la tesis.

A todos mis ex-compis de piso: Juanan, Miquel, Achus, Fo, Fer, Saúl, Noemi, Yael **et al.** con los que he pasado unos grandes momentos durante este tiempo en Tres Cantos. Al igual que a todas las personas que han pasado por mi vida en este tiempo por Madrid y en las estancias.

En estos agradecimientos no podrían faltar mis amigos de toda la vida, pese a estar lejos siempre he tenido un aliento de apoyo y amistad incondicional: Pablo, Laura, José, Abel, Iñaki, Fredo, Carpin, Xei, Cristian y como no a Jonathan que por fin me considera su amigo. Gracies guajes!!.

Y por último, quisiera agradecer y dedicar esta tesis a toda mi familia. Por estar en los malos y buenos momentos. Sin todos vosotros esto no podría haber llegado a tan buen puerto. Habéis sido mi pilar para poder seguir adelante. Por lo que muchas gracias a mis abuelos, mis primos, mis tíos y tías; en especial a mi tío y padrino Sebi al cuál extraño todos los días. Espero te sientas orgulloso de mí. Siempre estarás en mi corazón y mis pensamientos. Por supuesto a mis padres, Ovidio y Elisa, no hay palabras para poder explicar lo agradecido que estoy, gracias por vuestro sacrificio desde que era pequeño, siempre apoyándome y brindándome vuestro cariño; siempre aconsejándome y cuidándome. Que duda cabe que esta tesis sin vosotros no hubiera sido posible, OS QUIERO. Por supuesto muchas gracias a mis hermanitas, Tamara y Mónica, siempre estáis ahí y pensar siempre en lo mejor para mí, sin duda sois las mejores. A Amparo, por estar apoyandome de forma incondicional durante todo este tiempo, y sobre todo agradecer tu paciencia y cariño. Que

duda cabe que empezar a vivir con alguien durante el tiempo de escritura de tesis no es nada fácil y sobre todo adaptarte a mi menú “sin gluten”. Gracias por todo ello y por quererme.

MUCHES GRACIES